Novel mechanisms of diastolic dysfunction in diabetes

Parisa Koutsifeli

Bachelor of Engineering (Hons), Bachelor of Science (Hons), Master of Science

ORCID Identifier: 0000-0003-2274-4636

A thesis submitted in total fulfilment of the requirements for the degree of Doctor of Philosophy in Biomedical Science

December, 2019

Supervised by Dr. Kimberley Mellor, Prof. Lea Delbridge and Prof. Denis Loiselle

Cellular and Molecular Cardiology Laboratory

Department of Physiology

Faculty of Medical and Health Sciences

University of Auckland

Thesis Consent Form

This thesis may be consulted for the purposes of research or private study provided that due acknowledgement is made where appropriate and that permission is obtained before any material from the thesis is published. Students who do not wish their work to be available for reasons such as pending patents, copyright agreements, or future publication should seek advice from the Graduate Centre as to restricted use or embargo.

Author of thesis	Parisa Koutsifeli
Title of thesis	Novel mechanisms of diastolic dysfunction in diabetes
Name of degree	Doctor of Philosophy in Biomedical Science
Date Submitted	01/05/2020

Print Format (Tick the boxes that apply)	
☑	I agree that the University of Auckland Library may make a copy of this thesis available for the collection of another library on request from that library.
☑	I agree to this thesis being copied for supply to any person in accordance with the provisions of Section 56 of the Copyright Act 1994.

Digital Format - PhD theses

I certify that a digital copy of my thesis deposited with the University is the same as the final print version of my thesis. Except in the circumstances set out below, no emendation of content has occurred and I recognise that minor variations in formatting may occur as a result of the conversion to digital format.

Access to my thesis may be limited for a period of time specified by me at the time of deposit. I understand that if my thesis is available online for public access it can be used for criticism, review, news reporting, research and private study.

Digital Format - Masters theses

I certify that a digital copy of my thesis deposited with the University is the same as the final print version of my thesis. Except in the circumstances set out below, no emendation of content has occurred and I recognise that minor variations in formatting may occur as a result of the conversion to digital format.

Access will normally only be available to authenticated members of the University of Auckland, but I may choose to allow public access under special circumstances. I understand that if my thesis is available online for public access it can be used for criticism, review, news reporting, research and private study.

Copyright (Digital Format Theses) (Tick **ONE box only**)	
☑	I confirm that my thesis does not contain material for which the copyright belongs to a third party, ***(or)*** that the amounts copied fall within the limits permitted under the Copyright Act 1994.
☐	I confirm that for all third party copyright material in my thesis, I have obtained written permission to use the material and attach copies of each permission, ***(or)*** I have removed the material from the digital copy of the thesis, fully referenced the deleted materials and, where possible, provided links to electronic sources of the material.

Signature [redacted] Date 01/05/2020

Comments on access conditions

Faculty Student Centre / Graduate Centre only: Digital copy deposited ☐ Signature Date

Abstract

Diabetic cardiomyopathy is primarily characterised by diastolic dysfunction and deranged cardiomyocyte performance. The underlying mechanisms are unknown, and specific treatment targets are lacking. Recent findings (Mellor et al, publication pending) have shown that glycogen accumulation is a consistent observation in the myocardium in numerous model types of diabetes and is correlated with poor functional outcomes. The glycogen phenotype could not be explained by activation changes in the well described glycogen handling enzymes, glycogen synthase and glycogen phosphorylase. Related findings from the Mellor-Delbridge labs have identified that glycogen-selective autophagy (glycophagy) is a process of lysosomal glycogen degradation that may operate in the myocardium in parallel with conventional macro-protein autophagy, and involves selective molecular partners to tag glycogen cargo (STBD1) and to localize glycogen cargo to the engulfing autophagosome (GABARAPL1). Arising from these observations, a role for disrupted glycophagy in the aetiology of diabetic heart disease was hypothesized.

Thus, the goal of this Thesis was to address the following questions:

(1) What are the molecular alterations underlying increased glycogen deposition in the diabetic heart? (Chapter 3)
(2) What is the role of the key glycogen autophagy (glycophagy) protein, GABARAPL1, in regulating cardiac function and glycogen content? (Chapter 4)
(3) Can glycophagy-targeting interventions rescue cardiac function and provide therapeutic potential for diabetic cardiomyopathy? (Chapter 5)

Cardiac RNA from 3 rodent models of diabetes was analysed using a custom-designed PCR arrays to evaluate gene expression characteristics. Functional network analysis (STRING) was performed to identify molecular signalling pathways involved in glycogen handling disruption providing evidence of GABARAPL1 involvement. To investigate the role of disrupted cardiac glycophagy in cardiac pathophysiology, *Gabarapl1* gene deletion *in vivo* was achieved via CRISPR-Cas9 gene editing. Cardiac function in *Gabarapl1*-KO mice was assessed via transthoracic echocardiography and glycogen content was measured (calorimetric assay) in hearts extracted ex vivo. To determine whether a glycophagy-augmenting intervention could rescue cardiac function, an AAV9 *Gabarapl1*-

expressing virus was used to achieve cardiac-specific *Gabarapl1* upregulation in a type 2 diabetic (T2D) model induced by high fat/sugar diet feeding.

Key findings:

(1) **Molecular discovery**: The diabetic heart is characterised by glycophagy disturbance involving *Gabarapl1* downregulation.
(2) **Glycophagy proof of concept**: Reduction in GABARAPL1 availability is sufficient to induce cardiac glycogen accumulation and diastolic dysfunction *in vivo*.
(3) **Glycophagy disease intervention**: *Gabarapl1* upregulation rescues diabetes-induced cardiac glycogen accumulation and diastolic dysfunction *in vivo* in a T2D mouse model.

This Thesis presents original findings which link diabetic cardiac glycogen accumulation with disturbances in the novel glycogen autophagy pathway, glycophagy, and in particular identifies *Gabarapl1* downregulation as a pathogenic state in diabetes. Further, this Thesis provides the first demonstration that GABARAPL1 plays a central role in maintaining cardiac glycogen levels and is crucial for the preservation of cardiac contractile function. Finally, this study presents new evidence that upregulation of glycophagy by *Gabarapl1* gene delivery produces favourable functional outcomes for the diabetic heart. Collectively these investigations identify glycophagy disturbance as a novel mechanism of diastolic dysfunction in the diabetic heart. In overview these findings provide an evidence base for targeting glycophagy as a potential therapeutic strategy for treatment of diabetic heart disease.

Στην Έμμη και το Μήτσο,

‘Απόψε,
κοιτώντας πίσω,
στο μακρύ μονοπάτι,
δεν πιστεύω ότι θα είχα κάνει
τίποτα διαφορετικό’

Τσαρλς Μπουκόφσκι

Acknowledgements

My PhD has been an incredible journey during which I have had the privilege to receive unwavering support and guidance. For that I would like to express my sincere gratitude to my two main supervisors, Dr. Kim Mellor and Prof. Lea Delbridge. Your exceptional mentoring, scientific expertise, immense knowledge and inspiring work ethic have been invaluable to my development as a scientist. Kim, thank you for your enthusiasm, patience, diligence, perseverance and trust as I developed the skills, technical and intellectual, required to complete this body of work. And for the countless life lessons along the way. Lea, thank you for your motivation, persistence, attention to detail and encouragement. You taught me to strive to be the best I can, to stand on my feet and to believe in myself. For that I am forever grateful. To both, I would not be the scientist and person I am today without you. I am grateful for the opportunity to learn alongside you and I will be forever your student.

I acknowledge the financial support, in the form of PhD Scholarship from the Marsden Fund of the Royal Society of New Zealand and in the form of PhD support from the University of Auckland.

I would like to express sincere thank you all the members in the Cellular and Molecular Cardiology lab in Auckland, Dr. Lorna Daniels, Dr. Vicky Benson, Xun (Cookie) Li, Marco Annandale, Calum Macindoe and the Cardiac Phenomics lab in Melbourne, Dr. Jim Bell, Dr. Claire Curl, Dr. Upasna Varma, Dr. Wendy Ip, Dr. Hanneke Raaijmakers, Dr. Gabriel Bernasochi, Johannes Janssens, Simon Wells, Eleia Chan, Helen Waddell, for their ample support throughout this candidature. I would particularly like to thank Dr. Vicky Benson and Xun (Cookie) Li for dedicating their time to my training in numerous techniques used in this thesis.

A special section in these acknowledgements is dedicated to my friend and colleague, Johannes Janssens. JJ, you are an incredible scientist and amazing person. It has been a privilege to work and learn from you. Thank you for the countless hours or worrying, injecting, GTT-ing, analysing, discussing, listening. Thank you for being my friend. As always, work hard, play hard.

Dr. Lorna Daniels, working with you has been an absolute pleasure with colossal gains. Thank you for listening, for the positivity, endless conversations, whiteboard discussions, travelling adventures and helping me to think outside the box. Thank you for helping me flux my frustrations.

I would like to express my genuine thanks to Marcela María Irma Arias Bascuñan, Luis Alejandro Muñoz Maricura, Facundo Alejandro Muñoz Arias and Carles Raimundo Muñoz Arias for being my family away from home. I am incredibly grateful and lucky to have met you. Thank you for your love and support throughout these years. For opening your home to me, for taking care of me, for listening. I could not have done this without you. Julia Schmidt, thank you for all the laughs and for listening to my rambling after those long lab days. And for waiting for me with a hot cup of tea at 2am after long flights. Your la-la brain was great to come home to.

Shubham Rawal, thank you for all your support and understanding during this PhD. For gracefully dealing with my craziness, for being there for me, for knowing what to say to calm me down. Thank you for believing in me and pushing me to do better.

To all my family and friends, your love and understanding all these years leading to the completion of this candidature has been greatly appreciated.

The final section of these acknowledgements is dedicated to my parents, Emmi Avramidou and Dimitris Koutsifelis. Mom and Dad, thank you for your love and for believing in me. For giving me every opportunity. For allowing me to discover my strengths and weaknesses. For teaching me to go after what I want, fight and aim high. For the support during 14 years of being a student. For continuously being there for me and taking my side. This is my greatest achievement yet, and is dedicated to you.

Contributions to data collection

Many of the techniques used in this thesis required teamwork and the contribution of multiple investigators. This was greatly appreciated and acknowledged below. Type 1 and pre-type 2 diabetic rat cardiac tissue used in Chapter 3 was collected prior to commencement of this doctoral candidature by Dr. Vicky Benson and Jessica Liu. Cardiac RNA from Type 2 diabetic mice (T2D, db/db) was provided by A/Prof. Rebecca Ritchie and the PCR array for these samples was run by Dr. Chanchal Chandramouli (Chapter 3). Technical assistance for *in vivo* mouse studies was provided by Dr Upasna Varma, Dr. Wendy Ip, Johannes Janssens and Eleia Chan. Technical contribution to various aspects of molecular data (immunoblot, quantification of protein and glycogen levels) by Dr. Upasna Varma and Xun (Cookie) Li, is acknowledged. Image acquisition for echocardiography was performed by skilled investigators, Dr. Claire Curl and Dr. Hanneke Raaijmakers. Dr. Lorna Daniels and Eleia Chan assisted in neonatal cardiomyocyte cultures.

Table of contents

List of figures

List of tables

Glossary (abbreviations)

A wave	Late diastolic blood flow velocity through the mitral valve
AAV	Adeno-associated virus
AGEs	Advanced glycation end-products
AICAR	5-Aminoimidazole-4-carboxamide ribonucleotide
AIM	ATG8-interacting motif
AKT	RAC-alpha serine/threonine-protein kinase
AMP	Adenosine mono-phosphate
AMPK	5' AMP-activated protein kinase
ANOVA	Analysis of variance
ATG3	Autophagy-related 3
ATG5	Autophagy-related 5
ATG7	Autophagy-related 7
ATG8	Autophagy-related 8
ATG12	Autophagy-related 12
ATG14	Autophagy-related 14
ATG16	Autophagy-related 16
ATP	Adenosine tri-phosphate
bGH-poly(A)	Bovine growth hormone polyadenylation
BGL	Blood glucose levels
Ca^{2+}	Calcium ion
CAD	Coronary artery disease
cAMP	Cyclic adenosine mono-phosphate
CBM20	Carbohydrate-binding motif 20
cDNA	Complementary DNA
CRISPR	Clustered regularly interspaced short palindromic repeats
cTnTp	Cardiac Troponin promoter
db/db	Mouse model of leptin deficiency
ddPCR	Digital droplet PCR
DE	Differentially expressed
DMEM	Dulbecco’s modified essential medium
E wave	Early diastolic blood flow velocity through the mitral valve
E/A	Mitral peak early to late filling velocity ration
E/E’	Mitral peak early filling velocity to early diastolic mitral annular velocity ratio

E’	Early diastolic mitral annular velocity
EF	Ejection fraction
ER	Endoplasmic reticulum
ERT	Enzyme replacement therapy
FA	Fatty acid
FABPpm	Plasma membrane isoform of fatty acid binding protein
FS	Fractional shortening
G6P	Glucose-6-phosphate
GAA	alpha-acid glucosidase
GABARAP	Gamma-aminobutyric acid type A receptor-associated protein
GABARAPL1	Gamma-aminobutyric acid type A receptor-associated protein like 1
GABL1	GABARAPL1
GBE	Glycogen branching enzyme
gc	Genome copies
GDE	Glycogen debranching enzyme
GLUT1	Glucose transporter 1
GLUT4	Glucose transporter 4
GP	glycogen phosphorylase
gRNA	guide RNA
GS	glycogen synthase
GSD	Glycogen storage disease
GST	Glutathione S-transferase
GTT	Glucose tolerance test
HbA_{1c}	Glycated hemoglobin
HFD	High fat diet
HFDm	High fat diet mouse model
HFDr	High fat diet rat model
HFpEF	Heart failure with preserved ejection fraction
HG	High glucose
IGF	Insulin growth factor
IRS	Insulin receptor substrate
ITR	Inverted terminal repeat
KO	Knockout
LAMP2	Lysosome-associated membrane protein 2
LC3B	Light chain 3, paralog B
LIR	LC-interacting motif

LVEDP	Left ventricular end diastolic pressure
MAP1LC3	Microtubule-associated proteins 1A/1B light chain 3B
MCF-7	Michigan Cancer Foundation-7
MEM	Minimum essential medium
mM	milli-molar
MOI	Multiplicity of infection
mRNA	Messenger RNA
mTOR	Mammalian target of rapamycin
MV Dec T	Mitral valve deceleration time
NBCS	New-born bovine calf serum
NBR1	Neighbour of BRCA1
NG	Normal glucose
NIX	BCL2 interacting protein 3 like
NRVM	Neonatal rat ventricular myocytes
Opti-MEM	Reduced serum media
PCR	Polymerase chain reaction
PI3K	Phosphoinositide 3-kinase
PPC	Positive PCR control
Pre-T2D	pre-type 2 diabetes (glucose intolerance, insulin resistance)
PWD	Pulsewave Doppler
QC	Quality control
RAB5	Ras-related protein Rab-5A
RAB7	Ras-related protein Rab-7A
RNA	Ribonucleic acid
ROS	Reactive oxygen species
RTC	Reverse transcription control
RT-qPCR	Reverse transcription quantitative PCR
SAR	Soluble autophagy receptor
SNAP23	Synaptosome Associated Protein 23
SNAP25	Synaptosome Associated Protein 25
SNAREs	N-Ethylmaleimide-Sensitive Factor Attachment Protein Receptors
SQSTM1/p62	Sequestosome 1
SR	Sarcoplasmic reticulum
ssDNA	single-stranded DNA
STBD1	Starch binding domain 1
STRING	Functional netwark analysis

STX17	Syntaxin 17
STX7	Syntaxin 7
STX8	Syntaxin 8
STZ	Streptozotocin
STZr	Type 1 diabetic rat model
T1D	Type 1 diabetes
T2D	Type 2 diabetes
TGN	trans-Golgi network
UBL	Ubiquitin-like
ULK1	Unc-51 like autophagy activating kinase
UVRAG	UV Radiation Resistance Associated gene
VP	Viral proteins
VPS34	Phosphatidylinositol 3-kinase VPS34
WPRE	Woodchuck Hepatitis Virus Posttranscriptional Regulatory Element
WT	Wild-type

List of publications related to this work

U. Varma, **P. Koutsifeli**, V.L. Benson, K.M. Mellor, L.M.D. Delbridge. Molecular mechanisms of cardiac pathology in diabetes – Experimental insights. November 2017, BBA – Molecular Basis of Disease, 1864:(5 Pt B, 1949-1959)

List of collaborative publications during candidature

C. Chandramouli, M. Reichelt, C. Curl, U. Varma, L. Bienvenu, **P. Koutsifeli**, A.Raaijmakers, M. De Blasio, C. Qin, A. Jenkins, R. Ritchie, K. Mellor, and L. Delbridge. Diastolic dysfunction is more marked in diabetic female mice, despite less pronounced yperglycemia. 2018, Scientific Reports, 8:2346-2358

List of first author submitted abstracts

Koutsifeli P, Varma U, Daniels LJ, Chan E, Annandale M, Delbridge LM, Mellor KM. Characterizing the role of glycogen autophagy in regulating cardiac glycogen content in diabetes. 2019**.** *Proceedings from the Medical Sciences NZ Congress.* Queenstown, New Zealand – John Hubbard award finalist

Koutsifeli P, Varma U, Daniels LJ, Chan E, Annandale M, Delbridge LMD, Mellor KM, Glycogen autophagy is mediated by GABARAPL1 in cardiomyocytes. International Society for Heart Research, World Congress, June 2019, Beijing, China - poster

Koutsifeli P, Varma U, Chan E, Delbridge L, Mellor K, Glycogen autophagy plays an important role in glycogen overload in diabetic cardiomyocytes *in vitro*, 66th Annual Scientific Meeting of the Cardiac Society of Australia and New Zealand, August 2018, Brisbane, Australia. Short communication – student prize finalist

Koutsifeli P, Benson V, Liu J, Lamberts R, Delbridge L, Mellor K, Cardiac metabolic and autophagy gene networks are differentially regulated in models of type 1 diabetes, insulin resistance and type 2 diabetes, 65th Annual Scientific Meeting of the Cardiac Society of Australia and New Zealand, August 2017, Perth, Australia - Mini oral

List of collaborative abstracts

Daniels LJ, Annandale MA, **Koutsifeli P**, Li X, Delbridge L.M, Mellor K.M. Elevated cardiac fructose content may contribute to lipid accumulation in the diabetic heart. Proceedings from the Medical Sciences NZ Congress. Queenstown, New Zealand, 2019.

Mellor K.M, Varma U, Daniels L.J, **Koutsifeli P**, Annandale M, Li X, Nursalim Y, Benson V.L, Delbridge L.M.D. Diabetes is associated with cardiac glycogen mishandling. *Proceedings from the International Society for Heart Research World Congress*, Beijing, China 2019.

Daniels L.J, Annandale M, **Koutsifeli P**, Delbridge L.M.D, Mellor K.M. Cardiomyocyte fructose exposure *in vitro* impacts on glycolytic metabolic flux. *Proceedings from the International Society for Heart Research World Congress,* Beijing, China 2019.

Janssens J.V, Raaijmakers A.J.A, **Koutsifeli P**, Mellor K.M, Curl C.L, Delbridge L.M.D. Diabetic cardiomyocyte stiffness and defective length-dependence of Ca^{2+} sensitivity – a myofilament 'AGE' burden? *Proceedings from the International Society for Heart Research World Congress,* Beijing, China 2019.

Janssens J.V, Raaijmakers A.J.A, **Koutsifeli P**, Mellor K.M, Curl C.L, Delbridge L.M.D. Cardiomyocyte hypercontractility is an adaptational response to stiffness in high-fat diet mice. *Proceedings from the Basic Cardiovascular Science Scientific Sessions,* Boston, USA, 2019.

Janssens J.V, Raaijmakers A.J.A, **Koutsifeli P**, Chan E.J, Curl C.L, Mellor K.M, Delbridge L.M.D. Elevated cardiomyocyte stiffness is a key component of diastolic dysfunction in pre-diabetic high-fat fed mice. Proceedings from the International Society for Heart Research (Australasian Section) Meeting, Brisbane, Australia, 2018.

Chan E.J, Varma U, Curl C.L, **Koutsifeli P**, Mellor K.M, Delbridge L.M.D, STBD1 regulation of myocardial glycogen content, Proceedings from the Australian Physiology Society meeting, Sydney, Australia, 2018.

CHAPTER 1

A review of the literature

Introduction

Diabetes is one of the most prevalent diseases worldwide, affecting approximately 400 million people[1], although the estimates are expected to increase by 50% in the following 20 years[2]. More specifically in New Zealand, 6% of the population suffers from diabetes which makes the disease the largest health issue in the country[3]. Although diabetes is characterised by a spectrum of complications, the predominant cause of mortality is heart disease. Diabetes-induced functional and structural alterations are independent from vascular complications such as coronary artery disease, and diabetic cardiomyopathy is now recognised as a distinct cardiac pathology[4,5]. As shown in human patients and in various rodent models of type 1 or type 2 diabetes (T1D or T2D respectively), diastolic dysfunction is a primary manifestation of diabetic cardiomyopathy[6-8]. Diastolic dysfunction reflects cardiac functional abnormalities occurring in the period between aortic valve closure and mitral valve closure (diastole). It is commonly used to describe impaired passive filling and relaxation of the left ventricle and can be the result of 4 underlying mechanisms: loss of ventricular compliance, decreased trans-mitral pressure gradient (decreased peak filling rate), reduction in the rate of ventricular pressure decline and mechanical pericardial constriction[9]. In diabetes, decreased peak filling rates are evident and are most commonly associated with loss of ventricular compliance[10].

The metabolic environment of the diabetic heart is shaped by disease-induced systemic abnormalities including hyperglycemia, altered circulating levels of insulin and hyperlipidemia[11]. The cardiac diabetic metabolic profile is characterised by reduced glucose uptake and dramatic shifts in substrate utilization that in turn lead to dysregulation of homeostatic survival pathways including autophagy and glycogen handling[12]. Glycogen accumulation was first incidentally observed over 80 years ago in the human diabetic myocardium[13]. Additionally, extensive investigations in the Mellor-Delbridge labs demonstrated that increased glycogen deposition is a consistent phenotype in the diabetic heart and is correlated with diastolic functional decline (Mellor et al, publication pending). However, the molecular mechanisms underlying this phenomenon have not been previously investigated. Glycogen management, in the heart and other tissues, involves a network of cytosolic and lysosome-mediated processes[14]. Interestingly, diabetes-induced alterations in activity or expression of enzymes involved in cytosolic glycogen handling fail to account for cardiac glycogen

accumulation[12]. Recent findings from the Mellor-Delbridge labs have identified that glycophagy (glycogen-selective autophagy) is a process of lysosomal glycogen degradation that may operate in the myocardium in parallel with conventional, protein-targeting autophagy. Despite the lack of possible explanations for the diabetic cardiac glycogen phenotype, potential underlying mechanisms, such as glycophagy (glycogen autophagy) have not been investigated.

The purpose of this Literature Review is to highlight the key metabolic and signalling disturbances occurring in the diabetic heart and how they may be linked to glycogen mismanagement. Furthermore, it provides an account of evidence describing the molecular mechanisms of glycogen autophagy and identifies research areas warranting further investigation. Last, it provides the basis on which the studies presented in this Thesis have been conducted.

1.1. Diabetic cardiomyopathy is a distinct cardiac pathology

Diabetic heart disease was first characterised approximately 50 years ago following closer examination of post-mortem reports of 4 diabetic patients who presented symptoms of heart failure but had no further associated vascular abnormalities[15]. The Framingham Heart Study demonstrated that the risk of heart failure in diabetic patients, although sex-dependent, is on average 3.7 fold greater than in non-diabetic participants and was independent of other factors such as obesity, age and coronary artery disease (CAD)[16]. Follow up population studies using large cohorts of diabetic patients have demonstrated that reduced ventricular compliance and diastolic dysfunction are a primary manifestation of diabetic cardiomyopathy and are independent of the type of diabetic insult[17-19]. Diabetic heart disease is now recognized as a separate cardiopathology[11] that is characterised by early, in disease progression, diastolic dysfunction and is observed in approximately 50% of diabetic patients worldwide[20-22].

1.1.1. Functional demise of the diabetic heart

Although diabetes is characterised by a spectrum of complications, diabetic cardiomyopathy often presents in the absence of vascular abnormalities or hypertension[23-26]. As shown in human patients[27,28], and in various rodent models of type 1 or type 2 diabetes (T1D or T2D respectively)[6-8,29], diabetic diastolic dysfunction is most commonly associated with abnormal ventricular filling due

to increased cardiomyocyte stiffness[10,27]. In addition, diabetes-induced diastolic dysfunction may be followed by late systolic abnormalities[30] but is more commonly observed in complete absence of systolic dysfunction[21,31,32]. It is unclear whether glycaemic status can be directly related to cardiac dysfunction. A study using human cohorts of T2D patients, observed that 1% increase in glycated haemoglobin (HbA_{1c}) was associated with an 8 fold higher risk of heart failure development[18]. In contrast, an almost concurrent study also examining T2D patients, showed that glycaemic status is not necessarily indicative of cardiac dysfunction suggesting that maintaining euglycaemia is not sufficient to prevent cardiac abnormalities[33]. In T1D, tissue Doppler measurements suggest that both right and left ventricular diastolic dysfunction manifests as early as 13 years of age and is not accompanied by systolic functional decline. Interestingly, in this study diastolic dysfunction was concluded on the basis of the mitral and tricuspid valves E'/A' ratios but no differences were detected in E/E' values[17] which is considered a more traditional clinical measure of diastolic dysfunction[34]. Concurrent impairment of right and left ventricular relaxation is also evident in older T1D patients as shown by both Pulsed Wave (PWD) and tissue Doppler[35].

Diabetic cardiomyopathy is often accompanied by cardiac remodelling and interstitial fibrosis that may contribute to diastolic dysfunction. A recent European study examining diabetic patients demonstrated that concentric left ventricular hypertrophy often manifests before hyperglycemia and may be used as a predictive measure for diabetes[36]. Similarly, an earlier population study showed that echocardiographic parameters such as left ventricular mass can be indicative of predisposition to T2D[37]. In rodent diabetic models, interstitial fibrosis has been repeatedly reported both in association to pharmacologically-induced T1D and in genetic T2D models[38-46]. Often, fibrosis has been observed to accompany myocardial hypertrophy and diastolic dysfunction[40,41]. Hypertrophy and fibrosis have also been reported in animal models of pre-T2D or insulin resistance and were linked to diabetes-induced diastolic dysfunction[47,48]. In contrast, in humans, although late-stage diabetic cardiomyopathy can be accompanied by left ventricular hypertrophy, this phenotype is not commonly observed in pre-diabetic, glucose-intolerant subjects[49].

In addition to left ventricular diastolic dysfunction, in the last 20 years diabetic heart disease has been expanded to include atrial dysfunction in the form of arrhythmias and particularly atrial

fibrillation (AF). Multiple population studies have been conducted in order to identify whether there is a link between diabetes and AF incidence. The Framingham Heart Study identified diabetes as an independent contributor to AF as it was evident by a 38 year long follow up of diabetic participants[50]. However, later investigations did not detect a similar association and concluded that diabetes is not an independent risk factor for AF[51]. More recently, a large meta-analysis determined that pre-diabetic, glucose-intolerant patients present a 20% risk of developing AF while this increases to 28% in type 2 diabetic subjects[52]. Interestingly, this analysis identified a positive correlative link between the extent of hyperglycemia and prevalence of AF although an earlier report suggested that glycemic control is not linked to atrial dysfunction[52,53]. While it appears that published reports have not arrived at a consensus regarding the impact of diabetes on AF manifestation, it should be noted that comprehensive examination of these studies must take into consideration the inherent stratification of participants[54]. Furthermore, obesity, which is a common comorbidity in diabetic patients, has also been deemed as an independent risk factor for AF and other conduction abnormalities[55]. Thus, atrial arrhythmias and particularly atrial fibrillation, although less prevalent than diastolic dysfunction, has been identified as an important characteristic of the diabetic heart but the underlying mechanisms are not understood.

It is evident that in the past 50 years, extensive research has been conducted to decipher the clinical presentations of diabetic cardiomyopathy. It is now well understood that diabetes-induced heart disease manifests with early ventricular remodelling followed by progressive diastolic dysfunction and ultimately heart failure with preserved ejection fraction (HFpEF). Currently there are no effective treatment options for diastolic dysfunction indicating that further investigations into the underlying molecular mechanisms are warranted.

1.1.2. The interplay between glucose and fatty acids in the diabetic heart

The metabolic environment of the diabetic heart is shaped by disease-induced systemic abnormalities including hyperglycemia, altered circulating levels of insulin and hyperlipidaemia[11]. Under physiological conditions, cardiac energy production exhibits higher reliance of fatty acid (FA) oxidation (60%) than glycolysis-derived ATP (40%)[56]. Fatty acids enter cardiomyocytes either via passive diffusion or via receptor-mediated endocytosis[57]. Studies employing several rodent models

of diabetes, have confirmed that FA cardiomyocyte sarcolemmal uptake is increased and is associated with upregulation of FA transport proteins, such as the plasma membrane isoform of fatty acid binding protein (FABPpm)[58,59]. Following FA uptake, cardiomyocytes either directly drive energy production or promote lipid storage via formation of lipid droplets[57]. The diabetic heart is characterised by reduced glucose oxidation. Downregulation of the glucose transporters GLUT1 and GLUT4 and decreased insulin-stimulated, GLUT4-mediated glucose uptake is evident and has been demonstrated in rodent models of both T1D and T2D[60]. This is coincident with an even greater reliance on FA metabolism. Association between increased myocardial lipid content and higher mitochondrial capacity for FA oxidation has been observed in both genetic and dietary models of diabetes[61,62]. A recent study in T1D rat hearts demonstrated that the expression of genes involved in glucose and lipid metabolism is drastically changed 48 hours post-STZ administration with several glycolytic enzymes being significantly downregulated in contrast to upregulation of factors involved in lipid metabolism[63]. Interestingly, a decline in cardiac function has been associated with glucose-to-FA metabolic shifts in genetic murine models of T2D at ages when hyperglycemia had not yet manifested[64]. Conversely, normalization of the metabolic profile in T1D and T2D rat models, via pharmacological upregulation of glucose oxidation was shown to improve cardiac function[65,66].

Increased FA uptake in the diabetic heart has also been linked to elevated lipid droplet formation. It has been shown that the expression of the primary lipid droplet-associated protein in oxidative tissues, Perilipin 5 (PLIN5), is increased in hearts of both db/db and STZ-treated mice[67,68] suggesting that the primary cardiac response to steatosis is the promotion of lipid storage. Interestingly, in the cardiomyocyte cell line HL1 lipid accumulation leads to increased lipid droplet size and volume indicating droplet fusion via the actions of the SNARE system. It has been suggested that due to the involvement of SNAREs in transporting GLUT4-containing vesicles to the plasma membrane, the increased demand for lipid droplet fusion reduces GLUT4 translocation, thus contributing to insulin resistance[69]. Whether the same is true for isolated primary cardiomyocytes or for the *in vivo* heart remains to be examined.

FA oxidation in the diabetic heart has also been linked with elevated production of Reactive Oxygen Species (ROS) due to increased oxygen consumption[70-72]. In turn, ROS-mediated oxidative stress

can contribute to decline in cardiac function; this has been repeatedly observed in both diabetic patients and rodent models of diabetes[73-75]. Furthermore, increased ROS production can lead to compensatory upregulation of autophagy[76], which, as discussed further in section 1.3, has been linked to detrimental functional outcomes in the diabetic heart.

These investigations indicate that higher reliance on FA oxidation is an early metabolic adaptation in the diabetic heart and may be closely linked to cardiac dysfunction through different mechanisms. It may also contribute to exacerbation of insulin resistance. Thus, approaches aiming to upregulate glucose oxidation may be suitable therapeutic targets for diabetic cardiomyopathy.

1.1.3. Diabetic cardiomyopathy is associated with autophagy dysregulation

Autophagy (from the Greek 'self-eating') is a 'bulk' degradation process that utilizes the acidic environment of the lysosome to break down damaged proteins, organelles and macromolecules in order to regenerate energy and nutrients both basally and during periods of cellular stress. It is well established that the term autophagy encompasses a number of lysosome-dependent degradation processes, each with specialized protein machinery aiming to recycle specific cargo. These subtypes include macro-phagy which is the lysosomal recycling of aberrant ubiquitinated proteins but also others such as mito-phagy, ER-phagy, lipo-phagy, xeno-phagy and glyco-phagy. Despite the cargo-dependent selectivity, all autophagy subtypes share a common basic functional mechanism. In all cases, cargo that is marked for lysosomal breakdown, is tagged by soluble autophagy receptors (SARs) and is then sequestered to forming double-membrane vesicles called phagosomes. In phagosomes, the SARs bind to one of the membrane-tethered Autophagy-related protein 8 (ATG8) homologs through the ATG8-interacting motif (AIM). Lysosomal recycling of the cargo is achieved through phagosome-lysosome fusion[77-79].

The process of autophagy, in the heart and other tissues, involves the concerted participation of multiple proteins and protein-complexes and is carried out in several consequent steps. First, the ULK (ULK1/2, ATG13, FIP200, ATG101)[80,81] and PI3K (PI3-class III kinase, VPS34, ATG14, BECLIN1)[82] complexes are assembled at the omegasome, the site of autophagosome formation. The ULK complex is responsible for mTOR-activated autophagy[80] and the PI3K complex induces

nucleation of the phagophore membrane[82]. Elongation of the membrane involves the ATG12-ATG5-ATG16 complex in conjunction with ATG9 and WIPI1[83]. During maturation of the phagophore to phagosome, the ATG12-ATG5-ATG16 complex dissociates while lipidated ATG8 proteins such as LC3B (facilitated by ATG7-ATG3 complex) localize on both the luminal and cytoplasmic side of the phagosome membrane[83,84]. Interestingly, biotinylated peptide screens have shown that ATG8s interact with several members of the induction complexes thereby providing a spatial bridge for their assembly at the omegasome[85]. Cargo-carrying SARs (eg SQSTM1/p62, NBR1, NIX and others) anchor to phagosome-bound ATG8s while the vesicle is being formed[79]. The mature phagosome is then trafficked to and fused with the lysosome, in a process thought to require multiple proteins from the Syntaxin (STX17, STX7, STX8), Synaptobrevin (SNAP23, SNAP25) and Rab (RAB7, RAB5) families[86,87]. Substitution of ATG14 by UVRAG on the PI3K complex positively regulates phagosome-lysosome fusion while binding of RUBICON to UVRAG produces the opposite effect[88-90].

In the context of the diabetic heart, multiple studies have examined autophagy and have reported both upregulation and downregulation of the pathway in various pre-clinical models of diabetes and human patients[77,91-114]. Consequently, maladaptive responses have been attributed to both upregulation and downregulation of the pathway. For example, high fat diet-induced obesity, leads to downregulation of myocardial autophagy, evident by the decrease in LC3II/I ratio and can coincide with decline in systolic function and cardiomyocyte relaxation[91,94,96]. Similarly, in a different model of high fat diet-induced obesity, failure of autophagy induction was evident following fasting[92]. Contradictory findings have demonstrated that dietary induction of obesity induces cardiac autophagy in mice, as shown by upregulation of *Beclin1* mRNA expression[93]. Similarly, in a model of type 2 diabetes induced by high fat diet feeding accompanied by administration of a low dose of streptozotocin (STZ), myocardial autophagy, as measured by LC3II/I ratio and SQSTM1/p62 levels, was upregulated and the effects were exacerbated with longer disease duration[95]. Autophagy was also shown to be increased in both type 1 (STZ-induced diabetes) and type 2 (leptin receptor mutants db/db) diabetic mouse hearts. Interestingly, left ventricular end diastolic pressure (LVEDP), an indicator of diastolic dysfunction, was increased in db/db mice but was only increased in STZ mice following attenuation of autophagy with chloroquine[99] suggesting that in the type 1 diabetic

myocardium increased autophagy is adaptive. Interestingly a different study using STZ-induced diabetes in mice showed that diastolic dysfunction was evident and was coincident with a reduction in autophagy. Restoration of autophagic flux (by BECLIN1 upregulation) in that model exacerbated the functional outcomes indicating that the original reduction in autophagy was adaptive[109]. A limited number of studies have examined autophagy in diabetic patients. In type 2 diabetic patients without abnormalities in cardiac function (ejection fraction >50%, preserved diastolic function), autophagy was upregulated as shown by increased levels of BECLIN1, LC3B and reduced expression of SQSTM1/p62[114]. In contrast, a separate study has shown that in type 2 diabetic patients presenting with decreased intrinsic atrial contraction, ATG5 (phagophore elongation) was downregulated but LC3BII/I ratio was not changed[115].

Together, these contradictory findings indicate that autophagy in the diabetic myocardium presents as both an adaptive and a maladaptive response while there seems to be no agreement on the response of the autophagic pathway in the diabetic heart. It is likely that some of the different observations can be attributed to discrepancies in the pre-clinical models used such as age, sex and species of animals. Nevertheless, these inconsistencies highlight that further research is needed to resolve the role of autophagy in the diabetic heart and whether this pathway can serve as a suitable therapeutic approach.

1.1.4. The diabetic heart displays a paradoxical glycogen accumulation

Increased glycogen deposition has been previously sporadically observed in the diabetic heart but the causes or consequences of this phenomenon have received little attention[116-138]. Glycogen is a major energy storage molecule that has been extensively investigated in the liver and skeletal muscle, yet its role and management in the heart remain poorly understood. In diabetic rodents, decreased translocation of the insulin-dependent glucose transporter (GLUT4) to the plasma membrane has been reported and has been linked with reduced glucose uptake[139,140]. Consistently, diabetic skeletal muscle is characterised by glycogen depletion[141,142]. In diabetes, insulin-sensitive tissues operate under glucose-limited conditions induced either by absence of insulin (T1D) or localized insulin resistance (T2D). Extensive, comparative and systematic investigations carried out in the Mellor-Delbridge labs prior to this Thesis undertaking, have counterintuitively demonstrated

glycogen elevation to be a consistent feature of the diabetic myocardium (Mellor et al, publication pending). This extensive body of work is the first to systematically assess cardiac glycogen levels in both rodent models of diabetes and human tissues from patients undergoing coronary artery or valve replacement surgery. These unpublished findings demonstrate that glycogen accumulation is a consistent diabetic cardiac phenotype that does not depend on the type of diabetic insult (Fig 1.1a) and is cardiac specific because skeletal muscle does not exhibit the same phenotype (Fig 1.1b). Additionally, further unpublished data from our group demonstrate that glycogen content correlates with impaired cardiac relaxation in diabetes (Fig 1.1c). This is the first evidence that links glycogen accumulation in the diabetic heart with diastolic dysfunction that is the hallmark of diabetic cardiomyopathy.

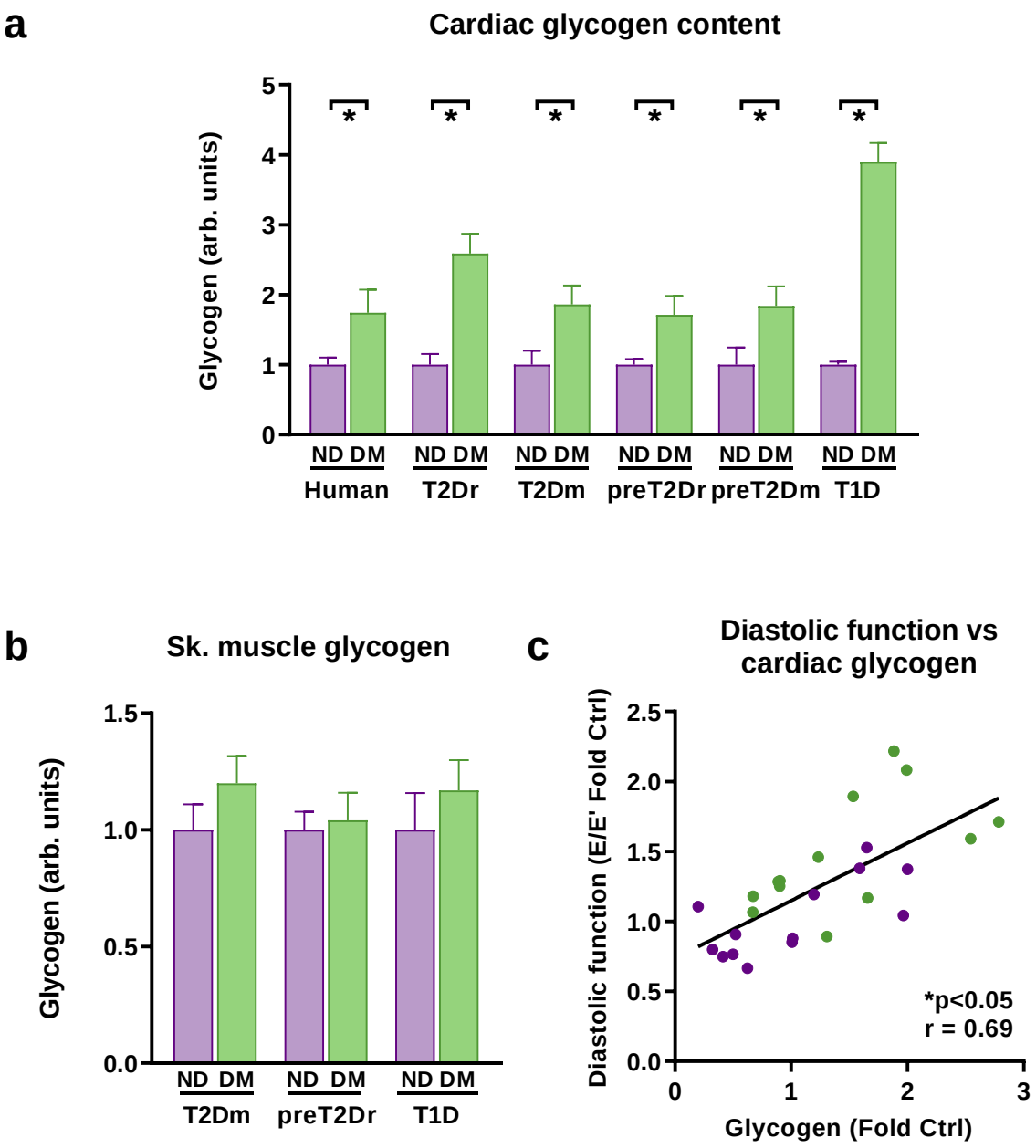

Figure 1.1: Cardiac glycogen is linked with diastolic dysfunction in diabetes. (a) Cardiac glycogen content is increased in human patients with diabetes mellitus (DM, n=4-7 patients) and diabetic (T2D, type 2 diabetes; T1D, type 1 diabetes) animal models. ZDF (Zucker diabetic fatty rat age 20 week); db/db (leptin receptor mutant mouse age 10 week); HFSDr (high fat/sugar diet-fed rat 14 weeks); HFSDm (high fat/sugar diet-fed mouse 14 weeks); STZr, (streptozotocin-treated rat 8 weeks), n≥7 animals. **(b)** No change in skeletal muscle glycogen content in diabetic animal models (db/db mice, high fat/sugar diet rats (HFSDr), STZ rat; n ≥ 7 animals). **(c)** Myocardial glycogen content and diastolic dysfunction (E/E' ratio) are correlated for control (purple) and diabetic (green, HFSD) mice (r, Pearson correlation coefficient). Mellor-Delbridge, unpublished.

1.2. Mechanisms of cardiac glycogen handling

Glycogen is a polymer composed of glucose-1-phosphate molecules that is elongated enzymatically by glycogen synthase (GS) and branched by glycogen branching enzyme (GBE)[143,144]. In absence of pathology, increased energy demand or nutrient deprivation leads to glycogen breakdown that occurs either in the cytosol via concerted actions of glycogen phosphorylase (GP) and glycogen debranching enzyme (GDE)[145] or in the lysosome. In the past decade lysosomal glycogenolysis has been placed in the context of autophagy and is referred to as a novel selective autophagy branch termed glycophagy (glycogen autophagy). While macro-autophagy has been extensively investigated and its molecular mediators identified, glycophagy and the key proteins involved in the process are not well characterised. There are some indications that glycophagy requires glycogen to be tagged by Starch-binding domain 1 (STBD1) so that it can be sequestered to the forming phagosome [146]. There, STBD1 anchors to γ-aminobutyric acid receptor-associated protein-like 1 (GABARAPL1)[147], one of the mammalian ATG8 proteins. In the final stage of the process, the phagosome fuses with the lysosome where GAA hydrolyses the glycosidic bonds thereby releasing glucose monomers (Fig 1.2) [148,149]. The following sections discuss the mechanisms and regulation of glycogen in the heart and highlight the key signalling pathways governing glycogen management.

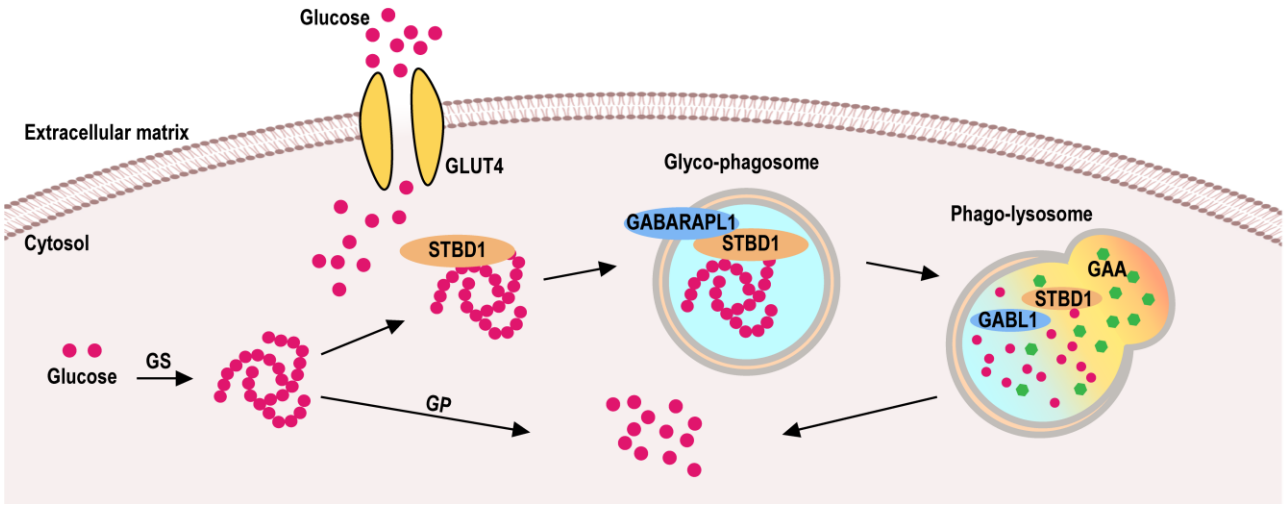

Figure 1.2: Schematic illustrating three stages of glycophagy. Glucose enters the cell via GLUT4-mediated uptake. Glycogen synthesis from glucose monomers is catalysed by glycogen synthase (GS). Glycogen breakdown is either cytosolic, mediated by glycogen phosphorylase (GP) or occurs via glycophagy. For glycophagy to proceed, STBD1 (orange) tags glycogen and binds to the Atg8 protein, GABARAPL1 (blue) at the forming autophagosome membrane. The mature glyco-phagosome fuses with a lysosome where GAA (green) degrades glycogen to free glucose for metabolic recycling.

1.2.1. Cytosolic glycogen management

Glycogen accumulation in the diabetic heart may be expected to be the result of diabetes-induced disturbances in glycogen handling mechanisms. Glycogen is a polymer composed of glucose-1-phosphate (G1P) molecules and is synthesized enzymatically in the cytosol. Circulating glucose enters the cell via glucose transporters (in the heart mainly GLUT1 and GLUT4[150]) and is immediately phosphorylated by Hexokinase (HK) to produce glucose-6-phosphate (G6P). In order for G6P to participate in glycogen synthesis, it must first be converted to uridine diphosphate-glucose (UDP-glucose). Glycogenin subsequently catalyses covalent self-attachment of several UDP-glucose molecules in a reaction that provides the first few monomers of the glycogen strand. Glucose chains are then elongated by glycogen synthase (GS) that catalyses the formation of α-1,4-glycosidic bonds between UDP-glucose molecules. Glycogen branching occurs every 10-14 residues by the glycogen branching enzyme (GBE) via α-1,6-glycosidic bonds[143-145,151]. Cytosolic glycogen breakdown is achieved by actions of glycogen phosphorylase in conjunction with glycogen debranching enzyme (GDE)[145]. GP catalyses cleavage of the α-1,4-glycosidic bonds resulting in release of G1P molecules. The activity of GP comes to arrest 4 residues prior to a branch-point (limit-dextrin)[145], when GDE is required to first transfer a 3-residue linear strand to a neighbouring strand and subsequently cleave the α-1,6-glycosidic bond, thus allowing GP to proceed with glycogen breakdown[143].

In the diabetic context, several studies using rodent models of both T1D and T2D have shown decreased activity of glycogen synthase (GS) and unchanged or increased activity of glycogen phosphorylase (GP)[120,126,131,137,152]- a response which would be more consistent with glycogen depletion than accumulation. For example, in rats where T1D was induced pharmacologically by pancreatic β-cell destruction, myocardial glycogen content was increased and coincided with increased GP activity[120]. Similarly, in a rat model of spontaneous diabetes, ex-vivo activity assessment of glycogen handling enzymes showed that GP activity was increased while that of GS was decreased[131]. Further, in the genetic T2D model db/db mouse, increased myocardial glycogen deposition was coincident with decreased GS activity[137]. Taken together, these findings illustrate that alterations in activity of cytosolic glycogen regulatory enzymes do not explain the diabetic cardiac

phenotype. It is possible that perturbation in glycogen storage is an early response in diabetes and that single time-point measurements of glycogen regulatory enzymes may not necessarily reflect the progression of the phenotype and may indicate a compensatory response. There is also the possibility that other glycogen handling mechanisms, such as lysosomal glycogenolysis (glycophagy), may play a role in the manifestation of glycogen disturbance although this has not been investigated in the diabetic heart.

1.2.2. Tagging glycogen for lysosomal breakdown

In the past decade lysosomal glycogenolysis has been placed in the context of autophagy due to the discovery of Starch binding domain 1 (STBD1) as a protein that contains both a carbohydrate binding motif (CBM20)[153] and seven ATG8-intracting motifs (AIMs)[147]. Even though STBD1 was initially shown to exhibit higher expression levels in muscle tissues than the liver[154,155], it was the analysis of rodent hepatic glycogen proteomes that identified STBD1 as a glycogen-binding protein[156]. Interestingly, a yeast 2-hybrid screen where the 'bait' was N-terminal-lacking STBD1 identified two members of the ATG8 family, GABARAP and GABARAPL1, as binding partners[146]. Follow up co-expression experiments however, indicated that STBD1 only partially co-localizes with GABARAP while its cellular distribution pattern fully aligns with that of GABARAPL1[146]. In addition, compelling evidence demonstrated that STBD1 co-localizes with lysosomal-associated membrane protein 1 (LAMP1) in COS cells[146]. Together these findings indicated a potential role of STBD1 in the lysosomal breakdown of glycogen but little further research has been conducted. In support of STBD1-involvement in glycophagy, treatment of cells with the lysosome inhibitor bafilomycin, resulted in accumulation, albeit small, of both wild type (WT) and AIM-mutant STBD1[157]. The accumulation of AIM-mutant STBD1 following bafilomycin treatment may indicate either that STBD1-mediated transfer of glycogen to the lysosome is not always reliant on the occupancy of the AIM by GABARAPL1 or that lysosome blockade increases glycogen deposition thereby driving an increase in STBD1 expression. Indeed, in a murine model of Pompe disease (GAA-KO), skeletal muscle expression of STBD1 was increased to reflect the extent of glycogen accumulation, although neither the cardiac nor the hepatic STBD1 expression was altered despite elevated glycogen levels in these tissues. Interestingly however, muscle-specific STBD1 knockdown did not compromise glycogen

sequestration to the lysosome in the GAA-KO mice[158] indicating either that transfer of glycogen to the lysosome is STBD1-independent or that there is perhaps an additional, yet unidentified glycophagy receptor acting to compensate for reduction in STBD1 availability. Indeed, it has been shown that in the skeletal muscle of *D. melanogaster*, the AIM of the glycogen synthase (GS) homolog is required for sequestration of glycogen to phagosomes following chloroquine (lysosome inhibitor) administration[159]. Similarly, simultaneous global knockout (KO) of both STBD1 and GAA in rodents did not affect cardiac glycogen accumulation induced by the GAA knockout alone. In contrast, GAA-KO-induced hepatic glycogen accumulation was hindered in absence of STBD1[158], suggesting a different role for STBD1 in the liver.

Despite the limited number of glycophagy-focused investigations, it has become increasingly evident that STBD1 plays a central role in both the lysosome-mediated glycogen. It is likely that the regulation of STBD1 varies between different tissues and cell types making further examination of the precise involvement of STBD1 in the glycophagy pathway warranted.

1.2.3. Glycogen sequestration to the phagosome

The phagosome-residing ATG8 (from yeast 'Autophagy-related 8') proteins are thought to be essential for the maturation of cargo-containing phagosomes. The mammalian ATG8 protein family consists of two subfamilies: Microtubule-associated Protein 1 Light chain 3 (MAP1LC3) and GABA type A receptor-associated protein (GABARAP), each being comprised of 3 members[160]. All six members are classified as small ubiquitin-like proteins due to sharing the same UBL fold with ubiquitin[78] and are thought to be integral to the maturation of autophagic phagosomes. Soluble cargo receptors (SARs) bind to members of the ATG8 family that, when C-terminally lipidated, are anchored to the phagosomal membrane[78].

Binding of SARs to the ATG8 proteins is facilitated by an ATG8-interaction motif (AIM, otherwise known as LC3-interaction motif or LIR). Recently, a biotinylated peptide screen using AIMs from 30 different autophagy adaptors (proteins associated with autophagy but do not carry cargo) and SARs revealed that in their vast majority, ATG8-interacting proteins displayed a higher binding preference for the GABARAP subfamily members over the MAP1LC3s, while binding preferences between

members of the same subfamily was invariant. Strikingly, STBD1 displayed an almost 10-fold higher preference for GABARAP (member of the GABARAP subfamily) than LC3B (member of the MAP1LC3 subfamily). The preference for GABARAPL1 was not specifically measured but further crystallography analysis of the ATG8-AIM interactions shows that binding to GABARAPL1 is likely to be very similar to GABARAP[161]. Therefore, it can be speculated that GABARAPL1 and GABARAP may be interchangeably used in glycophagosomes, although STBD1 was shown to display complete co-localization with GABARAPL1 but only partially co-localized with GABARAP[146]. In addition to the yeast-2 hybrid screen that identified STBD1-binding to members of the GABARAP subfamily, STBD1 was shown to interact with all three GABARAP subfamily members in 293T cells following GST-pulldown assays but also with all MAP1LC3s[162].

Of all the six mammalian ATG8 members, GABARAPL1 is thought to be glycophagy-specific because it was shown to display complete co-localization with STBD1[146]. Indeed, even when overexpressed alone in CHO cells, GABARAPL1 localized in proximity to the Endoplasmic Reticulum (ER) and *trans*-Golgi Network (TGN)[163] which is similar to the pattern exhibited by overexpressed STBD1[146,157]. Despite numerous studies, GABARAPL1 has not yet been assigned a specific function over other members of the GABARAP subfamily and particularly over GABARAP with which it shares 87% similarity[160]. Only recently it was shown that starvation enhances the binding of ULK1 to GABARAPL1 but has no effects on its interaction with GABARAP or GABARAPL2, indicating a diverse functionality. The same study demonstrated that GABARAPL1 lipidation does not proceed in presence of LC3B, potentially revealing a preference for the participation of the latter during cargo sequestration[164]. In addition, it has been argued that in MCF-7 cells, lipidation of GABARAPL1, and therefore phagosome conjugation, is not necessary for its participation in autophagy induction through facilitation of ULK1 phosphorylation[165]. Taken together, these findings imply that GABARAPL1 may not necessarily be involved in the formation of the phagosome but instead may closely mediate autophagy induction. However, there can also be a case of GABARAPL1-specific cargo sequestration. It is likely that there might be a degree of redundancy between the members of the GABARAP subfamily and therefore glycophagy does not utilize solely GABARAPL1 but also GABARAP although differential co-localization with STBD1 may indicate otherwise. Although

glycophagy has not received attention in the cardiac field, the evidence pointing towards GABARAPL1 being the glycophagy-specific ATG8 indicate that it may be an important target protein for approaches aiming to intervene in this pathway.

1.2.4. Lysosomal glycogenolysis

The concept of lysosomal glycogen breakdown is not novel in nature. It is known for a long time that Pompe disease, a genetic glycogen storage disorder (GSD) that results in glycogen accumulation in a number of tissues, is caused by mutations in the lysosome-residing α-acid glucosidase (GAA) enzyme[166]. By comparison, lysosomal glycogen breakdown is expected to be more efficient because in contrast to the limitations imposed by branching on the enzymatic pathway (carried out by GP and GDE), GAA is able to cleave both α-1,4-glycosidic and α-1,6-glycosidic bonds, thereby degrading the entire granule to α-glucose[148,149,167]. It is likely that substrate specificity and kinetic properties of GAA are similar between different cell types. It has been shown that in humans there are no differences in the kinetics of the liver-residing GAA to that in the heart[168]. Interestingly, it has been hypothesised that lower hepatic GAA activity activates an unidentified feedback loop mechanism aiming to reduce lysosomal glycogen sequestration[169,170]. In addition, our group has demonstrated that glycogen synthesis and glycophagy are concurrently upregulated in cardiomyocytes both in response to fasting and following insulin exposure[171,172]. Taken together, these findings indicate that there is a regulatory interplay between glycogen levels and GAA activity. Within the context of GAA regulation, it is noteworthy that induction of lysosomal Ca^{2+} release in rat hepatocytes was shown to result in reduction of GAA activity[173]. Furthermore, it has been shown that lysosomal Ca^{2+} release is triggered by treatment with ATP or thapsigargin (Ca^{2+}-ATPase inhibitor)[174], and results in autophagy inhibition in hepatocytes[175], indicating that lysosomal-mediated breakdown depends on localized Ca^{2+} stores. In contrast, it was shown that a rise in the levels of cAMP leads to an increase in GAA activity[176], suggesting that glycophagy may depend on the cellular energetic status. It would be interesting to investigate the dependence of glycophagy on Ca^{2+} in contractile cells that follow a patterned SR-depletion of intracellular Ca^{2+} stores and determine whether the cytoplasmic levels of the cation, which may reflect contractile abnormalities, also have the ability to regulate lysosome-mediated breakdown processes.

1.2.5. Lysosomal glycogenolysis is linked to cardiac dysfunction

The vital role of glycophagy in the heart is evidenced by contractile abnormalities observed in inherited glycogen storage diseases (GSDs) where mutations in α-acid glucosidase (*Gaa*, GSD type II, Pompe disease) or Lysosome-associated membrane protein 2 (*Lamp2*, GSD type IV, Danon disease) lead to glycogen accumulation[177,178]. Severe GAA deficiency has been linked to hypertrophic or dilated cardiomyopathy with decline in both systolic and diastolic function. Clinically, ventricular pre-excitation/conduction defects are evident in some cases and are associated with sudden cardiac death[179,180]. In genetic animal models of Pompe disease (GAA-KO) and in human patients, enzyme replacement therapy (ERT) delivering recombinant GAA has been demonstrated to reduce left ventricular wall thickening thereby reducing hypertrophy and improving cardiac function. GAA-ERT has also been used in GSD type III, which manifests due to mutations in GDE, and was shown to reduce glycogen levels in skeletal muscle. Unsurprisingly, hypertrophy and diastolic dysfunction are also evident in GSD type III, further highlighting the link between glycogen accumulation and detrimental functional outcomes for the heart. Similarly, conduction abnormalities, hypertrophy, systolic and diastolic functional decline are clinically and pre-clinically observed in Danon disease[14,166,177,181]. Taken together, pre-clinical and clinical evidence suggest that lysosomal glycogenolysis is important for the preservation of physiological cardiac function and highlight that further investigations are required to determine the mechanism via which glycogen is trafficked to the lysosome. In addition, these findings indicate that lysosome-mediated glycogen breakdown and glycophagy could be target pathways of particular interest in non-Mendelian diseases, such as diabetes, where cardiac glycogen accumulation is also evident.

1.3. Signalling and regulation of cardiac glycogen handling and glycophagy

Cytosolic cardiac glycogen handling has been well investigated and is governed by a multitude of pathways including insulin and 5' AMP-activated protein kinase (AMPK) signalling that act in concert to activate or inhibit glycogen synthesis via different mechanisms depending on the cellular energy status[182-191]. In contrast, very little is known about the regulation of cardiac glycophagy but some insight may be gained through examination of pathways that regulate glycogen and autophagy. In

addition to signalling regulation, the morphological structure of the glycogen particle may determine glycophagy involvement.

1.3.1. Morphological determinants of glycogen particle fate

The molecular structure of glycogen varies between different cell types, even between subcellular compartments, and it may determine whether glycogenolysis occurs in the cytosol or the lysosome. Glycogen is one of the largest cellular macromolecules with its particles reaching a diameter of up to 300nm and containing up to 55,000 glucose residues[192]. Morphologically, glycogen can appear in particles of different sizes that may determine the preferred mechanism of glycogenolysis, although this has not been directly investigated. It is recognised that highly branched α-particles are formed by aggregating, smaller in diameter, β-particles (<50nm). In turn, β-particles are characterised by smaller degree of branching and are thought to be the first to break down upon energy demand due to their high surface-to-volume ratio[193]. It has been shown that glycogen pools in skeletal muscle are solely composed by β particles whereas α-particles are abundant in the liver, consistent with the physiological roles of the two tissues[193,194]. In contrast, cardiac glycogen has been observed to exist in both α and β particles[171,195] indicating that in the heart glycogen metabolism may serve to provide energy both basally and under increased demand. In the liver, lysosome-residing glycogen particles have been identified as larger than those in the cytosol[196]. Taken together, these investigations may indicate that glycophagy is a process employed under stress to provide energy, similar to all selective autophagy branches, by rapidly degrading densely branched α particles. Despite the logical nature of this assumption however, how particle size is a determinant of particle fate remains unclear.

Detection of glycogen-containing phagosomes in the liver of new-born rats lead to the hypothesis that hepatic glycophagy may be employed shortly after birth as the primary glycogen breakdown mechanism[197,198]. Interestingly, measurements of the optical rotatory dispersion of rodent foetal hepatic glycogen showed that it differs in structure compared to the adult[199]. In addition, hepatic glycogen-containing phagosomes seem to be short-lived and cannot be detected past postnatal day two[199] indicating that potentially the selectivity of neonatal glycophagy is morphology-dependent. Despite the number of studies showing that glycophagy is highly operational in neonatal hepatocytes, it has also been shown that the activity of GP is increased in the hours after birth and

that the liver is characterised by considerable degrees of glycogenolysis[200]. Therefore, it appears likely that under conditions of increased energy demand such as the postnatal starvation period, lysosomal and cytosolic glycogen breakdown pathways act in concert to maintain energy balance. In the cardiac context, it has been shown that the neonatal cardiomyocytes are dependent on glycolysis-derived ATP[201] but whether glycophagy plays a central role in maintaining glucose availability in the neonatal heart remains to be determined. An interesting finding linking glycogen morphology and glycophagy was the observed increased association of STBD1, the protein thought to tag glycogen for lysosomal glycogenolysis, with skeletal muscle glycogen from Laforin-KO mice[146]. Absence or mutations in Laforin lead to progressively increased glycogen phosphorylation with age causing poor branching and solubility and eventually aggregates, called Lafora bodies[202-204]. Thus, glycophagy may be a process employed under pathophysiological conditions to degrade aberrant, poorly branched glycogen. Noticeably, multiple studies have examined glycophagy in the liver and to a lesser extent in the skeletal muscle. In contrast, cardiac glycophagy remains insufficiently investigated.

1.3.2. Regulation by insulin

Insulin signalling has been repeatedly implicated in regulation of glycogen handling. Insulin-activated AKT Serine/Threonine Kinase 1 (AKT) has been shown to inhibit, through phosphorylation, glycogen synthase kinases 3α and 3β (GSK3α/β) thereby alleviating the inhibition on GS and promoting glycogen synthesis[188,189,191]. In mice expressing non-phosphorylatable (mutant) GSK3β insulin failed to induce cardiac glycogen synthesis suggesting a central role of GSK3β in glycogen handling[188]. In ex-vivo experiments, cardiac perfusion with insulin was shown to decrease the rate of glycogen breakdown while simultaneously increasing synthesis rate. Interestingly, this was also evident in diabetic hearts in the same setup although the effects were much less pronounced[131]. Insulin can also positively regulate glycogen synthesis via promoting GLUT4 translocation to the plasma membrane thereby increasing glucose uptake and levels of G6P. In turn, G6P can allosterically regulate GS by preventing its phosphorylation, thereby promoting glycogen synthesis[183].

Cardiac macro-autophagy has been shown to be negatively and positively regulated by insulin. In mice deficient in insulin receptor substrate (IRS), progressive post-natal autophagy results in heart

failure[205]. In contrast, in neonatal rat ventricular myocytes cultured under high glucose conditions, autophagy was shown to be upregulated following insulin stimulation, evidenced by decreased LC3B-II/-I ratio. Interestingly, expression of STBD1 was also increased under these conditions suggesting that glycophagy was also positively regulated[172]. Collectively, the research on insulin-mediated regulation of glycogen handling indicates that in the diabetic heart, where insulin signalling is impaired, either due to decreased circulating insulin (T1D) or insulin resistance (T2D), glycogen synthesis and content would be expected to decrease. As discussed in section 1.1.4 however, glycogen accumulation is consistently observed in the diabetic heart, making this phenomenon increasingly paradoxical.

1.3.3. Regulation by AMPK

AMPK has also been reported to regulate glycogen handling. AMPK is composed of 3 subunits (α-catalytic, β,/γ-regulatory) and is the cellular energy sensor; it is activated when ATP levels fall and those of AMP rise. In the heart, the link between AMPK and glycogen is evident in patients presenting with ventricular pre-excitation abnormalities and increased cardiomyocyte glycogen levels (Wolf-Parkinson-White syndrome) because of mutations in the γ2 regulatory subunit (*Prkag2*)[206-208]. Elevated glycogen and mutations in the γ2 subunit have also been linked with cardiac hypertrophy in humans[209,210]. AMPK is allosterically activated by rising levels of AMP that has also been shown to enhance phosphorylation (thus activation) of AMPK at Threonine172 (T172)[211]. It has been demonstrated that AMPK can directly phosphorylate GS and GP thereby inhibiting glycogen synthesis and promoting glycogenolysis[184,190]. Interestingly, the mutations causing pre-excitation defects coincident with glycogen accumulation inhibit AMP binding and should therefore reduce the activity of AMPK[212]. Thus, it is unclear how myocardial glycogen deposition is increased in these settings. Another role for AMPK in glycogen metabolism can be deduced from *in vivo* experiments showing that activation of AMPK enhances GLUT4 translocation to the plasma membrane thereby promoting glucose uptake and increasing cellular G6P content[187]. Since G6P is an allosteric activator of GS, it can be hypothesised that AMPK activation can indirectly promote glycogen synthesis. Intriguingly, the β-regulatory subunit of AMPK contains a carbohydrate binding motif that has been shown to directly bind to glycogen[213,214]. In skeletal muscle, it has been demonstrated that increased

glycogen binding inhibits AMPK activity[190], which may indicate the presence of a negative feedback loop. In the heart, counterintuitively, fasting induces concurrent AMPK activation and glycogen accumulation[171]. Interestingly, pharmacological activation of AMPK with aminoimidazole carboxamide riboside (AICAR) has been shown to both increase and decrease glycogen levels[215-218] indicating that further investigation is needed to decipher the precise involvement of AMPK in glycogen metabolism. This may be particularly important in diabetic settings where myocardial glycogen accumulation is evident and AMPK agonists (Metformin) are routine therapeutic approaches.

A role for AMPK, in conjunction with mTOR has also been described in autophagy initiation. When mTOR is activated (under amino acid plentiful conditions), the ULK complex and by extension autophagy is inhibited[219]. Under periods of nutrient stress, high levels of AMP activate AMPK which in turn phosphorylates mTOR thereby lifting the inhibition on autophagy[220]. In addition, AMPK has been shown to directly positively regulate ULK1[221]. This interaction is necessary for mitochondrial autophagy (mitophagy)[222]. Interestingly, mTOR signalling has also been implicated in the regulation of glycophagy. A recent study using mouse embryonic fibroblasts showed that amino acid starvation (traditionally an mTOR activator) resulted in decreased glycogen levels. This was due to glycophagy induction as shown by concurrent treatment with the lysosome inhibitor Bafilomycin A[223]. Thus, it is likely that glycophagy regulation is similar to that of autophagy but further research into glycophagy stimuli, particularly in the heart, is critical.

1.4. Research questions

Extensive investigations by the Mellor-Delbridge labs have demonstrated that the diabetic heart is consistently characterised by glycogen accumulation that is in turn associated and correlated with diastolic dysfunction. This phenotype cannot be explained by diabetes-induced alterations in metabolic signalling or by disturbances in the well-characterised cytosolic glycogen handling pathway. A role for glycophagy in the heart has emerged through previous experimental investigations showing that this pathway may be operational in the heart[172] and through evidence linking lysosomal glycogenolysis with poor functional outcomes in inherited glycogen storage diseases but investigations of this pathway in the heart are limited. Thus, it seems that glycogen accumulation in the diabetic heart has detrimental consequences for cardiac function but the molecular mechanisms contributing to this phenotype remain poorly understood. The outline of the research presented in this thesis is schematically depicted in Figure 1.3.

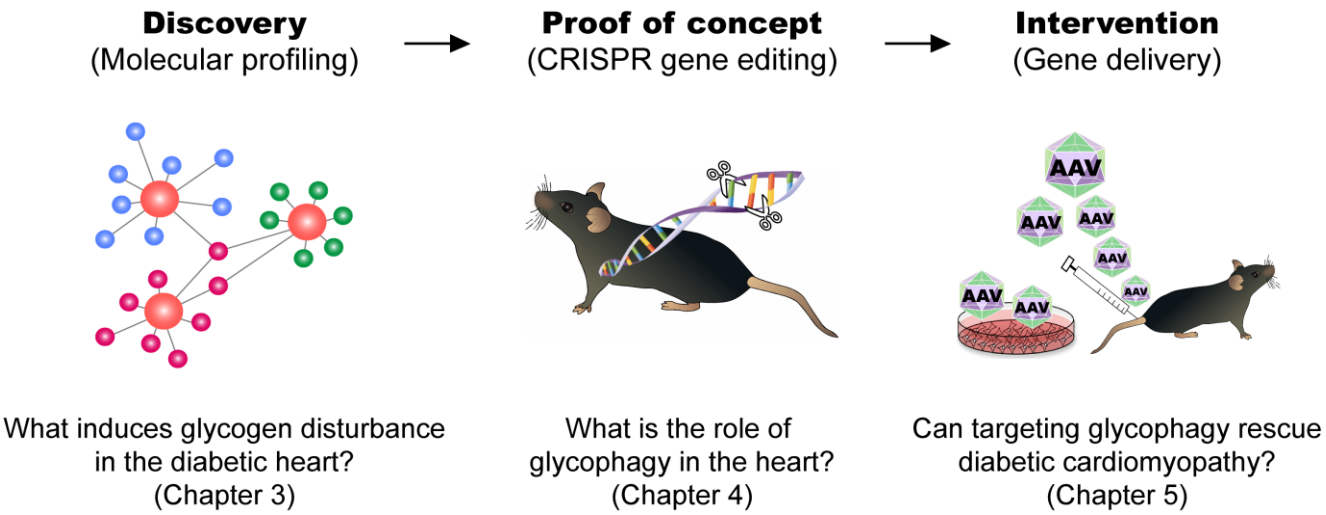

Figure 1.3: Direction of research presented in this Thesis.

The investigations conducted during this doctoral candidature aimed to identify the underlying molecular mechanisms responsible for the diabetic cardiac glycogen pathology. The glycophagy process and its potential for use as a therapeutic approach for diabetic cardiomyopathy are also characterised.

Research questions addressed in this Thesis:

(1) What are the molecular alterations underlying increased glycogen deposition in the diabetic heart? (Chapter 3)
(2) What is the role of the key glycogen autophagy (glycophagy) protein, GABARAPL1, in regulating cardiac function and glycogen content? (Chapter 4)
(3) Can glycophagy-targeting interventions rescue cardiac function and provide therapeutic potential for diabetic cardiomyopathy? (Chapter 5)

CHAPTER 2

General methodology

2.1. Ethical statements

All animal studies reported in this Thesis were approved by the Animal Ethics Committee of the University of Auckland (Approval number: 01422) or the Animal Ethics Committee of The University of Melbourne (Approval Numbers: 1714147, 1614056) as applicable. For studies conducted in Auckland, the care of animals was in accordance with the *Good Practice Guide for the Use of Animals in Research, Testing and Teaching* (NAEAC). For studies conducted in Melbourne, the care of animals was according to the *Australian Code for the Care and Use of Animals for Scientific Purposes* (NHMRC, 2013). Animals were housed in the Vernon Jensen Unit at the University of Auckland or the Biomedical Sciences Animal Facility at the University of Melbourne. Animals were maintained under temperature controlled conditions and a 12:12 hour light:dark cycle.

2.2. Echocardiography

In vivo cardiac function of the animals used in the study presented in Chapters 4 and 5 was determined via transthoracic echocardiography as previously described[171]. Isoflurane (4%, Baxter Healthcare) mixed with oxygen and room air was used to induce anaesthesia which was subsequently maintained with 1.5% Isoflurane for the duration of the echocardiographic assessment (<30 minutes per mouse). Echocardiography was performed using the GE vivid 9 Dimension echocardiography system with a 15MHz i13L linear array transducer (GE Healthcare). The GE EchoPac software was used for image acquisition and analysis. Image acquisition was performed by the experienced investigators, Dr. Claire Curl and Dr. Hanneke Raaijmakers.

2.3. Glucose Tolerance Test

Glucose tolerance test was performed as previously described[224]. Briefly, a baseline blood glucose measurement was taken using a tail prick performed with a 23G needle and calibrated glucometer (ACCUCHECK® Advantage, Roche). Subsequently, glucose was administered intraperitoneally at a dose of 1.5g/kg (1.25mM in saline) and blood glucose concentrations were measured at 5, 15, 30, 60, 90 and 120 minutes to determine glucose tolerance. Glucose concentration was plotted against time to generate glucose clearance curves. The area under these curves is used as an index of

glucose clearance from plasma[225] and was calculated in Prism (Graphpad Software) using the trapezoid rule.

2.4. Extraction of cardiac tissue

Cardiac tissue used for molecular analyses was extracted from animals that were anesthetised with sodium pentobarbitone (100mg/kg) via intraperitoneal injection. The heart was rapidly excised following opening of the thoracic cavity. Cardiac arrest was achieved by complete immersion and palpitation of the heart in cold HEPES-Krebs buffer (Table 2.1) supplemented with 1mM $CaCl_2$ (Sigma, cat – 21115). The cardiac muscle was subsequently transferred to a calcium-free buffer to achieve relaxation. Following determination of whole heart wet weight, atrial tissue was removed and ventricular tissue was dissected into equal portions, snap-frozen in liquid N_2 and stored at -80ºC prior to analysis. Tibia length was measured using an electronic calibrated calliper following isolation of the tibia from the femur and patella through gentle dislocation and from the calcaneus (heel bone) through delicate displacement of the flexor retinaculum of the foot.

2.5. Protein extraction from frozen cardiac tissue

Cardiac tissue homogenates were generated using a Polytron PT2500E with a PT-DA 1207/2EC-E dispersing aggregate. The homogenization buffer is summarized in Table 2.2 and was supplemented with protease (Complete, EDTA-free, Roche, cat – 04693132001) and phosphatase (PhosSTOP, Roche, cat – 04906837001) inhibitors. Following complete homogenization of the tissue, separate aliquots were snap-frozen in liquid N_2, each to be used for molecular analyses. Separate aliquots were blended with equal volume of 2 times concentrated sample buffer (Table 2.3) supplemented with 5% 2-mercaptoethanol (Sigma, cat – M3148) and were stored at -20ºC for immunoblotting.

2.6. Lowry assay for assessment of protein concentration

The protein concentration of cardiac tissue homogenates and NRVM cell lysates was determined in a 2-step calorimetric assay. First, samples were subjected to a 10 minute incubation with an SDS-containing solution (solution ‘A’, Table 2.4). Subsequently, samples were incubated with Folin reagent (solution ‘B’, Biorad, cat – 5000114) for 30 minutes. Each sample was assayed in triplicate

in a clear 96 well plate. Absorbance was measured at 750nm. Protein concentration was determined via a standard curve constructed with Bovine Serum Albumin (Biorad, cat – 5000007) at various concentrations. A standard curve was included in each assay.

2.7. Glycogen assay

The glycogen content of cardiac tissue homogenates and NRVM cell lysates was determined in a 2-step enzymatic calorimetric assay as described previously[171,172]. Briefly, duplicate aliquots were incubated at 50ºC in presence or absence (1 aliquot per condition) of amyloglucosidase (Roche, cat – 10102857001, diluted in 0.1M sodium acetate) for 1 hour. Amyloglucosidase-positive and negative samples were subsequently centrifuged for 2 minutes at 4ºC at 16,000g. The supernatant was collected and incubated with glucose oxidase/peroxidase (PGO enzyme capsules, Sigma, cat – P7119) diluted in H_2O/1% o-dianisdine dihydrochloride (Sigma, cat – D3252) for 30 minutes at room temperature. Absorbance was measured at 450nm. The absorbance of each amyloglucosidase-positive and negative sample was measured in triplicate. Glucose concentration was determined via a standard curve constructed with glucose (glucose standard solution, Sigma, cat – G6918). A standard curve was included in each assay. Glycogen was determined by subtracting the glucose content of the amyloglucosidase-negative reaction from that of the positive reaction for each sample.

2.8. RNA extraction

RNA was extracted and purified (PureLink RNA mini kit, Invitrogen, cat - 12183018A) from frozen cardiac tissue by homogenization in TRizol™ reagent (Ambion/Thermofisher, cat – 15596026). NRVM cells were lysed in TRizol™ reagent prior to carrying out the remaining of the protocol. Homogenates (and lysates) were subsequently supplemented with Chloroform (5:1 v/v) and centrifuged for 15 minutes at 4ºC at 12,000g. As per manufacturer's instructions, the aqueous phase was removed and mixed with equal volume of 70% ethanol to achieve RNA precipitation and was subsequently treated on-column with DNase (RureLink® DNase, Invitrogen cat - 12185010). Purified RNA was eluted in DEPC-treated, RNase-free H_2O (Thermofisher, cat - AM9906). The concentration and quality of the extracted RNA was measured with NanoDrop™ 2000/2000c Spectrophotometer (Thermofisher, cat - ND2000).

2.9. Reverse transcription

RNA samples extracted from frozen cardiac tissue or NRVM cell lysates were reverse-transcribed to cDNA using the SuperScript™ III First-Strand Synthesis System (Invitrogen/Thermofisher, cat - 18080051) as per manufacturer's instructions. Up to 5µg of RNA per sample were incubated with random primers (hexamers) and dideoxyribonucleotides (dNTPs) for 5 minutes at 65ºC and were allowed to cool down by incubation at 4ºC for at least 2 minutes. Each sample was then combined with the reverse transcriptase mix (Table 2.5) and incubated at 25ºC for 10 minutes followed by 50 minutes at 50ºC and 5 minutes at 85ºC. Samples were allowed to cool down at 4ºC for at least 2 minutes prior to the addition of RNaseH (Invitrogen/Thermofisher, cat - EN0201) and final incubation at 37ºC for 20 minutes. All incubations were performed using a T100™ Thermal cycler (Biorad). cDNA samples were stored at -20ºC prior to further analysis. For each set of samples that were reverse-transcribed as part of 1 experiment, one of the samples was used as template for an RT-negative reaction in which reverse-transcriptase was not added. RT-negative samples were incorporated in qPCR to verify that the extracted RNA samples were DNA-free.

2.10. Real-time quantitative polymerase chain reaction (RT-qPCR)

Primers targeting genes of interest (GOIs) and housekeeping genes (HKs) used for normalization are summarized in Table 2.6. Primers were manually designed so that (where possible) (1) the Guanine-Cytosine (GC) content did not exceed 50%, (2) there was GC clamp in the 3' end, (3) there was no stretch of more than 2 of the same nucleotide, (4) the target sequence to be amplified by a primer pair in qPCR did not exceed 150 base-pairs in length and (5) they were located either on exon-exon junctions or were exon-spanning. Specificity of the primers was confirmed with Basic Logical Alignment Search Tool (BLAST) against both the genomic and trancriptomic sequences for human, mouse and rat. qPCR was performed using Platinum™ SYBR™ Green qPCR SuperMix-UDG (Invitrogen, cat – 11733038) and the QuantStudio™ 12K Flex Real-time PCR System (Thermofisher, cat – 4471090). All PCRs were optimized so that the amplification efficiency of GOIs and HKs were 100%±5%. The cycling conditions were the same for all qPCRs and are summarized in Table 2.7. Gene expression was determined using the ΔC_T method as previously described[226].

2.11. Immunoblot

Equal protein amount per sample was loaded onto polyacrylamide gels (Biorad precast 4-15% acrylamide gels, cat - 4561083) and separated by gel electrophoresis (SDS-page, 45 minutes, 150V). Protein was transferred to polyvinylidene difluoride membranes (PVDF) using a Trans-Blot® Turbo™ Transfer System (Biorad, cat – 1704274). To avoid non-specific primary antibody binding, membranes were incubated in 5% milk/PBS-T (phosphate buffer saline containing 0.1% Tween) for 2 hours (with the exception of GABARAPL1-targeting blots where the membranes were incubated in 5% milk/TBS-T (tris buffer saline containing 0.1% Tween). Primary antibody incubation occurred overnight at 4ºC followed by 1 hour incubation with secondary antibody (HRP-conjugated anti-Rabbit, GE healthcare life sciences, cat - NA934) at room temperature. Primary antibody details and conditions are summarized in Table 2.8. Following incubation with the secondary antibody, membranes were incubated with Amersham™ ECL Prime (GE healthcare life sciences, cat - RPN2236) for 3 minutes at room temperature and were imaged using a ChemiDoc™ XRS+ system (Biorad, cat – 1708265). Images were analysed with Image Lab© v6.0 (Biorad). Equal protein loading was confirmed by Coomassie Brilliand Blue (Briorad, cat – 1610400) staining of the PVDF membranes. Coommassie staining was imaged with the ChemiDoc™ XRS+ System and analysed with Image Lab©. Band intensities of the proteins of interest were normalized to the intensity of the corresponding Coomassie staining to account for differences in protein loading.

2.12. Statistical analysis

All statistical analyses were performed using Prism Software v.8 (Graphpad Software). In instances where comparisons between 2 groups were required, Student's t-Test was used. In instances where comparisons were made between 3 or 4 groups, one-way ANOVA or two-way ANOVA were used respectively. The significance of glucose tolerance tests was determined using two-way ANOVA with repeated measures. Parametric assumptions (normal distribution and equal variance) were verified for all datasets prior to applying parametric statistical tests. For datasets with 2 groups, F-test was used to verify equal variance whereas for those containing 3 or 4 groups, equal variance was verified using the Brown-Forsythe test. Normality was verified with the Shapiro-Wilk test. If parametric

assumptions were not met, the data was transformed using either the x=log(y) or the x=sin(y) function prior to statistical analysis. In cases where datasets continued to fail parametric assumptions after application of the above 2 transformations, non-parametric tests were used. This is clearly indicated in the Figure legends.

Table 2.1: HEPES-Krebs buffer used in extraction of cardiac tissue

	Concentration
NaCl (Sigma, cat – S5886)	146mM
KCl (Sigma, cat – P5405)	4.69mM
D-Glucose (Sigma, cat – G7021)	1.11mM
NaH_2PO_4 (Sigma, cat – S5136)	0.35mM
$MgSO_4$ (Sigma, cat – 246972)	1mM
HEPES (Sigma, cat – H4034)	10mM
	pH 7.40

Table 2.2: Tris-HCl buffer used in protein extraction from frozen cardiac tissue

	Concentration
Tris-HCl (Trizma base, Sigma, cat – T1503)	100mM
EGTA (Sigma, cat – E3889)	5mM
EDTA (Sigma, cat – E6758)	5mM
	pH 7.00

Table 2.3: Sample buffer used for generation of samples used for immunoblotting

	Concentration
Tris-HCl (Trizma base, Sigma, cat – T1503)	100mM
SDS (Sigma, cat – L3771)	4%
Glycerol (Sigma, cat – G5516)	20%
Bromophenol blue (Sigma, cat – B5525)	0.2%
	pH 6.8

Table 2.4: Solution 'A' used in the Lowry assay

	Final concentration
10% SDS (Sigma, cat – L3771)	4%
0.8M NaOH (Sigma, cat – S8045)	0.2M
12.5% Na_2CO_3 (Sigma, cat – S7795)	5%
2% NaK Tartrate (Sigma, cat – S2377)	0.8%
1% $CuSO_4$ (Sigma, cat – 451657)	0.4%

Table 2.5: Reverse transcription reaction components

	Concentration per reaction
10X RT buffer	1X
$MgCl_2$	5mM
Dithiothreitol	10mM
Superscript III	200 Units
RNaseOUT®	40 Units

Table 2.6: Summary of primer sequences and concentrations used in qPCR

Species	Gene	Accession number	Primer sequences	[primer] (nM)
Homo sapiens	*GABARAPL1*	NM_031412	FWD: 5'-CCTCTGACCTTACTGTTGGC-3' REV: 5'-CCTCATGATTGTCCTCATACAGT-3'	250
	18S	NR_146152	FWD: 5'-TCGAGGCCCTGTAATTGGAA-3' REV: 5'-CCCTCCAATGGATCCTCGTT-3'	200
Mus musculus	*Gabarapl1*	NM_020590	FWD: 5'-GGTCATCGTGGAGAAGGCTC-3' REV: 5'-TAGAACTGGCCAACAGTGAGG-3'	200
	Stbd1	NM_175096	FWD: 5'-AAGCAGAGCATCTTCGAGAAAGC-3' REV: 5'-ACCCAGTCTGCTCCAACATTC-3'	200
	Gaa	NM_008064	FWD: 5'-TACATGATGATCGTGGACCCT-3' REV: 5'-GTGGTTCCAGGCCAAACCTTCC-3'	200
	Map1lc3b	NM_026160	FWD: 5'-TTATAGAGCGATACAAGGGGGAG-3' REV: 5'-CGCCGTCTGATTATCTTGATGAG-3'	200
	Gabarap	NM_019749	FWD: 5'-AAGAGGAGCATCCGTTCGAGA-3' REV: 5'-GCTTTGGGGGCTTTTTCCAC-3'	200
	Gabarapl2	NM_026693	FWD: 5'-TGGCTCAGTTCATGTGGATCA-3' REV: 5'-AAGCTGTCCCATAGTTAGGCT-3'	200
	18S	NR_003278	FWD: 5'-TCGAGGCCCTGTAATTGGAA-3' REV: 5'-CCCTCCAATGGATCCTCGTT-3'	50
	B2m	NM_009735	FWD: 5'-TTCTGGTGCTTGTCTCACTGA-3' REV: 5'-CAGTATGTTCGGCTTCCCATTC-3'	100
Rattus norvegicus	*Gabarapl1*	NM_001044294	FWD: 5'-GGTCATCGTGGAGAAGGCTC-3' REV: 5'-TAGAACTGGCCAACAGTGAGG-3'	100
	Stbd1	NM_001013988	FWD: 5'-CTCCAAAGCAGAGCATCTTCGAG-3' REV: 5'-CCACAGGAACATATTCTCTGGC-3'	100
	Gaa	NM_199118	FWD: 5'-ATGCCATGGATGTGGTCCTGCAGC-3' REV: 5'-GGGTATCCCACGACATCCAGGTA-3'	100
	18S	NR_046237	FWD: 5'-TCGAGGCCCTGTAATTGGAA-3' REV: 5'-CCCTCCAATGGATCCTCGTT-3'	50

Table 2.7: qPCR cycling conditions

Temperature	Time	
50°C	2 minutes	
95°C	2 minutes	
95°C	15 seconds	**40 cycles**
60°C	1 minute	
60°C to 99°C	1°C/min	Melt curve

Table 2.8: Details and conditions of the primary antibodies used in immunoblotting

Protein of interest	Antibody supplier	Catalog number	Antibody concentration	Expected band size
Phosphor-AMPK (Thr172)	Cell Signaling Technology	2535	1:1,000	62kDa
AMPK	Cell Signaling Technology	2532	1:1,000	62kDa
GABARAPL1	Cell Signaling Technology	26632	1:6,000	18kDa
Phospho-GP (Ser14)	Supplied by David Stapleton (University of Melbourne)	NA	1:5,000	97kDa
GP	Supplied by David Stapleton (University of Melbourne)	NA	1:5,000	97kDa
Phospho-GS (Ser641)	Abcam	Ab81230	1:2,000	85kDa
GS	Cell Signaling Technology	3893	1:1,000	85kDa
MAP1LC3B	Cell Signaling Technology	2775	1:2,000	16kDa (LC3B-I), 14kDa (LC3B-II)
SERCA2a	Badrilla	A010-20	1:20,000	100kDa
SQSTM1/p62	Sigma	P0067	1:2,000	62kDa

CHAPTER 3

Gene profiling identifies glycophagy disturbance as a novel feature of the type 2 diabetic heart

3.1. Introduction

Investigation carried out in the Mellor-Delbridge labs is the first to systematically demonstrate that cardiac glycogen accumulation is a consistent phenotype in rodent models of diabetes and in the human diabetic myocardium. Additionally, the extent of glycogen accumulation correlates positively with diastolic dysfunction (Mellor et al, publication pending). This suggests that diabetes-induced cardiac glycogen accumulation may be a contributing factor to diastolic dysfunction. Thus, deciphering the molecular mechanisms underlying diabetic cardiac glycogen pathology may provide novel therapeutic targets for diabetic cardiomyopathy.

3.1.1. Heart disease is highly prevalent in diabetes

According to the International Diabetes Federation, 425 million people are currently living with diabetes worldwide[2]. Approximately half of the diagnosed patients develop a distinct type of heart disease[11] that is characterised by early manifestation of diastolic dysfunction[20-22] and is not necessarily accompanied by systolic functional decline[21,31,32]. Furthermore, diabetic cardiomyopathy is often displayed in absence of hypertension or vascular complications[23-26] suggesting that the molecular mechanisms underlying this pathology are distinct. Numerous studies using rodent models of both type 1 (T1D) and type 2 diabetes (T2D) have indicated that diabetes-induced diastolic dysfunction is most often the result of increased cardiomyocyte stiffness leading to aberrant ventricular filling[6-8,10,27]. Currently, there are no therapeutic approaches for diabetic cardiomyopathy. Thus, further research into novel molecular pathways is needed to provide potential therapeutic targets.

3.1.2. The diabetic heart is paradoxically characterised by glycogen accumulation

In addition to the functional disturbances, there have been incidental reports of altered glycogen levels in the diabetic heart[116-138]. Glycogen is a glucose polymer that serves as an energy storage molecule and is synthesized enzymatically in the cytosol upon insulin-stimulated glucose influx[145,151]. In diabetes, insulin-sensitive tissues operate under glucose-limited conditions, induced either by absence of insulin (T1D) or localized insulin resistance (T2D), and are characterised by reduced

glucose uptake[25]. Thus, these sporadic observations of diabetic cardiac glycogen accumulation would be unexpected and paradoxical and the causes or consequences of elevated cardiac glycogen have not been previously investigated. As discussed in Chapter 1 (Section 1.1.4), extensive research in the Mellor-Delbridge labs has demonstrated that glycogen accumulation is a consistent feature of the diabetic heart and that there is a direct positive correlation between the extent of cardiac glycogen deposition and diastolic dysfunction. Although the mechanisms via which glycogen may influence the manifestation of diastolic dysfunction are not understood, it seems that glycogen handling pathways may be potential therapeutic targets for diabetic heart disease.

3.1.3. Molecular regulation of glycogen handling

Glycogen is a polymer of glucose-1-phosphate molecules that is elongated enzymatically by glycogen synthase (GS) and branched by glycogen branching enzyme (GBE)[143,144]. In the absence of pathology, increased energy demand or nutrient deprivation leads to glycogen breakdown that occurs either in the cytosol via concerted actions of glycogen phosphorylase (GP) and glycogen debranching enzyme (GDE)[145] or in the lysosome, through pH-activation of α-acid glucosidase (GAA)[148,149,167]. Cytosolic cardiac glycogen handling has been well investigated and is governed by a multitude of pathways including insulin and 5' AMP-activated protein kinase (AMPK) signalling. These pathways act in concert to activate or inhibit glycogen synthesis via different mechanisms depending on the cellular energy status[182-191]. For example, insulin-activated AKT Serine/Threonine Kinase 1 (AKT) has been shown to inhibit glycogen synthase kinases 3α and 3β thereby alleviating the inhibition on GS and promoting glycogen synthesis[188,189,191]. Similarly, AMPK has been reported to act directly on GS and GP thereby inhibiting glycogen synthesis and promoting glycogenolysis[184,190]. In the past decade, lysosomal glycogen breakdown has been placed in context of selective autophagy due to the discovery of Starch binding domain 1 (STBD1); a glycogen binding protein that interacts with phagosome-residing molecules (Autophagy related 8, ATG8s)[146,147,162]. Insulin signalling and AMPK have also been implicated in the regulation of autophagy in the heart and have been shown to have opposing roles in activation of the pathway[98,205,227-229]. Low energy status is linked to AMPK-induced activation of mammalian Target of rapamycin (mTOR) thereby promoting autophagy via phosphorylation of Unc-51 like autophagy activating kinase (ULK1)[227]. In

contrast, insulin-induced AKT activation suppresses mTOR leading to inhibition of autophagy[205]. Interestingly, a recent study using mouse embryonic fibroblasts showed that amino acid starvation (traditionally an mTOR activator) resulted in decreased glycogen levels. This was due to glycogen autophagy (glycophagy) induction as shown by concurrent treatment with the lysosome inhibitor Bafilomycin A[223]. Thus, it is likely that glycophagy regulation is similar to that of autophagy but further research into glycophagy stimuli, particularly in the heart, is critical. In the diabetic heart, pathways traditionally known to regulate glycogen content are disturbed but the changes appear compensatory relative to increased glycogen deposition. For example, decreased or unchanged activity of GS and increased activity of GP have been reported in studies using rodent models of diabetes[120,126,131,137,152,166]. Similarly, autophagy disturbances in the diabetic heart have been extensively investigated in both diabetic models and human patients but there appears to be no agreement on the response of the pathway to diabetic stimuli[77,91-113]. Thus, further research is warranted to determine the molecular mechanisms underlying the cardiac diabetic glycogen pathology.

3.1.4. Aims of study

The study presented in this Chapter aims to determine the key molecular alterations associated with increased glycogen deposition in the diabetic heart. Gene expression was measured using cardiac RNA extracted from T1D and insulin resistant (pre-T2D) rats and T2D mice. Previous investigations by our group have shown that cardiac glycogen accumulation coincident with diastolic dysfunction is a consistent phenotype in these models. RNA was subsequently subjected to custom-designed PCR arrays targeting genes involved in metabolism, glycogen handling, autophagy and apoptosis. Additionally, human RNA was obtained from type 2 diabetic and non-diabetic patients. This study is the first to demonstrate that the key glycophagy gene, *Gabarapl1*, is downregulated in both pre-T2D and T2D rodent models of disease also in the human T2D heart.

3.2. Specific methodology

3.2.1. Human myocardial RNA

Following establishment of consensual study participation, human myocardial RNA was extracted from right atrial appendage tissues obtained from male diabetic and non-diabetic patients undergoing coronary artery bypass or aortic valve replacement surgery. Limited amount of these RNA samples were provided by Dr Kim Powell (collaborator, Royal Melbourne Hospital, Australia). The protocols were approved by the Melbourne Health Human Research and Ethics Committee.

3.2.2. Animal models of diabetes

Rodent diabetic models representing T1D, pre-T2D and T2D were used in the RT^2 Profiler PCR Array. Tissues from the dietary pre-type 2 diabetic (pre-T2D) and type 1 diabetic (T1D) models were collected prior to commencement of this doctoral candidature by Dr. Victoria Benson and Jessica Liu at the University of Auckland. Cardiac mRNA samples from type 2 diabetic (T2D) mice (db/db) were obtained from A/Prof. Rebecca Ritchie's laboratory (collaborator, Baker Heart and Diabetes Institute, Melbourne, Australia).

Type 1 diabetes was induced pharmacologically in 10 week old Sprague Dawley rats by Streptozotocin (STZ, 55mg/kg, i.v, Sigma, cat - S0130). Levels of circulating glucose were measured with a calibrated glucometer (ACCUCHECK® Advantage, Roche) weekly. Animals had access to water and diet *ad libitum*. Extraction of cardiac tissue was performed 8 weeks post-STZ administration and as described in Chapter 2 (2.4).

Glucose intolerance (pre-type 2 diabetes) was induced in 8 week old Sprague Dawley rats following high fat/sugar diet feeding (23.5% fat w/w, 20.1% sucrose w/w, SF04-001, Specialty Feeds). Control rats were fed a regular chow (6.2% fat w/w, 5% sucrose w/w, 2018, Envigo). Animals had access to water and diet *ad libitum* and were monitored weekly. Similarly, 8 week old C57/Bl6J mice were fed a high fat/high sugar diet (HFSD, 23% fat w/w, 20.1% sucrose w/w, SF04-001, Specialty Feeds) or a control diet (7% fat w/w, 10% sucrose w/w, AIN93G, Specialty Feeds). Extraction of cardiac tissue was performed as described in Chapter 2 (Section 2.4) 13 weeks post-diet commencement. At this

diet duration, blood glucose levels were confirmed to be unchanged and glucose intolerance was evident (glucose tolerance test).

Type 2 diabetes was investigated using 10 week old C57BLKS/J lepr^{db}/lepr^{db} mice[230]. This model is characterised by leptin deficiency induced by a mutation in the leptin receptor gene. Leptin deficiency induces hyperinsulinemia as early as 10 days of age while hyperglycemia and obesity become apparent at 8 weeks of age[231]. Left ventricular RNA from these mice was extracted as previously described[41,42,232].

3.2.3. Gene expression analysis – RT^2 profiler PCR Array

RNA was extracted from frozen cardiac tissue as described in Chapter 2 (Section 2.8). For RNA samples extracted from T1D and pre-T2D myocardia, 937.6ng of RNA was subjected to reverse transcription using the RT^2 First Strand Kit (Qiagen, cat – 330404) as per manufacturer's instructions and as previously described[29]. RNA was combined with the provided Genomic DNA elimination mix and incubated at 42ºC for 5 minutes. Samples were subsequently combined with the Reverse Transcription mix (2% BC3 Buffer, 0.5% P2 control, 1% RE3 Reverse transcriptase) and incubated at 42ºC for 15 minutes prior to heat-induced reaction arrest. RNA and cDNA quality was verified as per manufacturer's instructions using the RT^2 RNA QC PCR Array (Qiagen, cat – 330291). Detailed explanation of the different controls and sample quality can be found in Supplement 1 (Tables A1.1, A1.2). The custom PCR array plates were designed in house and purchased from Qiagen. The plates were designed so that 57 genes of interest and 2 housekeeping genes (18S and β-actin) were included in all assays. In addition to genes, each assay contained a reverse transcription control (RTC) and a positive PCR control (PPC). The target genes are summarized in Table 3.1. Real time PCR was performed as described in Chapter 2 (2.10). Gene expression was determined using the comparative ΔC_T method as previously described[226]. Ribosomal biogenesis has been shown to be altered in the T1D heart[233]. Thus, 18S was not a stable housekeeper in this setting. Both pre-T2D (HFSD rat) and T2D (db/db mouse) animals displayed significant cardiac hypertrophy which is linked to altered expression of cytoskeletal genes including β-actin[234]. Thus, 18S was chosen as the normalizing gene for these models. The PCR array for db/db samples was designed and run by Dr. Chanchal Chandramouli prior to commencement of this PhD candidature. As a result, there are 13

genes that were different between the mouse- and rat-targeting arrays. This is indicated in Table 3.1. All subsequent analysis and in silico modelling was performed by the author of this Thesis.

3.2.4. Jensen DISEASE classification

The Jensen DISEASE resource combines text-mining with manually curated gene-disease associations, genome-wide association studies and cancer mutation data to determine the likelihood that a single gene or set of candidate genes are associated with a particular human condition[235]. When targeted approaches have been pursued, such as examining gene expression in a tissue of interest under certain conditions, the Jensen DISEASE classification can be interpreted as the resulting associated phenotype in the tissue of interest. To identify the diabetes-associated cardiac phenotype resulting from differential gene expression detected in the RT^2-profiler PCR array, genes found to be statistically significantly different in each model were entered separately into the Enrichr database for curated gene sets[236] to subsequently determine the Jensen DISEASE classification. A p-value and odds ratio was assigned to each human disease linked to a single gene or group of genes in the input dataset. The first 10 diseases (lowest p-value/highest odds ratio) were plotted against the combined score calculated as [*ln(p-val) x odds ratio*].

3.2.5. Functional Network Analysis (STRING)

The genes found to be significantly, statistically different in the myocardia of all 3 diabetic models, were entered into the STRING protein-protein association network analysis[237] to determine common pathways or associations that may be affected in the heart in T2D models. Each association determined by STRING was the result of a combination of text-mining and experimentally determined evidence. The minimum accepted confidence score (minimum probability) for an association was set at 0.7 (0.1:1, lowest:highest). In STRING, confidence scores are calculated by combining the different sources of evidence (e.g. text-mining) and adding the 'true'-positive probabilities for an interaction while simultaneously correcting for the probability of association between 2 randomly chosen proteins, thereby accounting for random observations[238].

Table 3.1: Summary of genes of interest included in the RT^2-profiler PCR arrays for each diabetic model.

		Accession number	
Gene name	**Gene ID**	***Rattus norvegicus***	***Mus musculus***
Amylo-Alpha-1, 6-Glucosidase, 4-Alpha-Glucanotransferase	*Agl*	NM_001108564	NM_001081326
Akt Serine/Threonine Kinase 1	*Akt1*	NM_033230	NM_009652
Autophagy And Beclin 1 Regulator 1	*Ambra1*	NM_001134341	NM_172669
Autophagy Related 12	*Atg12*	NM_001038495	NM_026217
Autophagy Related 16-Like 1	*Atg16l1*	NM_001108809	NM_029846
Autophagy Related 16-Like 2	*Atg16l2*	NM_001191560	NM_001111111
Autophagy Related 3	*Atg3*	NM_134394	NM_026402
Autophagy Related 4b, Cysteine Peptidase	*Atg4b*	NM_001025711	NM_174874
Autophagy Related 4c, Cysteine Peptidase	*Atg4c*	NM_001107948	NM_175029
Autophagy Related 5	*Atg5*	NM_001014250	NM_053069
Autophagy Related 7	*Atg7*	NM_001012097	NM_028835
Autophagy Related 9a	*Atg9a*	NM_001014218	NM_001003917
Bcl2-Associated Agonist Of Cell Death	*Bad*	NM_022698	NM_007522
B-Cell Cll/Lymphoma 2	*Bcl2*	NM_016993	NM_009741
Bcl2-Like 1	*Bcl2l1*		NM_009743
Beclin 1	*Becn1*	NM_053739	NM_019584
Bcl2/Adenovirus E1B Interacting Protein 3	*Bnip3*	NM_053420	NM_009760
Caspase 3	*Casp3*	NM_012922	NM_009810
Cathepsin b	*Ctsb*	NM_022597	NM_007798
Cathepsin d	*Ctsd*		NM_009983
Cathepsin s	*Ctss*	NM_017320	NM_021281
Death Associated Protein Kinase 1	*Dapk1*	NM_001107335	NM_029653
DNA-Damage Regulated Autophagy Modulator 2	*Dram2*	NM_001025018	NM_026013
Epilepsy, Progressive Myoclonus Type 2A	*Epm2a*	NM_001276762	
Forkhead Box O1	*FoxO1*	NM_001191846	
Forkhead Box O3	*FoxO3*	NM_001106395	
Glucosidase, Alpha, Acid	*Gaa*	NM_199118	NM_008064
Gaba Type A Receptor-Associated Protein	*Gabarap*	NM_172036	NM_019749
Gaba Type A Receptor Associated Protein Like 1	*Gabarapl1*	NM_001044294	NM_020590
Gaba Type A Receptor Associated Protein Like 2	*Gabarapl2*	NM_022706	NM_026693
Glucokinase	*Gck*	NM_012565	NM_010292
Solute Carrier Family 2 Member 1	*GLUT1*	NM_138827	
Solute Carrier Family 2 Member 4	*GLUT4*	NM_012751	
Solute Carrier Family 2 Member 8	*GLUT8*	NM_053494	
Glucose-6-Phosphate Isomerase	*Gpi1*		NM_008155
Glycogen Synthase Kinase 3 Alpha	*Gsk3a*	NM_017344	NM_001031667
Glycogen Synthase Kinase 3 Beta	*Gsk3b*	NM_032080	NM_019827
Glycogen Synthase 1	*Gys1*	NM_001109615	NM_030678
Hexokinase 2	*Hk2*	NM_012735	NM_013820
Insulin-Like Growth Factor 1	*Igf1*	NM_178866	NM_010512
Lysosomal-Associated Membrane Protein 1	*Lamp1*	NM_012857	NM_010684
Lysosomal-Associated Membrane Protein 2	*Lamp2*	NM_017068.2	NM_010685
Microtubule-Associated Protein 1 Light Chain 3 Alpha	*Map1lc3a*	NM_199500	NM_025735
Microtubule-Associated Protein 1 Light Chain 3 Beta	*Map1lc3b*	NM_022867	NM_026160
Mechanistic Target Of Rapamycin	*Mtor*	NM_019906	NM_020009

		Accession number	
Gene name	**Gene ID**	***Rattus norvegicus***	***Mus musculus***
Phosphofructokinase, Muscle	*Pfkm*	NM_031715	NM_021514
Phosphoglucomutase 1	*Pgm1*		NM_025700
Phosphoglucomutase 2	*Pgm2*		NM_028132
Phosphoglucomutase 3	*Pgm3*		NM_028352
Phosphorylase Kinase, Alpha 1	*Phka1*	NM_022626	NM_173021
Phosphorylase Kinase Beta Subunit	*Phkb*	NM_001014152	NM_199446
Phosphorylase Kinase, Gamma 1	*Phkg1*	NM_031573	NM_011079
Phosphatidylinositol 3-Kinase, Catalytic Subunit Type 3	*Pik3c3*	NM_022958	NM_181414
Phosphatidylinositol-4,5-Bisphosphate 3-Kinase, Catalytic Subunit Gamma	*Pik3cg*	NM_001106723	NM_020272
Phosphoinositide-3-Kinase, Regulatory Subunit 4	*Pik3r4*	NM_001108777	NM_001081309
PTEN Induced Putative Kinase 1	*Pink1*	NM_001106694	NM_026880
Protein Kinase Amp-Activated Catalytic Subunit Alpha 1	*Prkaa1*	NM_019142	NM_001013367
Phosphorylase, Glycogen, Muscle	*Pygm*	NM_012638	NM_011224
Sirtuin 1	*Sirt1*	NM_001107627	
Sequestosome 1	*Sqstm1*	NM_181550	NM_011018
Starch Binding Domain 1	*Stbd1*	NM_001013988	NM_175096
Tripartite Motif Containing 72	*Trim72*	NM_001077675	
UDP-Glucose Pyrophosphorylase 2	*Ugp2*	NM_001024743	NM_139297
Unc-51 Like Autophagy Activating Kinase 1	*Ulk1*	NM_001108341	NM_009469
WD Repeat Domain, Phosphoinositide Interacting 1	*Wipi1*	NM_001127297	NM_145940

3.3 Results

3.3.1. Cardiac gene expression profiling depends on the type of diabetic insult

Gene expression profiling arrays targeting genes involved in glucose handling, autophagy, metabolism and apoptosis were performed using RNA extracted from type 1 (STZr, T1D) and diet-induced pre-type 2 (HFSDr, pre-T2D) diabetic rat and type 2 (db/db, T2D) diabetic mouse hearts. With the exception of a subset of glucose handling genes, overall the different types of diabetic insult resulted in different cardiac gene expression profiles as evidenced by the contrasting colour patterns depicted in the heat-maps (Fig 3.1). The precise fold change differential expression of each gene relative to the respective control group of each model and the p-values are summarized in Table 3.2.

Glucose handling genes were found to be downregulated in T1D hearts (65-71% decrease, Glucose transporter 1/*Slc2a1*/*Glut1*, Glucose transporter 4/*Slc2a4*/*Glut4*, Hexokinase 2/*Hk2*, $p<0.05$, Fig 3.1, Table 3.2). *Hk2* and *Glut4* were similarly significantly downregulated in pre-T2D (17-41%, $p<0.05$, Fig 3.1, Table 3.2) hearts. In T2D hearts, mRNA expression of *Hk2* was decreased by 45% but it did not reach statistical significance ($p=0.07$, Table 3.2). No changes were detected in the mRNA expression of Phosphofructokinase/*Pfkm* in any diabetic model examined.

Autophagy machinery gene expression was also altered in response to diabetes. In T1D hearts upregulation of autophagy machinery genes was evident (25-53%, Autophagy related 16 like 1/*Atg16l1*, *Atg16l2*, Autophagy related 4b/*Atg4b*, *Atg4c*, *Atg5*, *Atg7*, *Atg9a*, *Atg12*, $p<0.05$, Fig 3.1, Table 3.2). In contrast, pre-T2D cardiac genes involved in autophagy were downregulated (19-41%, *Atg16l1*, *Atg16l2*, *Wipi1*, *Atg3*, *Atg4c*, *Atg12*, $p<0.05$, Fig 3.1, Table 3.2). Similarly, in T2D hearts, expression of autophagy genes was decreased (33-55%, *Atg16l1*, *Atg16l2*, *Atg4c*, *Atg5*, *Atg9a*, *Atg12*, $p<0.05$, Fig 3.1, Table 3.2). Differential expression was also detected in genes involved in autophagic cargo recruitment, autophagosome formation and lysosomal function. In T1D hearts, upregulation of the cargo receptor *Sqstm1* was evident (2-fold, $p<0.05$, Fig 3.1, Table 3.2) and was accompanied by increased expression of autophagosome (37-44%, Microtubule associated protein 1 light chain 3a/*Map1lc3a*, *Map1lc3b*, γ-aminobutyric acid receptor-associated protein like 1/*Gabarapl1*, $p<0.05$, Fig 3.1, Table 3.2) and lysosome markers (27-62%, Lysosome-associated

membrane protein 2/*Lamp2*, Cathepsin b/*Ctsb*, *Ctss*, p<0.05, Fig 3.1, Table 3.2). In contrast, the phagosome markers *Gabarapl1* and *Gabarap* were downregulated in pre-T2D (20-25%, p<0.05, Fig 3.1, Table 3.2) hearts. *Gabarapl1* downregulation was also evident in T2D hearts (57%, p<0.05, Fig 3.1, Table 3.2). This was not coincident with changes in expression of other phagosome or lysosome markers with the exception of a 33% decrease in the expression of *Sqstm1* in T2D hearts (p<0.05, Fig 3.1, Table 3.2).

Autophagy induction signalling displayed variable differential expression according to the type of diabetic insult. In T1D hearts, members of the phosphatidyl-inositol 3 kinase (PI3K) complex were upregulated (29-30%, Phosphatidylinositol 3-kinase catalytic subunit type 3/*Pik3c3*, Phosphatidylinositol 3-kinase regulatory subunit type 4/*Pik3r4*, p<0.05, Fig 3.1, Table 3.2) but this was not accompanied by changes in expression of Beclin1/*Becn1* (core member of the kinase complex). In contrast, in pre-T2D and T2D hearts, downregulation of *Pik3c3* (24-44%, p<0.05, Fig 3.1, Table 3.2) was evident while in pre-T2D hearts, this was coincident with decreased expression of *Becn1* (26%, p<0.05, Fig 3.1, Table 3.2). Unc-51 like Autophagy Activating Kinase 1/*Ulk1* was decreased by 52% in T2D (p<0.05, Fig 3.1, Table 3.2) and by 23% decreased in pre-T2D (p=0.051, Table 3.2) and was not changed in T1D hearts.

Metabolic and insulin signalling was evidently altered in response to different diabetic insults. Protein Kinase AMP-Activated Catalytic Subunit α 1/*Prkaa1* was significantly upregulated in T1D (53%, Fig 3.1, Table 3.2) but was downregulated in both pre-T2D (49%, p<0.05, Fig 3.1, Table 3.2) and T2D (43%, p<0.05, Fig 3.1, Table 3.2) hearts. In pre-T2D hearts, reduction in expression of *Prkaa1* was coincident with downregulation of AKT Serine/Threonine Kinase 1/*Akt1* (21%, p<0.05, Fig 3.1, Table 3.2) and Phosphatidylinositol-4,5-Bisphosphate 3-Kinase Catalytic Subunit γ/*Pik3cg* (26%, p<0.05, Fig 3.1, Table 3.2).

Apoptosis genes were significantly upregulated in T1D hearts (26-93%, Bcl2-associated Agonist of Cell Death/*Bad*, B-cell lymphoma 2/*Bcl2*, Bcl2-interacting Protein 3/*Bnip3*, Caspase 3/*Casp3*, Death-associated Protein Kinase 1/*Dapk1*, p<0.05, Fig 3.1, Table 3.2). In contrast, *Bad*, *Bcl2* and *Bnip3* were downregulated in pre-T2D hearts (22-26%, p<0.05, Fig 3.1, Table 3.2). In T2D hearts, expression of genes involved in apoptosis was not changed.

3.3.2. The diabetic cardiac phenotype is classified as a 'Glycogen storage disease'

Given the absence of consistent differences in gene expression between models it was necessary to evaluate whether collectively, the changes in gene expression contribute to particular phenotypes in the heart. The differentially expressed (DE) genes were entered into the Enrichr database to determine their Jensen DISEASE classification. The diseases associated with each DE gene, along with the p-value, odds ratio and combined score for each model are summarised in Tables A1.3-A1.5. The top 10 conditions with the highest combined score are shown in Figure 3.2. For both T1D and T2D hearts, 'Glycogen storage disease' was the classification with the highest combined score (1033.122 and 2517.013 respectively), while 'Glycogen storage disease type V' (comb. score 405.885) was also ranked amongst the top 9 diseases with the highest score in T1D. The pre-T2D cardiac phenotype, resulting from the changes in gene profiling, was associated with 'Glycogen storage disease' (Table A1.3, comb. score 175.444) but also a multitude of lysosomal storage disorders.

3.3.2. Diabetic cardiac glycogen accumulation is not associated with changes in expression of cytosolic glycogen handling enzymes

To determine whether diabetes-induced cardiac glycogen accumulation was associated with changes in cytosolic glycogen handling proteins, several enzymes involved in glycogen metabolism were included in the RT^2 profiler PCR arrays. No differences were detected in mRNA expression of glycogen synthase (GS, *Gys1*) in any model (Fig 3.3a). Expression of glycogen phosphorylase (GP, *Pygm*) was significantly increased in T1D (26%, $p<0.05$) but remained unchanged in pre-T2D and T2D hearts (Fig 3.3b). Glycogen debranching enzyme (GDE, *Agl*) was downregulated by 37% ($p<0.05$) in T2D but no difference was detected in neither T1D nor pre-T2D hearts (Fig 3.3c). Activation of GP is achieved by phosphorylation and is carried out by glycogen phosphorylase kinases. Consequently, glycogen phosphorylase kinases α1 (*Phkα1*), β (*Phkβ1*) and γ1 (*Phkγ1*) were also targeted in the RT^2 profiler PCR arrays. No differences were detected in mRNA expression of *Phkα1* in any model (Fig 3.3d). *Phkβ* was upregulated by 66% ($p<0.05$) in T1D myocardia and mRNA expression of *Phkγ1* was decreased in T2D hearts (47%, $p<0.05$) (Fig 3.3e-f). No further or

consistent differences were detected in the mRNA expression of cytosolic glycogen handling enzymes.

3.3.3. Functional network analysis identifies glycophagy as a target of interest in the diabetic heart

Out of the 57 target genes included in the RT^2 profiler PCR arrays, 35 were significantly differentially expressed in T1D, 24 in pre-T2D and 16 in T2D hearts. As depicted in the venn diagrams in Figure 3.4a, the T1D model exhibited a contrasting gene expression profile to the T2D models. No common genes were detected to be differentially expressed in all 3 models. In contrast, 8 genes (*Prkaa1*, *Pik3c3*, *Atg12*, *Atg16l1*, *Atg16l2, Gabarapl1, Gaa and Dram2)* exhibited significant downregulation (20-57%, $p<0.05$) in both pre-T2D and T2D models (Fig 3.4b). Thus, follow up investigation focused on the T2D state with closer analysis of these common genes. To determine the interactions or associations that could be consistently downregulated in the pre-T2D and T2D heart, the 8 genes that were found to be significantly downregulated were subjected to functional network analysis (STRING, Fig 3.5a). The associations were derived from a combination of experimentally determined interactions and text-mining approaches. The annotation and accession numbers of the 8 input genes and 50 genes identified by STRING analysis are summarized in Table A1.6. In total, 443 associations were identified, out of which 126 were between the 8 input genes and those identified ('discovered') in the analysis (primary interactions, Table A1.7). The remaining 317 associations were detected between 'discovered' genes identified in STRING (secondary interactions, Table A1.8). Interestingly, a key glycogen-binding element, Stbd1 (starch-binding domain 1), was identified to have a primary association with the differentially expressed gene Gabarapl1 (combined score 0.815). Further STRING analysis using the same lines of evidence and *Stbd1* alone as the input gene, showed that its association with *Gabarapl1* provides a link between glycogen handling and autophagy (Fig 3.5b). The annotations, primary and secondary interactions identified in the *Stbd1* network analysis are summarized in Tables A1.9 – A1.11.

3.3.4. Glycogen autophagy is disturbed in the diabetic heart

Following identification of glycogen autophagy (glycophagy) as a pathway that may be downregulated in the pre-T2D and T2D heart, closer examination of the mRNA expression of 3 key glycophagy-involved markers was performed. A pre-T2D mouse model (high fat/sugar diet, HFSD) was included in these analyses to ensure validation of findings in a feasible model for future *in vivo* gene manipulation studies. Expression of the gene encoding for the glycogen-tagging protein STBD1 was unchanged in pre-T2D and T2D models (Fig 3.6a). The Atg8 homologue, Gabarapl1 mRNA expression was significantly downregulated in pre-T2D and T2D rodent models of diabetes (25% pre-T2D rat, 63% pre-T2D mouse, 57% T2D mouse) and was trending towards downregulation in atrial appendage tissues extracted from human patients undergoing coronary artery bypass or aortic valve replacement surgery (30%, $p=0.06$, Fig 3.6b). The lysosomal glycogen degrading enzyme, α-acid glucosidase (Gaa), was either unchanged (pre-T2D mouse) or downregulated (21% pre-T2D rat, 23% T2D mouse, $p<0.05$) in the diabetic hearts (Fig 3.6c). Together, these data suggest that glycophagy may be consistently downregulated in the pre-T2D and T2D heart.

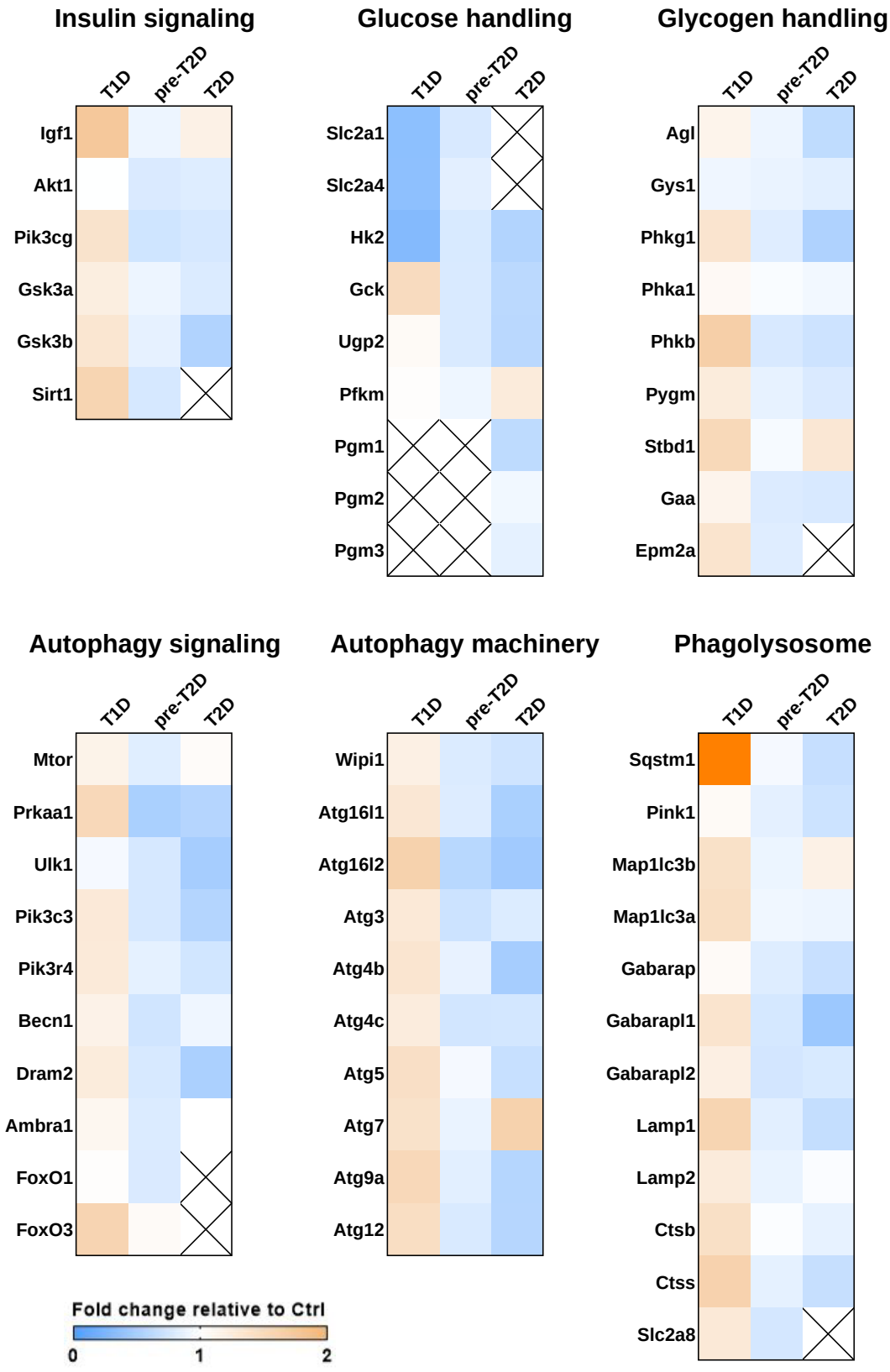

Figure 3.1: Diabetic cardiac glycogen overload cannot be explained by consistent differences in gene expression. Type 1 diabetes (T1D, 8 week STZ rat), pre-type 2 diabetes (pre-T2D, 13 week high-fat/sugar diet) and type 2 diabetes (T2D, leptin receptor mutant, db/db mouse). Genes are grouped by functional association into Insulin signalling, Glucose handling, Glycogen handling, Autophagy signalling, Autophagy machinery and phagolysosome factors. Data are presented as fold change relative to control for each model (n=3-7 animals per group). Upregulation (fold change >1) and downregulation (fold change <1) are shown in orange and blue respectively. Genes not included in some assays are indicated by a cross.

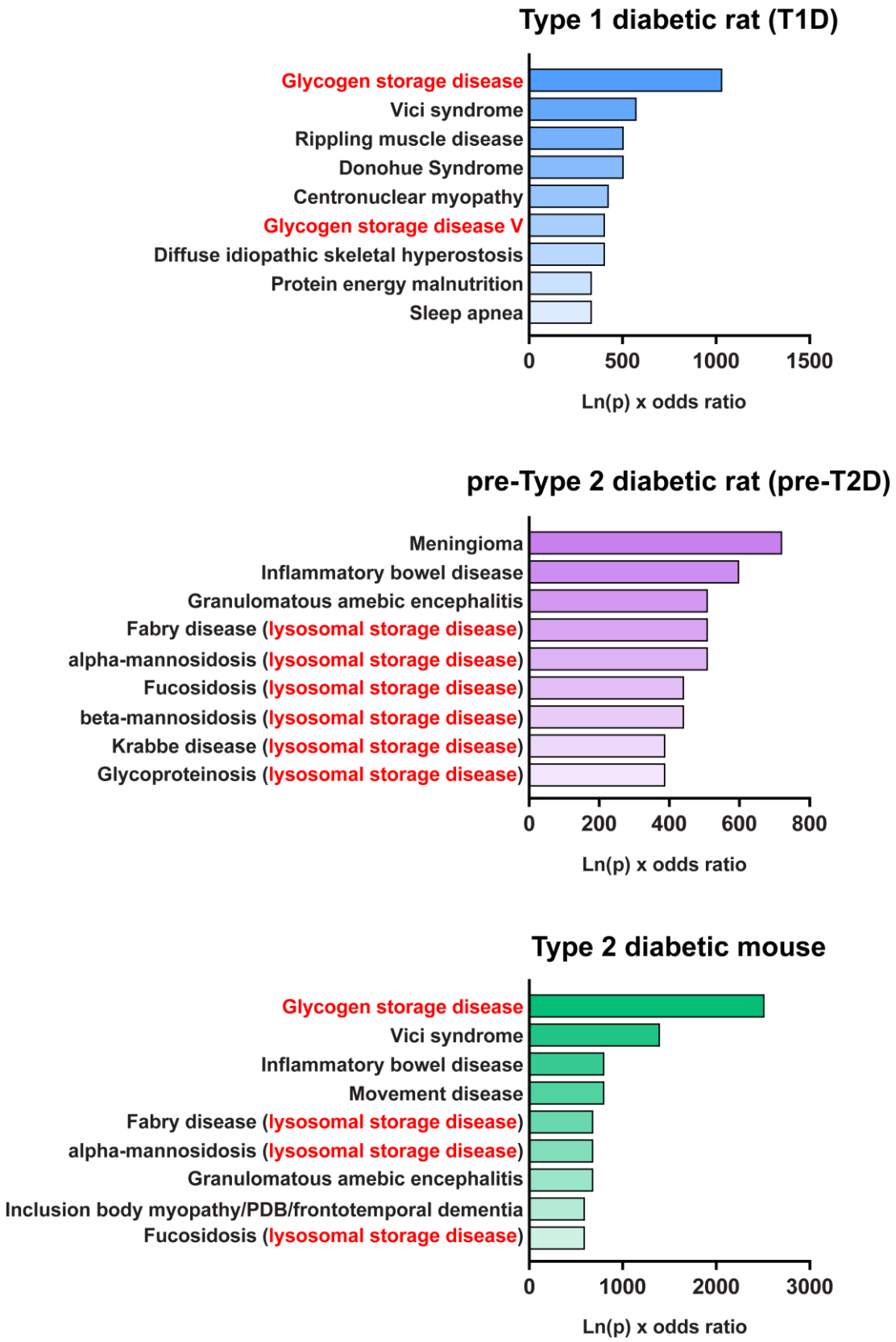

Figure 3.2: The diabetic heart is phenotypically classified as a Glycogen storage disease. type 1 diabetes (T1D, 8 week STZ rat, blue), pre-type 2 diabetes (pre-T2D, 13 week high fat/sugar diet, purple) and type 2 diabetes (T2D, leptin receptor mutant, db/db mouse, green). Diseases are plotted against the combined score derived from the p-value (signifying the statistical significance of the association) and the odds ratio (strength of association between observation and outcome).

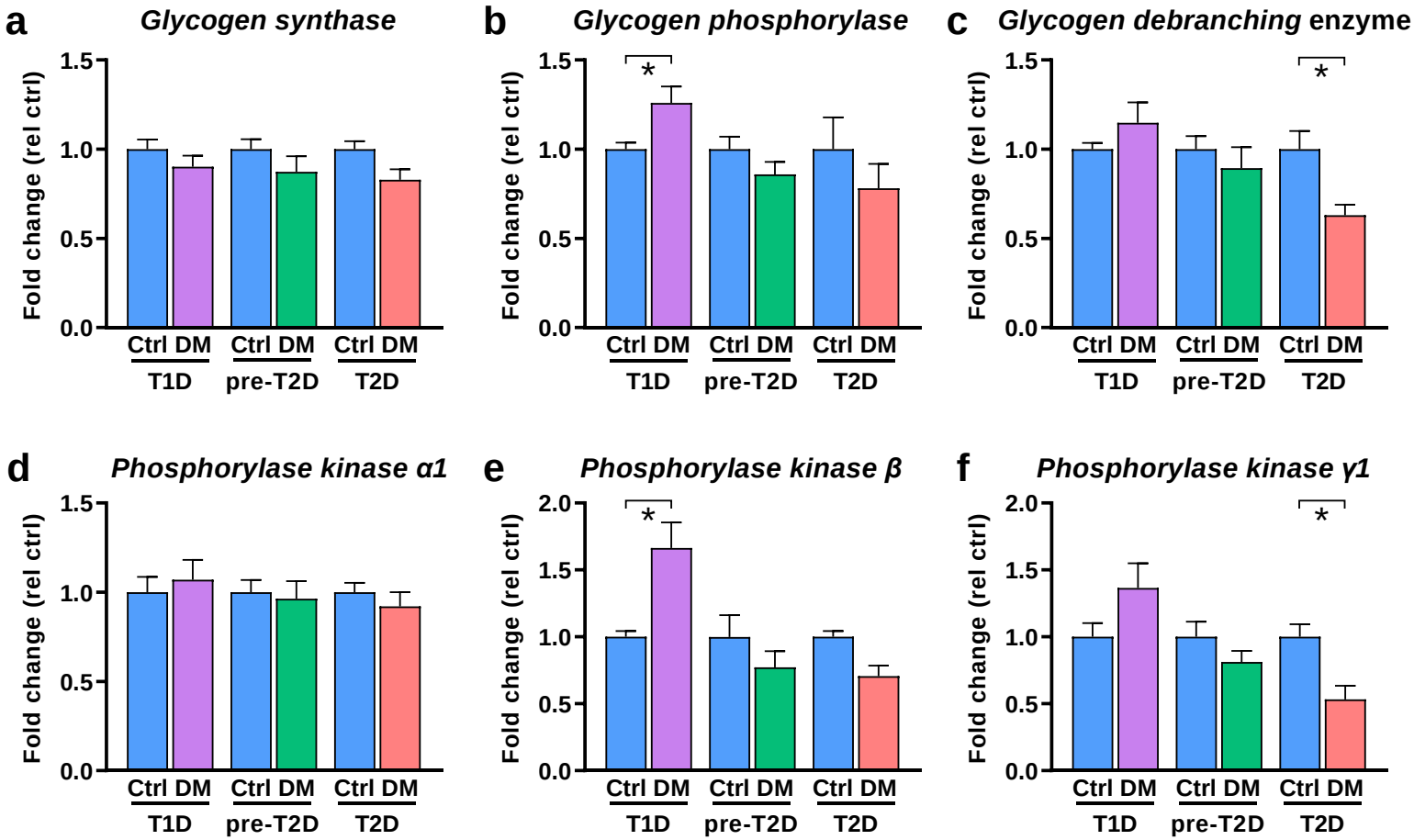

Figure 3.3: Diabetic cardiac glycogen accumulation cannot be explained by differences in the expression of the cytoplasmic glycogen handling enzymes. **(a)** Glycogen synthase (*GS*) mRNA expression, **(b)** Glycogen phosphorylase (*GP*) mRNA expression, **(c)** Glycogen debranching enzyme (*GDE or Agl*) mRNA expression, **(d)** Phosphorylase kinase α1 (*Phkα1*) mRNA expression, **(e)** Phosphorylase kinase β (*Phkβ*) mRNA expression and **(f)** Phosphorylase kinase γ (*Phkγ1*) mRNA expression in the type 1 diabetic rat heart (STZr, purple), pre-type 2 diabetic rat heart (HFSDr, green) and type 2 diabetic mouse heart (db/db, pink)**.** Data analysed with Student's t-test for each model and gene. Data presented as mean fold change (relative to the respective control group for each model) ±SEM, *p<0.05, n=3-7 animals per group.

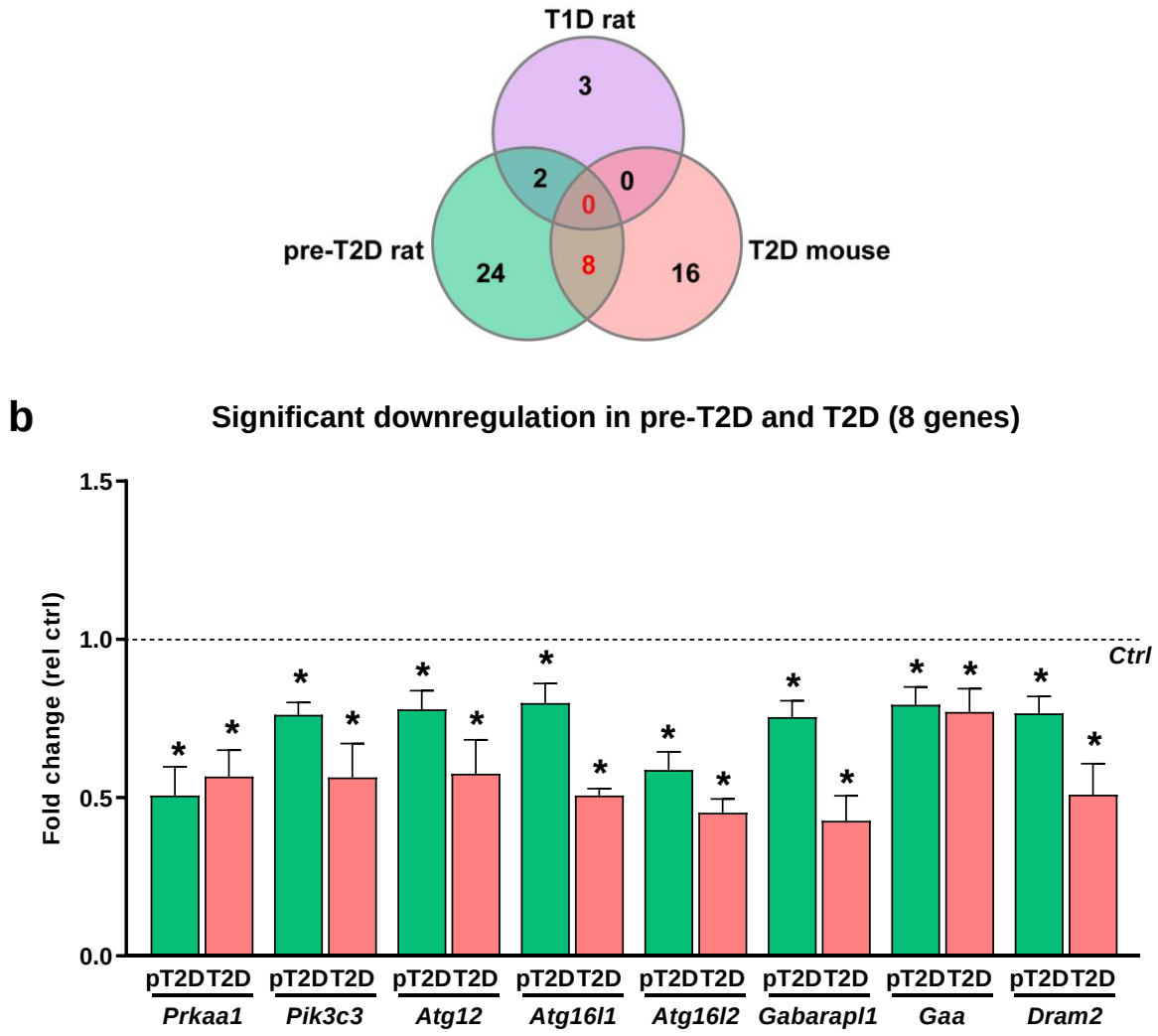

Figure 3.4: Significant downregulation in pre-T2D and T2D rodent models. (a) Venn diagram depicting the number of genes found to be significantly downregulated in each diabetic model separately, the overlapping gene numbers between pairs of models and all models collectively. (b) mRNA expression of the 8 statistically significantly downregulated genes (Prkaa, Pik3c3, Atg12, Atg16l1, Atg16l2, Gabarapl1, Gaa and Dram2) in pre-type 2 diabetic rat heart (pT2D, HFSDr, green) and type 2 diabetic mouse heart (db/db, pink) (n=3-7 animals per group). Data were analysed by Student's t-test. Data are presented as mean fold change (relative to the respective control group for each model) ±SEM, control is set to 1, *p<0.05.

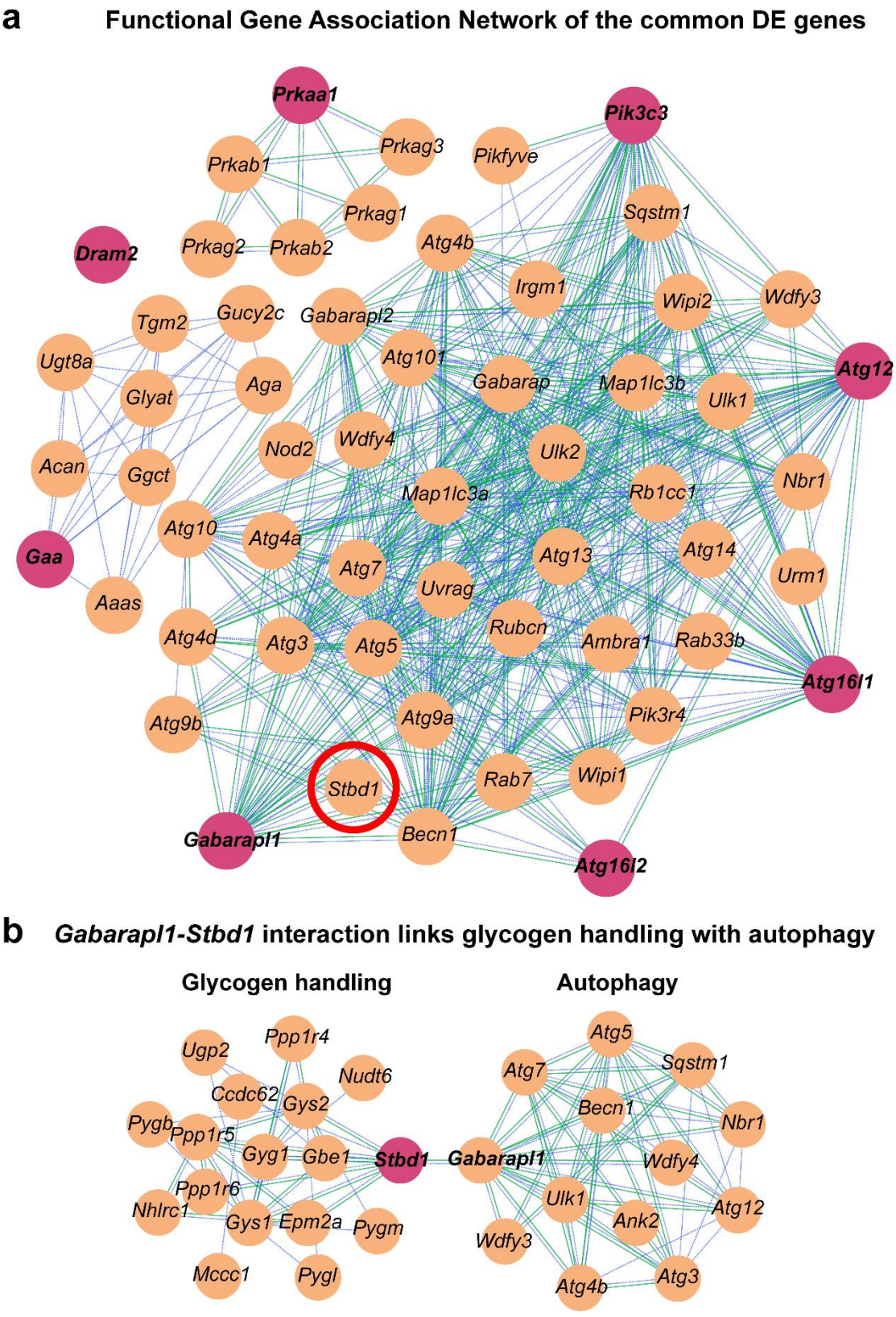

Figure 3.5: Functional Association analysis (STRING) identifies glycophagy as a potential pathway of interest in the type 2 diabetic heart. (a) Interactions affected by the differential expression of the 6 consistently downregulated genes detected in type 2 diabetic models. DE genes are shown in dark pink nodes and associated genes are shown in orange nodes. **(b)** The interaction between *Stbd1* and *Gabarapl1* links autophagy and glycogen handling. Blue dotted lines represent text-mining evidence. Green lines depict experimentally determined interactions.

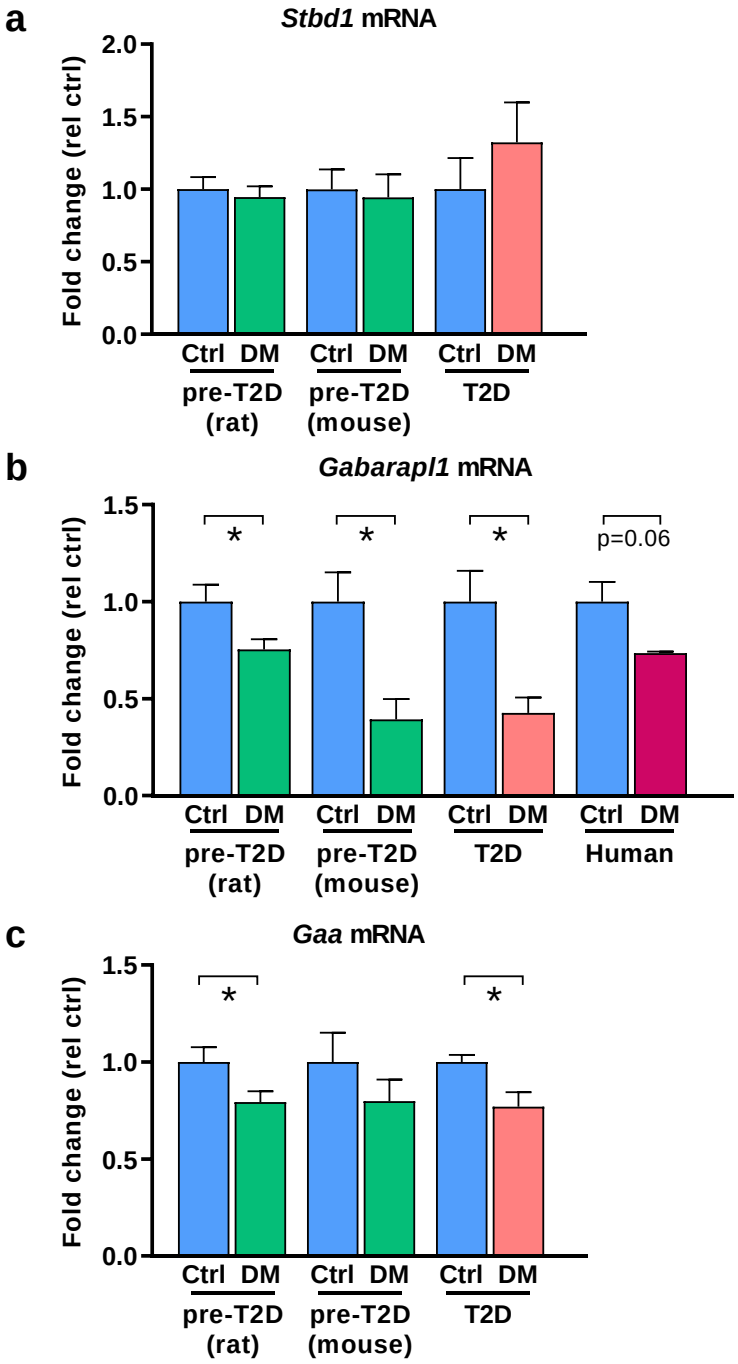

Figure 3.6: Glycophagy genes are downregulated in the diabetic myocardium. (a) Cardiac *Stbd1* mRNA expression in rodent diabetic models (pre-T2D rat, pre-T2D mouse and T2D mouse, n=3-9 animals per group). **(b)** Cardiac *Gabarapl1* mRNA expression in rodent diabetic models (pre-T2D rat, pre-T2D mouse and T2D mouse, n=3-9 animals per group) and human diabetic patients (n=3 samples per group). **(c)** Cardiac *Gaa* mRNA expression in rodent diabetic models (pre-T2D rat, pre-T2D mouse and T2D mouse, n=3-9 animals per group). Data analysed with Student's t-test for each model and gene. Data presented as mean fold change (relative to the respective control group for each model) ±SEM, *p<0.05.

Table 3.2: Summary of gene expression detected in the RT^2-profiler PCR arrays for each diabetic model.

	T1D (STZ rat)		pre-T2D (HFSD rat)		T2D (db/db mouse)	
Gene ID	**Fold change**	**p-value**	**Fold change**	**p-value**	**Fold change**	**p-value**
Agl	1.15	0.31	0.89	0.46	0.63	0.03
Akt1	0.99	0.94	0.78	0.03	0.80	0.31
Ambra1	1.11	0.25	0.79	0.049	1.00	0.98
Atg12	1.45	<0.01	0.78	0.01	0.58	0.03
Atg16l1	1.33	0.02	0.80	0.03	0.51	<0.01
Atg16l2	1.62	<0.01	0.59	<0.01	0.45	<0.01
Atg3	1.30	0.07	0.70	<0.01	0.80	0.35
Atg4b	1.36	<0.01	0.87	0.17	0.48	<0.01
Atg4c	1.25	0.048	0.74	0.02	0.74	0.10
Atg5	1.44	<0.01	0.94	0.47	0.67	0.02
Atg7	1.40	0.02	0.87	0.22	1.62	0.34
Atg9a	1.53	<0.01	0.83	0.11	0.57	<0.01
Bad	1.26	<0.01	0.78	0.048	0.89	0.63
Bcl2	1.41	<0.01	0.73	<0.01	0.61	0.23
Bcl2l1					0.82	0.53
Becn1	1.17	0.21	0.73	<0.01	0.91	0.70
Bnip3	1.33	0.02	0.73	<0.01	0.62	0.10
Casp3	1.38	<0.01	0.82	0.15	0.52	0.26
Ctsb	1.43	<0.01	0.98	0.8	0.86	0.56
Ctsd					0.89	0.58
Ctss	1.62	<0.01	0.85	0.15	0.67	0.47
Dapk1	1.93	<0.01	0.96	0.78	0.66	0.05
Dram2	1.26	0.06	0.77	0.04	0.51	0.04
Epm2a	1.37	<0.01	0.81	0.09		
FoxO1	1.02	0.85	0.78	0.08		
FoxO3	1.58	<0.01	1.06	0.58		
Gaa	1.14	0.06	0.79	0.048	0.77	0.049
Gabarap	1.06	0.6	0.80	0.03	0.68	0.31
Gabarapl1	1.37	0.01	0.75	0.03	0.43	0.03
Gabarapl2	1.21	0.08	0.74	0.07	0.77	0.40
Gck	1.49	0.31	0.78	0.24	0.61	0.11
GLUT1	0.34	<0.01	0.77	0.12		
GLUT4	0.34	<0.01	0.83	0.02		
GLUT8	1.30	0.02	0.75	0.03		
Gpi1					0.98	0.96
Gsk3a	1.23	0.01	0.89	0.22	0.79	0.20
Gsk3b	1.34	<0.01	0.85	0.14	0.54	0.06
Gys1	0.90	0.26	0.87	0.24	0.83	0.08
Hk2	0.29	<0.01	0.77	0.02	0.55	0.07
Igf1	1.76	0.06	0.89	0.34	1.19	0.77
Lamp1	1.58	0.09	0.83	0.41	0.66	0.06
Lamp2	1.27	<0.01	0.87	0.17	0.97	0.86
Map1lc3a	1.44	<0.01	0.91	0.63	0.89	0.70
Map1lc3b	1.41	<0.01	0.89	0.22	1.19	0.58
Mtor	1.16	0.07	0.82	0.06	1.04	0.84
Pfkm	1.02	0.86	0.90	0.35	1.27	0.44
Pgm1					0.62	0.07
Pgm2					0.92	0.60
Pgm3					0.85	0.62

	T1D (STZ rat)		pre-T2D (HFSD rat)		T2D (db/db mouse)	
Gene ID	**Fold change**	**p-value**	**Fold change**	**p-value**	**Fold change**	**p-value**
Phka1	1.07	0.63	0.96	0.2	0.92	0.46
Phkb	1.66	<0.01	0.77	0.28	0.71	0.10
Phkg1	1.37	0.08	0.81	0.2	0.53	0.03
Pik3c3	1.30	0.01	0.76	0.02	0.56	0.02
Pik3cg	1.39	0.11	0.72	0.02	0.76	0.59
Pik3r4	1.29	<0.01	0.85	0.13	0.73	0.09
Pink1	1.07	0.44	0.84	0.21	0.70	0.02
Prkaa1	1.53	0.01	0.51	<0.01	0.57	0.04
Pygm	1.26	0.02	0.86	0.18	0.78	0.39
Sirt1	1.58	0.02	0.76	0.01		
Sqstm1	2.10	<0.01	0.94	0.56	0.67	0.049
Stbd1	1.53	0.02	0.95	0.64	1.32	0.41
Trim72	1.13	0.18	0.79	0.12		
Ugp2	1.06	0.59	0.78	0.01	0.60	0.09
Ulk1	0.94	0.48	0.76	0.05	0.48	0.03
Wipi1	1.20	0.08	0.79	0.04	0.72	0.46

Data analysed with Student's t-test for each model and gene. Data presented as mean fold change (relative to the respective control group for each model), *p<0.05.

3.4. Discussion

The study presented in this Chapter is a systematic evaluation of myocardial gene expression in rodent models representing 3 types of diabetes, type 1 (T1D), type 2 (T2D) and glucose intolerance (pre-T2D). This is the first investigation to phenotypically characterize the diabetic cardiac phenotype as a Glycogen storage disease and link diabetic cardiac glycogen accumulation, systematically demonstrated by investigation in the Mellor-Delbridge labs, with disturbances in the glycogen-specific autophagy pathway, glycophagy. Glycophagy was identified as a pathway of interest in the diabetic heart through computational functional network analysis and was subsequently demonstrated experimentally to be consistently downregulated in rodent models of pre-T2D and T2D and also in the human T2D myocardium.

3.4.1. Cardiac gene expression profiles depend on the underlying diabetic aetiology

The aim of this study was to assess cardiac gene expression profiles in order to identify consistent maladaptations that could be the underlying source of diabetes-induced glycogen accumulation. It is evident that expression of genes included in the study depends largely on the type of diabetic aetiology and that no consistent differences between 3 diabetic models were identified that could profoundly explain the diabetic cardiac glycogen phenotype. Glycogen accumulation in the diabetic heart is a rather paradoxical phenomenon due to the decreased glucose uptake by the myocardium. In this study, expression of *Glut4* (Solute carrier family 2, facilitated glucose transporter member 4/*Slc2a4*), the primary glucose transporter responsible for glucose uptake, was decreased in both T1D and pre-T2D hearts (not measured in T2D) indicating that there is reduced glucose influx. Interestingly, expression of *Akt1* in T1D hearts was not changed indicating that despite reduced insulin stimulation, downstream signalling remains, at least partially, intact and may not fully account for downregulation of *Glut4*. In contrast, in pre-T2D hearts *Akt1* was downregulated, which can result in downregulation of *Glut4* as AKT-mediated transcriptional regulation of this glucose transporter has been previously reported[239]. Reduced glucose uptake is also reflected by significant downregulation of Hexokinase 2 (*Hk2*) in both T1D and pre-T2D hearts (45% reduced, not significant in T2D hearts). Together, these findings demonstrate that glucose uptake in the diabetic heart is decreased and

highlight the paradoxical nature of the diabetic cardiac glycogen phenotype. Thus, further research is required to identify the mechanisms associated with glycogen accumulation in the diabetic heart.

Autophagic maladaptation has also been reported in the diabetic heart although there is currently no agreement in the literature on whether autophagic alterations depend on diabetic aetiology. In this study, autophagy was upregulated in T1D hearts as evidenced by increased mRNA expression of genes involved in autophagy induction, phagosome and lysosome markers. Similar to this study, autophagy upregulation in T1D rat hearts has also been reported in the literature[172,240] and interestingly, to date, there are no investigations reporting downregulation of autophagy in this model indicating that the severe STZ-induced energy deprivation drives a maladaptive pathway response. Increased autophagy may also lead to apoptosis[241], which could explain the upregulation detected in apoptosis-related factors (*Bad*, *Bcl2*, *Bnip3*, *Casp3*, *and Dapk1*). In contrast to T1D, autophagy was downregulated in pre-T2D rat and T2D mouse hearts. The finding that autophagy is downregulated in T2D hearts is in agreement with reports in the literature that have also shown autophagic downregulation in the db/db mouse myocardium[102,103]. In contrast, counter to this study, investigations have only reported increased protein and mRNA expression in the diet-induced glucose intolerant myocardium[95,100]. However, the reported assessments were performed at different diet durations than this study indicating that a relationship between disease progression and autophagy response may exist. In this study, pre-T2D hearts were also characterised by downregulation of apoptotic markers which was absent from the T2D myocardia even though increased apoptosis has been previously shown in the db/db hearts[242]. Further investigations involving histological staining or quantification of protein expression may elucidate the activity of the apoptotic pathway in these hearts.

Interestingly, and despite the absence of consistent differences in gene expression, model-specific enrichment of the significantly altered genes for pathological associations in the Jensen DISEASE database resulted in phenotypical classification of the diabetic heart as a glycogen or lysosomal storage disorder. This indicates that even though the underlying molecular disturbances may be dependent on the type of diabetes, the resulting associated glycogen phenotype is common across the diabetic spectrum.

3.4.2. Changes in cytosolic glycogen handling cannot be linked with glycogen accumulation in the diabetic heart

The findings presented in this Chapter indicate that changes in mRNA expression of cytosolic glycogen-handling enzymes fail to account for the diabetes-induced myocardial glycogen accumulation. Cardiac gene expression of glycogen synthase (GS, *Gys1*) was unchanged in all models included in this study. This implies that increased glycogen deposition is unlikely to be the result of increased synthesis. While mRNA expression is not always indicative of enzyme activity, unpublished data generated in the Mellor lab showed that in T1D rat hearts GS is highly phosphorylated (7-fold increase of pGS relative to total) indicating enzyme inactivity. In this study, *Gsk3α* and *Gsk3β* were upregulated in T1D hearts which could explain the inhibition of GS[188,189,191] demonstrated in previous experiments. Phosphorylation of GS was also increased in T2D mouse myocardia (Mellor-Delbridge labs, unpublished) although expression of *Gsk3α* and *Gsk3β* was not changed in this model. In pre-T2D rat hearts, mRNA expression of GS was not changed and neither were phosphorylated levels of the enzyme (Mellor-Delbridge labs, unpublished) although insulin signalling was downregulated as evidenced by decreased expression of *Akt1*. In addition to findings presented in this Chapter and unpublished data from the Mellor lab, GS has been reported unchanged or inactive in rodent models of diabetes in the literature[126,131,137]. Thus, diabetic cardiac glycogen accumulation is unlikely to be the result of elevated polysaccharide synthesis. Furthermore, GS phosphorylation may be a compensatory response to the increased glycogen deposition, although it is likely that the molecular signals underlying enzyme inhibition depend on the diabetic aetiology.

Similarly to GS, changes in mRNA expression of GP (*Pygm*), or the enzymes regulating its activity, cannot account for diabetes-induced cardiac glycogen overload. In T1D rat hearts, mRNA expression of GP and *Phkβ* (regulatory subunit of Phosphorylase kinase β that phosphorylates and activates GP) were increased, reiteratively indicating the presence of a compensatory response. Furthermore, immunoblot data showed increased phosphorylation of GP in these hearts indicating enzyme activation (Mellor-Delbridge labs, unpublished). Interestingly, phosphorylated GP levels have been shown to be increased in rat hearts as early as 2 days following streptozotocin

administration[120], indicating that glycogen mishandling in the diabetic myocardium appears early on in the progression of the disease. In T2D mouse hearts mRNA expression of GP was not changed but expression of *Phkγ1*, catalytic subunit of Phosphorylase kinase β, was decreased indicating that cytosolic glycogen breakdown may be impaired due to decreased GP activation. In addition, AMPK (catalytic subunit, *Prkaa1*), that has been shown to directly activate GP[184,190], was also decreased in T2D hearts indicating that there may be reduced availability of GP activators. Intriguingly however, phosphorylated GP levels were unchanged in T2D mouse hearts following immunoblot assessment (Mellor lab, unpublished) implying that decrease in mRNA expression of *Phkγ1* or AMPK did not have a profound impact on the activity of GP. Together, findings presented in this Chapter in conjunction with unpublished data and published reports demonstrate that diabetes-induced cardiac glycogen accumulation cannot be attributed to alterations in expression or activity of GP.

3.4.3. Glycophagy is disturbed in the pre-type 2 and type 2 diabetic heart

The findings presented in this Chapter, through experimental and computational means, identified glycophagy as a pathway consistently downregulated in the pre-type 2 and type 2 diabetic heart. Broadly, and as in all selective autophagy branches, glycophagy can be divided into three stages. First, for glycophagy to proceed, glycogen must be tagged for lysosomal breakdown by the glycophagy-specific cargo receptor Starch-binding domain 1 (STBD1)[146]. The STBD1-glycogen complex is subsequently transferred to the forming phagosome where STBD1 anchors to membrane-bound γ-aminobutyric acid receptor-associated protein like 1 (GABARAPL1)[147], thereby tethering glycogen in the phagosome. At the late stages of the process, mature glycogen-containing phagosomes fuse with lysosomes where α-acid glucosidase (GAA) hydrolyzes the glycosidic bonds thereby releasing glucose-1-phosphate molecules[148,149,167]. In this study, *Stbd1* mRNA expression was found to be unchanged in the diabetic hearts from pre-T2D (HFSD rat, HFSD mouse) and T2D (db/db mouse) rodent diabetic models, potentially implying that tagging of glycogen for lysosomal breakdown remains intact. In contrast to *Stbd1*, cardiac *Gabarapl1* was found to be downregulated in all pre-T2D and T2D rodent models included in the study and in atrial appendage tissues collected from diabetic patients. This demonstrates that in these models, even though glycogen tagging by STBD1 appears intact, sequestration of tagged glycogen to the forming phagosome may be

disturbed due to reduced availability of *Gabarapl1*. Interestingly, mRNA expression of *Foxo3*, a known transcription factor for *Gabarapl1*[243], was not changed in pre-T2D hearts, indicating that *Gabarapl1* transcriptional downregulation was the result of different mechanism. *Gaa* mRNA expression displayed an approximate 20% reduction in pre-T2D rat and T2D mouse myocardia. *Gaa* mutations are associated with Glycogen storage disease type II (Pompe's disease) which results in glycogen accumulation in various tissues including the heart[166,244]. It is therefore likely that in pre-T2D and T2D hearts, multi-stage dysregulation of glycophagy contributes to the glycogen phenotype.

This study demonstrates that glycophagy is dysregulated in the diabetic heart and in particular, the phagosome marker *Gabarapl1* is downregulated in pre-T2D and T2D rodent models of disease. While the importance of cardiac lysosomal glycogenolysis is evident from the multitude of cardiac abnormalities associated with glycogen storage diseases[244,245], a role for glycophagy has not been described in the heart. It is therefore important to determine whether GABARAPL1 can be linked with cardiac glycogen pathology in order to identify with certainty that glycophagy disturbances contribute to the diabetic cardiac glycogen phenotype.

3.5 Conclusions and next steps

The study presented in this Chapter is the first to provide a link between diabetic cardiac glycogen accumulation and the glycogen-specific autophagy pathway, glycophagy. It is demonstrated that the mRNA expression of the key molecular mediator of glycophagy, *Gabarapl1*, is decreased in the diabetic heart and that downregulation is a consistent observation across rodent models of pre-T2D and T2D and also in the human diabetic myocardium. However, the role of GABARAPL1 and glycophagy in the heart has not yet been described. This shaped the direction of this Thesis to investigate, through genetic manipulations, the impact of reduced *Gabarapl1* availability on cardiac glycogen handling.

3.6. Limitations

Whilst this study has provided key evidence to suggest that glycophagy disturbance is associated with glycogen mishandling in diabetes, there are certain limitations to these studies to consider. STRING is primarily a protein association analysis tool that is built on protein-protein interaction data.

Since within the context of this study this tool was used in association with gene expression data, the interactions identified should be considered indicative and should be followed up by further investigations. In this Thesis, key findings were followed up by examination of mRNA expression of glycophagy markers in several rodent models of diabetes and in human atrial appendage tissues. Noticeably, there was a high degree of variability in gene expression data from the T2D, db/db mouse, likely due to low sample size (n=3/group). The RNA used for this study was extracted from an animal cohort in our collaborator's laboratory, prior to the commencement of this PhD candidature, thus additional samples could not be obtained at this time. Within the context of limited sample availability, it should be mentioned the small amounts of human RNA, derived from atrial appendage tissues, that was provided by our collaborators at Royal Melbourne Hospital did not allow for measurements of mRNA expression of all three glycophagy markers. *GABARAPL1* was chosen because it displayed consistent downregulation in the rodent models of diabetes. It should be mentioned that while the remaining investigations of this Thesis examined ventricular functional and structural alterations as they relate to diabetes-induced diastolic dysfunction, it is evident that human *GABARAPL1* mRNA measurements were performed using atrial tissues. This was due to the fact that human ventricular biopsies were not available. Given the functional differences between the two tissues, it could be expected that reduction in atrial GABARAPL1 mRNA expression would not necessarily be translated to the ventricular phenotype. However, as mentioned in Chapter 1 of this Thesis, atrial glycogen accumulation has been linked with conduction abnormalities, in addition to ventricular dysfunction, in Pompe disease where glycophagy dysregulation is caused by genetic GAA deficiency[246]. Thus, it could be anticipated that in humans, diabetes-induced atrial glycophagy downregulation could reflect a similar ventricular phenotype. Furthermore, it would usually be expected that changes observed at the mRNA level (e.g. Gabarapl1 mRNA downregulation) would be corroborated by measurements of protein levels via immunoblot. ATG8 proteins (including GABARAPL1) constantly shuttle between non-lipidated (cytosolic, inactive) and lipidated (membrane-bound, active) conformations, and a sub-pool of the protein is degraded in the lysosome. Thus, static measurements of protein levels do not necessarily reflect protein or pathway activity. For example, increased ATG8 protein may reflect either ATG8 accumulation due to impaired autophagy flux, or upregulation of the autophagy machinery for increased autophagic drive. As a

result, flux measurements obtained by lysosomal blockade are considered a more robust indication of activity. Parallel studies in the Mellor-Delbridge labs have shown that GABARAPL1 flux through the lysosome is lower in HL1 cardiomyocytes under diabetic conditions (using GFP-tagged GABARAPL1). Similarly, diabetic rat hearts exhibit reduced glycophagy flux (measured by *in vivo* chloroquine lysosomal blockade effect on glycogen). Finally, the data presented in this Chapter have provided mRNA expression evidence to indicate that glucose uptake is reduced in the diabetic heart. However, these findings should be interpreted with caution as they were not followed either by direct protein expression measurements or by examination of downstream enzymes involved in insulin signalling and glucose transporter trafficking.

CHAPTER 4

Gabarapl1 deletion is linked with cardiac glycogen accumulation and diastolic dysfunction *in vivo*

4.1. Introduction

Extensive and comparative research conducted in the Mellor-Delbridge labs has demonstrated that the diabetic heart is consistently characterised by increased glycogen deposition that correlates with diastolic dysfunction (See Fig 1.1, Mellor et al, publication pending). The research findings presented in Chapter 3 of this Thesis highlighted that the diabetic cardiac glycogen pathology is not the result of alterations in expression of cytosolic glycogen handling enzymes but may be due to dysregulated glycophagy (glycogen-specific autophagy). More specifically, the use of computational approaches coupled to mRNA expression data, showed that in pre-T2D and T2D rodent diabetic models and in the human diabetic myocardium, *Gabarapl1* mRNA expression was decreased. This finding provided the basis for the studies undertaken in this Chapter, which aimed to examine the role of GABARAPL1 and glycophagy in the heart.

4.1.1. The role of autophagy in cardiac pathology

Autophagy (from the Greek 'self-eating') is a 'bulk' degradation process that utilizes the acidic environment of the lysosome to break down damaged proteins, organelles and macromolecules in order to regenerate energy and nutrients both basally and during periods of cellular stress. For autophagy to proceed, cargo that is marked for lysosomal breakdown, is tagged by soluble autophagy receptors (SARs) and is then sequestered to forming double-membrane vesicles called phagosomes. In the phagosome, the SARs bind to one of the membrane-tethered Autophagy-related protein 8 (ATG8) homologs through ATG8-interacting motifs (AIMs). Lysosomal recycling of cargo is achieved through phagosome-lysosome fusion. Autophagy has been examined in a multitude of cardiac conditions such as cardiac hypertrophy, heart failure, ischemia/reperfusion and diabetic cardiomyopathy but collectively, there appears to be no agreement on whether alterations in the pathway reflect adaptive or maladaptive responses. For example, inhibition of phagophore elongation by *Atg5* deletion has been shown to induce cardiomyocyte structural disorganization, apoptosis and systolic dysfunction in addition to increasing cardiac susceptibility to pressure overload[247]. In contrast, autophagy inhibition through cardiac-specific *Beclin1* knockdown was shown to protect systolic function in the event of hypertrophic insult[248]. Similarly, multiple studies (and

Chapter 3 of this Thesis) have examined autophagy in the diabetic heart and report both upregulation and downregulation of the pathway in various pre-clinical models of diabetes and human patients[91-113]. Despite the extensive investigations, to date limited number of studies have followed autophagy-targeting strategies in the diabetic heart. A recent study using high fat diet-induced diabetes in mice, demonstrated that cardiac inhibition of ATG8 lipidation (via ATG7-KO) exacerbates diabetes-induced diastolic dysfunction due to reduced clearance of damaged mitochondria[249]. Thus, manipulation of autophagy has not yet been successful at rescuing cardiac disease. Autophagy requires the concerted actions of several proteins and protein complexes that are shared to a great extent between the selective autophagy branches. Thus, it is interesting that the studies reported to date target protein molecules that largely operate at upstream stages of the pathway while there is lack of studies targeting downstream factors that may provide higher specificity.

4.1.2. The role of GABARAPL1 in autophagy

GABARAPL1 is one of the 6 mammalian Atg8's and more specifically, it belongs to the GABA type A receptor-associated protein subfamily along with 2 additional members, GABARAP and GABARAPL2[160]. Extensive research in the past decade has attempted to identify specific roles for each of the members of the GABARAP subfamily. Proteomic analyses using human tumorigenic cell lines and *in vitro* biotinylated peptide arrays have shown that GABARAP proteins interact with several autophagy-regulatory molecules[85,162,250]. This is in addition to their role as phagosome-localized, cargo-tethering proteins, indicating that there may be a degree of redundancy or functional compensation. Only recently, diverse functionality was demonstrated through experiments showing that nutrient deprivation enhances the binding of ULK1, a protein necessary for autophagy induction, to GABARAPL1 but has no effects on its interaction with GABARAP or GABARAPL2[164]. Together, findings reported in recent years indicate that GABARAPL1 may play a specific role in the regulation of autophagy induction that is independent of its role as an autophagosome-residing protein. Due to its original identification as a $GABA_A$ receptor interacting protein, the role of GABARAPL1 in the Central Nervous System (CNS) has been well investigated but its role in other tissues remains poorly understood[163,251-253]. Interestingly, a single report has shown that in the neonatal mouse heart, G*abarapl1* is upregulated following ischemia[254] indicating a cardioprotective role under these

conditions. However, more research is warranted to determine the precise function of GABARAPL1 in the heart.

4.1.3. Gabarapl1 is linked with glycogen-specific autophagy: Glycophagy

In recent years, it has been recognised that the term autophagy encompasses a number of lysosome-dependent degradation processes, each with specialized protein machinery aiming to recycle specific cargo[78]. Out of all the selective autophagy branches, glycophagy remains the least investigated. While the process of lysosomal glycogen degradation by GAA has been extensively examined in the context of Glycogen Storage Diseases (GSDs)[148,149,166,167], the molecular mechanisms governing glycogen sequestration to the lysosome remain elusive. Glycophagy has recently received attention due to the discovery of Starch-binding domain 1 (STBD1) as both a glycogen-binding and autophagy receptor protein[146,156]. Further examination indicated that STBD1 displays complete co-localization with GABARAPL1 when the two are co-expressed *in vitro*[146]. Together, these findings led to identifying GABARAPL1 as the glycophagy-specific ATG8 protein. This indicates that the diverse functionality of GABARAPL1 may not only include roles in autophagy induction but also GABARAPL1-specific cargo sequestration. In Chapter 3, glycophagy was demonstrated to be dysregulated in the diabetic heart and more specifically *Gabarapl1* was downregulated in pre-T2D and T2D myocardia. However, very little is known about the role of GABARAPL1 in the heart. Thus, in order to determine whether *Gabarapl1* downregulation is responsible for the diabetic cardiac glycogen pathology, further investigation on the role of GABARAPL1 in heart is warranted.

4.1.4. Aims of study

The study presented in this Chapter aims to determine how reduced availability or absence of GABARAPL1 influences cardiac function and glycogen content. CRISPR/Cas9 gene editing was used to induce *Gabarapl1* gene deletion *in vivo*. This study is the first to demonstrate that absence of GABARAPL1 is not compensated for by upregulation of ATG8 paralogs and is sufficient to induce both cardiac glycogen accumulation and diastolic dysfunction in absence of systemic abnormalities.

4.2. Specific methodology

4.2.1. Design of the CRISPR/Cas9 Gabarapl1 gene deletion model

The Clustered Regularly Interspaced Short Palindromic Repeat (CRISPR) system evolved as an anti-viral immunity mechanism in bacteria and archaea and is now a widely used genome editing approach. In its core, this system involves an endonuclease (Cas9 and others) forming a nucleoprotein complex with an RNA molecule (guide RNA, gRNA). gRNAs are in part homologous to sequences targeted for cleavage by Cas9. Base-pair complementarity between gRNAs and target sequences ensures the specificity of the approach. This inherent bacterial mechanism, coupled to evolved DNA repair processes such as non-homologous DNA end joining, has been adapted for targeted genome editing in mammalian cells and organisms. There are 2 requirements for CRISPR genome editing. The first is that the gRNA(s) are designed so that they are homologous only to the sequence of interest, thus preventing off-target effects. The second involves the presence of a 2-6 base-pair sequence called 'Protospacer Adjacent Motif (PAM) right after the end of the gRNA homologous region[255].

To create the *Gabarapl1*-knockout (KO) mouse, 2 gRNAs were designed so that the target sequences for Cas9-mediated 'cutting', were located within the first intron and within the exo-genic region post the fourth exon (Fig 4.1). In this approach, 3 of 4 exons of the *Gabarapl1* gene were deleted (6,052bp). Table 4.1 summarizes the gRNA homologous sequences, the PAMs and the target location in the mouse genome (genome annotation release GRCm38.p4). To produce the founder generation (F0), fertilized eggs of C57/Bl6J background were injected with Cas9 from *Streptococcus pyogenes* mixed with the gRNAs and were subsequently implanted into pseudo-pregnant females (previously mated with a vasectomised male thus 'hormonally' pregnant). In total, 20 mice were born following the intervention and 8 were confirmed to have the KO allele and were selected for further breeding and colony establishment.

The model design was performed in house while the development of the F0 generation was outsourced to the Walter+Eliza Hall Institute of Medical Research (WEHI, Melbourne, Australia).

4.2.2. DNA extraction

DNA was extracted from tail clips following incubation with DirectPCR Lysis reagent (Viagen, cat – 102-T) supplemented with 160µg of PCR-grade Proteinase K (Sigma, cat – P6556), at 55ºC until the tissue was visibly dissolved. Reaction arrest was achieved by incubation at 85ºC for 45 minutes. The samples were then centrifuged at 12,000g, at room temperature for 2 minutes to precipitate keratinous tissue remnants. The supernatant was removed and supplemented with equal volume of 500mM NaCl (Sigma, cat – S6191) and Isopropanol (final concentration 80%, Sigma, cat – I9516) to precipitate the DNA. The samples were similarly centrifuged again, the supernatant was discarded and the DNA-containing pellet was washed with 70% ethanol twice. The pellet was left to dry and was subsequently resuspended in 10mM Tris-HCl, pH 8.0 (Sigma, cat – 10812846001).

4.2.3. Genotyping

The primer pairs used for detection of either the wild-type (WT) or knockout (KO) alleles are summarized in Table 4.2. Briefly, the primers detecting the KO allele were located in the first intron prior to the Cas9 cut-site and in the exogenic region following the second Cas9 cut-site, thereby amplifying a 309bp product only if the KO allele was present. In contrast, the WT primers were designed to amplify a region in the third intron, only present in the WT allele. Extracted DNA (2µl per sample) was combined with GoTaq MasterMix (Promega, cat – M7833) and primers (10µM) for PCR amplification using a Bio-Rad T100™ Thermal cycler. PCR conditions differed for the WT and KO alleles and are summarized in Table 4.3. Following completion of the PCR reaction, each sample was supplemented with DNA Gel Loading Dye 6X (Thermofisher, cat – R0611) and was loaded onto a 2% agarose DNA electrophoresis gel supplemented with SYBR Safe (Invitrogen, cat – S33102). For determination of amplicon size, GeneRuler 50bp DNA Ladder (Thermofisher, cat – SM0371) was also loaded. Electrophoresis was allowed to proceed for 45 minutes at 90V prior to imaging with a ChemiDoc™ XRS+ System (Biorad, cat – 1708265). Image analysis was performed with Image Lab© v6.0 (Biorad).

4.2.4. Sanger Sequencing

PCR amplification products from samples that were shown to contain the *Gabarapl1*-KO allele along with aliquots of the reverse KO primer were submitted for Sanger Sequencing at the Australian Genome Research Facility (Melbourne, Australia). Analysis of sequencing data was performed with Geneious software v11.0.5 (Biomatters Ltd).

4.2.5. Echocardiography

In vivo assessment of cardiac function of 29 week old mice was performed via transthoracic echocardiography as described in Chapter 2 (Section 2.2).

4.2.6. Glucose Tolerance Test

Glucose tolerance test of 28 week old mice was performed as described in Chapter 2 (Section 2.3).

4.2.7. Extraction of cardiac tissue

Cardiac tissue used for molecular analyses was extracted from neonatal (p2), 20 and 30 week old mice as described in Chapter 2 (Section 2.4).

4.2.8. Molecular analyses

Frozen cardiac tissue from 20 week old mice was used to determine glycogen and protein content as described in Chapter 2 (Sections 2.5-2.7). RNA extraction, reverse transcription and RT-qPCR was performed using frozen cardiac tissue from 30 week old mice as described in Chapter 2 (Sections 2.8-2.10). Immunoblot was performed as described in Section 11 of Chapter 2.

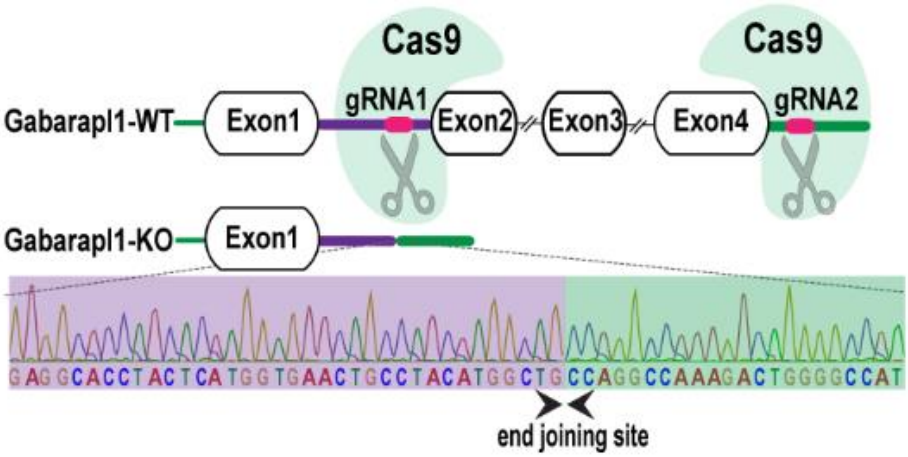

Figure 4.1: Schematic representation of the CRISPR/Cas9 *Gabarapl1* knockout mouse. Gene KO was induced by 2 gRNA-determined Cas9 genomic incisions, prior to exon 2 and post exon 4, resulting in deletion of 3 out of 4 gene exons. A representative Sanger Sequencing-derived KO allele DNA sequence is shown and the non-homologous end-joining site is indicated.

Table 4.1: Guide RNA sequences used for CRISPR-induced *Gabarapl1* knockout

	Spacer sequence (5'-3')	Strand	PAM (5'-3')	Location	Genomic location*
gRNA1	ggtggtgcgtcaaactatcg	+	cctggtg	Intron	Chr6:129,536,697
gRNA2	ggtctggtcccagatttgac	+	actggc	post-gene	Chr6:129,542,735

Table 4.2: Primer pairs used to detect the WT and KO alleles in genotyping of the *Gabarapl1*-KO mice

Target allele	Primer sequences	Amplicon size
KO	FWD: 5'-AGGTGGACATCGAAGGACAG-3' REV: 5'-TCAGTGAGTAAAGGCTTGGCC-3'	**309bp**
WT	FWD: 5'-AGTGGACATCGAAGGACAG-3' REV: 5'-TCAGTGAGTAAAGGCTTGCC-3'	**250bp**

Table 4.3: PCR amplification conditions for the WT and *Gabarapl1*-KO alleles

	Gabarapl1-WT		Gabarapl1-KO	
	Temperature	**Time**	**Temperature**	**Time**
Initial denaturation	95°C	2 minutes	95°C	2 minutes
	34 cycles		**35 cycles**	
Denaturation	95°C	30 sec	95°C	30 sec
Annealing	60°C	30 sec	55°C	30 sec
Extension	72°C	30 sec	72°C	30 sec
Final extension	72°C	5 min	72°C	5 min

4.3 Results

4.3.1. Validation of the CRISPR-induced *Gabarapl1* gene deletion model

The CRISPR/Cas9-induced *Gabarapl1* gene knockout (KO) was continuously verified by genotyping where PCR specifically designed to detect the KO allele produced a 309bp sequence which was present solely in heterozygous or homozygous KO animals but not wild-type. (Fig 4.2a). The KO was also confirmed by immunoblot where the 18kDa GABARAPL1 band was absent from the homozygous KO sample (Fig 4.2b). Further, qPCR quantifying the *Gabarapl1* mRNA detected a 40% reduction ($p<0.05$) in the heterozygous animals and complete absence in the homozygous KO mice (Fig 4.2c). To determine the exact edited sequence for each strain, DNA from descendants from each of the 8 original colony strains was PCR amplified for the *Gabarapl1*-KO allele and the PCR product was Sanger-sequenced. The sequences were subsequently aligned with the predicted KO sequence to confirm absence of the genomic region between the 2 guide RNAs (Fig 4.2d).

4.3.2. *Gabarapl1* gene deletion was not compensated for by upregulation of ATG8 paralogs

To ensure that potential phenotypic effects of the *Gabarapl1* gene deletion would not be masked by inherent upregulation of ATG8 paralogs, myocardial mRNA expression of *Gabarap*, *Gabarapl2* and *Map1lc3b* was measured by qPCR. No significant differences were detected in the expression of any paralog in either the heterozygous or homozygous KO adult animals (Fig 4.3 a-c).

4.3.2. *Gabarapl1*-KO does not induce a systemic phenotype or changes in cardiac morphology

The systemic phenotype of adult *Gabarapl1*-KO mice was examined prior to their endpoint and tissue collection. Neither the heterozygous nor the homozygous KO mice exhibited differences in their body weight or fed-state blood glucose levels relative to their wild-type littermates (Fig 4.4a-b). The glucose tolerance test revealed a mild insulin resistance in the homozygous KO mice, but not the heterozygous, relative to wild-type (Fig 4.4c). This was not resolved as a statistically significant difference in the calculation of the area under the glucose tolerance curve (Fig 4.4d). The wet cardiac

weight was measured at tissue collection and was found to be consistent across the 3 genotypes (Fig 4.4e). The endpoint characteristics of the mice are summarized in Table 4.4.

4.3.3. Reduced availability of *Gabarapl1* results in cardiac glycogen accumulation

To determine the involvement of GABARAPL1 in regulating cardiac glycogen content, hearts from neonatal and adult male mice were collected, homogenized and subjected to enzymatic glycogen measurements. Myocardial glycogen accumulation was observed in the neonatal (26%, $p<0.05$) and adult (46%, $p=0.05$) heterozygous animals relative to their wild-type littermates (Fig 4.5a-b).

4.3.4. *Gabarapl1* gene deletion induces diastolic dysfunction *in vivo*

The *in vivo* cardiac diastolic function of the adult heterozygous and homozygous KO mice was determined via Pulsed wave and tissue Doppler echocardiography, one week prior to tissue collection. Diastolic dysfunction in the homozygous KO mice was evident by the significant increase in E/E' ratio relative to the wild-type animals (Fig 4.6a) while no differences were detected in the E/A ratio (Fig 4.6b). As an indicator of ventricular compliance, MV DecT was measured and was found to be unchanged in the heterozygous animals relative to wild-type but significantly reduced in the homozygous KO mice relative to the heterozygous littermates (Fig 4.6c). The E'/A' ratio was not significantly different between groups but a progressive decrease depending on genotype was observed (Fig 4.6d). Pulsed wave and tissue Doppler peak wave velocities are summarized in Table 4.5.

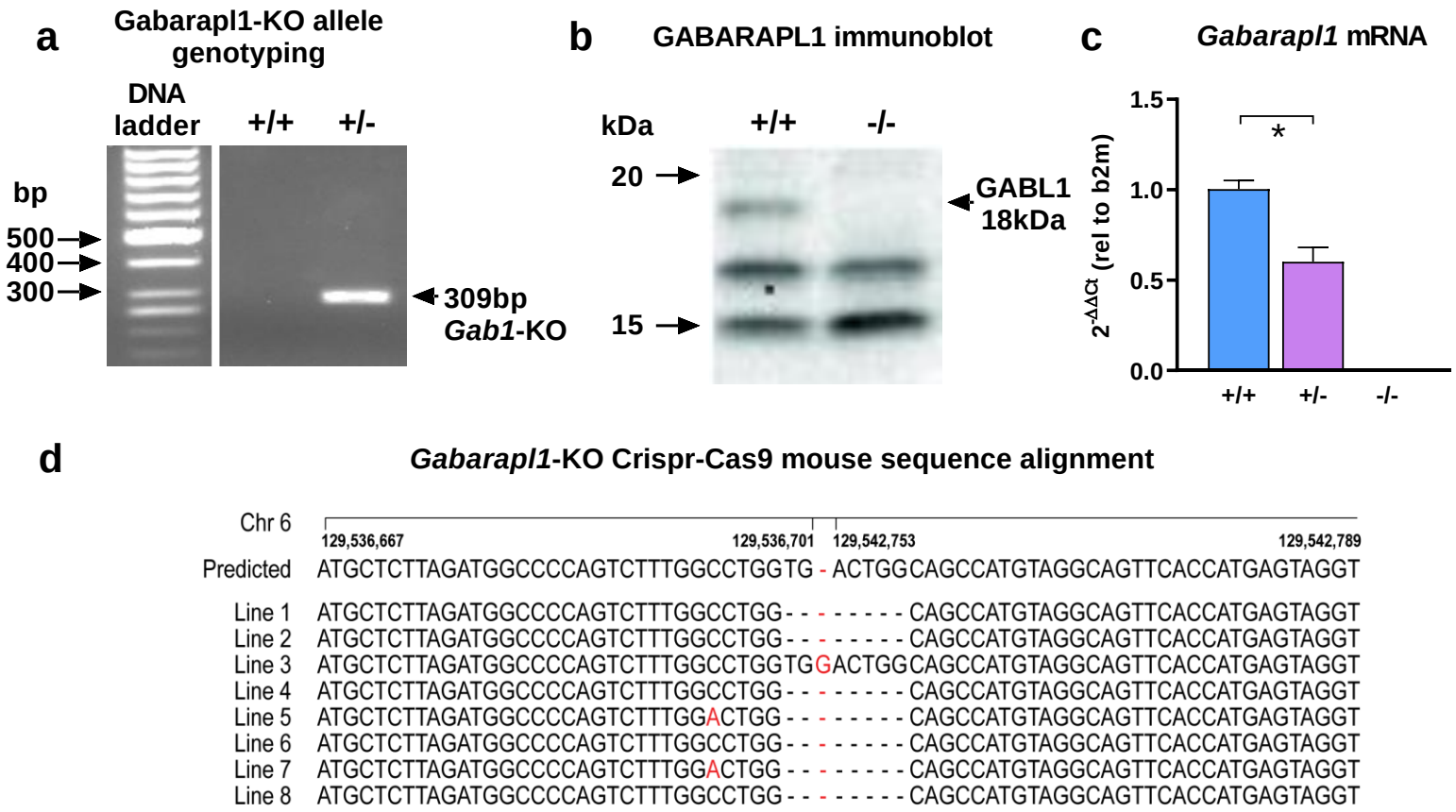

Figure 4.2: Validation of the *in vivo* CRISPR/Cas9 *Gabarapl1*-KO model. (a) Representative DNA gel electrophoresis obtained from genotyping a heterozygous *Gabarapl1*-KO mouse. The 309bp product amplified by primers located before and after the 2 Cas9 cut sites is present in the heterozygous KO but not the wild-type animal. **(b)** Representative immunoblot showing absence of the 18kDa GABARAPL1 band in the homozygous KO mouse. **(c)** *Gabarapl1* mRNA expression in the heterozygous and homozygous KO myocardium relative to the WT (n=4-5 animals per group). **(d)** KO sequence alignments obtained by Sanger Sequencing from each of the 8 original colony strains. Data analysed by one-way ANOVA with Bonferroni post-hoc test. Data presented as mean±SEM, *p<0.05. (+/+: wild-type, +/-: heterozygous, -/-: homozygous KO).

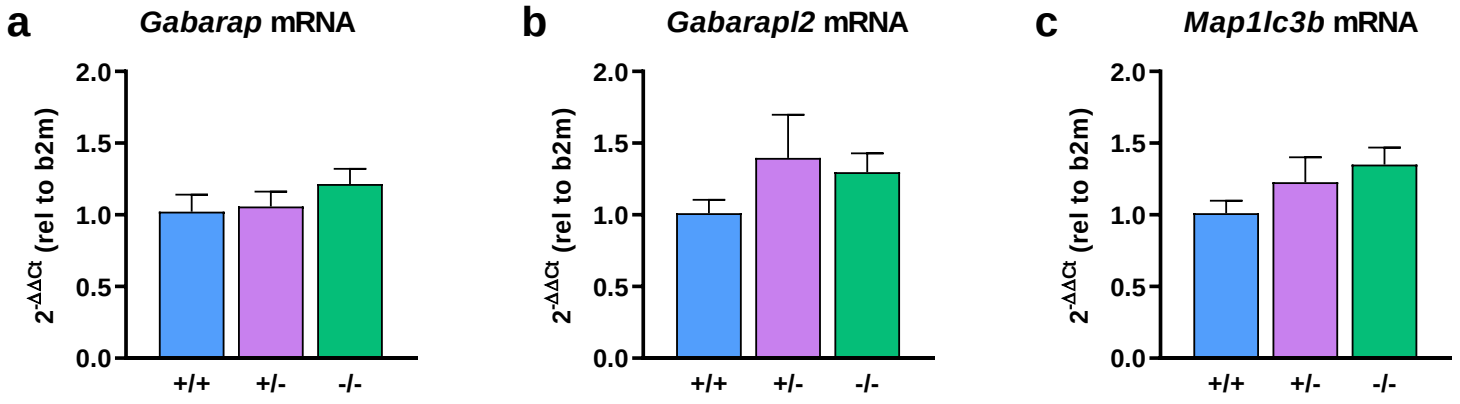

Figure 4.3: *Gabarapl1* deletion is not compensated by upregulation of ATG8 paralogs. **(a)** *Gabarap* mRNA expression in adult heterozygous and homozygous KO myocardium relative to wild-type (n=4-5 animals per group). **(b)** *Gabarapl2* mRNA expression in adult heterozygous and homozygous KO myocardium relative to wild-type (n=4-5 animals per group). **(c)** *Map1lc3b* mRNA expression in adult heterozygous and homozygous KO myocardium relative to wild-type (n=4-5 animals per group). Data analysed by one-way ANOVA with Bonferroni post-hoc test. Data presented as mean±SEM, *p<0.05. (+/+: wild-type, +/-: heterozygous, -/-: homozygous KO).

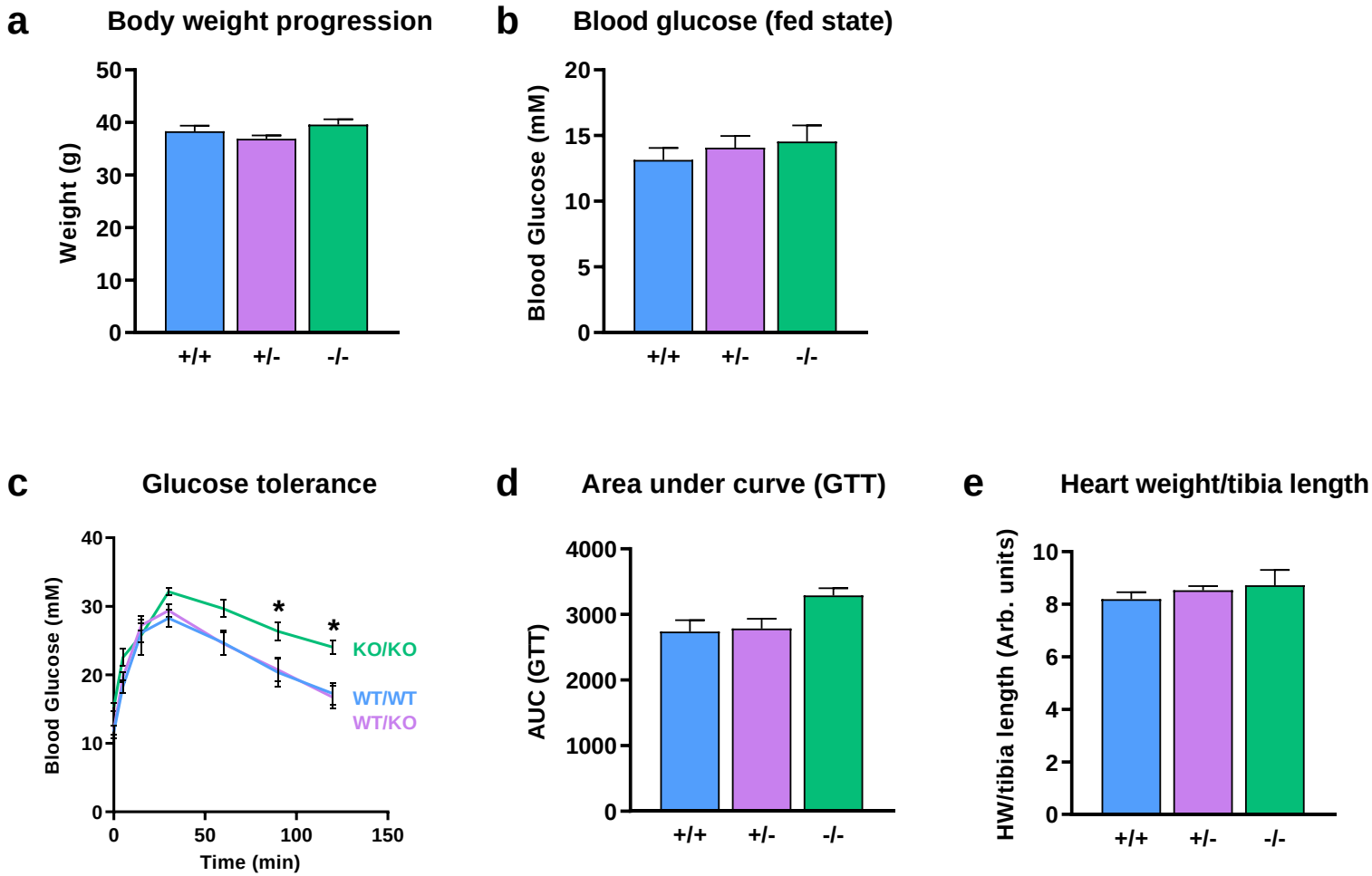

Figure 4.4: *Gabarapl1* gene deletion does not induce an apparent diabetic systemic phenotype. **(a)** Body weight measurements of adult male wild-type, heterozygous or homozygous KO mice (n=5-12 animals per group). **(b)** Fed- state blood glucose levels at the time of heart extraction (n=5-13 animals per group). **(c)** Glucose tolerance test (n=5-11 animals per group). **(d)** Area under curved derived from the glucose tolerance test. p=0.14 wild-type versus homozygous KO, p=0.19 heterozygous KO versus homozygous KO (n=5-11 animals per group). **(e)** Wet heart weight normalized to tibia length (n=5-13 animals per group). Data analysed by 2-way ANOVA with repeated measures or one-way ANOVA and Bonferroni post-hoc test. Data presented as mean±SEM, *p<0.05. (+/+: wild-type, +/-: heterozygous, -/-: homozygous KO).

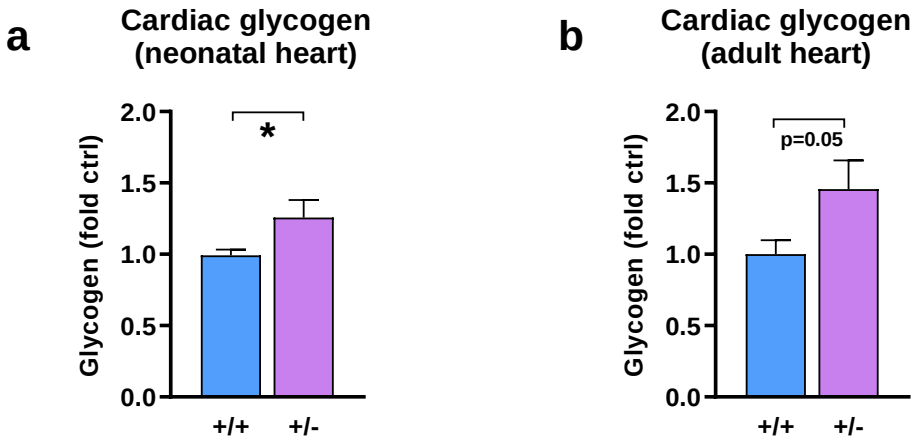

Figure 4.5: *Gabarapl1* gene deletion induces cardiac glycogen accumulation. (a) Cardiac glycogen content of heterozygous neonatal mice relative to wild-type (n=9-12 animals per group). **(b)** Cardiac glycogen content of heterozygous adult male mice relative to wild-type (n=5-7 animals per group). Data was analysed with Student's t-test. Data presented as mean±SEM, *p<0.05. (+/+: wild-type, +/-: heterozygous).

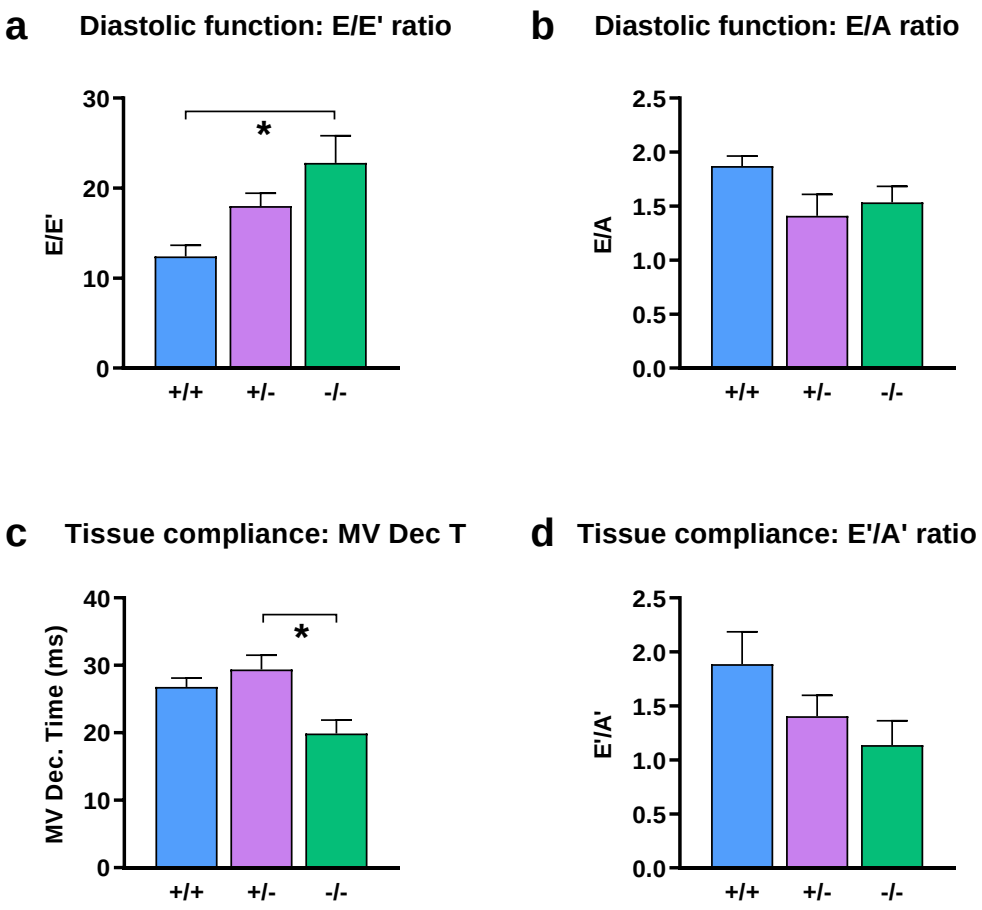

Figure 4.6: *Gabarapl1* gene deletion induces diastolic dysfunction *in vivo*. (a) E/E' ratio in adult, male wild-type, heterozygous or homozygous KO mice (n=4-5 animals per group). **(b)** Echocardiographic E/A ratio in adult, male wild-type, heterozygous or homozygous KO mice (n=4-5 animals per group). **(c)** Mitral valve deceleration time in adult, male wild-type, heterozygous or homozygous KO mice (n=4-5 animals per group). **(d)** E/A' ratio in adult, male wild-type, heterozygous or homozygous KO mice (n=4-5 animals per group). Data analysed by one-way ANOVA with Bonferroni post-hoc test. Data presented as mean±SEM, *p<0.05. (+/+: wild-type, +/-: heterozygous, -/-: homozygous KO).

Table 4.4: Systemic characteristics and cardiac morphology of adult *Gabarapl1*-KO mice.

	WT/WT	WT/KO	p value rel. WT/WT	KO/KO	p value rel. WT/WT	p value rel. WT/KO
Body weight (g)	38.30±1.06	36.88±0.64	0.69	39.62±1.01	>0.99	0.21
Blood glucose (mM)	13.15±0.90	14.07±0.91	>0.99	14.54±1.23	>0.99	>0.99
Heart weight (mg)	146.5±6.24	149.5±3.54	>0.99	148.3±7.44	>0.99	>0.99
Heart weight/body weight (mg/g)	3.78±0.18	3.98±0.09	0.89	3.75±0.19	0.99	0.99
Tibia length (mm)	17.31±0.12	17.50±0.13	>0.99	17.08±0.36	>0.99	0.41
Heart weight/tibia length (arb. Units)	8.19±0.26	8.53±0.16	>0.99	8.72±0.59	0.75	>0.99

Data analysed by one-way ANOVA with Bonferroni post-hoc test. Data presented as mean±SEM, *p<0.05.

Table 4.5: Diastolic echocardiography parameters of adult *Gabarapl1*-KO mice

	WT/WT	WT/KO	p value rel. WT/WT	KO/KO	p value rel. WT/WT	p value rel. WT/KO
MV E (mm/s)	431.5±33.37	455.8±49.79	>0.99	502.6±56.53	>0.99	>0.99
MV A (mm/s)	231.3±12.91	345.5±52.06	0.19	336.7±30.41	0.25	>0.99
MV E’ (mm/s)	36.07±4.29	24.74±1.81	0.12	25.36±3.77	0.15	>0.99
MV A’ (mm/s)	20.06±3.02	19.81±4.07	>0.99	24.14±3.85	>0.99	>0.99
MV E/E’	12.4±1.24	18.00±1.42	0.31	22.79±3.04	0.02	0.41
MV E/A	1.87±0.09	1.41±0.2	>0.99	1.53±0.15	>0.99	0.55
MV Deceleration time (ms)	26.82±1.3	29.4±2.09	>0.99	19.9±1.2	0.09	0.01
MV E’/A’	1.89±0.3	1.4±0.19	0.74	1.14±0.22	0.15	0.97

Data analysed by one-way ANOVA with Bonferroni post-hoc test. Data presented as mean±SEM, *p<0.05.

4.4. Discussion

The study presented in this Chapter is the first to show that the autophagy-related protein GABARAPL1 is crucial for maintaining physiological cardiac glycogen levels and diastolic function. CRISPR/Cas9-induced deletion of the *Gabarapl1* gene in mice was sufficient to induce diastolic dysfunction in adult male mice. Furthermore, cardiac glycogen accumulation was induced as early as 2 days post-birth and was maintained into adulthood.

4.4.1. *Gabarapl1* gene deletion is sufficient to cause cardiac glycogen accumulation

The finding that *Gabarapl1* gene deletion induced cardiac glycogen accumulation, even at heterozygosity, at the neonate and adult stages indicates that GABARAPL1 plays a pivotal role in myocardial glycogen handling. This observation corroborates unpublished evidence from the Delbridge lab showing that *Gabarapl1* siRNA-mediated knockdown induced glycogen accumulation *in vitro* in Neonatal Rat Ventricular Myocytes (NRVMs) and is the first study to demonstrate that maintenance of cardiac glycogen content *in vivo* relies on the availability of GABARAPL1. The precise mechanisms via which GABARAPL1 exerts regulatory functions over glycogen handling are not dissected in this study but the observed increase in myocardial glycogen deposition could be through a number of processes. Evidence supporting the involvement of GABARAPL1 in glycophagy arise from *in vitro* experiments showing that the glycophagy receptor STBD1 interacts with GABARAPL1[147,161,162]. However, STBD1 has been shown to interact not only with GABARAPL1 but also with GABARAP and all 3 members of the MAP1LC3 family[162]. Thus it could be expected that decreased GABARAPL1 availability could be compensated for by other ATG8 paralogs. However, as in this model cardiac glycogen accumulation was not coincident with upregulation of *Gabarap*, *Gabarapl2* or *Map1lc3b*, it is unlikely that the GABARAPL1-specific glycophagy functions were executed by another ATG8 protein. In addition, it has been shown, albeit in non-cardiac cells, that presence of ATG8 proteins is not necessary for phagosome formation but rather, it is required for fusion of the autophagic vesicles with the lysosome[256,257]. Thus, a reduction in GABARAPL1 may not necessarily inhibit glycogen sequestration to the phagosome but may obstruct delivery of the latter to the lysosome thereby resulting in accumulation of glycogen-containing vesicles. Furthermore, in

recent years, a distinct role for the GABARAP family proteins in autophagy induction has been described. Particularly, GABARAPL1 has recently been shown to strongly associate with ULK1 upon starvation in HeLa cells[164]. In addition, previous findings in MCF-7 cells reported that association of GABARAPL1 with ULK1 is independent of conjugation of the former to phosphatidyl-ethanolamine (PE)[165], indicating that GABARAPL1 has autophagy-related functionality that is independent of its association with the phagosome membrane. Collectively, these reported findings imply that in the absence of GABARAPL1, the autophagy process, with all its selective branches, including glycophagy, is inhibited or highly inefficient. As it was shown in Chapter 3, *Gabarapl1* was downregulated in the pre-T2D and T2D myocardium. This, together with the findings presented in this Chapter indicate that diabetic cardiac glycogen accumulation may be associated with *Gabarapl1* downregulation and glycophagy inhibition.

4.4.2. *Gabarapl1* deficiency induces diastolic dysfunction

The study presented in this Chapter is the first to show that *Gabarapl1* gene deletion is sufficient to induce diastolic dysfunction, as evidenced by the increase in E/E' ratio, in the absence of any underlying systemic pathology. Additionally, a parallel study in the Mellor-Delbridge labs has demonstrated that systolic function is preserved in adult *Gabarapl1*-deficient mice, suggesting a specific link between GABARAPL1 and cardiac relaxation. While several studies have examined autophagy in relation to cardiac function, only a limited number of reports exist where investigations were carried out in absence of cardiopathology. In addition, in its majority, the published literature characterizes cardiac function following genetic interventions targeting upstream, regulatory autophagy proteins[247,248]. This is the first study to demonstrate a link between a downstream, autophagosome-related molecule and cardiac function. GABARAPL1 has been implicated to a number of processes that could in turn be linked to cardiac dysfunction. In the study presented in this Chapter, the GABARAPL1-KO-induced diastolic dysfunction was coincident with cardiac glycogen accumulation. Additionally, related findings from the Mellor-Delbridge labs have demonstrated that in the diabetic heart, the extent of glycogen deposition positively correlates with diastolic dysfunction (Mellor et al, publication pending). Therefore, it would be interesting to explore a possible link between the two observations. In gastric cancer cell lines, siRNA-induced *Gabarapl1*

silencing lead to a decrease of the overall cellular ATP content. Interestingly, it has been proposed that Ca^{2+} uptake during relaxation relies on the use of glycolysis-derived ATP by SERCA2a[258]. Taken together, these reported findings imply that a possible mechanism via which *Gabarapl1*-deletion induced diastolic dysfunction is through reduction of glycolytic ATP caused by reduced supply of glycogen-derived glucose. Furthermore, recent findings centralizing around hepatic glycogen have shown that the glycogen metabolite produced by the anhydrofructose pathway[259] can drive formation of Advanced Glycation End products (AGEs)[260]. In the heart, recent findings from the Mellor and Delbridge labs have detected AGE modifications in contractile proteins, in regions essential for the functionality of contractile complexes during myocardial relaxation[261]. Thus, it is possible that in GABARAPL1-depleted hearts, where increased glycogen deposition is evident, glycogen-derived AGEs permanently modify contractile proteins thereby contributing to diastolic dysfunction.

In addition to glycophagy, GABARAPL1 has been implicated in mitochondrial autophagy (mitophagy). In immature red blood cells, inhibition of binding of the mitophagy receptor NIX to GABARAPL1 has been shown to hinder mitochondrial clearance resulting in accumulation of damaged mitochondria. In the heart, mitochondrial damage derived from genetic manipulations targeting mitophagy-implicated molecules have been linked to cardiomyocyte apoptosis-induced cardiomyopathy and increased susceptibility to ischemia/reperfusion injury[262-265]. This is presumably due to failure of the antioxidant response resulting in overproduction of Reactive Oxygen Species (ROS)[266], that in turn has direct effects on the cardiac phenotype promoting left ventricular hypertrophy and heart failure[267,268]. ROS-mediated cardiac dysfunction has also been linked to Ca^{2+} homeostasis affecting both the Ca^{2+}-mediated calcium release by the Ryanodine receptor (RyR) and the phospholamban-driven efficiency of Ca^{2+} uptake during relaxation[269,270]. In addition, inhibition of mitophagy has been demonstrated to have greater impact on cardiac function during aging inducing contractile impairments, hypertrophy and eventually heart failure[267,268,271]. Intriguingly, even though impaired mitophagy has repeatedly been associated with cardiac hypertrophy, enlargement of the cardiac muscle was not observed in this study under either partial deficiency or complete absence of GABARAPL1. Interestingly, recent findings derived from HeLa cells and electron microscopy have demonstrated that mitochondria continue to be engulfed in phagosomes in complete absence of

ATG8 proteins[256]. Therefore, while it is possible that mitophagy disturbances could be contributing to diastolic dysfunction observed in the GABARAPL1-KO mice in the study presented here, it is unlikely that the process would be completely abolished.

4.5 Conclusions and next steps

This study provides the first demonstration that the autophagy-related protein, GABARAPL1, plays a central role in the maintenance of cardiac glycogen levels and is crucial for the preservation of cardiac diastolic function. *Gabarapl1* gene deletion resulted in myocardial glycogen accumulation and had detrimental consequences for cardiac diastolic function in the absence of systemic pathology. The precise mechanisms via which GABARAPL1 deficiency induced glycogen accumulation and diastolic dysfunction remain to be understood, but the potential for targeting GABARAPL1 and glycophagy in situations where glycogen disturbance coincides with impaired cardiac relaxation, such as diabetic cardiomyopathy, becomes apparent.

4.6. Limitations

Technical limitations in the study presented in this Chapter centralize around the development and management of the *Gabarapl1*-KO mouse colony. During the maintenance of this colony breeding issues were evident and resulted in limited animal availability. Thus, there is only 5 animals in the homozygous KO group. Additionally, previous studies have shown that glycogen handling may be different in males and females[171]. In the study presented in this Chapter only males were used in order to minimise variability. A follow up study directly comparing the role of glycophagy in males and females is now warranted. Finally, while this Chapter has shown that the role of GABARAPL1 in cardiac glycophagy is unlikely to be carried out by other ATG8 paralogs, complete characterization of the response of members of the ATG8 by immunoblot to measure protein levels was not performed. This is in part due to lack of reliable antibodies (with the exception of those targeting LC3B). Further investigation is required to determine whether there were difference in protein levels of the ATG8 paralogs in response to partial or complete absence of GABARAPL1.

CHAPTER 5

Gabarapl1 gene delivery rescues glycogen accumulation and diastolic dysfunction in diabetes

5.1. Introduction

5.1.1. Diabetic cardiomyopathy is a distinct cardiac pathology

Diabetic heart disease is recognized as a distinct cardiopathology[11] that is characterised by early manifestation of diastolic dysfunction and is observed in approximately 50% of diabetic patients worldwide[20-22]. Although diabetes is characterised by a spectrum of complications, diabetic cardiomyopathy often presents in absence of vascular abnormalities or hypertension[23-26]. As shown in human patients[27,28], and in various rodent models of either type 1 or type 2 diabetes (T1D or T2D respectively)[6-8], diabetic diastolic dysfunction is most commonly associated with abnormal ventricular filling due to reduced ventricular wall compliance[10,27]. In addition, diabetes-induced diastolic dysfunction may be followed by late systolic abnormalities[30] but can also be observed in complete absence of systolic dysfunction[21,31,32]. Late-stage diabetic cardiomyopathy can be associated with left ventricular hypertrophy but this phenotype is not commonly observed in pre-diabetic, glucose-intolerant subjects[49]. Interestingly glycaemic status is not necessarily indicative of cardiac dysfunction suggesting that controlled blood glucose levels are not sufficient to prevent cardiac abnormalities[33]. Currently there are no effective treatment options for diastolic dysfunction indicating that further investigations into the underlying molecular mechanisms are warranted.

5.1.2. Dysregulated glycogen storage in the diabetic heart

Together with the mechanical disturbances in the diabetic heart, there have been sporadic reports of altered glycogen levels in cardiac tissues in some (but not all) contexts[116-138]. In diabetes, reduced glucose uptake is evident in insulin-sensitive tissues, and consistent with this, in skeletal muscle glycogen levels are depleted[43,44]. In diabetes, insulin-sensitive tissues operate under glucose-limited conditions induced either by absence of insulin (T1D) or localized insulin resistance (T2D). Thus, the incidental observations of diabetic cardiac glycogen accumulation would be unexpected and paradoxical and the causes or consequences of elevated cardiac glycogen have not been previously investigated. As described in Chapter 1 (see Figure 1.1, Mellor et al, publication pending) experiments which provided rationale for the current work, comprising an extensive, comparative and systematic investigation of glycogen levels in myocardial tissues derived from a variety of animal models and from clinical samples, have demonstrated glycogen elevation to be a consistent feature

of the diabetic myocardium. Interestingly, several studies (including investigations preliminary to this Thesis undertaking) using rodent models of both T1D and T2D have shown decreased activity of cardiac glycogen synthase (GS) and unchanged or increased activity of glycogen phosphorylase (GP)[120,126,131,137,152,166]. Therefore, it seems that alterations in the activity of glycogen regulatory enzymes do not explain diabetes-induced cardiac glycogen accumulation. It is possible that perturbation in glycogen storage is an early response in diabetes and that single time-point measurements of glycogen regulatory enzymes may not necessarily reflect the progression of the phenotype and may indicate a compensatory response. There is also the possibility that other glycogen handling mechanisms, such as glycophagy, may play a role in the manifestation of diabetic cardiac glycogen disturbance[77].

5.1.3. Glycophagy disturbances are linked with cardiac pathologies

The vital role of glycophagy in the heart is evidenced by contractile abnormalities observed in inherited glycogen storage diseases (GSDs) where mutations in α-acid glucosidase (GAA, Pompe disease) or Lysosome-associated membrane protein 2 (LAMP2, Danon disease) lead to glycogen accumulation[177,178]. The glycophagy process requires glycogen to be tagged by Starch-binding domain 1 (STBD1) so that it can be sequestered to the forming phagosome[146]. Subsequently, STBD1 anchors to γ-aminobutyric acid receptor-associated protein-like 1 (GABARAPL1)[147] that in its lipidated form localizes to the phagosome membrane[78]. In the final stage of the process, phagosomes fuse with lysosomes where GAA hydrolyses the glycosidic bonds thereby releasing glucose monomers[148,149]. In Chapter 3, glycophagy was demonstrated to be dysregulated in the diabetic heart. More specifically, *Gabarapl1* mRNA expression was decreased in rodent models of pre-T2D and T2D and was also downregulated in cardiac tissues from human diabetic patients. Additionally, the importance of glycophagy in the healthy heart was highlighted in Chapter 4 where knockout of *Gabarapl1* induced concurrent cardiac glycogen accumulation and diastolic dysfunction.

5.1.4. Aims of study

The aim of the study presented in this Chapter was to induce cardiac-specific GABARAPL1 upregulation and assess whether this intervention exerts favourable cardiac functional outcomes. Glycophagy was upregulated by viral *Gabarapl1* gene delivery both *in vitro* in cardiomyocytes and

in vivo in the diabetic heart. This study is the first to demonstrate that upregulating GABARAPL1 *in vivo* in the diabetic heart rescues both glycogen accumulation and diastolic dysfunction thereby providing a therapeutic potential for diabetic heart disease.

5.2. Specific methodology

5.2.1. Design of *Gabarapl1*-expressing Adeno-associated virus

To achieve *in vitro* and *in vivo Gabarapl1* gene delivery to non-dividing cardiomyocytes, Adeno-Associated virus of serotype 9 (AAV9) was chosen as the carrier vector. AAVs are non-enveloped icosahedral nucleocapsids of approximately 25nm in diameter and are so called due to their inability to replicate in absence of an Adenovirus. The genome of a wild-type AAV is single-stranded DNA (ssDNA) of approximately 4.7kb in length and contains 4 *Rep* genes involved in life cycle and host-genome integration and 3 *Cap* genes encoding for the viral proteins (VP) responsible for constructing the capsid. Importantly, the AAV genome is flagged by approximately 146b-long sequences called Inverted Terminal Repeats (ITRs) that are essential for the production of recombinant AAVs. Any sequence flagged by ITRs can be recognised as viral genome and can be encapsulated by the capsid[272,273].

Multiple AAV serotypes have been discovered. In this study AAV9 was chosen as the preferred vector because it displays higher cardiac tropism[274-281]. The entire mouse *Gabarapl1* cDNA (NM_020590.4) was inserted in the viral genome. To prevent non-cardiac over-expression of *Gabarapl1*, the viral genome was designed so that the transgene is under the regulation of the cardiac Troponin promoter (cTnTp)[282]. To ensure stable transgene expression in mammalian cells, the Woodchuck Hepatitis Virus (WHP) Posttranscriptional Regulatory Element (WPRE) and the Bovine Growth Hormone polyadenylation (bGH-poly(A)) sequences were added on the 3' end of the *Gabarapl1* cDNA (Fig 5.1). The annotated AAV9-cTnTp-m*Gabarapl1*-WPRE sequence can be found in Supplement 2 (Table A2.1 and Fig A2.1). As a negative control, an AAV9-cTnTp-Null virus was designed to lack the *Gabarapl1* cDNA but was otherwise identical to the *Gabarapl1*-expressing virus. The design of the viral genome was devised in house. Production of the viral particles was outsourced to Vector Biolabs (Philadelphia, USA).

5.2.2. Isolation and culture of Neonatal Rat Ventricular Myocytes

Neonatal rat ventricular myocytes (NRVMs) were isolated from p1-2 Sprague Dawley pups (of equal sex) following chunk collagenase digestion as previously described[172]. NRVMs were seeded in 6-well plates at density 1,187,500 cells/well. To evaluate the effects of *Gabarapl1* over-expression, following isolation, the cells were cultured in minimum essential media (MEM, Invitrogen – cat: 61100-061) supplemented with 10% newborn calf serum (NBCS, Invitrogen – cat: 16010-159) for 24 hours. The MEM was subsequently replaced with serum-free, antibiotic-free OptiMEM (Thermo Fisher – cat: 31985070) containing either AAV9-cTnT-*Gabarapl1* or AAV9-cTnT-Null virus with multiplicity of infection (MOI) of 10^4 gc/cell. The cells were cultured in transduction media for 24 hours and were then maintained in Dulbecco's modified essential medium (DMEM) supplemented with 5mM D-glucose (Sigma – cat: G7021) for 48 hours prior to receiving their experimental high glucose (HG, 30mM) or normal glucose (5mM, supplemented with 25mM Mannitol (Sigma – cat: M4125)) media supplemented with 1nM insulin for the final 24 hours. During the 48 hour maintenance period, the media was refreshed daily. Cells were lysed in RIPA buffer containing protease (Complete, EDTA-free, Roche, cat – 04693132001) and phosphatase inhibitors (PhosSTOP, Roche, cat – 04906837001) for molecular analysis. A schematic of the design of the *in vitro* experiments can be found in figure 5.2. To evaluate the extent of AAV-induced *Gabarapl1* overexpression, the cells were lysed in TriZol 72 hours post-transduction to obtain total RNA. Reverse transcription and *Gabarapl1*-targeting qPCR was performed as described in Chapter 2 (Sections 2.9, 2.10).

5.2.3. High Fat/Sugar Diet mouse study design

To develop the diabetic model used in this study, 8 week old C57/Bl6J mice were fed a high fat/sugar diet (HFSD, 23% fat w/w, 20.1% sucrose w/w, SF04-001, Specialty Feeds) or a control diet (7% fat w/w, 10% sucrose w/w, AIN93G, Specialty Feeds) for 26 weeks. HFSD-fed animals consumed 2 fold more lipid- and sugar-derived energy than control-fed animals. The diet compositions are summarized in Table 5.2. The animals first went through a 'transition week' during which they were fed their experimental diet for 12 'daylight' hours and their standard diet during the nocturnal 12 hours. At week 13 of full-time feeding, the systemic diabetic phenotype of the mice was evaluated via glucose tolerance test and the cardiac function via echocardiography as described in Chapter 2

(Sections 2.2 and 2.3). Mice were divided randomly into 2 groups and received 10^{12} gc/mouse of either the AAV9-*Gabarapl1* or the null virus via tail-vein injection. The body weight of the mice and their food intake was monitored weekly. Cardiac function was assessed longitudinally at 5, 8 and 11 weeks post-AAV administration. The systemic diabetic phenotype of the mice was re-assessed 10 weeks post-AAV administration prior to tissue collection at week 12 post-viral delivery. Selection of this timeframe was based on the requirement to allow enough time to achieve concurrent restoration of cardiac function and rescue of glycogen accumulation. A later study end point could have resulted in depletion of the viral load while earlier study conclusion could have proven inadequate time for glycogen accumulation to resolve. At this time point blood glucose levels of HFSD mice were significantly increased relative to control. Thus this model was considered type 2 diabetic. Extraction of cardiac tissue was performed as described in Chapter 2 (Section 2.4). A timeline schematic of this study can be found in figure 5.3.

5.2.4. DNA extraction

Myocardial DNA was extracted as per manufacturer's instructions using the Genomic DNA Purification kit (Invitrogen/Thermo Fisher Cat - 00572102/K0152). Briefly, ventricular samples were homogenized in 1X Tris-EDTA-Lysis buffer solution and were subsequently heated at 65ºC for 10 minutes. DNA was extracted following a chloroform – ethanol precipitation procedure. The concentration and quality of the extracted DNA was measured with Nanodrop. Table A2.2 summarizes the concentration and quality of the extracted DNA.

5.2.5. Digital Droplet PCR

Digital droplet PCR (ddPCR, Biorad) targeting the WPRE element of the AAV genome was performed as per manufacturer's instructions to quantify the viral copies remaining in the myocardium 12 weeks post-viral administration. The ddPCR EvaGreen supermix (Biorad – Cat: 1864034), specifically designed for this technique, contains the polymerase and the green fluorescent DNA intercalating agent. Droplets were generated using the QX200™ Droplet Generation Oil for EvaGreen (Biorad – Cat: 1864005) and the QX200™ Droplet Digital™ PCR System (Biorad – Cat: 1864001). The primer sequences and PCR conditions are shown in Table

5.1. The target WPRE sequence was used as a positive control. Analysis was performed using QuantaSoft™ Analysis Pro.

5.2.6. Molecular analyses

Frozen cardiac tissue was used to determine glycogen and protein content as described in Chapter 2 (Sections 2.5-2.7). RNA extraction, reverse transcription and RT-qPCR was performed using frozen cardiac tissue as described in Chapter 2 (Sections 2.8-2.10). Immunoblot was performed as described in Section 11 of Chapter 2.

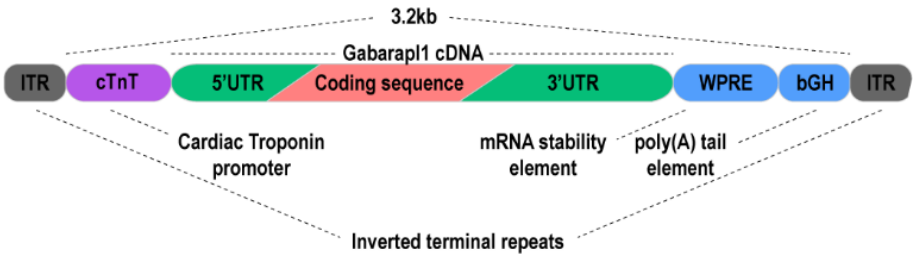

Figure 5.1: Design of the *Gabarapl1*-expressing AAV. The mouse *Gabarapl1* cDNA is preceded by the cardiac Troponin promorter (cTnTp) and followed by the Woodchuck Hepatitis Virus (WHP) Posttranscriptional Regulatory Element (WPRE) and the Bovine Growth Hormone polyadenylation (bGH-poly(A)) sequences. The recombinant sequence is flagged by the inverted terminal repeats (ITRs) to facilitate packaging of the transgene into viral capsids.

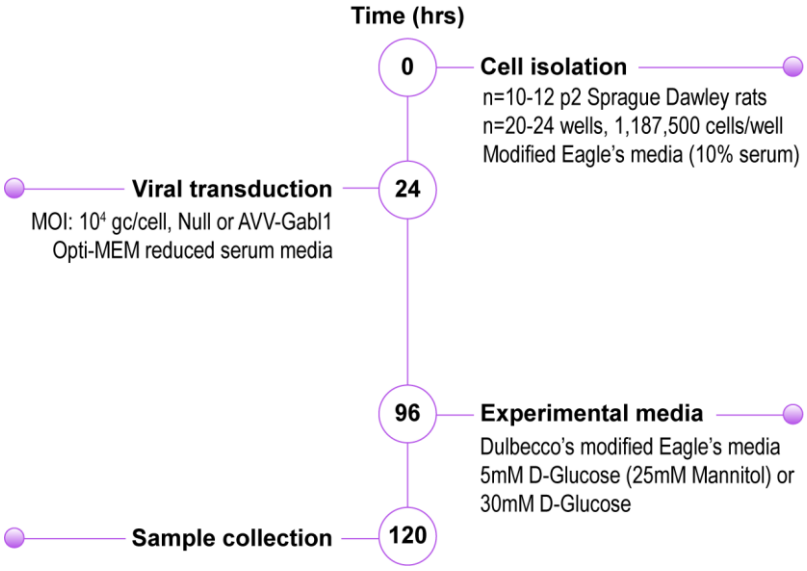

Figure 5.2: Timeline schematic of the *in vitro* NRVM viral transduction and high glucose experimental conditions.

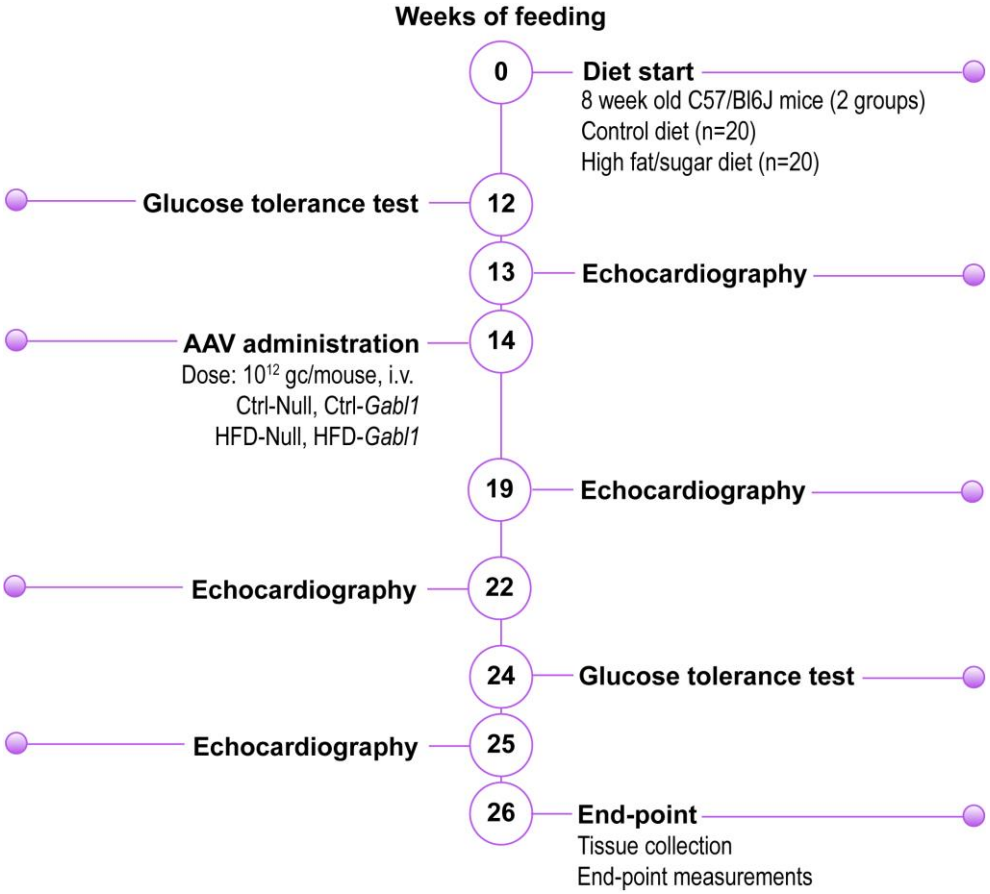

Figure 5.3: Timeline schematic of the *in vivo* high fat/high sugar diet (HFSD) AAV-*Gabarapl1* (*Gabl1*) study.

Table 5.1: Primer sequences and concentrations used for detection of AAV viral copies

Primer sequences	[primer] (nM)	[DNA] ng/rxn
FWD: 5' - CTGGTTGCTGTCTCTTTATGAGGAG - 3'	100	80
REV: 5' - CACTGTGTTTGCTGACGCAACC - 3'	100	

Table 5.2: Control and high fat/sugar diet compositions

	AIN93G (Ctrl)	**SF04-001 (HFSD)**
Protein (w/w)	19.40%	22.60%
Total fat (w/w)	7.00%	23.50%
Sucrose (w/w)	10%	20.10%
Crude fibre (w/w)	4.60%	5.40%
AD fibre (w/w)	4.70%	5.40%
Total digestible energy from lipids (rel. total)	16%	43%
Total digestible energy from protein (rel. total)	21%	21%
Total digestible energy from sucrose (rel. total)	10.10%	17.75%
Total digestible energy (kcal/g)	3.86 kcal/g	4.45 kcal/g

5.3 Results

5.3.1. *Gabarapl1* over-expression rescues high glucose-induced glycogen accumulation *in vitro*

Transduction of NRVM with AAV9-cTnTp-m*Gabarapl1* increased *Gabarapl1* mRNA expression by 87% 72 hours post-administration relative to null-treated cells (Fig 5.4a). Treatment of null-treated NRVM with high glucose (HG) lead to a 52% increase in glycogen relative to those maintained under normal glucose (NG) conditions. *Gabarapl1* over-expression in normal glucose conditions did not have a significant effect on cellular glycogen. *Gabarapl1* overexpression was sufficient to prevent HG-induced glycogen accumulation in NRVM (Fig 5.4b).

5.3.2. Establishment of a type 2 diabetic mouse model

Mice were matched for body weight and age prior to the start of the diet. HFSD-fed mice displayed significantly increased body weight (Fig 5.5a) 13 weeks post-diet commencement and were glucose intolerant (Fig 5.5b-c). In addition to the obese, glucose intolerant phenotype, the HFSD-fed mice displayed significant diastolic dysfunction evident by increased E/E' and E'/A' ratios (Fig 5.6a-b). No significant differences were detect in E/A ratio (Fig 5.6c).

5.3.3. Cardiac-specific *Gabarapl1* gene delivery did not affect the systemic diabetic phenotype or cardiac morphology

At 14 weeks on diet, mice were randomly divided into 4 groups and received either the *Gabarapl1*-expressing AAV or the null virus. Cardiac *Gabarapl1* gene delivery had no impact on the body weight of control mice or the progression of obesity of HFSD-fed mice (Fig 5.7a-b). Similarly, *Gabarapl1* gene delivery had no effect on the diabetic phenotype as *Gabarapl1*-treated HFSD-fed mice continued to exhibit glucose intolerance relative to their *Gabarapl1*-treated control littermates (Fig 5.7c-e). Although at 13 weeks of feeding fed blood glucose levels (BGL) were not different between control and HFSD-fed mice, at 26 weeks on diet, HFSD animals displayed increased BGL. This indicates the progression of the diabetic phenotype from glucose-intolerant pre-T2D to T2D. HFSD feeding induced significant cardiac hypertrophy as shown by the increase in heart weight-to-tibia length ratio. This phenotype was not affected by *Gabarapl1* gene delivery (Fig 5.7f). Table 5.3

summarizes the systemic and cardiac characteristics of the HFSD-fed mice at the study end-point, 12 weeks following AAV administration (26 weeks on diet).

5.3.4. *Gabarapl1* gene delivery rescued the diabetes-induced cardiac glycogen accumulation and diastolic dysfunction

At 12 weeks post AAV infection, viral copies were detectable in mouse hearts at similar levels between groups (445-700 gc/ug of extracted DNA, Fig A2.2). HFSD-fed, null-treated mice exhibited 86% increase in cardiac glycogen ($p<0.05$) relative to control-fed null treated mice. Cardiac *Gabarapl1* gene delivery rescued HFSD-induced glycogen accumulation, as cardiac glycogen levels of *Gabarapl1*-treated mice were comparable to null-treated, control-fed mice (Fig 5.8a). Similarly to glycogen, *Gabarapl1* gene delivery rescued HFSD-induced diastolic dysfunction, as early as 5 weeks post-administration, as shown by the decrease in E/E' ratio to control levels. E/E' values remained comparable to control until the study end-point, 12 weeks post-AAV administration (Fig 5.8b). There was a direct relationship between the levels of GABARAPL1 and cardiac function as shown by the significant correlation between membrane-bound GABARAPL1 protein and the end-point E/E' ratio (Fig 5.8c). The obtained echocardiography parameters are summarised in Table 5.4.

5.3.5. *Gabarapl1* upregulation did not induce significant alterations in macro-autophagy

As GABARAPL1 has been shown to modulate macro-autophagy[78], the autophagosome markers SQSTM1/p62, LC3B-I (non-lipidated form) and LC3B-II (lipidated form) were measured to determine whether they were altered as a result of *Gabarapl1* gene delivery. HFSD feeding alone increased the expression of SQSTM1/p62 by 51% ($p=0.06$, Fig 5.9b) which was not evident in the in the HFSD, *Gabarapl1*-treated animals. No changes were detected in LC3B-I, LC3B-II or the ratio LC3B-II/I (Fig 5.9c-e).

5.3.6. Diabetes reduces AMPK activation in a setting of *Gabarapl1* overexpression

Phosphorylation of AMPK occurs in ATP-depletion conditions and is a known macrophagy inducer. To determine whether the effects of *Gabarapl1* overexpression could involve AMPK, total and phosphorylated AMPK were measured by immunoblot. HFSD-fed, *Gabarapl1*-treated mice displayed decreased phosphorylation of AMPK at T172 by 52% relative to control-fed, *Gabarapl1*-treated mice ($p<0.05$, Fig 5.10b) but no differences were detected in total cardiac expression of

AMPK (Fig 5.10c). HFSD-fed, *Gabarapl1*-treated mice displayed decreased ratio of phosphorylated-to-total AMPK by 66% relative to their control-fed *Gabarapl1*-treated littermates (Fig 5.10d).

5.3.7. High fat diet feeding or *Gabarapl1* gene delivery do not induce changes in the cytosolic glycogen handling enzymes.

To assess whether *Gabarapl1*-induced effects on glycogen are due to changes in expression or activity of glycogen handling enzymes, glycogen phosphorylase (GP) and synthase (GS) levels were measured by immunoblot. No differences were detected in phosphorylated (S14, active) or total expression of GP (inactive) or the ratio of phosphorylated-to-total GP (Fig 5.11b-d). Similarly, neither HFSD feeding nor *Gabarapl1* gene delivery induced any changes in phosphorylated (S641, inactive) or total expression of GS (active) or the ratio of phosphorylated-to-total GS (Fig 5.12b-d).

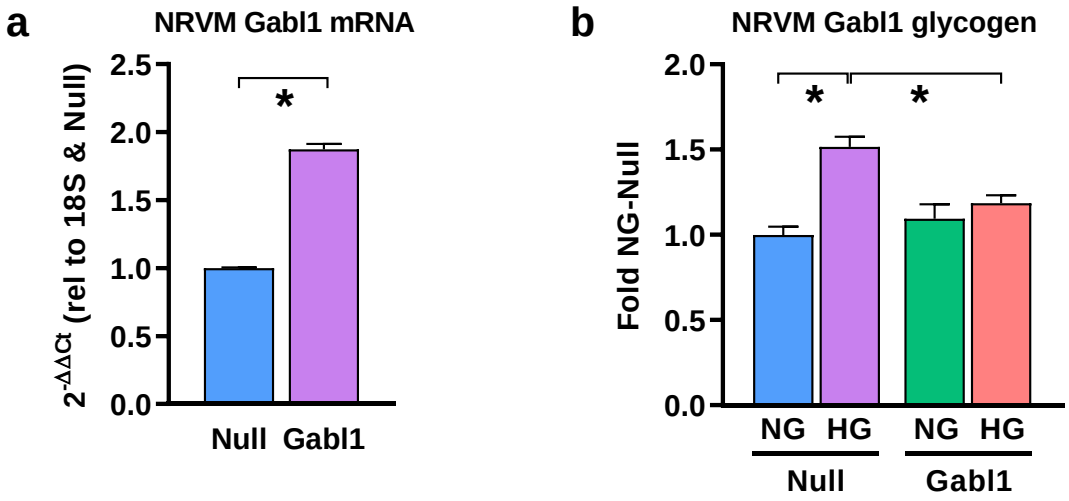

Figure 5.4: *Gabarapl1* over-expression prevents high glucose-induced glycogen accumulation *in vitro*. **(a)** Confirmation of AAV-induced *Gabarapl1* over-expression by qPCR (n=3 independent wells). **(b)** NRVM glycogen content in response to high glucose (HG) or *Gabarapl1* over-expression (n= 8-17 wells from 4 biologically independent cultures). Data analysed by Mann–Whitney U test or by 2-way ANOVA with Bonferroni post-hoc test. Data presented as mean±SEM, *p<0.05.

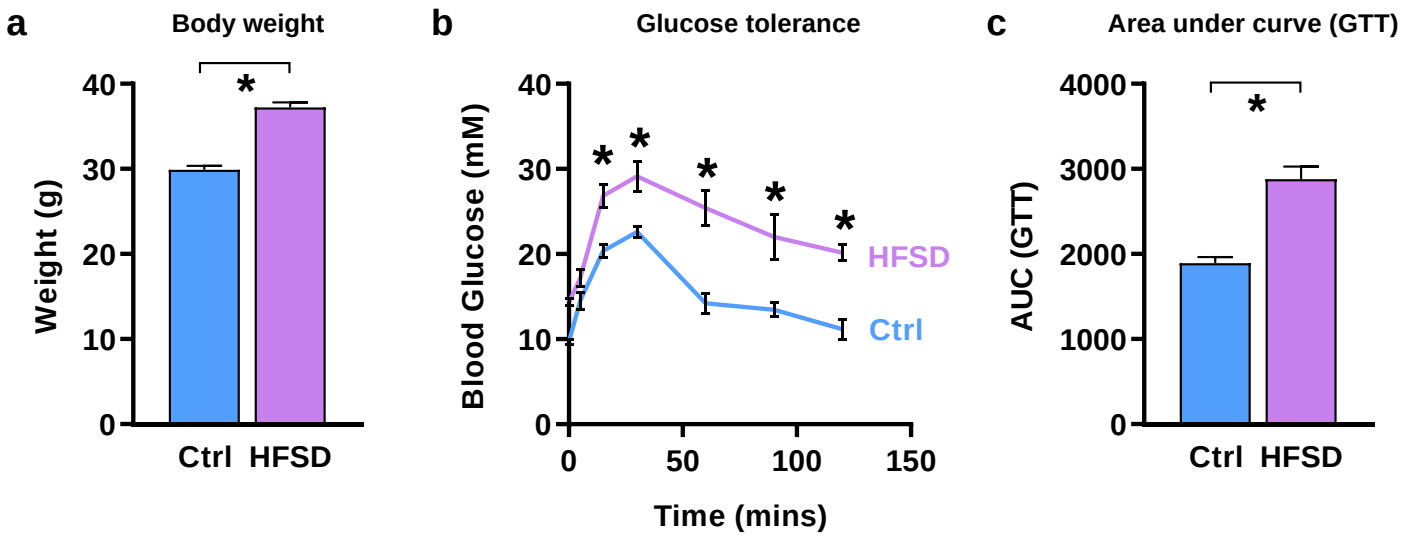

Figure 5.5: Establishment of a Type 2 Diabetic mouse model. (a) Body weight of the HFSD-fed mice prior to AAV administration (week 13 of diet, n=20 animals per group). **(b)** Glucose tolerance test (n=5-6 animals per group). **(c)** Area under curve derived from the glucose tolerance test (n=5-6 animals per group). Data analysed by 2-way ANOVA with repeated measures and Bonferroni post-hoc test or by Student's t-test. Data presented as mean±SEM, *p<0.05.

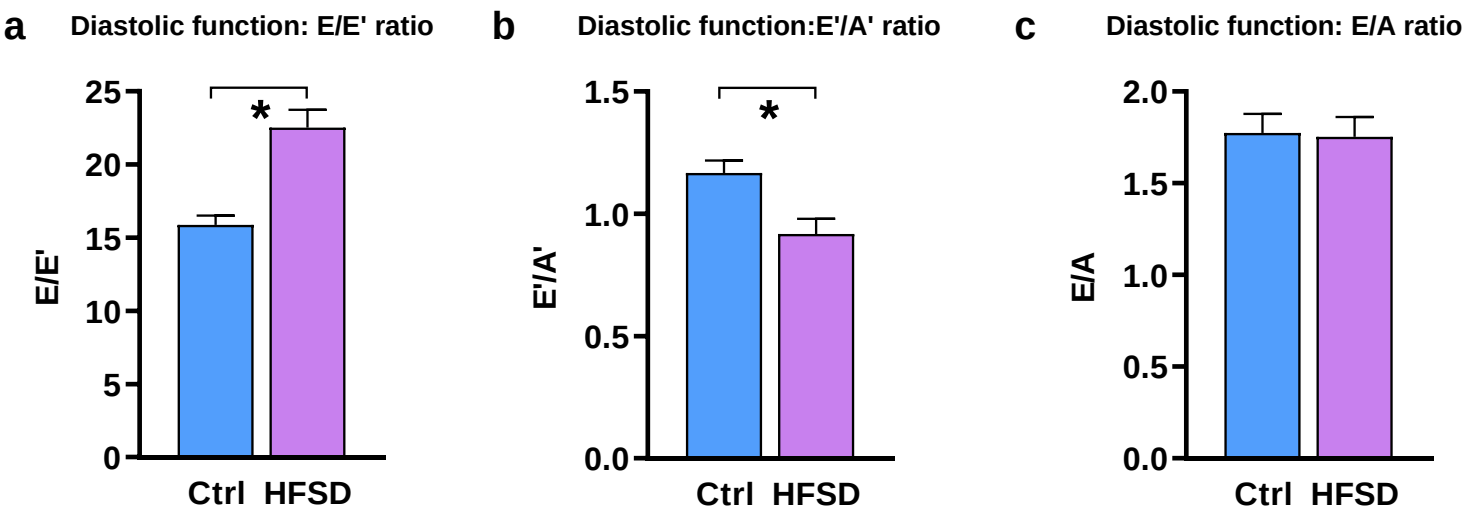

Figure 5.6: HFSD feeding induced diastolic dysfunction at 13 weeks post start of diet. (a) E/E' ratio (n=20-24 animals per group) **(b**) E'/A' ratio (n=20-24 animals per group). **(c)** E/A ratio (n=20-24 animals per group). Data analysed by Student's t-test. Data presented as mean±SEM, *p<0.05.

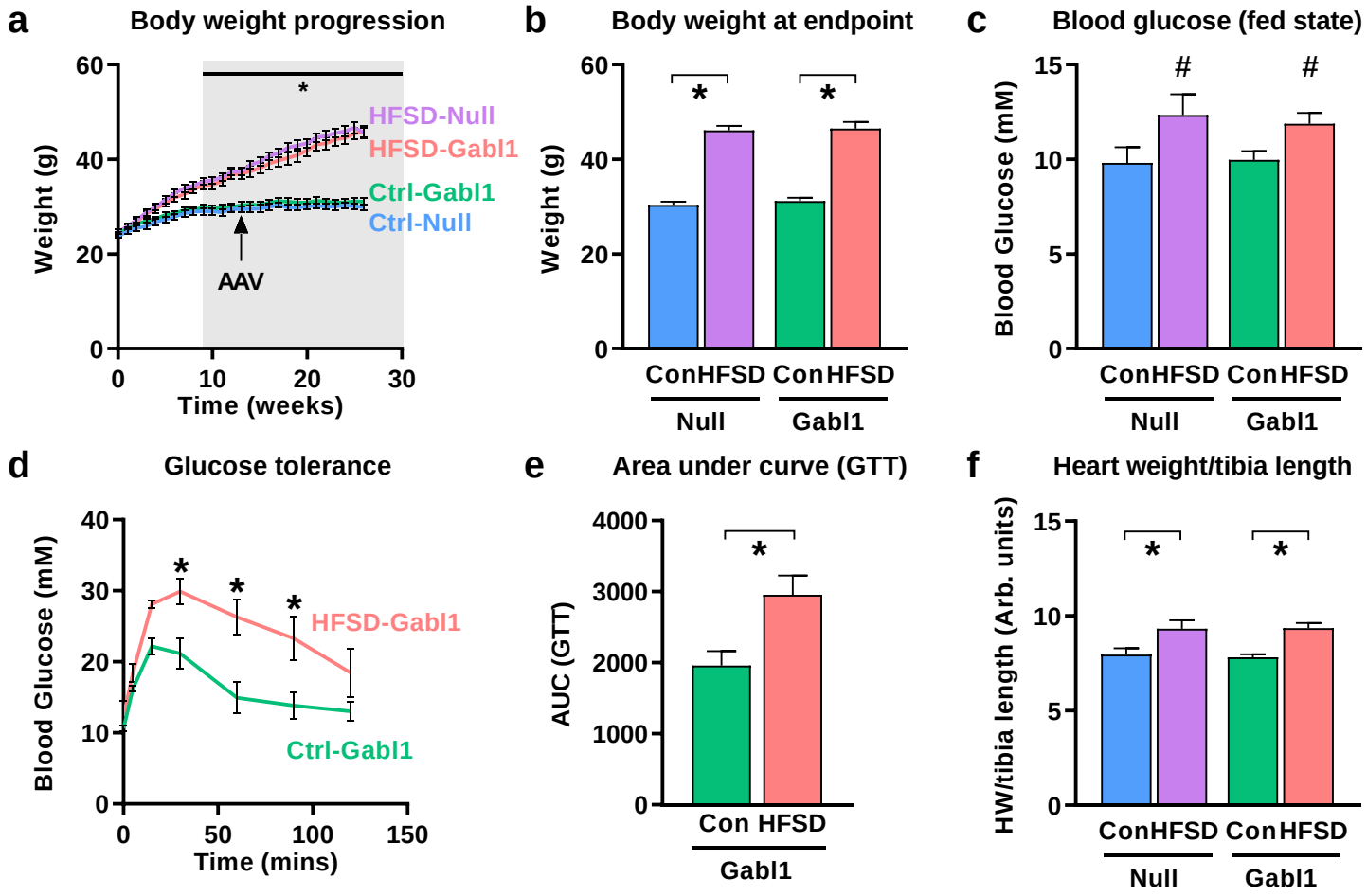

Figure 5.7: Cardiac-specific *Gabarapl1* gene delivery does not affect the systemic diabetic phenotype. (a) Progression of body weight gain of the HFSD-fed mice (n=10 animals per group). **(b)** Final body weight measurement, 12 weeks post-AAV injection (n=10 animals per group). **(c)** Fed-state blood glucose levels at the time of heart extraction (n=10 animals per group). **(d)** Glucose tolerance test (n=3 animals per group) **(e)** Area under curve derived from the glucose tolerance test (n=3 animals per group) **(f)** Wet heart weight normalized to tibia length (n=10 animals per group). Data analysed by 2-way ANOVA with or without repeated measures and Bonferroni post-hoc test or Student's t-test. Data presented as mean±SEM, *p<0.05, #p<0.05 2-way ANOVA diet factor effect.

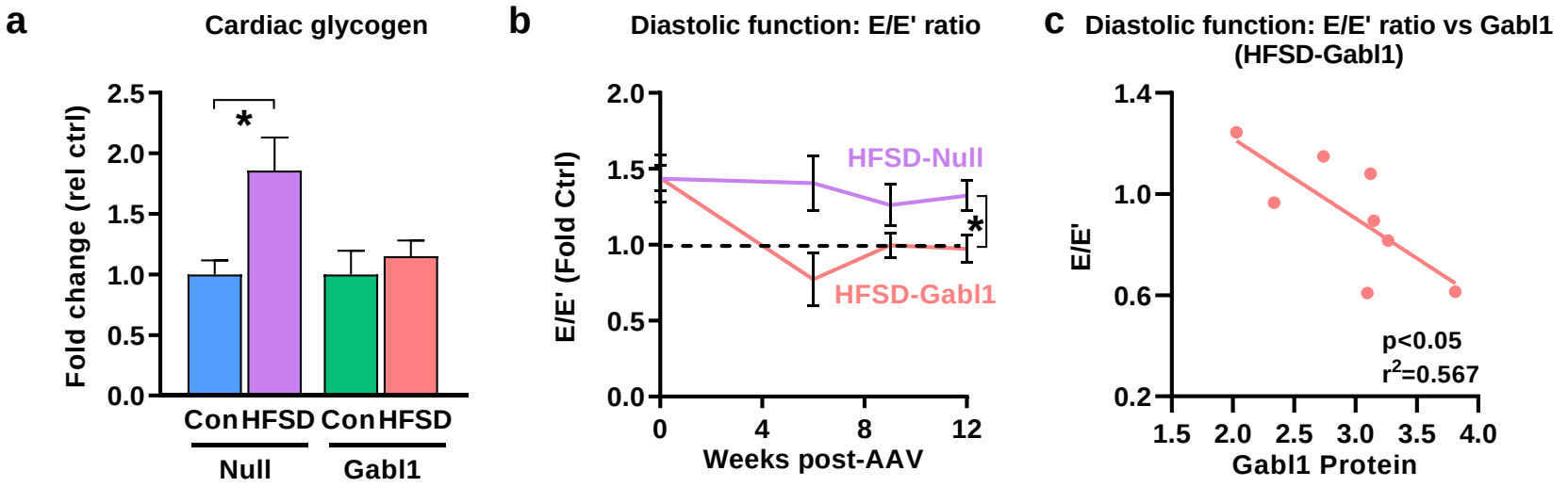

Figure 5.8: *Gabarapl1* gene delivery rescues glycogen accumulation and diastolic dysfunction in the diabetic heart. (a) Cardiac glycogen content in response to HFSD-induced diabetes or *Gabarapl1* gene delivery (n=9-12 animals per group) **(b)** Longitudinal representation of echocardiographic E/E' ratio (data presented as fold-change relative to control for each viral group, n=9-13 animals per group). **(c)** Correlation between membrane-bound Gabarapl1 protein and E/E' ratio in the HFSD-Gabl1 group (r, Pearson correlation coefficient). Raw (non-normalized) data was analysed by 2-way ANOVA with Bonferroni post-hoc test. Data presented as mean±SEM, *p<0.05.

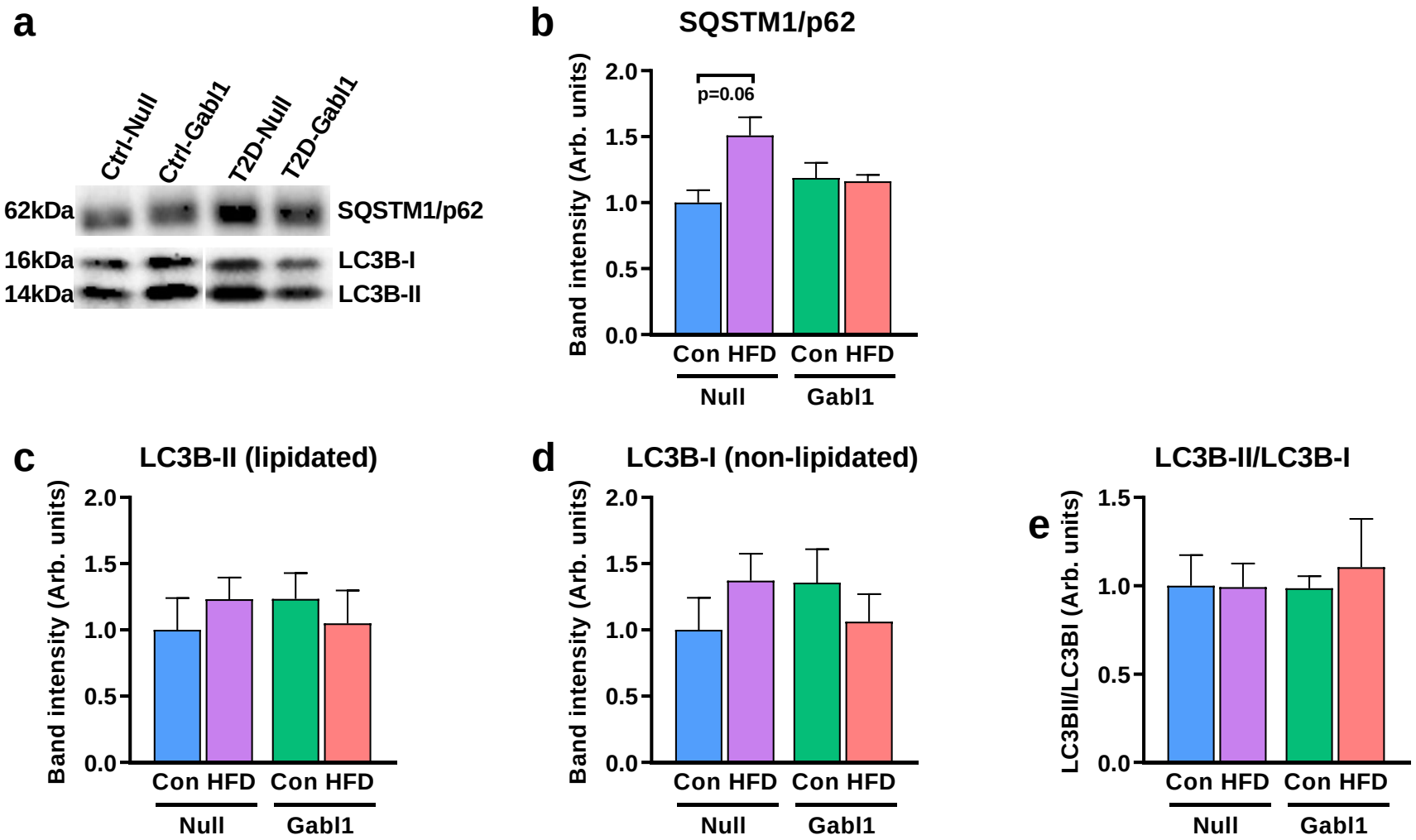

Figure 5.9: *Gabarapl1* gene delivery does not significantly affect macrophagy. (a) Representative immunoblots for SQSTM1/p62, LC3B-I (non-lipidated) and LC3B-II (lipidated). **(b)** Immunoblot quantification of SQSTM1/p62 (n=6 animals per group). **(c)** Immunoblot quantification of LC3B-II (n=6 animals per group)**. (d)** Immunoblot quantification of LC3B-I (n=6 animals per group)**. (e)** Ratio of lipidated-to-non-lipidated LC3 (LC3B-II/I) (n=6 animals per group). Data analysed by 2-way ANOVA with Bonferroni post-hoc test. Data presented as mean±SEM, *p<0.05.

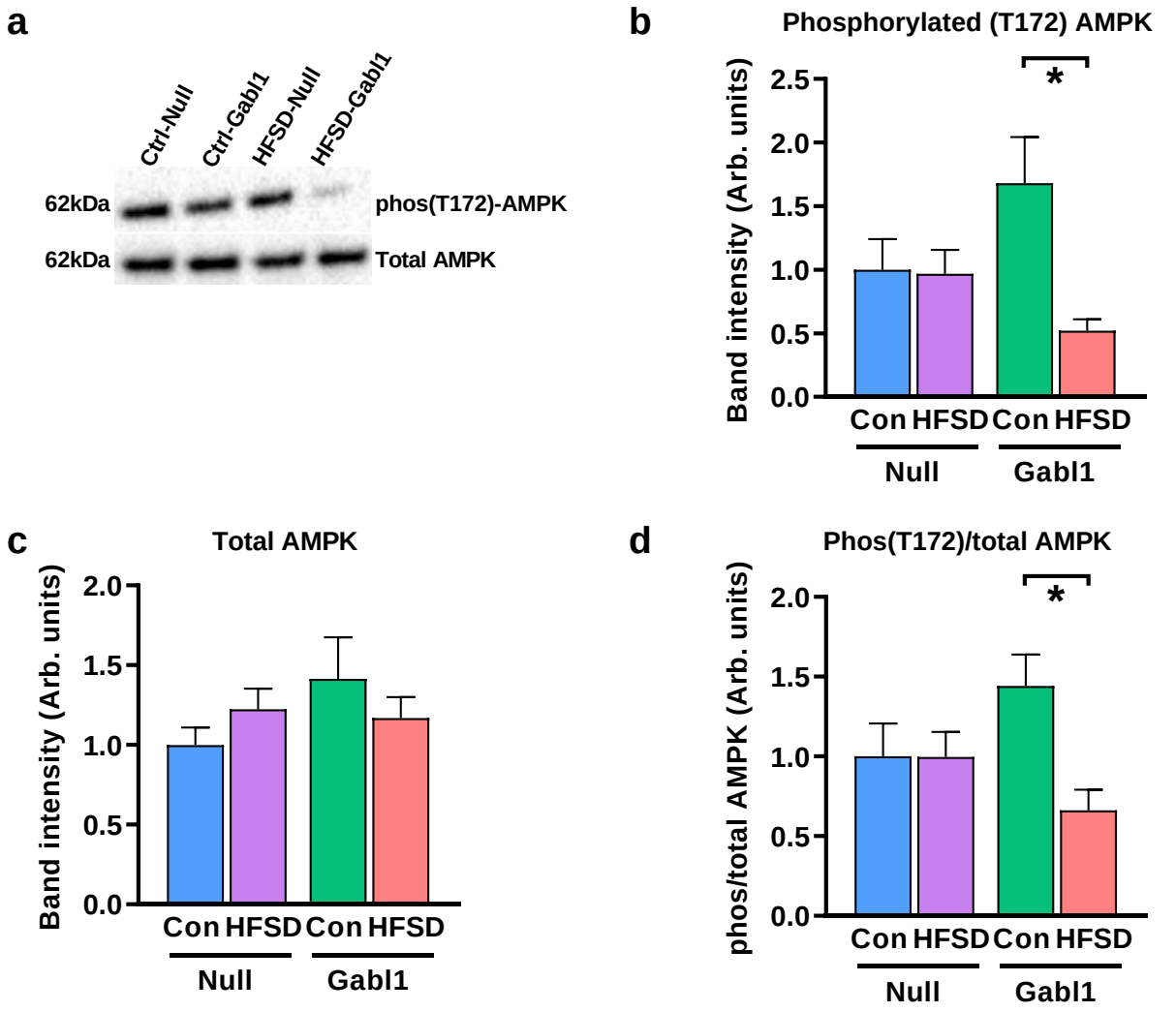

Figure 5.10: Diabetes reduces AMPK activation in a setting of *Gabarapl1* overexpression. (a) Representative immunoblots for total and phosphorylated AMPK. **(b)** Immunoblot quantification of phosphorylated (T172) AMPK (n=9-11 animals per group). **(c)** Immunoblot quantification of total AMPK (n=10-11 animals per group). **(d)** Ratio of phosphorylated-to-total AMPK (n=9-11 animals per group). Data analysed by 2-way ANOVA with Bonferroni post-hoc test. Data presented as mean±SEM, *p<0.05.

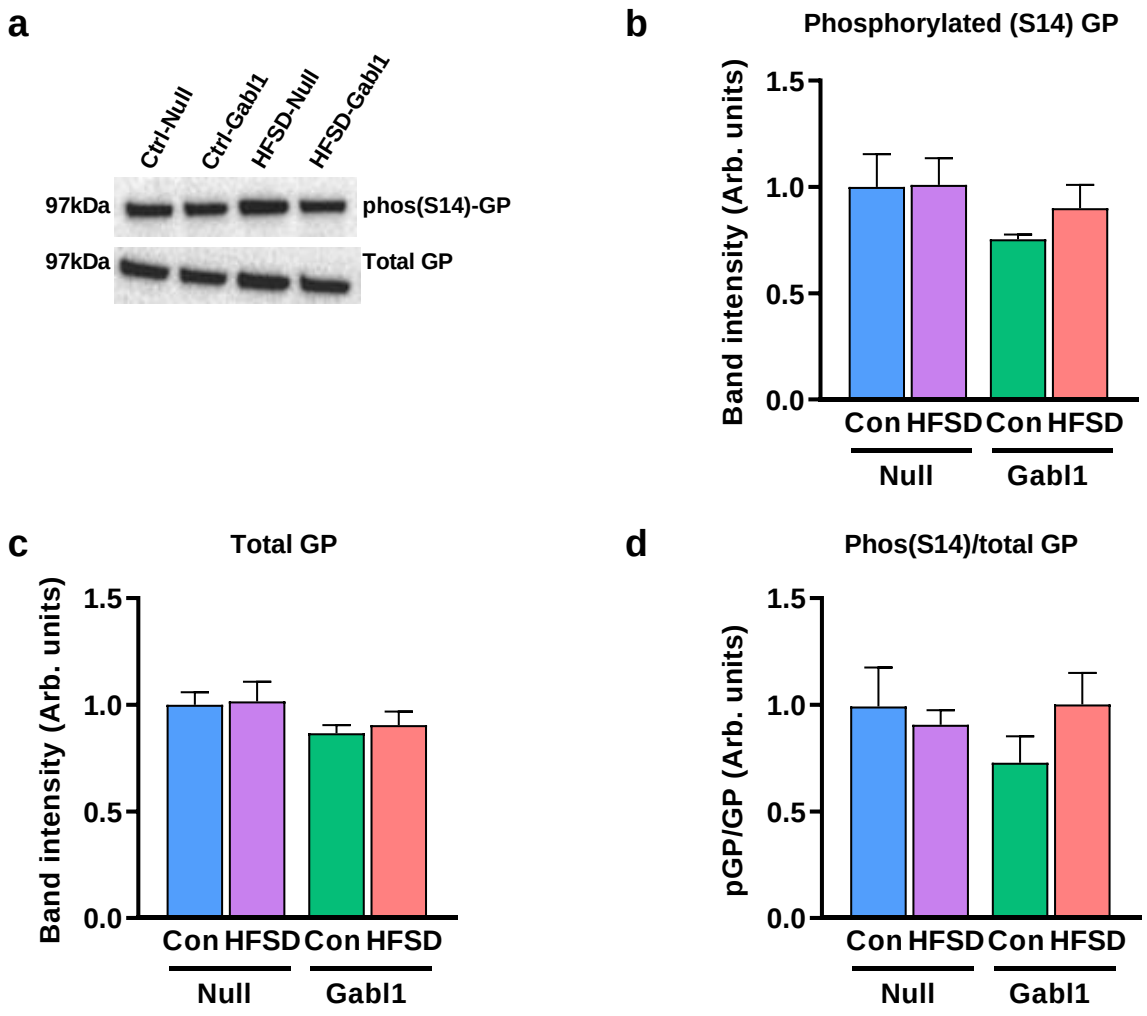

Figure 5.11: *Gabarapl1* gene delivery reduces glycogen independently of glycogen phosphorylase. (a) Representative immunoblots for phosphorylated (active) and total (inactive) glycogen phosphorylase (GP). **(b)** Immunoblot quantification of phosphorylated (S14) GP (n=6 animals per group). **(c)** Immunoblot quantification of total GP (n=5-6 animals per group). **(d)** Ratio of phosphorylated-to-total GP (n=5-6 animals per group). Data analysed by 2-way ANOVA with Bonferroni post-hoc test. Data presented as mean±SEM, *p<0.05.

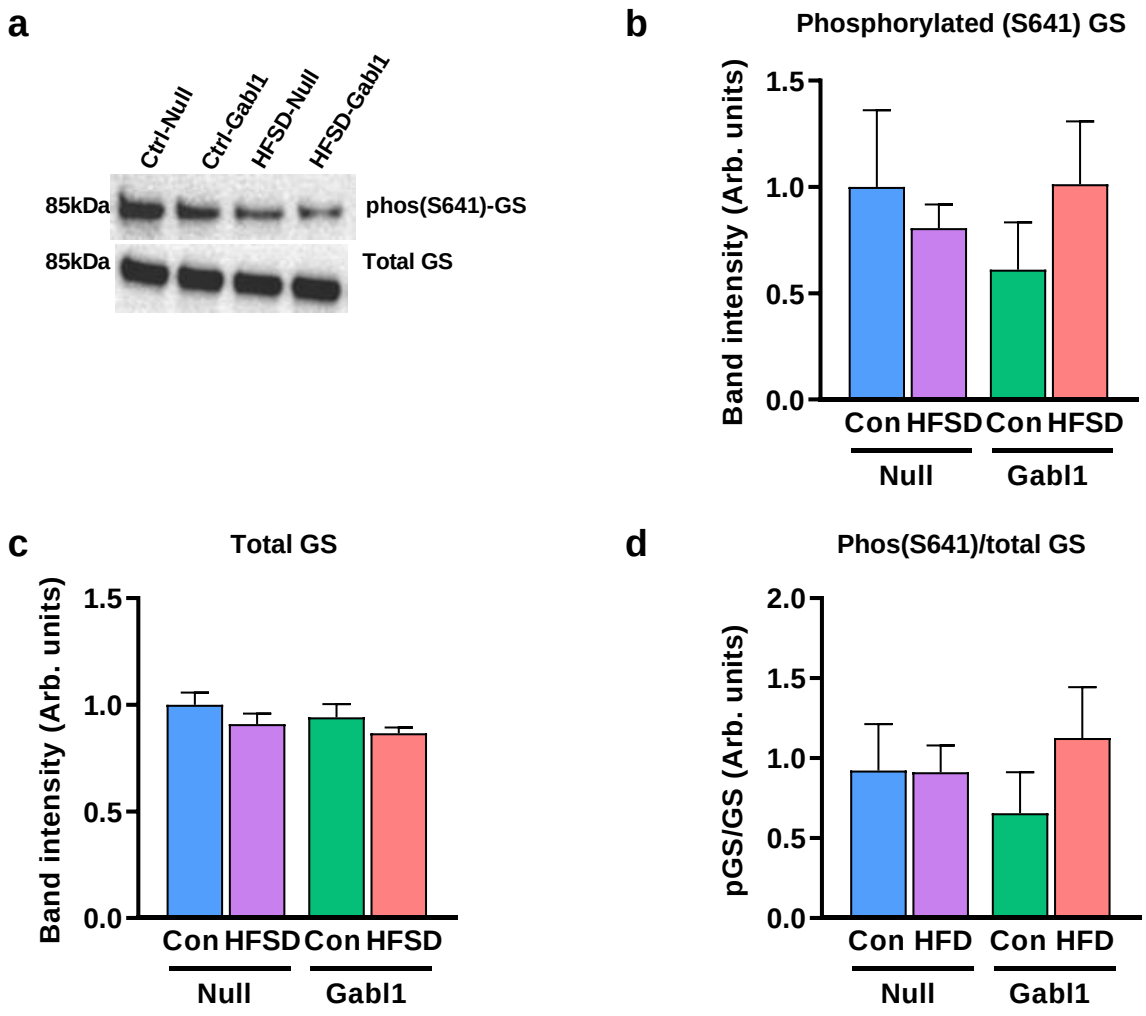

Figure 5.12: *Gabarapl1* gene delivery reduces glycogen independently of glycogen synthase. (a) Representative immunoblots for phosphorylated (inactive) and total (active) glycogen synthase (GS). **(b)** Immunoblot quantification of phosphorylated (S641) GS (n=5-6 animals per group). **(c)** Immunoblot quantification of total GS (n=5-6 animals per group). **(d)** Ratio of phosphorylated-to-total GS (n=5-6 animals per group). Data analysed by 2-way ANOVA with Bonferroni post-hoc test. Data presented as mean±SEM, *p<0.05.

Table 5.3: Endpoint characteristics of the HFSD mice

	AAV-Null		AAV-Gabl1	
	Ctrl	**HFSD**	**Ctrl**	**HFSD**
Body weight (g)	30.4 ± 0.7	46.1 ± 1.0*	31.2 ± 0.7	46.5 ±1.4*
Blood glucose (mM)	9.8 ± 0.8	12.3 ± 1.1	10.0 ± 0.5	11.9 ± 0.6
Heart weight (mg)	145.4 ± 6.0	169.1 ± 8.0*	142.2 ± 3.0	171.4 ± 5.6*
Heart weight/body weight (mg/g)	4.78 ± 0.1	3.68 ± 0.2*	4.58 ± 0.1	3.70 ± 0.1*
Tibia length (mm)	18.3 ± 0.1	18.1 ± 0.1	18.2 ± 0.1	18.3 ± 0.1
Heart weight/tibia length (arb. Units)	7.95 ± 0.33	9.32 ± 0.44*	7.8 ± 0.14	9.35 ± 0.27*

Data analysed by two-way ANOVA with Bonferroni post-hoc test. Data presented as mean±SEM, *p<0.05.

Table 5.4: Diastolic and systolic echocardiography parameters of the HFSD-fed and *Gabarapl1*-treated mice 11 weeks post-AAV administration

	AAV-Null		AAV-Gabl1	
	Ctrl	**HFSD**	**Ctrl**	**HFSD**
MV E (mm/s)	502.33±33.4	586.03±31.97	533.83±20.69	589.67±25.57
MV A (mm/s)	349.54±37.78	387.86±37.17	360.49±28.62	432.79±33.14
MV E/A	1.69±0.18	1.50±0.10	1.60±0.11	1.44±0.10
MV E' (mm/s)	28.08±1.87	24.64±1.14	25.70±2.38	25.0±1.39
MV A' (mm/s)	23.45±1.57	23.31±2.12	23.40±2.53	23.58±1.98
MV E'/A'	1.24±0.07	1.15±0.12	1.18±0.12	1.15±0.13
LV internal diameter (mm)	3.60±0.06	4.16±0.15*	3.70±0.07	4.09±0.1*
End diastolic volume (ml)	0.026±0.002	0.03±0.003	0.03±0.002	0.026±0.001
LV posterior wall thickness (mm)	0.94±0.01	0.94±0.03	0.94±0.03	0.91±0.03
Ejection fraction (EF, %)	70.7±2.0	69.4±1.6	66.3±0.9	62.8±2.2
Fractional shortening (FS, %)	31.8±1.1	29.8±1.0	29.6±0.6	26.8±1.0

Data analysed by two-way ANOVA with Bonferroni post-hoc test. Data presented as mean±SEM, *p<0.05.

Table 5.5: Pulse wave and tissue Doppler echocardiography parameters of the HFSD-fed and *Gabarapl1*-treated mice 5 weeks post-AAV administration

	AAV-Null		AAV-Gabl1	
	Ctrl	**HFSD**	**Ctrl**	**HFSD**
MV E (mm/s)	511.8±42.22	509.1±31.44	427.1±11.84	507.2±38.62
MV A (mm/s)	370.7±64.58	389.0±52.24	228.5±17.4	237.0±28.69
MV E/A	1.48±0.12	1.39±0.20	1.91±0.09	2.40±0.57
MV E' (mm/s)	37.62±4.66	29.15±4.19	30.38±3.84	35.3±4.38
MV A' (mm/s)	28.27±1.96	25.47±4.14	28.92±2.81	25.02±4.03
MV E'/A'	1.34±0.16	1.26±0.30	1.11±0.22	1.46±0.12

Data analysed by two-way ANOVA with Bonferroni post-hoc test. Data presented as mean±SEM, *p<0.05. MV A, MV A' and MV E/A datasets did not meet parametric assumptions. Statistical significance was determined using Kruskal-Wallis non-parametric test.

5.4. Discussion

This study is the first to show that a cardiac-specific, glycophagy-targeting genetic manipulation is beneficial with respect to cardiac functional outcomes in diabetic heart disease. Cardiac *Gabarapl1* gene delivery in mice fed a high-fat/sugar diet for a period of 26 weeks reduced diabetes-induced glycogen accumulation and exerted favourable influence on cardiac diastolic function while no effects on systolic function were evident. Amelioration of diabetes-induced glycogen accumulation with cardiac *Gabarapl1* gene delivery appeared independent of changes in glycogen handling enzymes (glycogen synthase and glycogen phosphorylase), AMPK or macro-autophagy markers. Thus disease rescue in this context is likely driven by *Gabarapl1*-induced glycophagy-mediated glycogen breakdown.

5.4.1. *Gabarapl1* gene delivery rescues diastolic dysfunction in diabetes

The study presented in this Chapter demonstrated that *Gabarapl1* upregulation reduced E/E' to levels comparable to control. Additionally increased membrane-bound GABARAPL1 protein levels correlated with decreased E/E' values. These findings corroborate the research presented in Chapter 4 where reduction in GABARAPL1 availability induced diastolic dysfunction in the form of increased E/E' ratio. Additionally, HFSD feeding did not induce systolic dysfunction, which is consistent with reports in the literature indicating that diabetic cardiomyopathy often presents without systolic abnormalities[21,31,32,283,284]. It is remarkable that at the whole organ level E/E' was resolved following *Gabarapl1* gene delivery, indicating rescue of the high fat diet-induced diastolic dysfunction. In support of GABARAPL1 rescuing diastolic dysfunction, an unpublished parallel study by our collaborators, conducted using human cardiac organoids, showed that the high glucose-induced delay to 50% relaxation of force was rescued following transduction with AAV-*Gabarapl1*. Furthermore, experiments conducted using isolated cardiomyocytes from HFSD-fed mice showed that *Gabarapl1* gene delivery restored the diastolic force-length relationship (measure of diastolic stiffness, Mellor-Delbridge, unpublished). It is evident that although ventricular compliance was restored, diabetes-induced chamber dilation was not rescued following *Gabarapl1* gene delivery as left ventricular internal diameter remained significantly augmented. Thus, although the precise mechanisms are unclear, it appears that the genetic intervention employed in this study, specifically

and separately operated in mediating cardiomyocyte mechanics but did not have an effect on cellular dimensions or morphology.

Taken together, these parallel studies indicate that cardiac-specific upregulation of GABARAPL1 has the capacity to rescue diabetes-induced diastolic dysfunction by restoring muscle compliance. It is interesting that E/E', but not E/A (additional parameter used to assess diastolic dysfunction) was restored following *Gabarapl1* gene delivery. Changes in E/E' without changes in E/A have been previously reported[285] and could be attributed to pseudo-normalization of the E/A ratio[286]. E/E' is derived on a combinatory basis of both pulsed wave Doppler and tissue Doppler and is therefore considered a concurrent comprehensive measure of impaired filling and ventricular compliance, making it the most clinically-accepted parameter for assessment of diastolic dysfunction[34].

5.4.2. GABARAPL1-mediated alleviation of cardiac dysfunction is likely linked to glycophagy upregulation

The study presented in this Chapter assessed the hypothesis that GABARAPL1 upregulation will result in rescue of diabetes-induced diastolic dysfunction through restoration of cardiac glycogen levels. Indeed, cardiac-specific *Gabarapl1* gene delivery both prevented high glucose-induced increase in glycogen deposition in cardiomyocytes *in vitro* and rescued diabetes-induced cardiac glycogen accumulation *in vivo*. Given that GABARAPL1 has been implicated in glycophagy in published reports[146,147,157] and its reduced availability was demonstrated to increase myocardial glycogen deposition in Chapter 4, it can be speculated that the GABARAPL1-mediated effects on glycogen and cardiac function were through glycophagy upregulation. It is important however to consider other glycophagy-independent mechanisms via which GABARAPL1 upregulation could have exerted its beneficial effects on cardiac function. Primarily, as it has been reviewed in Chapter 1 of this Thesis, GABARAPL1 plays an important role in macro-autophagy by both tethering cargo receptors to the phagosome and by providing a scaffold for assembly of numerous proteins involved in autophagy induction[78,85,164,250]. In addition, autophagy disturbances have been linked with diabetes-induced cardiopathology both in rodent models[91-112,287] and in human patients[114,115], although there appear to be no consistent differences, even between studies using the same diabetic models. Consequently, the macro-autophagy markers LC3B-I, LC3B-II and SQSTM1/p62 were

examined in the context of this study but neither HFSD feeding nor *Gabarapl1* gene delivery were found to induce any detectable significant differences. It should be noted that there was a trend for increase of SQSTM1/p62 following HFSD feeding, which was absent in the *Gabarapl1*-treated mice. Accumulation of this protein is traditionally thought of as a marker of macro-autophagy impairment but it usually coincides with alterations in LC3-II[288] which were not detected in this study. It is therefore unlikely that *Gabarapl1*-induced functional benefits are through a macro-autophagy mechanism.

Glycogen handling has been shown to be regulated by the energy sensor AMPK. Under energetically plentiful conditions, AMPK is inhibited thereby allowing energy storage processes to proceed, including glycogen synthesis[289]. In contrast, when nutrients are scarce AMPK activation promotes glucose uptake[216,290] and glycogen breakdown and inhibits synthesis[289,291,292]. Consequently, total and active (phosphorylated) AMPK were measured in this study. Interestingly, it was shown that HFSD feeding decreased AMPK phosphorylation only under conditions of *Gabarapl1* overexpression. A decrease in AMPK phosphorylation could lead to a concurrent upregulation of glycogen synthase and inhibition of glycogen phosphorylase[184,190] thereby inducing a subsequent increase in glycogen content, which would be the opposite phenotype to what was observed in the study. However, total expression or phosphorylation of neither GS nor GP were different in *Gabarapl1*-treated hearts, indicating that *Gabarapl1*-induced decrease of glycogen deposition is not through altered regulation of cytosolic glycogen handling enzymes. The observed reduction in phosphorylation of AMPK could be due to increased ATP levels derived from *Gabarapl1*-induced upregulation of glycophagy. Increased lysosomal glycogen breakdown, could result in higher glucose availability and therefore an increase in glycolytic energy production. The increased ATP availability would lower the AMP/ATP ratio thereby reducing phosphorylation of AMPK in the *Gabarapl1*-treated mice. It has been suggested that Ca^{2+} reuptake by the SR Ca^{2+} pumps during relaxation relies on glycolysis-derived ATP that depends on the levels of glycogen[258]. Therefore, and although the precise mechanism has not been identified in this study, it could be argued that the *Gabarapl1*-induced rescue of diastolic dysfunction at both the single cardiomyocyte and whole heart

levels could be through glycophagy-derived increase of glycolytic ATP that ultimately results in improved Ca^{2+} re-uptake by the SR during relaxation.

5.4.3. Cardiac-specific targeting of glycophagy could offer therapeutic potential for diabetic cardiomyopathy

This study is one of a limited number of investigations utilizing an autophagy-related, cardiac-specific intervention with aim to assess cardiac function in diabetes. Additionally, this is the first study reporting beneficial functional outcomes following a cardiac-specific genetic manipulation. A number of studies have been conducted aiming to either upregulate or inhibit autophagic pathways in a diabetic context but in their majority, these studies involved either systemic pharmacological administrations or global genetic manipulations, and had discrepant results with respect to cardiac function[98,99,103,107-109,287]. In other words, activation and inhibition of autophagy was shown to be both beneficial and detrimental to cardiac function, which may be due to systemic homeostatic alterations resulting from global autophagy targeting. There has been one report utilizing cardiac-specific *Beclin 1* upregulation in a rodent model of T1D, which was shown to aggravate diabetes-induced cardiac dysfunction even though autophagy was upregulated[109]. Similarly, cardiac-specific deletion of *Ulk1* was shown to exacerbate cardiac dysfunction in mice fed a high fat diet[91]. Even though these studies involved cardiac-specific interventions, the target molecules are upstream autophagy modulators, which may indicate that more targeted, downstream approaches are required in order to exert favourable functional outcomes. This indeed, may be the basis of success of the study presented in this Chapter. This investigation is the first to demonstrate that cardiac-specific upregulation of the selective autophagy branch, glycophagy, results in alleviation of diabetes-induced diastolic dysfunction. Thus, targeting glycophagy in the diabetic heart may provide a novel therapeutic approach for diabetic cardiomyopathy.

5.5 Conclusions

This study is the first to show that upregulating glycophagy exerts favourable functional outcomes for the diabetic heart. It is demonstrated that cardiac-specific gene delivery of the key glycophagy molecular mediator, GABARAPL1, simultaneously rescues diabetes-induced cardiac glycogen

accumulation and diastolic dysfunction in a rodent model of type 2 diabetes. The mechanisms via which restoration of glycogen levels alleviate diabetic diastolic dysfunction are not dissected in this investigation but the beneficial functional outcomes are evident. Thus, further research into the precise mechanisms via which GABARAPL1 mediates cardiac glycogen handling now warranted.

5.6. Limitations

In this study AAV9 gene delivery was employed for targeted gene manipulation as a first step in demonstrating the therapeutic potential of targeting the glycophagy pathway in the diabetic heart. Although AAV transgene vectors have been successfully used in humans, some limitations in the clinical translation of AAV gene therapy have been recognised and mainly involve capsid-elicited immunogenicity. This is dose dependent and particularly evident following systemic administration of recombinant vectors although it can be prevented by simultaneous administration of immunosuppressant formulations[293-295]. Thus, targeting glycophagy in the human heart may require employment of alternative approaches such as small molecule administration or localized gene delivery. An additional note should be made here regarding the use of NRVMs as the *in vitro* preparation to verify that *Gabarapl1* gene delivery can rescue glycogen accumulation in cardiomyocytes. Although, the use of neonatal cells, as opposed to adult, was technically favourable due to the difficulty of maintaining adult cardiomyocytes in culture, there are certain limitations that should be mentioned. Neonatal cardiomyocytes are metabolically different to the adult heart[56]. The neonatal cardiac muscle is primarily glycolytically driven in contrast to an augmented reliance on FA oxidation exhibited by the adult heart. Thus, there was the possibility that the role of GABARAPL1 in the neonatal heart as it relates to glycogen handling and glycophagy, would diverge from its role in the adult heart. However, as indicated by the findings presented in Chapter 4, *Gabarapl1* gene deletion induced glycogen accumulation in both the neonatal and adult mouse heart. Thus it was expected that the findings from the *in vitro* studies employing NRVMs would translate to adult *in vivo* settings. Additionally, NRVMs were cultured under high glucose conditions to mimic the diabetic environment but it should be acknowledged that diabetes involves numerous insults in addition to hyperglycemia. Furthermore, it is evident that direct GABARAPL1 protein quantification was not provided to verify AAV-induced overexpression. This is due to lack of reliable antibodies that would

confer the ability to accurately quantify the GABARAPL1 band in immunoblots. The correlation presented in Figure 5.8c utilizes GABARAPL1 protein amount as it was quantified in membrane fractions of cardiac samples. However, given the dynamic nature of the glycophagy process and the constant shuttling of its mediators, including GABARAPL1, between the cytosol and phagosomes, using the presence of GABARAPL1 in the membrane fractions to infer overexpression would be inaccurate. Instead, the approach taken in this Thesis was to verify the presence and quantify the amount of cardiac viral load at the study end-point (Appendix 2). Finally it should be noted that figures 5.7c and 5.7e include Ctrl-Gabl1 and T2D-Gabl1 groups but not the equivalent null-treated groups. This approach was taken because the effect of HFSD on glucose tolerance was established and presented earlier in the Thesis (Fig 5.5b-c). A similar effect of HFSD on glucose tolerance was observed in the AAV-null groups although the data is not shown. Additionally, this approach prevented the line graphs from being overcrowded.

CHAPTER 6

General discussion

Overview

Diabetic cardiomyopathy was first described over 40 years ago and has since been established as a distinct cardiac pathology. The Framingham study concluded that diabetic individuals have higher risk of heart failure and indeed this is the main cause of mortality in diabetes. In humans, diabetic cardiomyopathy manifests with early diastolic dysfunction, which may or may not be followed by systolic functional defects. In addition, diabetes-induced deterioration of cardiac function is not necessarily associated with vascular abnormalities including coronary artery disease (CAD) or hypertension. As shown in human patients[27,28], and in various rodent models of either type 1 or type 2 diabetes (T1D or T2D respectively)[6-8], diabetic diastolic dysfunction is most commonly associated with abnormal ventricular filling due to increased cardiomyocyte stiffness[10,27]. Currently there are no effective treatment options for diastolic dysfunction indicating that further investigations into the underlying molecular mechanisms are warranted.

Diabetic cardiomyopathy is associated with a multitude of cardiac metabolic disturbances including reduced glucose uptake, altered substrate utilization, increased lipid deposition, mitochondrial stress and autophagy dysregulation[12]. Additionally, the diabetic heart is characterised by glycogen accumulation. This paradoxical phenomenon is consistent across the diabetic spectrum, correlates significantly with diastolic dysfunction and cannot be attributed to alterations in the well-characterised cytosolic glycogen-handling pathway (Mellor-Delbridge, unpublished). Glycogen accumulation has been linked to deterioration of cardiac function in the context of inherited glycogen storage diseases but it has not been previously investigated in the context of the diabetic heart as a contributing factor to diastolic dysfunction.

The studies presented in this Thesis were devised to identify the molecular mechanisms underlying diabetic cardiac glycogen accumulation. The novel finding that glycogen autophagy (glycophagy) is disturbed in the diabetic myocardium in pre-T2D and T2D rodent models of disease, defined the course of this Thesis to investigate the role of this pathway in the heart in the absence and presence of systemic diabetes. The direction of the research undertaken during this candidature is depicted in Figure 6.1 and the main findings are stated below.

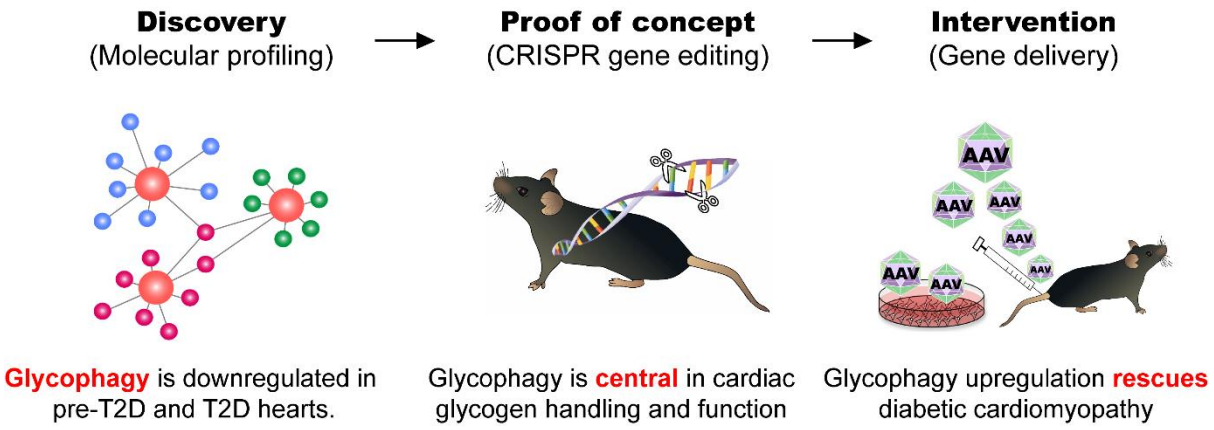

Figure 6.1: Direction of research conducted during candidature. First, glycophagy was identified as a pathway of interest in the diabetic heart. The role of glycophagy in the heart was subsequently established to be pivotal for physiological glycogen handling and cardiac function. Last, intervention in the form of viral gene delivery restored glycogen levels and rescued diastolic dysfunction in the diabetic heart *in vivo*.

The three main questions addressed in this Thesis are:

(4) What are the molecular alterations underlying increased glycogen deposition in the diabetic heart? (Chapter 3)

(5) What is the role of the key glycogen autophagy (glycophagy) protein, GABARAPL1, in regulating cardiac function and glycogen content? (Chapter 4)

(6) Can glycophagy-targeting interventions rescue cardiac function and provide therapeutic potential for diabetic cardiomyopathy? (Chapter 5)

The three main findings of this investigation are:

(4) **Molecular discovery**: The diabetic heart is characterised by glycophagy disturbance involving *Gabarapl1* downregulation.

(5) **Glycophagy proof of concept**: Reduction in GABARAPL1 availability is sufficient to induce cardiac glycogen accumulation and diastolic dysfunction *in vivo*.

(6) **Glycophagy disease intervention**: *Gabarapl1* upregulation rescues diabetes-induced cardiac glycogen accumulation and diastolic dysfunction *in vivo* in a T2D mouse model.

The importance and implications of these findings are discussed in more detail in the remainder of this Chapter.

6.1. Glycophagy disturbance may be the underlying cause of diabetic cardiac glycogen accumulation

Increased glycogen deposition in the diabetic myocardium was first observed in 1930[13] and has since been circumstantially reported in the literature[116-138]. Our group systematically showed that glycogen accumulation is a consistent phenotype in the diabetic heart and may be a contributing factor to diabetic cardiomyopathy. The findings presented in Chapter 3 demonstrated that gene alterations associated with the cardiac diabetic environment are aligned with Glycogen storage diseases but glycogen accumulation cannot be explained by alterations in cytosolic glycogen handling enzymes or upstream glycogen signalling. Further computational investigation indicated that this paradoxical phenomenon might be the result of disturbances in glycophagy (glycogen-specific autophagy). The presence of a lysosome-mediated glycogen breakdown pathway has been known for a long time due to the link between inherited diseases, caused by mutations in lysosomal genes, and phenotypic glycogen accumulation in various tissues[14,166,177,181]. The mechanisms however, via which glycogen is transported to lysosomal compartments remained largely unknown. Lysosomal glycogenolysis was placed in the context of selective autophagy in the last decade, following identification of STBD1 as a protein that contains both a carbohydrate-binding domain and an ATG8-interacting motif. In addition, STBD1 was shown to preferentially interact and co-localize with GABARAPL1. These findings lead to the conclusion that glycophagy (glycogen-specific autophagy) involves GABARAPL1-facilitated sequestration of STBD1-bound glycogen to phagosomes[146,147]. The findings presented in this Thesis demonstrate for the first time that the diabetic heart is characterised by irregular expression of glycophagy molecular mediators. In both diet-induced glucose intolerance (pre-T2D) and T2D rodent models, cardiac mRNA expression of *Gabarapl1* was reduced. Furthermore, *Gabarapl1* was downregulated in the human diabetic myocardium indicating that the experimental models accurately recapitulate human disease.

The research findings presented in Chapter 3 of this Thesis provide the first evidence that in the glucose intolerant and type 2 diabetic heart, sequestration of glycogen to the phagosome may be insufficient. This is the first investigation to provide a link between diabetic cardiac glycogen accumulation and *Gabarapl1* downregulation as an underlying, causal, molecular disturbance. While

cardiac dysfunction has been observed under conditions of impaired lysosomal glycogenolysis[177,179,181], glycophagy has not previously been investigated in the heart. Similarly, no research on the role of GABARAPL1 in the heart has been previously conducted. Thus, computational and experimental identification of glycophagy as a pathway of interest in the diabetic heart shaped the direction of this Thesis to next investigate the role of this process in the heart in the absence of prior underlying pathology.

6.2. Glycophagy: an active process in the healthy heart

This Thesis is the first to show that glycophagy is an active process in the heart and demonstrate a role for GABARAPL1 in mediating cardiac glycogen handling. It is shown that reduction in GABARAPL1 availability, via CRISPR/Cas9-induced gene deletion, is sufficient to induce myocardial glycogen accumulation *in vivo*. GABARAPL1 is one of the six mammalian ATG8 proteins. More specifically, it belongs to the GABARAP subfamily along with two additional members, GABARAP and GABARAPL2, with which it shares 87% and 61% sequence identity respectively[160]. GABARAPL1 has been implicated in glycophagy due to reported complete co-localization with STBD1 in CHO cells[146]. In addition, even when overexpressed alone, GABARAPL1 localized in proximity to the Endoplasmic Reticulum (ER) and *trans*-Golgi Network (TGN)[163] which is similar to the pattern exhibited by overexpressed STBD1[146,157]. Thus, the observed myocardial glycogen accumulation in this *Gabarapl1*-KO model is likely the result of glycophagy inhibition. It has been suggested that hepatic glycophagy is employed as the primary glycogen mechanism during the postnatal starvation period[197,198]. The findings presented in this Thesis show that inhibition of glycophagy via deletion of *Gabarapl1* induced significant glycogen accumulation in the neonatal mouse heart, suggesting a similar role for cardiac glycophagy. While this is the first evidence to show that an autophagy-related molecule mediates cardiac glycogen handling, it is perhaps not surprising given that the neonatal heart relies on glycolytic energy production (due to limited availability of circulating fatty acids)[201]. In contrast, the novel finding that glycophagy mediates glycogen handling in the adult heart is intriguing. Counter to the neonatal heart, adult cardiac energy derivation exhibits higher reliance on fatty acid (FA) oxidation (60%) than glycolysis-derived ATP (40%)[56]. This suggests that despite different utilization of metabolic substrates, glycophagy is evidently active in the adult

heart under basal conditions as no induction methods (e.g. starvation) were employed in this study. Thus, in the heart, there may be processes that rely on glucose-derived energy over FA oxidation and thus glycophagy operates to provide a constant supply of glucose residues.

While GABARAPL1 is thought to be the anchor for STBD1 in the phagosome and therefore the glycophagy-specific ATG8, it has also been implicated in autophagy induction. It has been suggested that binding of GABARAPL1 to autophagy regulatory proteins such as ULK1 provides a scaffold for assembling initiation complexes at the site of phagosome formation (omegasome) [85,250]. Additionally, there is emerging evidence suggesting that glycophagy initiation is similar to that of macro-autophagy in that it is regulated by mTOR[162,223]. Therefore, it is likely that reduction in GABARAPL1 availability could influence glycophagy at multiple stages. It could reduce sequestration of STBD1-bound glycogen to phagosomes but could also inhibit glycophagy induction. Furthermore, it has been shown that the GABARAP subfamily proteins are involved in phagosome-lysosome fusion[256,257]. Thus, in addition to glycogen sequestration to phagosomes and glycophagy initiation, reduction in GABARAPL1 availability could also negatively influence the later stages of glycophagy. Interestingly, a parallel study using the *Gabarapl1*-KO model and Electron Microscopy showed that the number of glycogen-containing phagosomes in the KO myocardium is markedly reduced compared to WT (Mellor-Delbridge, unpublished). Thus, it appears that GABARAPL1 deficiency inhibits glycophagy at earlier stages, either by negatively influencing initiation or by hindering glycogen sequestration to phagosomes.

6.3. *Gabarapl1* deletion is detrimental to cardiac function

Autophagy has been examined in a multitude of cardiac conditions such as cardiac hypertrophy, heart failure, ischemia/reperfusion and diabetic cardiomyopathy but collectively, there appears to be no agreement on whether alterations in the pathway reflect adaptive or maladaptive responses[77]. Furthermore, there is a limited number of reports examining the influence of autophagy-related molecules in absence of underlying pathology. It is interesting that these studies, although extensive, target proteins that operate during autophagy induction while studies targeting downstream factors such as the ATG8s are lacking[247,248]. The findings presented in this Thesis (Chapter 4) are first to

show that *Gabarapl1* deficiency is sufficient to induce diastolic dysfunction in absence of any underlying systemic pathology. This is the first study to demonstrate that a downstream phagosome-associated protein is implicated in cardiac function. The mechanisms via which *Gabarapl1* deletion influenced diastolic function in this model are unclear but it is likely that several mechanisms are involved. GABARAPL1 has been implicated in a number of autophagy processes including glycophagy. Given that glycogen has been observed to localize throughout the sarcomeres, it is possible that its presence could result in glycation of myofilament structures[260,261,296]. Thus, under conditions characterised by glycophagy impairment, excessive glycogen-derived glycation of contractile complexes could negatively influence cardiac function. Furthermore, siRNA-induced reduction in *Gabarapl1* availability in gastric cancer cell lines has been shown to reduce the overall cellular ATP content[297]. Thus, it would be interesting to consider the implications of ATP reduction in the myocardium. It has been proposed that Ca^{2+} uptake during relaxation relies on the use of glycolysis-derived ATP by SERCA2a[258]. Therefore, it could be hypothesised that *Gabarapl1* gene deletion could have prevented glycophagy-derived glucose release, thereby reducing supply of glycolytic ATP, thus inducing diastolic dysfunction. Although the precise mechanisms via which *Gabarapl1* deletion induces diastolic dysfunction are elusive, it is interesting that the genetically modified *Gabarapl1* deficient myocardium exhibits a similar phenotype to the diabetic heart in that it is characterised by both glycogen accumulation and diastolic dysfunction. This provides further confidence in the hypothesis that diabetes-induced glycophagy downregulation induces cardiac glycogen accumulation thereby contributing to diastolic dysfunction. The findings reported in this Thesis, that GABARAPL1 and glycophagy are involved in physiological cardiac glycogen handling, provide the basis for investigating glycophagy in other physiological and pathophysiological conditions characterised by cardiac glycogen accumulation such as fasting, exercise training, pregnancy and steroid toxicity[171,298-300].

6.4. Targeting glycophagy as a therapeutic approach for diabetic cardiomyopathy

Maintenance of physiological glycogen handling in the heart is vital for cardiac function. In particular, defects in lysosomal glycogenolysis have been linked to detrimental functional outcomes in inherited glycogen storage diseases (GDS type II and IV) where mutations in lysosome-residing proteins

induce glycogen accumulation and diastolic functional decline. Clinically, recombinant enzyme replacement therapy (ERT) for GAA is used to restore lysosomal glycogen breakdown and has been shown to improve cardiac functional outcomes in glycogen storage diseases[14,166,177,181]. In the context of the diabetic heart, our group has shown that glycogen accumulation is correlated with impaired relaxation. Furthermore, this Thesis has demonstrated that the cardiac environment is characterised as a glycogen storage disease but this phenotype is linked to upstream glycophagy defects as opposed to lysosomal abnormalities. Thus, developed and clinically used therapies for GSDs are likely to be an ineffective approach for diabetic cardiomyopathy.

The research findings presented in this Thesis have shown that inhibition of glycophagy in the healthy heart, via *Gabarapl1* deletion, is sufficient to induce glycogen accumulation and diastolic dysfunction. Additionally, *Gabarapl1* downregulation was evident in the diabetic heart in both rodent models of disease and human patients. These findings provided the impetus for investigating whether restoring GABARAPL1 availability in the diabetic heart *in vivo* could have beneficial functional outcomes. The study presented in Chapter 5 of this Thesis is the first to show that cardiac-specific GABARAPL1 upregulation simultaneously rescued the diabetic cardiac glycogen pathology and diastolic dysfunction as it relates to cardiomyocyte mechanics but not cardiac remodelling, in a model of diet-induced type 2 diabetes. Given that GABARAPL1 is identified as a key glycophagy protein and overexpression restored cardiac glycogen levels, it is speculated that rescue of diabetic cardiomyopathy in this settings is related to glycophagy-mediated glycogen breakdown. Investigations carried out as part of this work indicate that the involvement of cytosolic glycogen handling enzymes and autophagy in glycogen rescue is unlikely.

Additionally, upregulation of glycophagy may elicit favourable effects on cardiac function via increasing glucose availability for glycolytic ATP production. It has been demonstrated that key functional proteins such as SERCA2a rely on glycolysis-derived ATP that in turn depends on glycogen content[258]. Thus, upregulation of glycophagy could have restored ATP supply thereby positively influencing contractility. Early electron micrographs have demonstrated that in the healthy heart, glycogen granules can be found in the cytosol but also in and around the myofilaments indicating a diverse functionality of glycogen pools[296,301]. Therefore, it could be hypothesised that in

a pathophysiological setting characterised by increased glycogen deposition, ectopic glycogen presence could affect ventricular relaxation (Fig 6.2). Although further research is required to determine the precise mechanisms via which glycogen influences contractility, this study has provided the basis to pursue targeting of cardiac glycophagy as a therapeutic approach for diabetic heart disease.

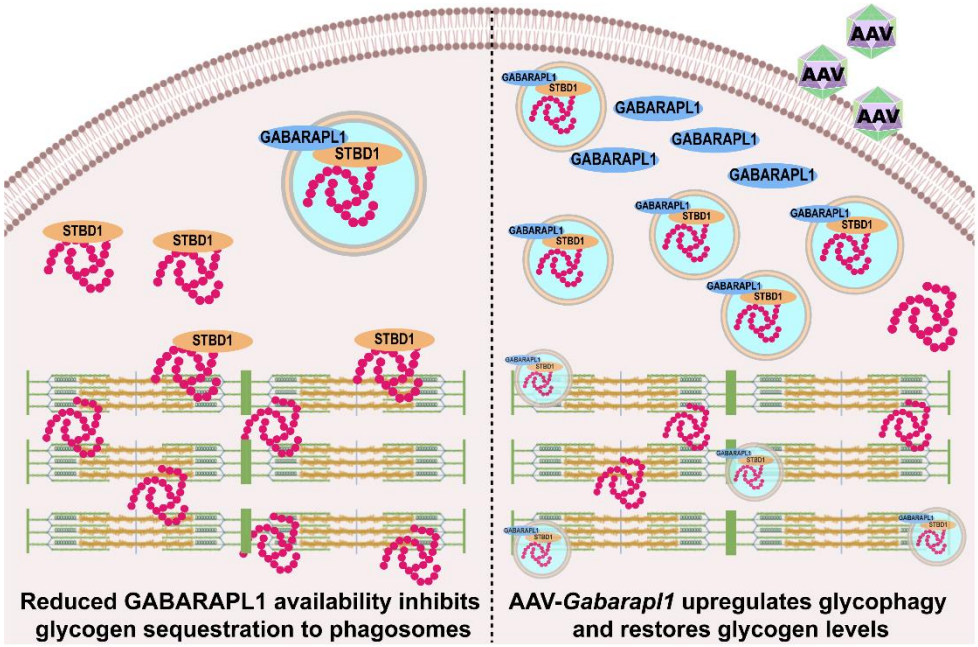

Figure 6.2: Schematic representation of GABARAPL1-mediated rescue of the diabetic glycogen pathology. Reduced availability of GABARAPL1 in the diabetic heart induces glycophagy impairment and results in glycogen accumulation in and around the myofilaments. *Gabarapl1* gene delivery induces glycophagosome formation thereby upregulating glycophagy. This results in glycogen breakdown thus alleviating spatial obstruction of the myofilaments and providing glycolysis-derived ATP for contractile proteins.

6.5. Future directions

The findings presented in this Thesis inspire new questions in the areas of cardiac glycogen handling and diabetic cardiomyopathy. The novel finding that glycophagy is an active process in both the neonatal and adult heart provides the incentive to investigate the signalling and regulatory pathways governing this process in the heart and determine whether there is indeed mechanistic overlap with macro-autophagy. The signals that determine the fate of a glycogen granule in the heart are yet to be investigated and would be informative in resolving the network of processes governing cardiac sugar metabolism. This is particularly important in the context of the diabetic heart where upstream metabolic signalling is disturbed.

This body of work emphasizes that there is a direct link between glycogen and cardiac function. It is now important to identify the mechanisms via which glycogen influences contractility. As discussed above in Sections 6.3 and 6.4, glycogen may influence relaxation in a variety of ways including AGE formation, spatial obstruction of contractile complexes and ATP production but the precise mechanisms require investigation.

GABARAPL1 is involved in a variety of autophagy-related processes. Thus, the precise mechanisms via which deletion or upregulation of GABARAPL1 influenced glycophagy are yet to be examined and would be informative in determining the potential of glycophagy targeting as a therapeutic approach for the diabetic cardiomyopathy.

6.6. Conclusions

The findings reported in this Thesis are the first to characterize the diabetic cardiac environment as a glycogen storage disease. This research provides a link between diabetic cardiac glycogen accumulation and disturbances in the glycogen-specific autophagy pathway, glycophagy. It is demonstrated that mRNA expression of the key molecular mediator of glycophagy, *Gabarapl1*, is decreased in the diabetic heart in both rodent models of disease and human patients. Additionally, it is shown for the first time that glycophagy is an operational process in the heart and that it is essential for physiological cardiac function. In diabetes, where diastolic dysfunction, glycogen accumulation and glycophagy disturbances are evident, it is demonstrated that cardiac-specific glycophagy upregulation rescues the glycogen phenotype and improves diastolic function.

Bibliography

1. Diabetes. 2019 [cited 2019 17/11]; Available from: https://www.who.int/health-topics/diabetes.
2. Federation, I.D. IDF DIABETES ATLAS - 8TH EDITION. 2017 [cited 2019 30/10/19]; Available from: https://diabetesatlas.org/.
3. New Zealand Ministry of Health. 18 June 2018 [cited 2019 17/11]; Available from: https://www.health.govt.nz/your-health/conditions-and-treatments/diseases-and-illnesses/diabetes.
4. Boudina, S. and E.D. Abel, Diabetic cardiomyopathy revisited. Circulation, 2007. 115(25): p. 3213-3223.
5. Boudina, S. and E.D. Abel, Diabetic cardiomyopathy, causes and effects. Rev Endocr Metab Disord, 2010. 11(1): p. 31-39.
6. Ternacle, J., F. Wan, D. Sawaki, M. Surenaud, M. Pini, R. Mercedes, L. Ernande, E. Audureau, J.L. Dubois-Rande, S. Adnot, S. Hue, G. Czibik, and G. Derumeaux, Short-term high-fat diet compromises myocardial function: a radial strain rate imaging study. Eur Heart J Cardiovasc Imaging, 2017. 18(11): p. 1283-1291.
7. Tate, M., M. Deo, A.H. Cao, S.G. Hood, K. Huynh, H. Kiriazis, X.J. Du, T.L. Julius, G.A. Figtree, G.J. Dusting, D.M. Kaye, and R.H. Ritchie, Insulin replacement limits progression of diabetic cardiomyopathy in the low-dose streptozotocin-induced diabetic rat. Diab Vasc Dis Res, 2017. 14(5): p. 423-433.
8. Raev, D.C., Which left ventricular function is impaired earlier in the evolution of diabetic cardiomyopathy? An echocardiographic study of young type I diabetic patients. Diabetes Care, 1994. 17(7): p. 633-639.
9. Kapila, R. and R.P. Mahajan, Diastolic dysfunction. Continuing Education in Anaesthesia Critical Care & Pain, 2009. 9(1): p. 29-33.
10. van Heerebeek, L., N. Hamdani, M.L. Handoko, I. Falcao-Pires, R.J. Musters, K. Kupreishvili, A.J. Ijsselmuiden, C.G. Schalkwijk, J.G. Bronzwaer, M. Diamant, A. Borbely, J. van der Velden, G.J. Stienen, G.J. Laarman, H.W. Niessen, and W.J. Paulus, Diastolic stiffness of the failing diabetic heart: importance of fibrosis, advanced glycation end products, and myocyte resting tension. Circulation, 2008. 117(1): p. 43-51.
11. Jia, G., A. Whaley-Connell, and J.R. Sowers, Diabetic cardiomyopathy: a hyperglycemia- and insulin-resistance-induced heart disease. Diabetologia, 2018. 61(1): p. 21-28.
12. Varma, U., P. Koutsifeli, V.L. Benson, K.M. Mellor, and L.M.D. Delbridge, Molecular mechanisms of cardiac pathology in diabetes - Experimental insights. Biochim Biophys Acta Mol Basis Dis, 2018. 1864(5 Pt B): p. 1949-1959.
13. Warren, S., The effect of insulin on pathologic glycogen deposits in diabetes mellitus. The American Journal of Medical Science, 1930. 179(4): p. 482-488.
14. Chandramouli, C., U. Varma, E.M. Stevens, R.P. Xiao, D.I. Stapleton, K.M. Mellor, and L.M. Delbridge, Myocardial glycogen dynamics: new perspectives on disease mechanisms. Clin Exp Pharmacol Physiol, 2015. 42(4): p. 415-425.
15. Rubler, S., J. Dlugash, Y.Z. Yuceoglu, T. Kumral, A.W. Branwood, and A. Grishman, New type of cardiomyopathy associated with diabetic glomerulosclerosis. Am J Cardiol, 1972. 30(6): p. 595-602.
16. Kannel, W.B., M. Hjortland, and W.P. Castelli, Role of diabetes in congestive heart failure: the Framingham study. Am J Cardiol, 1974. 34(1): p. 29-34.
17. Brunvand, L., D. Fugelseth, K.H. Stensaeth, K. Dahl-Jørgensen, and H.D. Margeirsdottir, Early reduced myocardial diastolic function in children and adolescents with type 1 diabetes mellitus a population-based study. BMC cardiovascular disorders, 2016. 16: p. 103-103.
18. Iribarren, C., A.J. Karter, A.S. Go, A. Ferrara, J.Y. Liu, S. Sidney, and J.V. Selby, Glycemic control and heart failure among adult patients with diabetes. Circulation, 2001. 103(22): p. 2668-2673.
19. Nichols, G.A., C.M. Gullion, C.E. Koro, S.A. Ephross, and J.B. Brown, The incidence of congestive heart failure in type 2 diabetes: an update. Diabetes Care, 2004. 27(8): p. 1879-1884.
20. Dandamudi, S., J. Slusser, D.W. Mahoney, M.M. Redfield, R.J. Rodeheffer, and H.H. Chen, The prevalence of diabetic cardiomyopathy: a population-based study in Olmsted County, Minnesota. J Card Fail, 2014. 20(5): p. 304-309.
21. Patil, V.C., H.V. Patil, K.B. Shah, J.D. Vasani, and P. Shetty, Diastolic dysfunction in asymptomatic type 2 diabetes mellitus with normal systolic function. J Cardiovasc Dis Res, 2011. 2(4): p. 213-222.
22. Shimabukuro, M., N. Higa, T. Asahi, K. Yamakawa, Y. Oshiro, M. Higa, and H. Masuzaki, Impaired glucose tolerance, but not impaired fasting glucose, underlies left ventricular diastolic dysfunction. Diabetes Care, 2011. 34(3): p. 686-690.
23. Huynh, K., B.C. Bernardo, J.R. McMullen, and R.H. Ritchie, Diabetic cardiomyopathy: mechanisms and new treatment strategies targeting antioxidant signaling pathways. Pharmacol Ther, 2014. 142(3): p. 375-415.
24. Lam, C.S., Diabetic cardiomyopathy: An expression of stage B heart failure with preserved ejection fraction. Diab Vasc Dis Res, 2015. 12(4): p. 234-238.

25. Bugger, H. and E.D. Abel, Molecular mechanisms of diabetic cardiomyopathy. Diabetologia, 2014. 57(4): p. 660-671.

26. Fisher, B.M., G. Gillen, G.B. Lindop, H.J. Dargie, and B.M. Frier, Cardiac function and coronary arteriography in asymptomatic type 1 (insulin-dependent) diabetic patients: evidence for a specific diabetic heart disease. Diabetologia, 1986. 29(10): p. 706-712.

27. Liu, J.E., V. Palmieri, M.J. Roman, J.N. Bella, R. Fabsitz, B.V. Howard, T.K. Welty, E.T. Lee, and R.B. Devereux, The impact of diabetes on left ventricular filling pattern in normotensive and hypertensive adults: the Strong Heart Study. J Am Coll Cardiol, 2001. 37(7): p. 1943-1949.

28. Araz, M., A. Bayrac, and H. Ciftci, The impact of diabetes on left ventricular diastolic function in patients with arterial hypertension. North Clin Istanb, 2015. 2(3): p. 177-181.

29. Chandramouli, C., M.E. Reichelt, C.L. Curl, U. Varma, L.A. Bienvenu, P. Koutsifeli, A.J.A. Raaijmakers, M.J. De Blasio, C.X. Qin, A.J. Jenkins, R.H. Ritchie, K.M. Mellor, and L.M.D. Delbridge, Diastolic dysfunction is more apparent in STZ-induced diabetic female mice, despite less pronounced hyperglycemia. Sci Rep, 2018. 8(1): p. 2346.

30. From, A.M., C.G. Scott, and H.H. Chen, The development of heart failure in patients with diabetes mellitus and pre-clinical diastolic dysfunction a population-based study. J Am Coll Cardiol, 2010. 55(4): p. 300-305.

31. Bradley, T.J., C. Slorach, F.H. Mahmud, D.B. Dunger, J. Deanfield, L. Deda, Y. Elia, R.L. Har, W. Hui, R. Moineddin, H.N. Reich, J.W. Scholey, L. Mertens, E. Sochett, and D.Z. Cherney, Early changes in cardiovascular structure and function in adolescents with type 1 diabetes. Cardiovasc Diabetol, 2016. 15: p. 31.

32. Nadeau, K.J., J.G. Regensteiner, T.A. Bauer, M.S. Brown, J.L. Dorosz, A. Hull, P. Zeitler, B. Draznin, and J.E. Reusch, Insulin resistance in adolescents with type 1 diabetes and its relationship to cardiovascular function. J Clin Endocrinol Metab, 2010. 95(2): p. 513-521.

33. Diamant, M., H.J. Lamb, Y. Groeneveld, E.L. Endert, J.W. Smit, J.J. Bax, J.A. Romijn, A. de Roos, and J.K. Radder, Diastolic dysfunction is associated with altered myocardial metabolism in asymptomatic normotensive patients with well-controlled type 2 diabetes mellitus. J Am Coll Cardiol, 2003. 42(2): p. 328-335.

34. Luke, P., C. Eggett, I. Spyridopoulos, and T. Irvine, A comparative analysis of British and American Society of Echocardiography recommendations for the assessment of left ventricular diastolic function. Echo research and practice, 2018. 5(4): p. 139-147.

35. Suran, D., A. Sinkovic, and F. Naji, Tissue Doppler imaging is a sensitive echocardiographic technique to detect subclinical systolic and diastolic dysfunction of both ventricles in type 1 diabetes mellitus. BMC cardiovascular disorders, 2016. 16: p. 72-72.

36. Modin, D., R. Møgelvang, P.G. Jørgensen, M.T. Jensen, J.P. Seferovic, and T. Biering-Sørensen, Left ventricular concentric geometry predicts incident diabetes mellitus independent of established risk factors in the general population: the Copenhagen City Heart Study. Cardiovasc Diabetol, 2019. 18(1): p. 37-37.

37. Park, J., J.-S. Kim, S.H. Kim, S. Kim, S.Y. Lim, H.-E. Lim, G.-Y. Cho, K.-C. Sung, J.-Y. Kim, I. Baik, K.K. Koh, J.B. Lee, S.K. Lee, and C. Shin, Subclinical left ventricular diastolic dysfunction and incident type 2 diabetes risk: the Korean Genome and Epidemiology Study. Cardiovasc Diabetol, 2017. 16(1): p. 36-36.

38. Khaidar, A., M. Marx, B. Lubec, and G. Lubec, L-arginine reduces heart collagen accumulation in the diabetic db/db mouse. Circulation, 1994. 90(1): p. 479-483.

39. Gonzalez-Quesada, C., M. Cavalera, A. Biernacka, P. Kong, D.W. Lee, A. Saxena, O. Frunza, M. Dobaczewski, A. Shinde, and N.G. Frangogiannis, Thrombospondin-1 induction in the diabetic myocardium stabilizes the cardiac matrix in addition to promoting vascular rarefaction through angiopoietin-2 upregulation. Circ Res, 2013. 113(12): p. 1331-1344.

40. Biernacka, A., M. Cavalera, J. Wang, I. Russo, A. Shinde, P. Kong, C. Gonzalez-Quesada, V. Rai, M. Dobaczewski, D.W. Lee, X.F. Wang, and N.G. Frangogiannis, Smad3 Signaling Promotes Fibrosis While Preserving Cardiac and Aortic Geometry in Obese Diabetic Mice. Circ Heart Fail, 2015. 8(4): p. 788-798.

41. Huynh, K., H. Kiriazis, X.J. Du, J.E. Love, K.A. Jandeleit-Dahm, J.M. Forbes, J.R. McMullen, and R.H. Ritchie, Coenzyme Q10 attenuates diastolic dysfunction, cardiomyocyte hypertrophy and cardiac fibrosis in the db/db mouse model of type 2 diabetes. Diabetologia, 2012. 55(5): p. 1544-1553.

42. Huynh, K., J.R. McMullen, T.L. Julius, J.W. Tan, J.E. Love, N. Cemerlang, H. Kiriazis, X.J. Du, and R.H. Ritchie, Cardiac-specific IGF-1 receptor transgenic expression protects against cardiac fibrosis and diastolic dysfunction in a mouse model of diabetic cardiomyopathy. Diabetes, 2010. 59(6): p. 1512-1520.

43. Ares-Carrasco, S., B. Picatoste, A. Benito-Martin, I. Zubiri, A.B. Sanz, M.D. Sanchez-Nino, A. Ortiz, J. Egido, J. Tunon, and O. Lorenzo, Myocardial fibrosis and apoptosis, but not inflammation, are present in long-term experimental diabetes. Am J Physiol Heart Circ Physiol, 2009. 297(6): p. H2109-2119.

44. Hao, P.P., J.M. Yang, M.X. Zhang, K. Zhang, Y.G. Chen, C. Zhang, and Y. Zhang, Angiotensin-(1-7) treatment mitigates right ventricular fibrosis as a distinctive feature of diabetic cardiomyopathy. Am J Physiol Heart Circ Physiol, 2015. 308(9): p. H1007-1019.

45. Meloni, M., B. Descamps, A. Caporali, L. Zentilin, I. Floris, M. Giacca, and C. Emanueli, Nerve growth factor gene therapy using adeno-associated viral vectors prevents cardiomyopathy in type 1 diabetic mice. Diabetes, 2012. 61(1): p. 229-240.

46. Li, J., H. Zhu, E. Shen, L. Wan, J.M. Arnold, and T. Peng, Deficiency of rac1 blocks NADPH oxidase activation, inhibits endoplasmic reticulum stress, and reduces myocardial remodeling in a mouse model of type 1 diabetes. Diabetes, 2010. 59(8): p. 2033-2042.

47. Watanabe, S., S. Kumazaki, K. Kusunoki, T. Inoue, Y. Maeda, S. Usui, R. Shinohata, T. Ohtsuki, S. Hirohata, S. Kusachi, K. Kitamori, M. Mori, Y. Yamori, and H. Oka, A High-Fat and High-Cholesterol Diet Induces Cardiac Fibrosis, Vascular Endothelial, and Left Ventricular Diastolic Dysfunction in SHRSP5/Dmcr Rats. J Atheroscler Thromb, 2018. 25(5): p. 439-453.

48. Li, S.-J., C.-H. Liu, H.-P. Chu, H.J. Mersmann, S.-T. Ding, C.-H. Chu, C.-Y. Wang, and C.-Y. Chen, The high-fat diet induces myocardial fibrosis in the metabolically healthy obese minipigs—The role of ER stress and oxidative stress. Clinical Nutrition, 2017. 36(3): p. 760-767.

49. Karason, K., L. Sjostrom, I. Wallentin, and M. Peltonen, Impact of blood pressure and insulin on the relationship between body fat and left ventricular structure. Eur Heart J, 2003. 24(16): p. 1500-1505.

50. Benjamin, E.J., D. Levy, S.M. Vaziri, R.B. D'Agostino, A.J. Belanger, and P.A. Wolf, Independent risk factors for atrial fibrillation in a population-based cohort. The Framingham Heart Study. JAMA, 1994. 271(11): p. 840-844.

51. Wilhelmsen, L., A. Rosengren, and G. Lappas, Hospitalizations for atrial fibrillation in the general male population: morbidity and risk factors. Journal of internal medicine, 2001. 250(5): p. 382-389.

52. Aune, D., T. Feng, S. Schlesinger, I. Janszky, T. Norat, and E. Riboli, Diabetes mellitus, blood glucose and the risk of atrial fibrillation: A systematic review and meta-analysis of cohort studies. J Diabetes Complications, 2018. 32(5): p. 501-511.

53. Fatemi, O., E. Yuriditsky, C. Tsioufis, D. Tsachris, T. Morgan, J. Basile, T. Bigger, W. Cushman, D. Goff, E.Z. Soliman, A. Thomas, and V. Papademetriou, Impact of intensive glycemic control on the incidence of atrial fibrillation and associated cardiovascular outcomes in patients with type 2 diabetes mellitus (from the Action to Control Cardiovascular Risk in Diabetes Study). Am J Cardiol, 2014. 114(8): p. 1217-1222.

54. Grisanti, L.A., Diabetes and Arrhythmias: Pathophysiology, Mechanisms and Therapeutic Outcomes. Frontiers in physiology, 2018. 9: p. 1669-1669.

55. Baek, Y.S., P.S. Yang, T.H. Kim, J.S. Uhm, J. Park, H.N. Pak, M.H. Lee, and B. Joung, Associations of Abdominal Obesity and New-Onset Atrial Fibrillation in the General Population. J Am Heart Assoc, 2017. 6(6).

56. Wisneski, J.A., E.W. Gertz, R.A. Neese, L.D. Gruenke, D.L. Morris, and J.C. Craig, Metabolic fate of extracted glucose in normal human myocardium. J Clin Invest, 1985. 76(5): p. 1819-1827.

57. Goldberg, I.J., C.M. Trent, and P.C. Schulze, Lipid metabolism and toxicity in the heart. Cell Metab, 2012. 15(6): p. 805-812.

58. Luiken, J.J., Y. Arumugam, D.J. Dyck, R.C. Bell, M.M. Pelsers, L.P. Turcotte, N.N. Tandon, J.F. Glatz, and A. Bonen, Increased rates of fatty acid uptake and plasmalemmal fatty acid transporters in obese Zucker rats. J Biol Chem, 2001. 276(44): p. 40567-40573.

59. Sreedhar, R., S. Arumugam, R.A. Thandavarayan, V. Karuppagounder, Y. Koga, T. Nakamura, M. Harima, and K. Watanabe, Role of 14-3-3eta protein on cardiac fatty acid metabolism and macrophage polarization after high fat diet induced type 2 diabetes mellitus. Int J Biochem Cell Biol, 2017. 88: p. 92-99.

60. Montessuit, C. and R. Lerch, Regulation and dysregulation of glucose transport in cardiomyocytes. Biochim Biophys Acta, 2013. 1833(4): p. 848-856.

61. Abdurrachim, D., M. Nabben, V. Hoerr, M.T. Kuhlmann, P. Bovenkamp, J. Ciapaite, I.M.E. Geraets, W. Coumans, J. Luiken, J.F.C. Glatz, M. Schafers, K. Nicolay, C. Faber, S. Hermann, and J.J. Prompers, Diabetic db/db mice do not develop heart failure upon pressure overload: a longitudinal in vivo PET, MRI, and MRS study on cardiac metabolic, structural, and functional adaptations. Cardiovasc Res, 2017. 113(10): p. 1148-1160.

62. de Gonzalo-Calvo, D., R.W. van der Meer, L.J. Rijzewijk, J.W. Smit, E. Revuelta-Lopez, L. Nasarre, J.C. Escola-Gil, H.J. Lamb, and V. Llorente-Cortes, Serum microRNA-1 and microRNA-133a levels reflect myocardial steatosis in uncomplicated type 2 diabetes. Sci Rep, 2017. 7(1): p. 47.

63. Cook, G.A., E.N. Lavrentyev, K. Pham, and E.A. Park, Streptozotocin diabetes increases mRNA expression of ketogenic enzymes in the rat heart. Biochim Biophys Acta Gen Subj, 2017. 1861(2): p. 307-312.

64. Buchanan, J., P.K. Mazumder, P. Hu, G. Chakrabarti, M.W. Roberts, U.J. Yun, R.C. Cooksey, S.E. Litwin, and E.D. Abel, Reduced cardiac efficiency and altered substrate metabolism precedes the

onset of hyperglycemia and contractile dysfunction in two mouse models of insulin resistance and obesity. Endocrinology, 2005. 146(12): p. 5341-5349.

65. Le Page, L.M., O.J. Rider, A.J. Lewis, V. Ball, K. Clarke, E. Johansson, C.A. Carr, L.C. Heather, and D.J. Tyler, Increasing Pyruvate Dehydrogenase Flux as a Treatment for Diabetic Cardiomyopathy: A Combined 13C Hyperpolarized Magnetic Resonance and Echocardiography Study. Diabetes, 2015. 64(8): p. 2735-2743.

66. Nicholl, T.A., G.D. Lopaschuk, and J.H. McNeill, Effects of free fatty acids and dichloroacetate on isolated working diabetic rat heart. Am J Physiol, 1991. 261(4 Pt 2): p. H1053-1059.

67. Kuramoto, K., F. Sakai, N. Yoshinori, T.Y. Nakamura, S. Wakabayashi, T. Kojidani, T. Haraguchi, F. Hirose, and T. Osumi, Deficiency of a lipid droplet protein, perilipin 5, suppresses myocardial lipid accumulation, thereby preventing type 1 diabetes-induced heart malfunction. Mol Cell Biol, 2014. 34(14): p. 2721-2731.

68. Wang, H., U. Sreenivasan, D.W. Gong, K.A. O'Connell, E.R. Dabkowski, P.A. Hecker, N. Ionica, M. Konig, A. Mahurkar, Y. Sun, W.C. Stanley, and C. Sztalryd, Cardiomyocyte-specific perilipin 5 overexpression leads to myocardial steatosis and modest cardiac dysfunction. J Lipid Res, 2013. 54(4): p. 953-965.

69. Bostrom, P., L. Andersson, M. Rutberg, J. Perman, U. Lidberg, B.R. Johansson, J. Fernandez-Rodriguez, J. Ericson, T. Nilsson, J. Boren, and S.O. Olofsson, SNARE proteins mediate fusion between cytosolic lipid droplets and are implicated in insulin sensitivity. Nat Cell Biol, 2007. 9(11): p. 1286-1293.

70. Faria, A. and S.J. Persaud, Cardiac oxidative stress in diabetes: Mechanisms and therapeutic potential. Pharmacol Ther, 2017. 172: p. 50-62.

71. How, O.-J., E. Aasum, D.L. Severson, W.Y.A. Chan, M.F. Essop, and T.S. Larsen, Increased Myocardial Oxygen Consumption Reduces Cardiac Efficiency in Diabetic Mice. Diabetes, 2006. 55(2): p. 466.

72. Mazumder, P.K., B.T. O'Neill, M.W. Roberts, J. Buchanan, U.J. Yun, R.C. Cooksey, S. Boudina, and E.D. Abel, Impaired Cardiac Efficiency and Increased Fatty Acid Oxidation in Insulin-Resistant ob/ob Mouse Hearts. Diabetes, 2004. 53(9): p. 2366.

73. De Blasio, M.J., K. Huynh, C. Qin, S. Rosli, H. Kiriazis, A. Ayer, N. Cemerlang, R. Stocker, X.-J. Du, J.R. McMullen, and R.H. Ritchie, Therapeutic targeting of oxidative stress with coenzyme Q10 counteracts exaggerated diabetic cardiomyopathy in a mouse model of diabetes with diminished PI3K(p110α) signaling. Free Radical Biology and Medicine, 2015. 87: p. 137-147.

74. Liang, D., P. Zhong, J. Hu, F. Lin, Y. Qian, Z. Xu, J. Wang, C. Zeng, X. Li, and G. Liang, EGFR inhibition protects cardiac damage and remodeling through attenuating oxidative stress in STZ-induced diabetic mouse model. J Mol Cell Cardiol, 2015. 82: p. 63-74.

75. Prakoso, D., M.J. De Blasio, C. Qin, S. Rosli, H. Kiriazis, H. Qian, X.J. Du, K.L. Weeks, P. Gregorevic, J.R. McMullen, and R.H. Ritchie, Phosphoinositide 3-kinase (p110α) gene delivery limits diabetes-induced cardiac NADPH oxidase and cardiomyopathy in a mouse model with established diastolic dysfunction. Clinical Science, 2017. 131(12): p. 1345-1360.

76. Yuan, H., C.N. Perry, C. Huang, E. Iwai-Kanai, R.S. Carreira, C.C. Glembotski, and R.A. Gottlieb, LPS-induced autophagy is mediated by oxidative signaling in cardiomyocytes and is associated with cytoprotection. American Journal of Physiology-Heart and Circulatory Physiology, 2009. 296(2): p. H470-H479.

77. Delbridge, L.M.D., K.M. Mellor, D.J. Taylor, and R.A. Gottlieb, Myocardial stress and autophagy: mechanisms and potential therapies. Nat Rev Cardiol, 2017. 14(7): p. 412-425.

78. Johansen, T. and T. Lamark, Selective Autophagy: ATG8 Family Proteins, LIR Motifs and Cargo Receptors. J Mol Biol, 2019.

79. Tanida, I., Autophagy basics. Microbiol Immunol, 2011. 55(1): p. 1-11.

80. Hosokawa, N., T. Hara, T. Kaizuka, C. Kishi, A. Takamura, Y. Miura, S. Iemura, T. Natsume, K. Takehana, N. Yamada, J.L. Guan, N. Oshiro, and N. Mizushima, Nutrient-dependent mTORC1 association with the ULK1-Atg13-FIP200 complex required for autophagy. Mol Biol Cell, 2009. 20(7): p. 1981-1991.

81. Hosokawa, N., T. Sasaki, S. Iemura, T. Natsume, T. Hara, and N. Mizushima, Atg101, a novel mammalian autophagy protein interacting with Atg13. Autophagy, 2009. 5(7): p. 973-979.

82. Itakura, E. and N. Mizushima, Characterization of autophagosome formation site by a hierarchical analysis of mammalian Atg proteins. Autophagy, 2010. 6(6): p. 764-776.

83. Mizushima, N., A. Yamamoto, M. Hatano, Y. Kobayashi, Y. Kabeya, K. Suzuki, T. Tokuhisa, Y. Ohsumi, and T. Yoshimori, Dissection of autophagosome formation using Apg5-deficient mouse embryonic stem cells. J Cell Biol, 2001. 152(4): p. 657-668.

84. Tanida, I., E. Tanida-Miyake, T. Ueno, and E. Kominami, The human homolog of Saccharomyces cerevisiae Apg7p is a Protein-activating enzyme for multiple substrates including human Apg12p, GATE-16, GABARAP, and MAP-LC3. J Biol Chem, 2001. 276(3): p. 1701-1706.

85. Alemu, E.A., T. Lamark, K.M. Torgersen, A.B. Birgisdottir, K.B. Larsen, A. Jain, H. Olsvik, A. Overvatn, V. Kirkin, and T. Johansen, ATG8 family proteins act as scaffolds for assembly of the ULK complex: sequence requirements for LC3-interacting region (LIR) motifs. J Biol Chem, 2012. 287(47): p. 39275-39290.

86. Huber, L.A. and D. Teis, Lysosomal signaling in control of degradation pathways. Curr Opin Cell Biol, 2016. 39: p. 8-14.

87. Itakura, E., C. Kishi-Itakura, and N. Mizushima, The hairpin-type tail-anchored SNARE syntaxin 17 targets to autophagosomes for fusion with endosomes/lysosomes. Cell, 2012. 151(6): p. 1256-1269.

88. Liang, C., P. Feng, B. Ku, I. Dotan, D. Canaani, B.H. Oh, and J.U. Jung, Autophagic and tumour suppressor activity of a novel Beclin1-binding protein UVRAG. Nat Cell Biol, 2006. 8(7): p. 688-699.

89. Itakura, E., C. Kishi, K. Inoue, and N. Mizushima, Beclin 1 forms two distinct phosphatidylinositol 3-kinase complexes with mammalian Atg14 and UVRAG. Mol Biol Cell, 2008. 19(12): p. 5360-5372.

90. Takahashi, Y., D. Coppola, N. Matsushita, H.D. Cualing, M. Sun, Y. Sato, C. Liang, J.U. Jung, J.Q. Cheng, J.J. Mule, W.J. Pledger, and H.G. Wang, Bif-1 interacts with Beclin 1 through UVRAG and regulates autophagy and tumorigenesis. Nat Cell Biol, 2007. 9(10): p. 1142-1151.

91. An, M., D.R. Ryu, J. Won Park, J. Ha Choi, E.M. Park, K. Eun Lee, M. Woo, and M. Kim, ULK1 prevents cardiac dysfunction in obesity through autophagy-meditated regulation of lipid metabolism. Cardiovasc Res, 2017. 113(10): p. 1137-1147.

92. Andres, A.M., J.A. Kooren, S.J. Parker, K.C. Tucker, N. Ravindran, B.R. Ito, C. Huang, V. Venkatraman, J.E. Van Eyk, R.A. Gottlieb, and R.M. Mentzer, Jr., Discordant signaling and autophagy response to fasting in hearts of obese mice: Implications for ischemia tolerance. Am J Physiol Heart Circ Physiol, 2016. 311(1): p. H219-228.

93. Chou, I.P., Y.P. Chiu, S.T. Ding, B.H. Liu, Y.Y. Lin, and C.Y. Chen, Adiponectin receptor 1 overexpression reduces lipid accumulation and hypertrophy in the heart of diet-induced obese mice--possible involvement of oxidative stress and autophagy. Endocr Res, 2014. 39(4): p. 173-179.

94. Cui, M., H. Yu, J. Wang, J. Gao, and J. Li, Chronic caloric restriction and exercise improve metabolic conditions of dietary-induced obese mice in autophagy correlated manner without involving AMPK. J Diabetes Res, 2013. 2013: p. 852754.

95. Gao, H., Q. Yang, R. Dong, F. Hou, and Y. Wu, Sequential changes in autophagy in diabetic cardiac fibrosis. Mol Med Rep, 2016. 13(1): p. 327-332.

96. Guo, R., Y. Zhang, S. Turdi, and J. Ren, Adiponectin knockout accentuates high fat diet-induced obesity and cardiac dysfunction: role of autophagy. Biochim Biophys Acta, 2013. 1832(8): p. 1136-1148.

97. He, C., M.C. Bassik, V. Moresi, K. Sun, Y. Wei, Z. Zou, Z. An, J. Loh, J. Fisher, Q. Sun, S. Korsmeyer, M. Packer, H.I. May, J.A. Hill, H.W. Virgin, C. Gilpin, G. Xiao, R. Bassel-Duby, P.E. Scherer, and B. Levine, Exercise-induced BCL2-regulated autophagy is required for muscle glucose homeostasis. Nature, 2012. 481(7382): p. 511-515.

98. He, C., H. Zhu, H. Li, M.H. Zou, and Z. Xie, Dissociation of Bcl-2-Beclin1 complex by activated AMPK enhances cardiac autophagy and protects against cardiomyocyte apoptosis in diabetes. Diabetes, 2013. 62(4): p. 1270-1281.

99. Kanamori, H., G. Takemura, K. Goto, A. Tsujimoto, A. Mikami, A. Ogino, T. Watanabe, K. Morishita, H. Okada, M. Kawasaki, M. Seishima, and S. Minatoguchi, Autophagic adaptations in diabetic cardiomyopathy differ between type 1 and type 2 diabetes. Autophagy, 2015. 11(7): p. 1146-1160.

100. Lai, C.H., C.C. Tsai, W.W. Kuo, T.J. Ho, C.H. Day, P.Y. Pai, L.C. Chung, C.C. Huang, H.F. Wang, P.H. Liao, and C.Y. Huang, Multi-Strain Probiotics Inhibit Cardiac Myopathies and Autophagy to Prevent Heart Injury in High-Fat Diet-Fed Rats. Int J Med Sci, 2016. 13(4): p. 277-285.

101. Lee, J.H., J.H. Lee, M. Jin, S.D. Han, G.R. Chon, I.H. Kim, S. Kim, S.Y. Kim, S.B. Choi, and Y.H. Noh, Diet control to achieve euglycemia induces significant loss of heart and liver weight via increased autophagy compared with ad libitum diet in diabetic rats. Exp Mol Med, 2014. 46: p. e111.

102. Marsh, S.A., P.C. Powell, L.J. Dell'italia, and J.C. Chatham, Cardiac O-GlcNAcylation blunts autophagic signaling in the diabetic heart. Life Sci, 2013. 92(11): p. 648-656.

103. Pei, X.M., B.Y. Yung, S.P. Yip, L.W. Chan, C.S. Wong, M. Ying, and P.M. Siu, Protective effects of desacyl ghrelin on diabetic cardiomyopathy. Acta Diabetol, 2015. 52(2): p. 293-306.

104. Russo, S.B., C.F. Baicu, A. Van Laer, T. Geng, H. Kasiganesan, M.R. Zile, and L.A. Cowart, Ceramide synthase 5 mediates lipid-induced autophagy and hypertrophy in cardiomyocytes. J Clin Invest, 2012. 122(11): p. 3919-3930.

105. Sun, S., M. Zhang, J. Lin, J. Hu, R. Zhang, C. Li, T. Wei, D. Sun, J. Wei, and H. Wang, Lin28a protects against diabetic cardiomyopathy via the PKA/ROCK2 pathway. Biochem Biophys Res Commun, 2016. 469(1): p. 29-36.

106. Trivedi, P.C., J.J. Bartlett, L.J. Perez, K.R. Brunt, J.F. Legare, A. Hassan, P.C. Kienesberger, and T. Pulinilkunnil, Glucolipotoxicity diminishes cardiomyocyte TFEB and inhibits lysosomal autophagy during obesity and diabetes. Biochim Biophys Acta, 2016. 1861(12 Pt A): p. 1893-1910.

107. Wang, B., Q. Yang, Y.Y. Sun, Y.F. Xing, Y.B. Wang, X.T. Lu, W.W. Bai, X.Q. Liu, and Y.X. Zhao, Resveratrol-enhanced autophagic flux ameliorates myocardial oxidative stress injury in diabetic mice. J Cell Mol Med, 2014. 18(8): p. 1599-1611.

108. Xie, Z., K. Lau, B. Eby, P. Lozano, C. He, B. Pennington, H. Li, S. Rathi, Y. Dong, R. Tian, D. Kem, and M.H. Zou, Improvement of cardiac functions by chronic metformin treatment is associated with enhanced cardiac autophagy in diabetic OVE26 mice. Diabetes, 2011. 60(6): p. 1770-1778.

109. Xu, X., S. Kobayashi, K. Chen, D. Timm, P. Volden, Y. Huang, J. Gulick, Z. Yue, J. Robbins, P.N. Epstein, and Q. Liang, Diminished autophagy limits cardiac injury in mouse models of type 1 diabetes. J Biol Chem, 2013. 288(25): p. 18077-18092.

110. Xu, X. and J. Ren, Macrophage migration inhibitory factor (MIF) knockout preserves cardiac homeostasis through alleviating Akt-mediated myocardial autophagy suppression in high-fat diet-induced obesity. Int J Obes (Lond), 2015. 39(3): p. 387-396.

111. Zhang, M., L. Zhang, J. Hu, J. Lin, T. Wang, Y. Duan, W. Man, J. Feng, L. Sun, H. Jia, C. Li, R. Zhang, H. Wang, and D. Sun, MST1 coordinately regulates autophagy and apoptosis in diabetic cardiomyopathy in mice. Diabetologia, 2016. 59(11): p. 2435-2447.

112. Zhao, Y., L. Zhang, Y. Qiao, X. Zhou, G. Wu, L. Wang, Y. Peng, X. Dong, H. Huang, L. Si, X. Zhang, L. Zhang, J. Li, W. Wang, L. Zhou, and X. Gao, Heme oxygenase-1 prevents cardiac dysfunction in streptozotocin-diabetic mice by reducing inflammation, oxidative stress, apoptosis and enhancing autophagy. PLoS One, 2013. 8(9): p. e75927.

113. Paula-Gomes, S., D.A. Goncalves, A.M. Baviera, N.M. Zanon, L.C. Navegantes, and I.C. Kettelhut, Insulin suppresses atrophy- and autophagy-related genes in heart tissue and cardiomyocytes through AKT/FOXO signaling. Horm Metab Res, 2013. 45(12): p. 849-855.

114. Munasinghe, P.E., F. Riu, P. Dixit, M. Edamatsu, P. Saxena, N.S. Hamer, I.F. Galvin, R.W. Bunton, S. Lequeux, G. Jones, R.R. Lamberts, C. Emanueli, P. Madeddu, and R. Katare, Type-2 diabetes increases autophagy in the human heart through promotion of Beclin-1 mediated pathway. Int J Cardiol, 2016. 202: p. 13-20.

115. Montaigne, D., X. Marechal, A. Coisne, N. Debry, T. Modine, G. Fayad, C. Potelle, J.M. El Arid, S. Mouton, Y. Sebti, H. Duez, S. Preau, I. Remy-Jouet, F. Zerimech, M. Koussa, V. Richard, R. Neviere, J.L. Edme, P. Lefebvre, and B. Staels, Myocardial contractile dysfunction is associated with impaired mitochondrial function and dynamics in type 2 diabetic but not in obese patients. Circulation, 2014. 130(7): p. 554-564.

116. Rizza, R.A., M.F. Crass, 3rd, and J.C. Shipp, Effect of insulin treatment in vivo on heart glycerides and glycogen of alloxan-diabetic rats. Metabolism, 1971. 20(6): p. 539-543.

117. Alfarano, C., S. Suffredini, O. Fantappie, A. Mugelli, E. Cerbai, M.E. Manni, and L. Raimondi, The effect of losartan treatment on the response of diabetic cardiomyocytes to ATP depletion. Pharmacol Res, 2011. 63(3): p. 225-232.

118. Bhimji, S., D.V. Godin, and J.H. McNeill, Myocardial ultrastructural changes in alloxan-induced diabetes in rabbits. Acta Anat (Basel), 1986. 125(3): p. 195-200.

119. Chen, V., C.D. Ianuzzo, B.C. Fong, and J.J. Spitzer, The effects of acute and chronic diabetes on myocardial metabolism in rats. Diabetes, 1984. 33(11): p. 1078-1084.

120. Dervisevik, M., S. Dinevska-Kovkarovska, M. Dimitrovska, N. Cipanovska, and B. Miova, High dose of aspirin moderates diabetes-induced changes of heart glycogen/glucose metabolism in rats. J Physiol Sci, 2014. 64(6): p. 411-420.

121. Eto, M., K. Watanabe, M. Sekiguchi, Y. Iwashima, A. Morikawa, E. Oshima, and K. Ishii, Metabolic and morphological changes of the heart in Chinese hamsters (CHAD strain) with spontaneous long-term diabetes. Diabetes Res Clin Pract, 1987. 3(6): p. 297-305.

122. He, J., M.T. Quintana, J. Sullivan, L.P. T, J.G. T, J.C. Schisler, J.A. Hill, C.C. Yates, R.F. Mapanga, M.F. Essop, W.E. Stansfield, J.R. Bain, C.B. Newgard, M.J. Muehlbauer, Y. Han, B.A. Clarke, and M.S. Willis, MuRF2 regulates PPARgamma1 activity to protect against diabetic cardiomyopathy and enhance weight gain induced by a high fat diet. Cardiovasc Diabetol, 2015. 14: p. 97.

123. Higuchi, M., K. Miyagi, J. Nakasone, and M. Sakanashi, Role of high glycogen in underperfused diabetic rat hearts with added norepinephrine. J Cardiovasc Pharmacol, 1995. 26(6): p. 899-907.

124. Hsiao, Y.C., K. Suzuki, H. Abe, and T. Toyota, Ultrastructural alterations in cardiac muscle of diabetic BB Wistar rats. Virchows Arch A Pathol Anat Histopathol, 1987. 411(1): p. 45-52.

125. Lajoie, C., A. Calderone, F. Trudeau, N. Lavoie, G. Massicotte, S. Gagnon, and L. Beliveau, Exercise training attenuated the PKB and GSK-3 dephosphorylation in the myocardium of ZDF rats. J Appl Physiol (1985), 2004. 96(5): p. 1606-1612.

126. Laughlin, M.R., W.A. Petit, Jr., R.G. Shulman, and E.J. Barrett, Measurement of myocardial glycogen synthesis in diabetic and fasted rats. Am J Physiol, 1990. 258(1 Pt 1): p. E184-190.

127. Lebkova, N.P., M.F. Bondarenko, O.E. Kolesova, and G.P. Azarian, [Ultrastructural manifestations of early metabolic disorders in the myocardium of dogs with alloxan diabetes]. Biull Eksp Biol Med, 1980. 89(5): p. 614-617.

128. Lebkova, N.P., O.E. Kolesova, V.D. Gorbunova, I. Bobkov Iu, and A. Petrovich Iu, [Intracellular transformation of fatty acids into glycogen in alloxan diabetic rats, based on electron autoradiographic data]. Biull Eksp Biol Med, 1984. 98(12): p. 734-736.

129. Liang, J.L., Z.K. Feng, X.Y. Liu, Q.X. Lin, Y.H. Fu, Z.X. Shan, J.N. Zhu, S.G. Lin, and X.Y. Yu, Effect of impaired glucose tolerance on cardiac dysfunction in a rat model of prediabetes. Chin Med J (Engl), 2011. 124(5): p. 734-739.

130. Malfitano, C., A.L. de Souza Junior, M. Carbonaro, A. Bolsoni-Lopes, D. Figueroa, L.E. de Souza, K.A. Silva, F. Consolim-Colombo, R. Curi, and M.C. Irigoyen, Glucose and fatty acid metabolism in infarcted heart from streptozotocin-induced diabetic rats after 2 weeks of tissue remodeling. Cardiovasc Diabetol, 2015. 14: p. 149.

131. Miller, T.B., Jr., Altered regulation of cardiac glycogen metabolism in spontaneously diabetic rats. Am J Physiol, 1983. 245(4): p. E379-383.

132. Nakao, M., T. Matsubara, and N. Sakamoto, Effects of diabetes on cardiac glycogen metabolism in rats. Heart Vessels, 1993. 8(4): p. 171-175.

133. Penpargkul, S., T. Schaible, T. Yipintsoi, and J. Scheuer, The effect of diabetes on performance and metabolism of rat hearts. Circ Res, 1980. 47(6): p. 911-921.

134. Plante, E., A. Menaouar, B.A. Danalache, T.L. Broderick, M. Jankowski, and J. Gutkowska, Treatment with brain natriuretic peptide prevents the development of cardiac dysfunction in obese diabetic db/db mice. Diabetologia, 2014. 57(6): p. 1257-1267.

135. Povlsen, J.A., B. Lofgren, C. Dalgas, R.I. Birkler, M. Johannsen, N.B. Stottrup, and H.E. Botker, Protection against myocardial ischemia-reperfusion injury at onset of type 2 diabetes in Zucker diabetic fatty rats is associated with altered glucose oxidation. PLoS One, 2013. 8(5): p. e64093.

136. Sakakibara, M., A. Hirashiki, X.W. Cheng, Y. Bando, K. Ohshima, T. Okumura, H. Funahashi, S. Ohshima, and T. Murohara, Association of diabetes mellitus with myocardial collagen accumulation and relaxation impairment in patients with dilated cardiomyopathy. Diabetes Res Clin Pract, 2011. 92(3): p. 348-355.

137. Shearer, J., K.D. Ross, C.C. Hughey, V.L. Johnsen, D.S. Hittel, and D.L. Severson, Exercise training does not correct abnormal cardiac glycogen accumulation in the db/db mouse model of type 2 diabetes. Am J Physiol Endocrinol Metab, 2011. 301(1): p. E31-39.

138. Virkamaki, A. and H. Yki-Jarvinen, Allosteric regulation of glycogen synthase and hexokinase by glucosamine-6-phosphate during glucosamine-induced insulin resistance in skeletal muscle and heart. Diabetes, 1999. 48(5): p. 1101-1107.

139. Abel, E.D., Glucose transport in the heart. Front Biosci, 2004. 9: p. 201-215.

140. Szablewski, L., Glucose transporters in healthy heart and in cardiac disease. Int J Cardiol, 2017. 230: p. 70-75.

141. He, J. and D.E. Kelley, Muscle glycogen content in type 2 diabetes mellitus. Am J Physiol Endocrinol Metab, 2004. 287(5): p. E1002-1007.

142. Thorburn, A.W., B. Gumbiner, F. Bulacan, G. Brechtel, and R.R. Henry, Multiple defects in muscle glycogen synthase activity contribute to reduced glycogen synthesis in non-insulin dependent diabetes mellitus. J Clin Invest, 1991. 87(2): p. 489-495.

143. Roach, P.J., A.A. Depaoli-Roach, T.D. Hurley, and V.S. Tagliabracci, Glycogen and its metabolism: some new developments and old themes. Biochem J, 2012. 441(3): p. 763-787.

144. Roach, P.J. and A.V. Skurat, Self-glucosylating initiator proteins and their role in glycogen biosynthesis. Prog Nucleic Acid Res Mol Biol, 1997. 57: p. 289-316.

145. Larner, J., B. Illingworth, G.T. Cori, and C.F. Cori, Structure of glycogens and amylopectins. II. Analysis by stepwise enzymatic degradation. J Biol Chem, 1952. 199(2): p. 641-651.

146. Jiang, S., B. Heller, V.S. Tagliabracci, L. Zhai, J.M. Irimia, A.A. DePaoli-Roach, C.D. Wells, A.V. Skurat, and P.J. Roach, Starch binding domain-containing protein 1/genethonin 1 is a novel participant in glycogen metabolism. J Biol Chem, 2010. 285(45): p. 34960-34971.

147. Jiang, S., C.D. Wells, and P.J. Roach, Starch-binding domain-containing protein 1 (Stbd1) and glycogen metabolism: Identification of the Atg8 family interacting motif (AIM) in Stbd1 required for interaction with GABARAPL1. Biochem Biophys Res Commun, 2011. 413(3): p. 420-425.

148. Palmer, T.N., The substrate specificity of acid -glucosidase from rabbit muscle. Biochem J, 1971. 124(4): p. 701-711.

149. Tashiro, K., T. Iwamasa, H. Kato, S. Ogata, and M. Anai, Purification and characterization of two components of acid alpha-glucosidase from pig liver. J Biochem, 1986. 99(3): p. 693-701.

150. Zhao, F.-Q. and A.F. Keating, Functional properties and genomics of glucose transporters. Current genomics, 2007. 8(2): p. 113-128.

151. Meyer, K.H., P. Bernfeld, R.A. Boissonnas, P. Gurtler, and G. Noelting, Starch Solutions and Pastes and their Molecular Interpretation. The Journal of Physical and Colloid Chemistry, 1949. 53(3): p. 319-334.

152. Miller, T.B., Jr., A dual role for insulin in the regulation of cardiac glycogen synthase. J Biol Chem, 1978. 253(15): p. 5389-5394.

153. Janecek, S., A motif of a microbial starch-binding domain found in human genethonin. Bioinformatics, 2002. 18(11): p. 1534-1537.

154. Bouju, S., M.F. Lignon, G. Pietu, M. Le Cunff, J.J. Leger, C. Auffray, and C.A. Dechesne, Molecular cloning and functional expression of a novel human gene encoding two 41-43 kDa skeletal muscle internal membrane proteins. Biochem J, 1998. 335((Pt 3)): p. 549-556.

155. Pietu, G., O. Alibert, V. Guichard, B. Lamy, F. Bois, E. Leroy, R. Mariage-Sampson, R. Houlgatte, P. Soularue, and C. Auffray, Novel gene transcripts preferentially expressed in human muscles revealed by quantitative hybridization of a high density cDNA array. Genome Res, 1996. 6(6): p. 492-503.

156. Stapleton, D., C. Nelson, K. Parsawar, D. McClain, R. Gilbert-Wilson, E. Barker, B. Rudd, K. Brown, W. Hendrix, P. O'Donnell, and G. Parker, Analysis of hepatic glycogen-associated proteins. Proteomics, 2010. 10(12): p. 2320-2329.

157. Zhu, Y., M. Zhang, A.R. Kelly, and A. Cheng, The carbohydrate-binding domain of overexpressed STBD1 is important for its stability and protein-protein interactions. Biosci Rep, 2014. 34(4).

158. Sun, T., H. Yi, C. Yang, P.S. Kishnani, and B. Sun, Starch Binding Domain-containing Protein 1 Plays a Dominant Role in Glycogen Transport to Lysosomes in Liver. J Biol Chem, 2016. 291(32): p. 16479-16484.

159. Zirin, J., J. Nieuwenhuis, and N. Perrimon, Role of autophagy in glycogen breakdown and its relevance to chloroquine myopathy. PLoS Biol, 2013. 11(11): p. e1001708.

160. Jatana, N., D.B. Ascher, D.E.V. Pires, R.S. Gokhale, and L. Thukral, Human LC3 and GABARAP subfamily members achieve functional specificity via specific structural modulations. Autophagy, 2019: p. 1-17.

161. Rogov, V.V., A. Stolz, A.C. Ravichandran, D.O. Rios-Szwed, H. Suzuki, A. Kniss, F. Lohr, S. Wakatsuki, V. Dotsch, I. Dikic, R.C. Dobson, and D.G. McEwan, Structural and functional analysis of the GABARAP interaction motif (GIM). EMBO Rep, 2017. 18(8): p. 1382-1396.

162. Behrends, C., M.E. Sowa, S.P. Gygi, and J.W. Harper, Network organization of the human autophagy system. Nature, 2010. 466(7302): p. 68-76.

163. Chen, C., J.G. Li, Y. Chen, P. Huang, Y. Wang, and L.Y. Liu-Chen, GEC1 interacts with the kappa opioid receptor and enhances expression of the receptor. J Biol Chem, 2006. 281(12): p. 7983-7993.

164. Grunwald, D.S., N.M. Otto, J.M. Park, D. Song, and D.H. Kim, GABARAPs and LC3s have opposite roles in regulating ULK1 for autophagy induction. Autophagy, 2019: p. 1-15.

165. Poillet-Perez, L., M. Jacquet, E. Hervouet, T. Gauthier, A. Fraichard, C. Borg, J.R. Pallandre, B.J. Gonzalez, Y. Ramdani, M. Boyer-Guittaut, R. Delage-Mourroux, and G. Despouy, GABARAPL1 tumor suppressive function is independent of its conjugation to autophagosomes in MCF-7 breast cancer cells. Oncotarget, 2017. 8(34): p. 55998-56020.

166. Chan, J., A.K. Desai, Z.B. Kazi, K. Corey, S. Austin, L.D. Hobson-Webb, L.E. Case, H.N. Jones, and P.S. Kishnani, The emerging phenotype of late-onset Pompe disease: A systematic literature review. Mol Genet Metab, 2017. 120(3): p. 163-172.

167. Onodera, S., H. Matsui, and S. Chiba, Substrate specificity and subsite affinities of rabbit liver acid alpha-glucosidase. J Biochem, 1994. 116(1): p. 7-11.

168. Chambers, J.P. and J.C. Williams, Acid alpha-glucosidase from human heart. Enzyme, 1983. 29(2): p. 109-119.

169. Geddes, R., D.E. Otter, G.K. Scott, and J.A. Taylor, Disturbance of lysosomal glycogen metabolism by liposomal anti-alpha-glucosidase and some anti-inflammatory drugs. Biochem J, 1983. 212(1): p. 99-103.

170. Geddes, R. and J.A. Taylor, Factors affecting the metabolic control of cytosolic and lysosomal glycogen levels in the liver. Biosci Rep, 1985. 5(4): p. 315-320.

171. Reichelt, M.E., K.M. Mellor, C.L. Curl, D. Stapleton, and L.M. Delbridge, Myocardial glycophagy - a specific glycogen handling response to metabolic stress is accentuated in the female heart. J Mol Cell Cardiol, 2013. 65: p. 67-75.

172. Mellor, K.M., U. Varma, D.I. Stapleton, and L.M. Delbridge, Cardiomyocyte glycophagy is regulated by insulin and exposure to high extracellular glucose. Am J Physiol Heart Circ Physiol, 2014. 306(8): p. H1240-1245.

173. Kalamidas, S.A., O.B. Kotoulas, and A.C. Hann, Studies on glycogen autophagy: effects of phorbol myristate acetate, ionophore A23187, or phentolamine. Microsc Res Tech, 2002. 57(6): p. 507-511.

174. Haller, T., P. Dietl, P. Deetjen, and H. Völkl, The lysosomal compartment as intracellular calcium store in MDCK cells: a possible involvement in InsP3-mediated Ca2+ release. Cell Calcium, 1996. 19(2): p. 157-165.

175. Gordon, P.B., I. Holen, M. Fosse, J.S. Rotnes, and P.O. Seglen, Dependence of hepatocytic autophagy on intracellularly sequestered calcium. J Biol Chem, 1993. 268(35): p. 26107-26112.

176. Kotoulas, O.B., The effects of cyclic 3',5'-AMP on the lysosomes of newborn rat hepatocytes. J Ultrastruct Mol Struct Res, 1986. 97(1-3): p. 210-215.

177. Fayssoil, A., O. Nardi, D. Annane, and D. Orlikowski, Right ventricular function in late-onset Pompe disease. J Clin Monit Comput, 2014. 28(4): p. 419-421.

178. Cheng, Z. and Q. Fang, Danon disease: focusing on heart. J Hum Genet, 2012. 57(7): p. 407-410.

179. Bulkley, B.H. and G.M. Hutchins, Pompe's disease presenting as hypertrophic myocardiopathy with Wolff-Parkinson-White syndrome. American heart journal, 1978. 96(2): p. 246-252.

180. Francesconi, M. and E. Auff, Cardiac arrhythmias and the adult form of type II glycogenosis. The New England journal of medicine, 1982. 306(15): p. 937-938.

181. Nair, V., E.C. Belanger, and J.P. Veinot, Lysosomal storage disorders affecting the heart: a review. Cardiovasc Pathol, 2019. 39: p. 12-24.

182. Banerjee, S.K., D.W. Wang, R. Alzamora, X.N. Huang, N.M. Pastor-Soler, K.R. Hallows, K.R. McGaffin, and F. Ahmad, SGLT1, a novel cardiac glucose transporter, mediates increased glucose uptake in PRKAG2 cardiomyopathy. J Mol Cell Cardiol, 2010. 49(4): p. 683-692.

183. Bouskila, M., R.W. Hunter, A.F. Ibrahim, L. Delattre, M. Peggie, J.A. van Diepen, P.J. Voshol, J. Jensen, and K. Sakamoto, Allosteric regulation of glycogen synthase controls glycogen synthesis in muscle. Cell Metab, 2010. 12(5): p. 456-466.

184. Carling, D. and D.G. Hardie, The substrate and sequence specificity of the AMP-activated protein kinase. Phosphorylation of glycogen synthase and phosphorylase kinase. Biochim Biophys Acta, 1989. 1012(1): p. 81-86.

185. De Luca, J.P., A.K. Garnache, J. Rulfs, and T.B. Miller, Jr., Wortmannin inhibits insulin-stimulated activation of protein phosphatase 1 in rat cardiomyocytes. Am J Physiol, 1999. 276(5): p. H1520-1526.

186. Goodwin, G.W., J.R. Arteaga, and H. Taegtmeyer, Glycogen turnover in the isolated working rat heart. J Biol Chem, 1995. 270(16): p. 9234-9240.

187. Hunter, R.W., J.T. Treebak, J.F. Wojtaszewski, and K. Sakamoto, Molecular mechanism by which AMP-activated protein kinase activation promotes glycogen accumulation in muscle. Diabetes, 2011. 60(3): p. 766-774.

188. Mora, A., K. Sakamoto, E.J. McManus, and D.R. Alessi, Role of the PDK1-PKB-GSK3 pathway in regulating glycogen synthase and glucose uptake in the heart. FEBS Lett, 2005. 579(17): p. 3632-3638.

189. Wang, L., X. Wang, and C.G. Proud, Activation of mRNA translation in rat cardiac myocytes by insulin involves multiple rapamycin-sensitive steps. Am J Physiol Heart Circ Physiol, 2000. 278(4): p. H1056-1068.

190. Wojtaszewski, J.F., S.B. Jorgensen, Y. Hellsten, D.G. Hardie, and E.A. Richter, Glycogen-dependent effects of 5-aminoimidazole-4-carboxamide (AICA)-riboside on AMP-activated protein kinase and glycogen synthase activities in rat skeletal muscle. Diabetes, 2002. 51(2): p. 284-292.

191. Wolleben, C.D., S.R. Jaspers, and T.B. Miller, Jr., Use of adult rat cardiomyocytes to study cardiac glycogen metabolism. Am J Physiol, 1987. 252(5 Pt 1): p. E673-678.

192. Bezborodkina, N.N., A.Y. Chestnova, M.L. Vorobev, and B.N. Kudryavtsev, Spatial Structure of Glycogen Molecules in Cells. Biochemistry (Mosc), 2018. 83(5): p. 467-482.

193. Ryu, J.-H., J. Drain, J.H. Kim, S. McGee, A. Gray-Weale, L. Waddington, G.J. Parker, M. Hargreaves, S.-H. Yoo, and D. Stapleton, Comparative structural analyses of purified glycogen particles from rat liver, human skeletal muscle and commercial preparations. International Journal of Biological Macromolecules, 2009. 45(5): p. 478-482.

194. Marchand, I., K. Chorneyko, M. Tarnopolsky, S. Hamilton, J. Shearer, J. Potvin, and T.E. Graham, Quantification of subcellular glycogen in resting human muscle: granule size, number, and location. J Appl Physiol (1985), 2002. 93(5): p. 1598-1607.

195. Besford, Q.A., M.A. Sullivan, L. Zheng, R.G. Gilbert, D. Stapleton, and A. Gray-Weale, The structure of cardiac glycogen in healthy mice. International Journal of Biological Macromolecules, 2012. 51(5): p. 887-891.

196. Geddes, R. and G.C. Stratton, The influence of lysosomes on glycogen metabolism. Biochem J, 1977. 163(2): p. 193-200.

197. Kotoulas, O.B. and M.J. Phillips, Fine structural aspects of the mobilization of hepatic glycogen. I. Acceleration of glycogen breakdown. Am J Pathol, 1971. 63(1): p. 1-22.

198. Kondomerkos, D.J., S.A. Kalamidas, O.B. Kotoulas, and A.C. Hann, Glycogen autophagy in the liver and heart of newborn rats. The effects of glucagon, adrenalin or rapamycin. Histol Histopathol, 2005. 20(3): p. 689-696.

199. Iwamasa, T., T. Tsuru, T. Hamada, and T. Takeuchi, Physicochemical and ultrastructural studies on glycogenosomes in newborn rat hepatocytes. Pathol Res Pract, 1980. 167(2-4): p. 363-373.

200. Margolis, R.N. and K. Tanner, Glycogen metabolism in neonatal liver of the rat. Arch Biochem Biophys, 1986. 249(2): p. 605-610.

201. Lopaschuk, G.D. and J.S. Jaswal, Energy metabolic phenotype of the cardiomyocyte during development, differentiation, and postnatal maturation. J Cardiovasc Pharmacol, 2010. 56(2): p. 130-140.

202. Tagliabracci, V.S., J. Turnbull, W. Wang, J.M. Girard, X. Zhao, A.V. Skurat, A.V. Delgado-Escueta, B.A. Minassian, A.A. Depaoli-Roach, and P.J. Roach, Laforin is a glycogen phosphatase, deficiency of which leads to elevated phosphorylation of glycogen in vivo. Proc Natl Acad Sci U S A, 2007. 104(49): p. 19262-19266.

203. Ganesh, S., R. Puri, S. Singh, S. Mittal, and D. Dubey, Recent advances in the molecular basis of Lafora's progressive myoclonus epilepsy. J Hum Genet, 2006. 51(1): p. 1-8.

204. Parihar, R., A. Rai, and S. Ganesh, Lafora disease: from genotype to phenotype. J Genet, 2018. 97(3): p. 611-624.

205. Riehle, C., A.R. Wende, S. Sena, K.M. Pires, R.O. Pereira, Y. Zhu, H. Bugger, D. Frank, J. Bevins, D. Chen, C.N. Perry, X.C. Dong, S. Valdez, M. Rech, X. Sheng, B.C. Weimer, R.A. Gottlieb, M.F. White, and E.D. Abel, Insulin receptor substrate signaling suppresses neonatal autophagy in the heart. J Clin Invest, 2013. 123(12): p. 5319-5333.

206. Arad, M., I.P. Moskowitz, V.V. Patel, F. Ahmad, A.R. Perez-Atayde, D.B. Sawyer, M. Walter, G.H. Li, P.G. Burgon, C.T. Maguire, D. Stapleton, J.P. Schmitt, X.X. Guo, A. Pizard, S. Kupershmidt, D.M. Roden, C.I. Berul, C.E. Seidman, and J.G. Seidman, Transgenic mice overexpressing mutant PRKAG2 define the cause of Wolff-Parkinson-White syndrome in glycogen storage cardiomyopathy. Circulation, 2003. 107(22): p. 2850-2856.

207. Sidhu, J.S., Y.S. Rajawat, T.G. Rami, M.H. Gollob, Z. Wang, R. Yuan, A.J. Marian, F.J. DeMayo, D. Weilbacher, G.E. Taffet, J.K. Davies, D. Carling, D.S. Khoury, and R. Roberts, Transgenic mouse model of ventricular preexcitation and atrioventricular reentrant tachycardia induced by an AMP-activated protein kinase loss-of-function mutation responsible for Wolff-Parkinson-White syndrome. Circulation, 2005. 111(1): p. 21-29.

208. Davies, J.K., D.J. Wells, K. Liu, H.R. Whitrow, T.D. Daniel, R. Grignani, C.A. Lygate, J.E. Schneider, G. Noel, H. Watkins, and D. Carling, Characterization of the role of gamma2 R531G mutation in AMP-activated protein kinase in cardiac hypertrophy and Wolff-Parkinson-White syndrome. Am J Physiol Heart Circ Physiol, 2006. 290(5): p. H1942-1951.

209. Akman, H.O., J.N. Sampayo, F.A. Ross, J.W. Scott, G. Wilson, L. Benson, C. Bruno, S. Shanske, D.G. Hardie, and S. Dimauro, Fatal infantile cardiac glycogenosis with phosphorylase kinase deficiency and a mutation in the gamma2-subunit of AMP-activated protein kinase. Pediatr Res, 2007. 62(4): p. 499-504.

210. Burwinkel, B., J.W. Scott, C. Buhrer, F.K. van Landeghem, G.F. Cox, C.J. Wilson, D. Grahame Hardie, and M.W. Kilimann, Fatal congenital heart glycogenosis caused by a recurrent activating R531Q mutation in the gamma 2-subunit of AMP-activated protein kinase (PRKAG2), not by phosphorylase kinase deficiency. Am J Hum Genet, 2005. 76(6): p. 1034-1049.

211. Gowans, G.J., S.A. Hawley, F.A. Ross, and D.G. Hardie, AMP is a true physiological regulator of AMP-activated protein kinase by both allosteric activation and enhancing net phosphorylation. Cell Metab, 2013. 18(4): p. 556-566.

212. Grahame Hardie, D., AMP-activated protein kinase: a key regulator of energy balance with many roles in human disease. Journal of internal medicine, 2014. 276(6): p. 543-559.

213. Hudson, E.R., D.A. Pan, J. James, J.M. Lucocq, S.A. Hawley, K.A. Green, O. Baba, T. Terashima, and D.G. Hardie, A novel domain in AMP-activated protein kinase causes glycogen storage bodies similar to those seen in hereditary cardiac arrhythmias. Curr Biol, 2003. 13(10): p. 861-866.

214. Polekhina, G., A. Gupta, B.J. van Denderen, S.C. Feil, B.E. Kemp, D. Stapleton, and M.W. Parker, Structural basis for glycogen recognition by AMP-activated protein kinase. Structure, 2005. 13(10): p. 1453-1462.

215. Kristiansen, S.B., L. Solskov, N. Jessen, B. Lofgren, O. Schmitz, J.E. Nielsen-Kudsk, T.T. Nielsen, H.E. Botker, and S. Lund, 5-Aminoimidazole-4-carboxamide-1-beta-D-ribofuranoside increases myocardial glucose uptake during reperfusion and induces late pre-conditioning: potential role of AMP-activated protein kinase. Basic Clin Pharmacol Toxicol, 2009. 105(1): p. 10-16.

216. Russell, R.R., 3rd, R. Bergeron, G.I. Shulman, and L.H. Young, Translocation of myocardial GLUT-4 and increased glucose uptake through activation of AMPK by AICAR. Am J Physiol, 1999. 277(2): p. H643-649.

217. Holmes, B.F., E.J. Kurth-Kraczek, and W.W. Winder, Chronic activation of 5'-AMP-activated protein kinase increases GLUT-4, hexokinase, and glycogen in muscle. J Appl Physiol (1985), 1999. 87(5): p. 1990-1995.

218. Longnus, S.L., R.B. Wambolt, H.L. Parsons, R.W. Brownsey, and M.F. Allard, 5-Aminoimidazole-4-carboxamide 1-beta -D-ribofuranoside (AICAR) stimulates myocardial glycogenolysis by allosteric mechanisms. Am J Physiol Regul Integr Comp Physiol, 2003. 284(4): p. R936-944.

219. Kim, J., M. Kundu, B. Viollet, and K.-L. Guan, AMPK and mTOR regulate autophagy through direct phosphorylation of Ulk1. Nat Cell Biol, 2011. 13(2): p. 132-141.

220. Egan, D., J. Kim, R.J. Shaw, and K.-L. Guan, The autophagy initiating kinase ULK1 is regulated via opposing phosphorylation by AMPK and mTOR. Autophagy, 2011. 7(6): p. 643-644.

221. Kim, J., M. Kundu, B. Viollet, and K.L. Guan, AMPK and mTOR regulate autophagy through direct phosphorylation of Ulk1. Nat Cell Biol, 2011. 13(2): p. 132-141.

222. Egan, D.F., D.B. Shackelford, M.M. Mihaylova, S. Gelino, R.A. Kohnz, W. Mair, D.S. Vasquez, A. Joshi, D.M. Gwinn, R. Taylor, J.M. Asara, J. Fitzpatrick, A. Dillin, B. Viollet, M. Kundu, M. Hansen, and R.J. Shaw, Phosphorylation of ULK1 (hATG1) by AMP-activated protein kinase connects energy sensing to mitophagy. Science, 2011. 331(6016): p. 456-461.

223. Pal, R., Y. Xiong, and M. Sardiello, Abnormal glycogen storage in tuberous sclerosis complex caused by impairment of mTORC1-dependent and -independent signaling pathways. Proc Natl Acad Sci U S A, 2019. 116(8): p. 2977-2986.

224. Mellor, K.M., J.R. Bell, M.J. Young, R.H. Ritchie, and L.M. Delbridge, Myocardial autophagy activation and suppressed survival signaling is associated with insulin resistance in fructose-fed mice. J Mol Cell Cardiol, 2011. 50(6): p. 1035-1043.

225. Sakaguchi, K., K. Takeda, M. Maeda, W. Ogawa, T. Sato, S. Okada, Y. Ohnishi, H. Nakajima, and A. Kashiwagi, Glucose area under the curve during oral glucose tolerance test as an index of glucose intolerance. Diabetol Int, 2016. 7(1): p. 53-58.

226. Livak, K.J. and T.D. Schmittgen, Analysis of relative gene expression data using real-time quantitative PCR and the 2(-Delta Delta C(T)) Method. Methods, 2001. 25(4): p. 402-408.

227. Egan, D., J. Kim, R.J. Shaw, and K.L. Guan, The autophagy initiating kinase ULK1 is regulated via opposing phosphorylation by AMPK and mTOR. Autophagy, 2011. 7(6): p. 643-644.

228. Martina, J.A., Y. Chen, M. Gucek, and R. Puertollano, MTORC1 functions as a transcriptional regulator of autophagy by preventing nuclear transport of TFEB. Autophagy, 2012. 8(6): p. 903-914.

229. Kuma, A., M. Hatano, M. Matsui, A. Yamamoto, H. Nakaya, T. Yoshimori, Y. Ohsumi, T. Tokuhisa, and N. Mizushima, The role of autophagy during the early neonatal starvation period. Nature, 2004. 432(7020): p. 1032-1036.

230. Bowden, M.A., G.H. Tesch, T.L. Julius, S. Rosli, J.E. Love, and R.H. Ritchie, Earlier onset of diabesity-Induced adverse cardiac remodeling in female compared to male mice. Obesity, 2015. 23(6): p. 1166-1177.

231. Susztak, K., E. Böttinger, A. Novetsky, D. Liang, Y. Zhu, E. Ciccone, D. Wu, S. Dunn, P. McCue, and K. Sharma, Molecular Profiling of Diabetic Mouse Kidney Reveals Novel Genes Linked to Glomerular Disease. Diabetes, 2004. 53(3): p. 784-794.

232. Huynh, K., H. Kiriazis, X.J. Du, J.E. Love, S.P. Gray, K.A. Jandeleit-Dahm, J.R. McMullen, and R.H. Ritchie, Targeting the upregulation of reactive oxygen species subsequent to hyperglycemia prevents type 1 diabetic cardiomyopathy in mice. Free Radic Biol Med, 2013. 60: p. 307-317.

233. Nutter, C.A. and M.N. Kuyumcu-Martinez, Emerging roles of RNA-binding proteins in diabetes and their therapeutic potential in diabetic complications. Wiley interdisciplinary reviews. RNA, 2018. 9(2): p. 10.1002/wrna.1459.

234. Balasubramanian, S., S.K. Mani, H. Kasiganesan, C.C. Baicu, and D. Kuppuswamy, Hypertrophic stimulation increases beta-actin dynamics in adult feline cardiomyocytes. PLoS One, 2010. 5(7): p. e11470-e11470.

235. Pletscher-Frankild, S., A. Palleja, K. Tsafou, J.X. Binder, and L.J. Jensen, DISEASES: text mining and data integration of disease-gene associations. Methods, 2015. 74: p. 83-89.

236. Kuleshov, M.V., M.R. Jones, A.D. Rouillard, N.F. Fernandez, Q. Duan, Z. Wang, S. Koplev, S.L. Jenkins, K.M. Jagodnik, A. Lachmann, M.G. McDermott, C.D. Monteiro, G.W. Gundersen, and A. Ma'ayan, Enrichr: a comprehensive gene set enrichment analysis web server 2016 update. Nucleic acids research, 2016. 44(W1): p. W90-W97.

237. Szklarczyk, D., A.L. Gable, D. Lyon, A. Junge, S. Wyder, J. Huerta-Cepas, M. Simonovic, N.T. Doncheva, J.H. Morris, P. Bork, L.J. Jensen, and C.V. Mering, STRING v11: protein-protein association networks with increased coverage, supporting functional discovery in genome-wide experimental datasets. Nucleic acids research, 2019. 47(D1): p. D607-D613.

238. von Mering, C., L.J. Jensen, B. Snel, S.D. Hooper, M. Krupp, M. Foglierini, N. Jouffre, M.A. Huynen, and P. Bork, STRING: known and predicted protein-protein associations, integrated and transferred across organisms. Nucleic acids research, 2005. 33(Database issue): p. D433-437.

239. Matsui, T., J. Tao, F. del Monte, K.H. Lee, L. Li, M. Picard, T.L. Force, T.F. Franke, R.J. Hajjar, and A. Rosenzweig, Akt activation preserves cardiac function and prevents injury after transient cardiac ischemia in vivo. Circulation, 2001. 104(3): p. 330-335.

240. Lee, Y., Y. Hong, S.R. Lee, K.T. Chang, and Y. Hong, Autophagy contributes to retardation of cardiac growth in diabetic rats. Lab Anim Res, 2012. 28(2): p. 99-107.

241. Booth, L.A., S. Tavallai, H.A. Hamed, N. Cruickshanks, and P. Dent, The role of cell signalling in the crosstalk between autophagy and apoptosis. Cell Signal, 2014. 26(3): p. 549-555.
242. Duan, P., J. Wang, Y. Li, S. Wei, F. Su, S. Zhang, Y. Duan, L. Wang, and Q. Zhu, Opening of mitoKATP improves cardiac function and inhibits apoptosis via the AKT-Foxo1 signaling pathway in diabetic cardiomyopathy. Int J Mol Med, 2018. 42(5): p. 2709-2719.
243. Sengupta, A., J.D. Molkentin, and K.E. Yutzey, FoxO transcription factors promote autophagy in cardiomyocytes. J Biol Chem, 2009. 284(41): p. 28319-28331.
244. Kohler, L., R. Puertollano, and N. Raben, Pompe Disease: From Basic Science to Therapy. Neurotherapeutics, 2018. 15(4): p. 928-942.
245. Ellingwood, S.S. and A. Cheng, Biochemical and clinical aspects of glycogen storage diseases. J Endocrinol, 2018. 238(3): p. R131-R141.
246. Mah, C., C.A. Pacak, K.O. Cresawn, L.R. DeRuisseau, S. Germain, M.A. Lewis, D.A. Cloutier, D.D. Fuller, and B.J. Byrne, Physiological Correction of Pompe Disease by Systemic Delivery of Adeno-associated Virus Serotype 1 Vectors. Molecular Therapy, 2007. 15(3): p. 501-507.
247. Nakai, A., O. Yamaguchi, T. Takeda, Y. Higuchi, S. Hikoso, M. Taniike, S. Omiya, I. Mizote, Y. Matsumura, M. Asahi, K. Nishida, M. Hori, N. Mizushima, and K. Otsu, The role of autophagy in cardiomyocytes in the basal state and in response to hemodynamic stress. Nat Med, 2007. 13(5): p. 619-624.
248. Zhu, H., P. Tannous, J.L. Johnstone, Y. Kong, J.M. Shelton, J.A. Richardson, V. Le, B. Levine, B.A. Rothermel, and J.A. Hill, Cardiac autophagy is a maladaptive response to hemodynamic stress. J Clin Invest, 2007. 117(7): p. 1782-1793.
249. Tong, M., T. Saito, P. Zhai, S.-i. Oka, W. Mizushima, M. Nakamura, S. Ikeda, A. Shirakabe, and J. Sadoshima, Mitophagy Is Essential for Maintaining Cardiac Function During High Fat Diet-Induced Diabetic Cardiomyopathy. Circ Res, 2019. 124(9): p. 1360-1371.
250. Birgisdottir, A.B., S. Mouilleron, Z. Bhujabal, M. Wirth, E. Sjottem, G. Evjen, W. Zhang, R. Lee, N. O'Reilly, S.A. Tooze, T. Lamark, and T. Johansen, Members of the autophagy class III phosphatidylinositol 3-kinase complex I interact with GABARAP and GABARAPL1 via LIR motifs. Autophagy, 2019. 15(8): p. 1333-1355.
251. Le Grand, J.N., K. Bon, A. Fraichard, J. Zhang, M. Jouvenot, P.Y. Risold, M. Boyer-Guittaut, and R. Delage-Mourroux, Specific distribution of the autophagic protein GABARAPL1/GEC1 in the developing and adult mouse brain and identification of neuronal populations expressing GABARAPL1/GEC1. PLoS One, 2013. 8(5): p. e63133.
252. Mansuy, V., W. Boireau, A. Fraichard, J.L. Schlick, M. Jouvenot, and R. Delage-Mourroux, GEC1, a protein related to GABARAP, interacts with tubulin and GABA(A) receptor. Biochem Biophys Res Commun, 2004. 325(2): p. 639-648.
253. Nemos, C., V. Mansuy, S. Vernier-Magnin, A. Fraichard, M. Jouvenot, and R. Delage-Mourroux, Expression of gec1/GABARAPL1 versus GABARAP mRNAs in human: predominance of gec1/GABARAPL1 in the central nervous system. Brain Res Mol Brain Res, 2003. 119(2): p. 216-219.
254. Quaife-Ryan, G.A., C.B. Sim, M. Ziemann, A. Kaspi, H. Rafehi, M. Ramialison, A. El-Osta, J.E. Hudson, and E.R. Porrello, Multicellular Transcriptional Analysis of Mammalian Heart Regeneration. Circulation, 2017. 136(12): p. 1123-1139.
255. Ishino, Y., M. Krupovic, and P. Forterre, History of CRISPR-Cas from Encounter with a Mysterious Repeated Sequence to Genome Editing Technology. J Bacteriol, 2018. 200(7).
256. Nguyen, T.N., B.S. Padman, J. Usher, V. Oorschot, G. Ramm, and M. Lazarou, Atg8 family LC3/GABARAP proteins are crucial for autophagosome-lysosome fusion but not autophagosome formation during PINK1/Parkin mitophagy and starvation. J Cell Biol, 2016. 215(6): p. 857-874.
257. McEwan, D.G., D. Popovic, A. Gubas, S. Terawaki, H. Suzuki, D. Stadel, F.P. Coxon, D. Miranda de Stegmann, S. Bhogaraju, K. Maddi, A. Kirchof, E. Gatti, M.H. Helfrich, S. Wakatsuki, C. Behrends, P. Pierre, and I. Dikic, PLEKHM1 regulates autophagosome-lysosome fusion through HOPS complex and LC3/GABARAP proteins. Mol Cell, 2015. 57(1): p. 39-54.
258. Priddy, T.S., C.R. Middaugh, and G.M. Carlson, Electrostatic changes in phosphorylase kinase induced by its obligatory allosteric activator Ca2+. Protein Sci, 2007. 16(3): p. 517-527.
259. Yu, S., L. Kenne, and M. Pedersen, Alpha-1,4-glucan lyase, a new class of starch/glycogen degrading enzyme. I. Efficient purification and characterization from red seaweeds. Biochim Biophys Acta, 1993. 1156(3): p. 313-320.
260. Sakasai-Sakai, A., T. Takata, H. Suzuki, I. Maruyama, Y. Motomiya, and M. Takeuchi, Immunological evidence for in vivo production of novel advanced glycation end-products from 1,5-anhydro-D-fructose, a glycogen metabolite. Sci Rep, 2019. 9(1): p. 10194-10194.
261. Janssens, J.V., B. Ma, M.A. Brimble, J.E. Van Eyk, L.M.D. Delbridge, and K.M. Mellor, Cardiac troponins may be irreversibly modified by glycation: novel potential mechanisms of cardiac performance modulation. Sci Rep, 2018. 8(1): p. 16084.

262. Diwan, A., M. Krenz, F.M. Syed, J. Wansapura, X. Ren, A.G. Koesters, H. Li, L.A. Kirshenbaum, H.S. Hahn, J. Robbins, W.K. Jones, and G.W. Dorn, Inhibition of ischemic cardiomyocyte apoptosis through targeted ablation of Bnip3 restrains postinfarction remodeling in mice. J Clin Invest, 2007. 117(10): p. 2825-2833.

263. Diwan, A., J. Wansapura, F.M. Syed, S.J. Matkovich, J.N. Lorenz, and G.W. Dorn, 2nd, Nix-mediated apoptosis links myocardial fibrosis, cardiac remodeling, and hypertrophy decompensation. Circulation, 2008. 117(3): p. 396-404.

264. Siddall, H.K., D.M. Yellon, S.B. Ong, U.A. Mukherjee, N. Burke, A.R. Hall, P.R. Angelova, M.H. Ludtmann, E. Deas, S.M. Davidson, M.M. Mocanu, and D.J. Hausenloy, Loss of PINK1 increases the heart's vulnerability to ischemia-reperfusion injury. PLoS One, 2013. 8(4): p. e62400.

265. Yussman, M.G., T. Toyokawa, A. Odley, R.A. Lynch, G. Wu, M.C. Colbert, B.J. Aronow, J.N. Lorenz, and G.W. Dorn, 2nd, Mitochondrial death protein Nix is induced in cardiac hypertrophy and triggers apoptotic cardiomyopathy. Nat Med, 2002. 8(7): p. 725-730.

266. Baines, C.P., The cardiac mitochondrion: nexus of stress. Annu Rev Physiol, 2010. 72: p. 61-80.

267. Kubli, D.A., M.N. Quinsay, and A.B. Gustafsson, Parkin deficiency results in accumulation of abnormal mitochondria in aging myocytes. Commun Integr Biol, 2013. 6(4): p. e24511.

268. Song, M., Y. Chen, G. Gong, E. Murphy, P.S. Rabinovitch, and G.W. Dorn, 2nd, Super-suppression of mitochondrial reactive oxygen species signaling impairs compensatory autophagy in primary mitophagic cardiomyopathy. Circ Res, 2014. 115(3): p. 348-353.

269. Kubin, A.M., R. Skoumal, P. Tavi, A. Konyi, A. Perjes, H. Leskinen, H. Ruskoaho, and I. Szokodi, Role of reactive oxygen species in the regulation of cardiac contractility. J Mol Cell Cardiol, 2011. 50(5): p. 884-893.

270. Terentyev, D., I. Gyorke, A.E. Belevych, R. Terentyeva, A. Sridhar, Y. Nishijima, E.C. de Blanco, S. Khanna, C.K. Sen, A.J. Cardounel, C.A. Carnes, and S. Gyorke, Redox modification of ryanodine receptors contributes to sarcoplasmic reticulum Ca2+ leak in chronic heart failure. Circ Res, 2008. 103(12): p. 1466-1472.

271. Dorn, G.W., 2nd, Mitochondrial pruning by Nix and BNip3: an essential function for cardiac-expressed death factors. J Cardiovasc Transl Res, 2010. 3(4): p. 374-383.

272. Wu, Z., A. Asokan, and R.J. Samulski, Adeno-associated virus serotypes: vector toolkit for human gene therapy. Molecular therapy : the journal of the American Society of Gene Therapy, 2006. 14(3): p. 316-327.

273. Russell, D.W. and M.A. Kay, Adeno-associated virus vectors and hematology. Blood, 1999. 94(3): p. 864-874.

274. Asokan, A. and R.J. Samulski, An emerging adeno-associated viral vector pipeline for cardiac gene therapy. Human gene therapy, 2013. 24(11): p. 906-913.

275. Bostick, B., A. Ghosh, Y. Yue, C. Long, and D. Duan, Systemic AAV-9 transduction in mice is influenced by animal age but not by the route of administration. Gene therapy, 2007. 14(22): p. 1605-1609.

276. Inagaki, K., S. Fuess, T.A. Storm, G.A. Gibson, C.F. McTiernan, M.A. Kay, and H. Nakai, Robust systemic transduction with AAV9 vectors in mice: efficient global cardiac gene transfer superior to that of AAV8. Molecular therapy : the journal of the American Society of Gene Therapy, 2006. 14(1): p. 45-53.

277. Kotchey, N.M., K. Adachi, M. Zahid, K. Inagaki, R. Charan, R.S. Parker, and H. Nakai, A potential role of distinctively delayed blood clearance of recombinant adeno-associated virus serotype 9 in robust cardiac transduction. Molecular therapy : the journal of the American Society of Gene Therapy, 2011. 19(6): p. 1079-1089.

278. Palomeque, J., E.R. Chemaly, P. Colosi, J.A. Wellman, S. Zhou, F. Del Monte, and R.J. Hajjar, Efficiency of eight different AAV serotypes in transducing rat myocardium in vivo. Gene therapy, 2007. 14(13): p. 989-997.

279. Zincarelli, C., S. Soltys, G. Rengo, and J.E. Rabinowitz, Analysis of AAV serotypes 1-9 mediated gene expression and tropism in mice after systemic injection. Molecular therapy : the journal of the American Society of Gene Therapy, 2008. 16(6): p. 1073-1080.

280. Konkalmatt, P.R., R.J. Beyers, D.M. O'Connor, Y. Xu, M.E. Seaman, and B.A. French, Cardiac-selective expression of extracellular superoxide dismutase after systemic injection of adeno-associated virus 9 protects the heart against post-myocardial infarction left ventricular remodeling. Circulation. Cardiovascular imaging, 2013. 6(3): p. 478-486.

281. Piras, B.A., D.M. O'Connor, and B.A. French, Systemic delivery of shRNA by AAV9 provides highly efficient knockdown of ubiquitously expressed GFP in mouse heart, but not liver. PLoS One, 2013. 8(9): p. e75894-e75894.

282. Ma, H., C.M. Sumbilla, I.K.G. Farrance, M.G. Klein, and G. Inesi, Cell-specific expression of SERCA, the exogenous Ca2+ transport ATPase, in cardiac myocytes. Am J Physiol Cell Physiol, 2004. 286(3): p. C556-C564.

283. Daniels, A., D. Linz, M. van Bilsen, H. Rutten, T. Sadowski, S. Ruf, H.P. Juretschke, C. Neumann-Haefelin, C. Munts, G.J. van der Vusse, and F.A. van Nieuwenhoven, Long-term severe diabetes only leads to mild cardiac diastolic dysfunction in Zucker diabetic fatty rats. Eur J Heart Fail, 2012. 14(2): p. 193-201.

284. Werner, R.A., C. Eissler, N. Hayakawa, P. Arias-Loza, H. Wakabayashi, M.S. Javadi, X. Chen, T. Shinaji, C. Lapa, T. Pelzer, and T. Higuchi, Left Ventricular Diastolic Dysfunction in a Rat Model of Diabetic Cardiomyopathy using ECG-gated (18)F-FDG PET. Sci Rep, 2018. 8(1): p. 17631.

285. Alex, L., I. Russo, V. Holoborodko, and N.G. Frangogiannis, Characterization of a mouse model of obesity-related fibrotic cardiomyopathy that recapitulates features of human heart failure with preserved ejection fraction. Am J Physiol Heart Circ Physiol, 2018. 315(4): p. H934-H949.

286. Dumesnil, J.G., G. Gaudreault, G.N. Honos, and J.G. Kingma, Jr., Use of Valsalva maneuver to unmask left ventricular diastolic function abnormalities by Doppler echocardiography in patients with coronary artery disease or systemic hypertension. Am J Cardiol, 1991. 68(5): p. 515-519.

287. Zhang, J., Y. Cheng, J. Gu, S. Wang, S. Zhou, Y. Wang, Y. Tan, W. Feng, Y. Fu, N. Mellen, R. Cheng, J. Ma, C. Zhang, Z. Li, and L. Cai, Fenofibrate increases cardiac autophagy via FGF21/SIRT1 and prevents fibrosis and inflammation in the hearts of Type 1 diabetic mice. Clin Sci (Lond), 2016. 130(8): p. 625-641.

288. Mizushima, N. and T. Yoshimori, How to interpret LC3 immunoblotting. Autophagy, 2007. 3(6): p. 542-545.

289. Gowans, G.J. and D.G. Hardie, AMPK: a cellular energy sensor primarily regulated by AMP. Biochem Soc Trans, 2014. 42(1): p. 71-75.

290. Lee, C.T., J.R. Ussher, A. Mohammad, A. Lam, and G.D. Lopaschuk, 5'-AMP-activated protein kinase increases glucose uptake independent of GLUT4 translocation in cardiac myocytes. Can J Physiol Pharmacol, 2014. 92(4): p. 307-314.

291. Jorgensen, S.B., J.N. Nielsen, J.B. Birk, G.S. Olsen, B. Viollet, F. Andreelli, P. Schjerling, S. Vaulont, D.G. Hardie, B.F. Hansen, E.A. Richter, and J.F. Wojtaszewski, The alpha2-5'AMP-activated protein kinase is a site 2 glycogen synthase kinase in skeletal muscle and is responsive to glucose loading. Diabetes, 2004. 53(12): p. 3074-3081.

292. Halse, R., L.G. Fryer, J.G. McCormack, D. Carling, and S.J. Yeaman, Regulation of glycogen synthase by glucose and glycogen: a possible role for AMP-activated protein kinase. Diabetes, 2003. 52(1): p. 9-15.

293. Colella, P., G. Ronzitti, and F. Mingozzi, Emerging Issues in AAV-Mediated In Vivo Gene Therapy. Molecular therapy. Methods & clinical development, 2017. 8: p. 87-104.

294. Nathwani, A.C., U.M. Reiss, E.G.D. Tuddenham, C. Rosales, P. Chowdary, J. McIntosh, M. Della Peruta, E. Lheriteau, N. Patel, D. Raj, A. Riddell, J. Pie, S. Rangarajan, D. Bevan, M. Recht, Y.-M. Shen, K.G. Halka, E. Basner-Tschakarjan, F. Mingozzi, K.A. High, J. Allay, M.A. Kay, C.Y.C. Ng, J. Zhou, M. Cancio, C.L. Morton, J.T. Gray, D. Srivastava, A.W. Nienhuis, and A.M. Davidoff, Long-term safety and efficacy of factor IX gene therapy in hemophilia B. The New England journal of medicine, 2014. 371(21): p. 1994-2004.

295. Nathwani, A.C., E.G.D. Tuddenham, S. Rangarajan, C. Rosales, J. McIntosh, D.C. Linch, P. Chowdary, A. Riddell, A.J. Pie, C. Harrington, J. O'Beirne, K. Smith, J. Pasi, B. Glader, P. Rustagi, C.Y.C. Ng, M.A. Kay, J. Zhou, Y. Spence, C.L. Morton, J. Allay, J. Coleman, S. Sleep, J.M. Cunningham, D. Srivastava, E. Basner-Tschakarjan, F. Mingozzi, K.A. High, J.T. Gray, U.M. Reiss, A.W. Nienhuis, and A.M. Davidoff, Adenovirus-associated virus vector-mediated gene transfer in hemophilia B. The New England journal of medicine, 2011. 365(25): p. 2357-2365.

296. Rybicka, K., Glycosomes (protein-glycogen complex) in the canine heart. Virchows Archiv B, 1979. 30(1): p. 335-347.

297. Zhang, X., Z. Li, Z. Xuan, P. Xu, W. Wang, Z. Chen, S. Wang, G. Sun, J. Xu, and Z. Xu, Novel role of miR-133a-3p in repressing gastric cancer growth and metastasis via blocking autophagy-mediated glutaminolysis. J Exp Clin Cancer Res, 2018. 37(1): p. 320.

298. Blake, C.A. and R.L. Hazelwood, Effect of pregnancy and exercise on actomyosin, nucleic acid, and glycogen content of the rat heart. Proc Soc Exp Biol Med, 1971. 136(2): p. 632-636.

299. Kokubun, E., S.M. Hirabara, J. Fiamoncini, R. Curi, and H. Haebisch, Changes of glycogen content in liver, skeletal muscle, and heart from fasted rats. Cell Biochem Funct, 2009. 27(7): p. 488-495.

300. Puthanveetil, P., F. Wang, G. Kewalramani, M.S. Kim, E. Hosseini-Beheshti, N. Ng, W. Lau, T. Pulinilkunnil, M. Allard, A. Abrahani, and B. Rodrigues, Cardiac glycogen accumulation after dexamethasone is regulated by AMPK. Am J Physiol Heart Circ Physiol, 2008. 295(4): p. H1753-1762.

301. Rybicka, K.K., Glycosomes--the organelles of glycogen metabolism. Tissue Cell, 1996. 28(3): p. 253-265.

Appendix 1

Table A1.1: Summary of RNA and cDNA quality controls (RT^2 RNA QC PCR Array)ray)

Control	Objective	Calculation	Optimum C_t value
Housekeeping controls (HK)	2 control genes (β-actin/*Actb* and Hypoxanthine phosphoribosyltransferase/*Hprt1* were used to estimate the Ct values at which genes of interest would cross the detection threshold.	-	Variable
Reverse transcription control (RTC)	This control examines the presence of RT-inhibitory contaminants in the RNA samples by amplifying a PCR-detectable internal control (P2) that is combined with the RNA samples during reverse transcription.	$\Delta C_T = [C_{T/RTC}] - [C_{T/PPC\text{-}H2O}] \leq 5$ A ΔC_T value ≤ 5 indicates no apparent inhibition of the RT reaction.	Variable
Positive PCR control (PPC)	Each PPC well in the QC plate contains a plasmid-based artificial sequence and primers. Failure to amplify this sequences denotes the presence of PCR-inhibitory contaminants. This sequence is amplified both in presence (PPC-cDNA) and absence (PPC-H2O) of cDNA template.	$\Delta C_T = [C_{T/PPC\text{-}cDNA}] - [C_{T/PPC\text{-}H2O}] \leq 3$ A ΔC_T value ≤ 3 indicates absence of PCR-inhibitory contaminants.	20±2 (per PPC control)
Genomic DNA control (GDC)	This assay specifically detects non-transcribed DNA.	-	≥35
No Reverse Transcription (NRT)	Amplification detected in assays using RNA as template indicate DNA contamination of the RNA samples	-	≥35
No Template control (NTC)	Amplification detected in assays using H2O as template indicate DNA contamination induced at experimental setup.	-	≥35

Table A1.2: Summary of the quality control values for each sample included in the RT^2 RNA QC PCR Array

Sample ID	C_T Actb	C_T Hprt1	C_T RTC	C_T PPC-cDNA	C_T GDC	C_T NRT	$[C_{T/RTC}] - [C_{T/PPC\text{-}H2O}]$	$[C_{T/PPC\text{-}cDNA}] - [C_{T/PPC\text{-}H2O}]$
STZr-1	19.87	20.87	23.61	18.59	>35	>35	4.36	-0.67
STZr-2	22.12	21.63	24.52	18.84	>35	>35	5.26	-0.41
STZr-3	20.49	20.63	23.71	18.57	>35	>35	4.46	-0.68
STZr-4	20.10	20.63	23.62	18.11	>35	>35	4.37	-1.14
STZr-5	20.51	20.84	23.90	18.86	>35	>35	4.65	-0.40
STZr-6	21.18	21.21	24.23	19.21	>35	>35	4.98	-0.04
STZr-7	19.89	20.70	23.65	18.56	>35	>35	4.40	-0.69
Lean-1	19.38	20.34	23.35	18.32	>35	>35	4.10	-0.93
Lean-2	19.76	20.40	23.77	18.84	>35	>35	4.52	-0.41
Lean-3	19.58	20.58	23.56	18.60	>35	>35	4.31	-0.66
Lean-4	18.91	20.36	23.45	18.16	>35	>35	4.20	-1.10
Lean-5	19.80	20.50	23.58	18.30	>35	>35	4.33	-0.96
Lean-6	20.56	20.78	23.79	19.13	>35	>35	4.53	-0.12
Lean-7	20.09	20.85	24.21	18.66	>35	>35	4.96	-0.60
Lean-8	19.74	20.50	23.79	18.20	>35	>35	4.53	-1.05
CHOW-1	20.65	21.01	24.24	18.78	>35	>35	4.99	-0.47
CHOW-2	20.79	21.33	23.96	18.49	>35	>35	4.71	-0.76
CHOW-3	20.96	21.24	24.13	18.65	>35	>35	4.87	-0.61
CHOW-4	19.65	20.33	23.53	18.61	>35	>35	4.27	-0.65
CHOW-5	19.20	20.47	23.59	18.53	>35	>35	4.34	-0.72
CHOW-6	20.02	20.82	24.23	19.72	>35	>35	4.98	0.46
CHOW-7	19.99	20.68	23.98	18.74	>35	>35	4.73	-0.51
CHOW-8	20.28	21.27	24.31	18.78	>35	>35	5.05	-0.48
CHOW-9	20.18	20.75	24.22	19.51	>35	>35	4.97	0.25
HFD-1	20.38	21.13	23.98	19.85	>35	>35	4.73	0.60
HFD-2	20.45	21.37	23.85	19.08	>35	>35	4.60	-0.18
HFD-3	20.27	20.92	24.36	19.13	>35	>35	5.11	-0.12
HFD-4	20.69	21.19	24.23	19.26	>35	>35	4.97	0.01
HFD-5	21.14	21.44	24.35	18.96	>35	>35	5.09	-0.29

Sample ID	C_T Actb	C_T Hprt1	C_T RTC	C_T PPC-cDNA	C_T GDC	C_T NRT	$[C_{T/RTC}] - [C_{T/PPC-H2O}]$	$[C_{T/PPC-cDNA}] - [C_{T/PPC-H2O}]$
HFD-6	20.61	21.53	23.99	18.81	>35	>35	4.74	-0.44
HFD-7	20.12	21.52	23.86	18.89	>35	>35	4.61	-0.36
HFD-8	19.66	20.79	23.65	18.78	>35	>35	4.40	-0.47
HFD-9	19.42	20.40	23.82	18.51	>35	>35	4.57	-0.75

Samples included in the RT^2 RNA QC PCR Array formed the T1D (STZ rat) and pre-T2D (HFSD rat) groups. All samples were deemed of good quality to proceed to the RT2 profiler PCR array assays, as there was no evidence of RT- or PCR-inhibitory contaminants. The mean NTC value returned from the QC assay was >39 cycles. This, together with the GDC values being >35 cycles indicated that there was no genomic DNA contamination introduced at either the RNA extraction/RT step (verified by GDC) nor during experimental setup (verified by NTC). The quality of the db/db samples was verified previously by Dr Chanchal Chandramouli.

Table A1.3: Type 1 diabetic rat (STZr) Jensen DISEASE classification

Jensen DISEASE	p-value	Odds Ratio	Comb. Score	Genes
Glycogen Storage Disease	5.53E-06	85.349	1033.122	*Lamp2, Pygm, Phkb*
Vici Syndrome	3.44E-04	72.072	574.683	*Gabarapl1, Atg5*
Rippling Muscle Disease	0.009	108.108	506.675	*Gsk3B*
Donohue Syndrome	0.009	108.108	506.675	*Igf1*
Centronuclear Myopathy	0.001	56.899	426.212	*Pik3R4, Pik3C3*
Glycogen Storage Disease V	0.011	90.090	405.885	*Pygm*
Diffuse Idiopathic Skeletal Hyperostosis	0.011	90.090	405.885	*Igf1*
Protein-Energy Malnutrition	0.013	77.220	336.067	*Igf1*
Sleep Apnea	0.013	77.220	336.067	*Igf1*
Laron Syndrome	0.013	77.220	336.067	*Igf1*
Inflammatory Bowel Disease	0.013	77.220	336.067	*Atg16L1*
Abdominal Aortic Aneurysm	0.015	67.568	285.097	*Ctss*
Granulomatous Amebic Encephalitis	0.015	67.568	285.097	*Gabarapl1*
Fabry Disease	0.015	67.568	285.097	*Lamp2*
Breast Disease	0.015	67.568	285.097	*Igf1*
Inclusion Body Myopathy With Paget Disease Of Bone And Frontotemporal Dementia	0.017	60.060	246.399	*Sqstm1*
Wolff-Parkinson-White Syndrome	0.017	60.060	246.399	*Lamp2*
Beta-Mannosidosis	0.017	60.060	246.399	*Bcl2*
Myoglobinuria	0.018	54.054	216.113	*Pygm*
Lysosomal Storage Disease	0.018	54.054	216.113	*Ctss*
Keratopathy	0.020	49.140	191.827	*Igf1*
Rem Sleep Behavior Disorder	0.022	45.045	171.962	*Atg4C*
Craniopharyngioma	0.024	41.580	155.444	*Igf1*
Vitelliform Macular Dystrophy	0.024	41.580	155.444	*Pygm*
Short Bowel Syndrome	0.027	36.036	129.626	*Igf1*
Mccune Albright Syndrome	0.027	36.036	129.626	*Igf1*
Hyperprolactinemia	0.029	33.784	119.374	*Igf1*
Hyperglycemia	0.001	15.015	103.117	*Casp3, Igf1, Sirt1*
Pituitary Hypoplasia	0.033	30.030	102.627	*Igf1*
Retinopathy Of Prematurity	0.033	30.030	102.627	*Igf1*
Anovulation	0.035	28.450	95.713	*Igf1*
Dementia	0.001	13.627	89.774	*Gsk3B, Casp3, Igf1*
Atypical Autism	0.042	23.502	74.661	*Atg4C*
Cone-Rod Dystrophy	0.042	23.502	74.661	*Dram2*
Connective Tissue Disease	0.043	22.523	70.612	*Atg5*
Goiter	0.043	22.523	70.612	*Igf1*
Diabetes Mellitus	0.008	14.609	70.049	*Gsk3B, Gsk3A*
Huntington'S Disease	0.0091	14.225	67.475	*Casp3, Sirt1*
Multiple Endocrine Neoplasia Type 1	0.045	21.622	66.924	*Pygm*
Brain Disease	0.009	14.040	66.245	*Casp3, Igf1*
Hyperandrogenism	0.049	20.020	60.462	*Igf1*
Pancreatitis	0.011	12.870	58.575	*Casp3, Ctsb*
Acromegaly	0.051	19.305	57.618	*Igf1*
Multiple System Atrophy	0.052	18.639	54.993	*Atg4C*
Hypopituitarism	0.054	18.018	52.566	*Igf1*
Pituitary Adenoma	0.056	17.437	50.314	*Igf1*
Arthritis	0.005	8.718	46.415	*Casp3, Ctss, Ctsb*
Hyperthyroidism	0.063	15.444	42.744	*Igf1*
Brain Ischemia	0.063	15.444	42.744	*Casp3*
Hyperparathyroidism	0.068	14.225	38.238	*Igf1*
Schistosomiasis	0.068	14.225	38.238	*Ctsb*
Diabetic Retinopathy	0.068	14.225	38.238	*Igf1*
Frontotemporal Dementia	0.070	13.860	36.910	*Sqstm1*

Jensen DISEASE	p-value	Odds Ratio	Comb. Score	Genes
Silver-Russell Syndrome	0.071	13.514	35.657	*Igf1*
Lung Disease	0.020	9.085	35.354	*Casp3, Igf1*
Skin Disease	0.073	13.184	34.474	*Igf1*
Toxic Encephalopathy	0.023	8.580	32.474	*Gsk3B, Casp3*
Metabolic Acidosis	0.090	10.599	25.495	*Igf1*
Cognitive Disorder	0.092	10.395	24.812	*Dapk1*
Amenorrhea	0.094	10.199	24.159	*Igf1*
Hyperinsulinism	0.095	10.010	23.533	*Igf1*
Alopecia Areata	0.099	9.653	22.359	*Bad*
Vasculitis	0.102	9.320	21.277	*Lamp2*
Prader-Willi Syndrome	0.102	9.320	21.277	*Igf1*
Muscular Atrophy	0.107	8.861	19.808	*Foxo3*
Hypogonadism	0.114	8.316	18.090	*Igf1*
Gout	0.120	7.834	16.601	*Pygm*
Paraplegia	0.127	7.405	15.300	*Bad*
Hypoglycemia	0.128	7.305	15.001	*Igf1*
Fundus Dystrophy	0.135	6.930	13.891	*Dram2*
Cerebrovascular Disease	0.065	4.805	13.141	*Casp3, Igf1*
Systemic Lupus Erythematosus	0.143	6.513	12.678	*Atg5*
Fatty Liver Disease	0.146	6.359	12.240	*Sirt1*
Parkinson'S Disease	0.168	5.460	9.744	*Ctsb*
Hypertension	0.100	3.741	8.626	*Casp3, Igf1*
Cancer	0.106	3.604	8.084	*Bcl2, Foxo3*
Osteoporosis	0.215	4.158	6.400	*Hk2*
Immune System Cancer	0.225	3.946	5.890	*Bcl2*
Pancreatic Cancer	0.225	3.946	5.890	*Dapk1*
Lymphoid Leukemia	0.246	3.556	4.985	*Bcl2*
Infertility	0.261	3.316	4.449	*Igf1*
Coronary Artery Disease	0.317	2.637	3.028	*Igf1*
Multiple Sclerosis	0.335	2.468	2.700	*Foxo3*
Kidney Cancer	0.194	1.464	2.402	*Gsk3B, Gsk3A, Dapk1, Atg16L1, Pik3R4, Phkb, Pik3C3*
Crohn'S Disease	0.370	2.180	2.167	*Atg16L1*
Type 2 Diabetes Mellitus	0.394	2.009	1.870	*Igf1*
Neurodegenerative Disease	0.421	1.845	1.596	*Sqstm1*
Acquired Metabolic Disease	0.468	1.599	1.214	*Igf1*
Carcinoma	0.429	1.051	0.889	*Epm2A, Gsk3B, Prkaa1, Gsk3A, Dapk1, Atg9A, Pik3R4, Pygm, Phkb, Foxo3, Sirt1, Hk2, Ctss, Map1Lc3B, Atg16L1, Stbd1, Lamp2, Atg4C, Atg4B, Pik3C3, Atg7, Ctsb*
Lung Cancer	0.527	1.351	0.866	*Pik3C3*
Liver Cancer	0.674	0.905	0.357	*Pik3R4*

Table A1.4: pre-type 2 diabetic rat (HFSDr) Jensen DISEASE classification

Jensen DISEASE	p-value	Odds Ratio	Comb. Score	Genes
Meningioma	0.007	144.928	721.594	*Akt1*
Inflammatory Bowel Disease	0.008	124.224	599.428	*Atg16L1*
Granulomatous Amebic Encephalitis	0.009	108.696	510.045	*Gabarapl1*
Fabry Disease	0.009	108.696	510.045	*Gaa*
Alpha-Mannosidosis	0.009	108.696	510.045	*Gaa*
Fucosidosis	0.010	96.618	442.046	*Gaa*
Beta-Mannosidosis	0.010	96.618	442.046	*Bcl2*
Krabbe Disease	0.011	86.957	388.728	*Gaa*
Glycoproteinosis	0.011	86.957	388.728	*Gaa*
Alcohol-Related Neurodevelopmental Disorder	0.011	86.957	388.728	*Wipi1*
Chorea-Acanthocytosis	0.011	86.957	388.728	*Wipi1*
Stiff-Person Syndrome	0.013	79.051	345.898	*Gabarap*
Rem Sleep Behavior Disorder	0.014	72.464	310.807	*Atg4C*
Upper Respiratory Tract Disease	0.015	66.890	281.582	*Pik3Cg*
Inclusion-Cell Disease	0.016	62.112	256.900	*Gaa*
Gangliosidosis	0.017	57.971	235.806	*Gaa*
Vici Syndrome	0.017	57.971	235.806	*Gabarapl1*
Cowden Disease	0.019	51.151	201.718	*Akt1*
Thyroid Cancer	0.021	48.309	187.776	*Akt1*
Galactosemia	0.022	45.767	175.444	*Ugp2*
Centronuclear Myopathy	0.022	45.767	175.444	*Pik3C3*
Glycogen Storage Disease	0.022	45.767	175.444	*Gaa*
Gaucher'S Disease	0.025	39.526	145.790	*Gaa*
Atypical Autism	0.026	37.807	137.792	*Atg4C*
Cone-Rod Dystrophy	0.026	37.807	137.792	*Dram2*
Fatty Liver Disease	0.004	20.460	111.674	*Akt1, Sirt1*
Multiple System Atrophy	0.033	29.985	102.431	*Atg4C*
Retinal Degeneration	0.038	25.575	83.370	*Akt1*
Hyperglycemia	0.007	16.103	80.397	*Akt1, Sirt1*
Bilirubin Metabolic Disorder	0.041	24.155	77.384	*Ugp2*
Diabetic Retinopathy	0.043	22.883	72.099	*Akt1*
Neurofibromatosis	0.043	22.883	72.099	*Akt1*
Skin Disease	0.046	21.209	65.246	*Akt1*
Toxic Encephalopathy	0.009	13.803	64.810	*Becn1, Akt1*
Ptosis	0.049	19.763	59.435	*Gaa*
Hyperinsulinism	0.060	16.103	45.218	*Akt1*
Alopecia Areata	0.062	15.528	43.056	*Bad*
Paraplegia	0.081	11.912	29.981	*Bad*
Lung Cancer	0.010	6.522	29.748	*Akt1, Pik3C3, Pik3Cg*
Huntington'S Disease	0.084	11.442	28.356	*Sirt1*
Brain Disease	0.085	11.293	27.846	*Akt1*
Fundus Dystrophy	0.086	11.148	27.351	*Dram2*
Doid:2627	0.101	9.452	21.701	*Pik3Cg*
Cancer	0.046	5.797	17.834	*Bcl2, Akt1*
Lung Disease	0.128	7.307	15.003	*Akt1*
Osteoporosis	0.139	6.689	13.182	*Hk2*
Immune System Cancer	0.146	6.347	12.200	*Bcl2*
Lymphoid Leukemia	0.161	5.721	10.448	*Bcl2*
Breast Cancer	0.088	4.007	9.733	*Akt1, Pik3Cg*
Arthritis	0.193	4.675	7.679	*Akt1*
Crohn'S Disease	0.250	3.506	4.866	*Atg16L1*
Endometrial Cancer	0.287	2.978	3.716	*Akt1*
Kidney Cancer	0.167	1.683	3.008	*Atg16L1, Akt1, Pik3C3, Ambra1, Pik3Cg*

Jensen DISEASE	p-value	Odds Ratio	Comb. Score	Genes
Skin Cancer	0.410	1.915	1.706	*Akt1*
Carcinoma	0.589	0.999	0.529	*Atg3, Prkaa1, Gaa, Wipi1, Ambra1, Sirt1, Hk2, Pik3Cg, Ugp2, Atg16L1, Atg4C, Akt1, Pik3C3*

Table A1.5: Type 2 diabetic mouse (db/db) Jensen DISEASE classification

Jensen DISEASE	p-value	Odds Ratio	Comb. Score	Genes
Glycogen Storage Disease	5.88E-07	175.439	2517.013	Gaa, Agl, Phkb
Vici Syndrome	7.98E-05	148.148	1397.979	Gabarapl1, Atg5
Inflammatory Bowel Disease	0.006	158.730	804.725	Atg16L1
Movement Disease	0.006	158.730	804.725	Pink1
Fabry Disease	0.007	138.889	685.647	Gaa
Alpha-Mannosidosis	0.007	138.889	685.647	Gaa
Granulomatous Amebic Encephalitis	0.007	138.889	685.647	Gabarapl1
Inclusion Body Myopathy With Paget Disease Of Bone And Frontotemporal Dementia	0.008	123.457	594.976	Sqstm1
Fucosidosis	0.008	123.457	594.976	Gaa
Krabbe Disease	0.009	111.111	523.818	Gaa
Myoglobinuria	0.009	111.111	523.818	Phkg1
Glycoproteinosis	0.009	111.111	523.818	Gaa
Inclusion-Cell Disease	0.013	79.365	347.587	Gaa
Gangliosidosis	0.013	74.074	319.335	Gaa
Centronuclear Myopathy	0.017	58.480	238.382	Pik3C3
Gaucher's Disease	0.020	50.505	198.535	Gaa
Cone-Rod Dystrophy	0.021	48.309	187.776	Dram2
Connective Tissue Disease	0.021	46.296	178.002	Atg5
Neurodegenerative Disease	0.028	7.584	27.108	Pink1, Sqstm1
Frontotemporal Dementia	0.035	28.490	95.888	Sqstm1
Ptosis	0.039	25.253	81.999	Gaa
Lung Cancer	0.049	5.556	16.706	Agl, Pik3C3
Hypoglycemia	0.065	15.015	41.141	Agl
Fundus Dystrophy	0.068	14.245	38.305	Dram2
Systemic Lupus Erythematosus	0.072	13.387	35.194	Atg5
Asthma	0.080	12.077	30.553	Agl
Kidney Cancer	0.196	1.720	2.807	Atg16L1, Agl, Phkb, Pik3C3
Crohn's Disease	0.201	4.480	7.183	Atg16L1
Carcinoma	0.631	0.982	0.452	Prkaa1, Phkg1, Atg16L1, Gaa, Agl, Atg9A, Atg4B, Phkb, Ulk1, Pik3C3

Table A1.6: Differential expression in DM models: STRING Network gene annotation (Fig 3.5a)

	Accession number (NCBI Gene)		
STRING network genes	**Rattus norvegicus**	**Mus musculus**	**Annotation**
Aaas	300259	223921	Aladin; Plays a role in the normal development of the peripheral and central nervous system.
Acan	58968	11595	Aggrecan core protein; This proteoglycan is a major component of extracellular matrix of cartilagenous tissues.
Aga	290923	11593	N(4)-(beta-N-acetylglucosaminyl)-L-asparaginase; Cleaves the GlcNAc-Asn bond which joins oligosaccharides to the peptide of asparagine-linked glycoproteins.
Ambra1	59319	228361	Autophagy/beclin 1 regulator 1.
Atg3	171415	67841	Ubiquitin-like-conjugating enzyme ATG3; E2 conjugating enzyme required for the cytoplasm to vacuole transport (Cvt), autophagy, and mitochondrial homeostasis. Responsible for the E2-like covalent binding of phosphatidylethanolamine to the C-terminal Gly of ATG8-like proteins (GABARAP, GABARAPL1, GABARAPL2 or MAP1LC3A).
Atg4a	678769	666468	Cysteine protease; Cysteine protease required for the cytoplasm to vacuole transport (Cvt) and autophagy.
Atg4b	316640	66615	Cysteine protease; Cysteine protease required for the cytoplasm to vacuole transport (Cvt) and autophagy.
Atg4d	686505	235040	Cysteine protease; Cysteine protease required for the cytoplasm to vacuole transport (Cvt) and autophagy.
Atg5	365601	11793	Autophagy protein 5; Involved in autophagic vesicle formation. Conjugation with ATG12, through a ubiquitin-like conjugating system involving ATG7 as an E1-like activating enzyme and ATG10 as an E2-like conjugating enzyme, is essential for its function. The ATG12-ATG5 conjugate acts as an E3-like enzyme which is required for lipidation of ATG8 family proteins and their association to the vesicle membranes.
Atg7	312647	74244	Ubiquitin-like modifier-activating enzyme ATG7; E1-like activating enzyme involved in the 2 ubiquitin- like systems required for cytoplasm to vacuole transport (Cvt) and autophagy. Activates ATG12 for its conjugation with ATG5 as well as the ATG8 family proteins for their conjugation with phosphatidylethanolamine. Both systems are needed for the ATG8 association to Cvt vesicles and autophagosomes membranes.

	Accession number (NCBI Gene)		
STRING network genes	**Rattus norvegicus**	**Mus musculus**	**Annotation**
Atg9a	363254	245860	Autophagy-related protein 9A; Involved in autophagy and cytoplasm to vacuole transport (Cvt) vesicle formation. Plays a key role in the organization of the preautophagosomal structure/phagophore assembly site (PAS), the nucleating site for formation of the sequestering vesicle.
Atg9b	499973	213948	Autophagy-related protein 9; Involved in autophagy and cytoplasm to vacuole transport (Cvt) vesicle formation. Plays a key role in the organization of the preautophagosomal structure/phagophore assembly site (PAS), the nucleating site for formation of the sequestering vesicle.
Atg10	688555	66795	RCG44366, isoform CRA_a; Autophagy related 10.
Atg12	67526	361321	Ubiquitin-like protein ATG12; Ubiquitin-like protein involved in autophagy vesicles formation. Conjugation with ATG5 through a ubiquitin-like conjugating system involving also ATG7 as an E1-like activating enzyme and ATG10 as an E2-like conjugating enzyme, is essential for its function. The ATG12-ATG5 conjugate acts as an E3-like enzyme which is required for lipidation of ATG8 family proteins and their association to the vesicle membranes.
Atg13	362164	51897	Autophagy-related protein 13; Autophagy related 13; Belongs to the ATG13 family. Metazoan subfamily.
Atg14	305831	100504663	Beclin 1-associated autophagy-related key regulator; Required for both basal and inducible autophagy. Determines the localization of the autophagy-specific PI3-kinase complex. Plays a role in autophagosome formation and MAP1LC3/LC3 conjugation to phosphatidylethanolamine.
Atg16l1	363278	77040	Autophagy related 16-like 1 (S. cerevisiae)
Atg16l2	308865	73683	Autophagy related 16-like 2 (S. cerevisiae)
Atg101	300240	68118	Autophagy-related protein 101; Autophagy factor required for autophagosome formation. Stabilizes ATG13, protecting it from proteasomal degradation.
Becn1	114558	56208	Beclin-1; Plays a central role in autophagy. Acts as core subunit of the PI3K complex that mediates formation of phosphatidylinositol 3-phosphate; different complex forms are believed to play a role in multiple membrane trafficking pathways: PI3KC3-C1 is involved in initiation of autophagosomes and PI3KC3- C2 in maturation of autophagosomes and endocytosis.

	Accession number (NCBI Gene)		
STRING network genes	**Rattus norvegicus**	**Mus musculus**	**Annotation**
Dram2	362011	67171	DNA damage-regulated autophagy modulator protein 2; Plays a role in the initiation of autophagy. In the retina, might be involved in the process of photoreceptor cells renewal and recycling to preserve visual function. Induces apoptotic cell death when coexpressed with DRAM1
Gaa	367562	14387	Lysosomal alpha-glucosidase; Essential for the degradation of glycogen in lysosomes. Has highest activity on alpha-1,4-linked glycosidic linkages, but can also hydrolyze alpha-1,6-linked glucans
Gabarap	58974	56486	Gamma-aminobutyric acid receptor-associated protein; Involved in apoptosis (By similarity). May play a role in intracellular transport of GABA(A) receptors and its interaction with the cytoskeleton. Involved in autophagy (By similarity).
Gabarapl1	689161	57436	Gamma-aminobutyric acid receptor-associated protein-like 1; Ubiquitin-like modifier that increases cell-surface expression of kappa-type opioid receptor through facilitating anterograde intracellular trafficking of the receptor. Involved in formation of autophagosomal vacuoles. Whereas LC3s are involved in elongation of the phagophore membrane, the GABARAP/GATE-16 subfamily is essential for a later stage in autophagosome maturation (By similarity).
Gabarapl2	64670	39739	Gamma-aminobutyric acid receptor-associated protein-like 2; Ubiquitin-like modifier that increases cell-surface expression of kappa-type opioid receptor through facilitating anterograde intracellular trafficking of the receptor. Involved in formation of autophagosomal vacuoles. Whereas LC3s are involved in elongation of the phagophore membrane, the GABARAP/GATE-16 subfamily is essential for a later stage in autophagosome maturation (By similarity).
Ggct	362368	79017	Gamma-glutamylcyclotransferase; Catalyzes the formation of 5-oxoproline from gamma- glutamyl dipeptides and may play a significant role in glutathione homeostasis.
Glyat	293779	107146	Glycine N-acyltransferase; Mitochondrial acyltransferase which transfers an acyl group to the N-terminus of glycine and glutamine, although much less efficiently.
Gucy2c	25711	14917	Heat-stable enterotoxin receptor; Receptor for the E.coli heat-stable enterotoxin (E.coli enterotoxin markedly stimulates the accumulation of cGMP in mammalian cells expressing GC-C).
Irgm1	15944	15944	Immunity-related GTPase family M protein 1; Putative GTPase which is required for IFNG-mediated clearance of acute protozoan and bacterial infections.

	Accession number (NCBI Gene)		
STRING network genes	**Rattus norvegicus**	**Mus musculus**	**Annotation**
Map1lc3a	66734	362245	Microtubule-associated proteins 1A/1B light chain 3A; Ubiquitin-like modifier involved in formation of autophagosomal vacuoles (autophagosomes).
Map1lc3b	64862	67443	Microtubule-associated proteins 1A/1B light chain 3B; Ubiquitin-like modifier involved in formation of autophagosomal vacuoles (autophagosomes). Plays a role in mitophagy which contributes to regulate mitochondrial quantity and quality by eliminating the mitochondria to a basal level to fulfill cellular energy requirements and preventing excess ROS production.
Nbr1	303554	17966	Next to BRCA1 gene 1 protein; Acts probably as a receptor for selective autophagosomal degradation of ubiquitinated targets.
Nod2	291912	257632	Nucleotide-binding oligomerization domain containing 2.
Pik3c3	65052	225326	Phosphatidylinositol 3-kinase catalytic subunit type 3; Catalytic subunit of the PI3K complex that mediates formation of phosphatidylinositol 3-phosphate; different complex forms are believed to play a role in multiple membrane trafficking pathways: PI3KC3-C1 is involved in initiation of autophagosomes and PI3KC3-C2 in maturation of autophagosomes and endocytosis.
Pik3r4	363131	75669	Phosphoinositide 3-kinase regulatory subunit 4; Regulatory subunit of the PI3K complex that mediates formation of phosphatidylinositol 3-phosphate; different complex forms are believed to play a role in multiple membrane trafficking pathways: PI3KC3-C1 is involved in initiation of autophagosomes and PI3KC3-C2 in maturation of autophagosomes and endocytosis.
Pikfyve	316457	18711	Phosphoinositide kinase, FYVE-type zinc finger-containing; Phosphoinositide kinase, FYVE finger containing.
Prkaa1	65248	105787	5'-AMP-activated protein kinase catalytic subunit alpha-1; Catalytic subunit of AMP-activated protein kinase (AMPK), an energy sensor protein kinase that plays a key role in regulating cellular energy metabolism. In response to reduction of intracellular ATP levels, AMPK activates energy-producing pathways and inhibits energy-consuming processes: inhibits protein, carbohydrate and lipid biosynthesis, as well as cell growth and proliferation. AMPK acts via direct phosphorylation of metabolic enzymes, and by longer-term effects via phosphorylation of transcription regulators.

	Accession number (NCBI Gene)		
STRING network genes	**Rattus norvegicus**	**Mus musculus**	**Annotation**
Prkab1	83803	19079	5'-AMP-activated protein kinase subunit beta-1; Non-catalytic subunit of AMP-activated protein kinase (AMPK), an energy sensor protein kinase that plays a key role in regulating cellular energy metabolism. In response to reduction of intracellular ATP levels, AMPK activates energy-producing pathways and inhibits energy-consuming processes: inhibits protein, carbohydrate and lipid biosynthesis, as well as cell growth and proliferation. AMPK acts via direct phosphorylation of metabolic enzymes, and by longer-term effects via phosphorylation of transcription regulators. Also acts as a reg [...]
Prkab2	64562	108097	5'-AMP-activated protein kinase subunit beta-2; Non-catalytic subunit of AMP-activated protein kinase (AMPK).
Prkag1	25520	19082	5'-AMP-activated protein kinase subunit gamma-1; AMP/ATP-binding subunit of AMP-activated protein kinase (AMPK).
Prkag2	373545	108099	Protein kinase, AMP-activated, gamma 2 non-catalytic subunit.
Prkag3	301518	241113	Protein kinase, AMP-activated, gamma 3 non-catalytic subunit.
Rab33b	365793	19338	Ras-related protein Rab-33B; Protein transport. Acts, in coordination with RAB6A, to regulate intra-Golgi retrograde trafficking (By similarity). It is involved in autophagy, acting as a modulator of autophagosome formation; Belongs to the small GTPase superfamily. Rab family.
Rab7	29448	19349	Ras-related protein Rab-7a; Key regulator in endo-lysosomal trafficking. Governs early-to-late endosomal maturation, microtubule minus-end as well as plus-end directed endosomal migration and positioning, and endosome-lysosome transport through different protein-protein interaction cascades (By similarity).
Rb1cc1	12927	12421	RB1-inducible coiled-coil 1.
Rubcn	303885	100502698	RUN and cysteine-rich domain-containing beclin 1-interacting protein; Similar to mKIAA0226 protein.
Sqstm1	113894	18412	Sequestosome-1; Autophagy receptor that interacts directly with both the cargo to become degraded and an autophagy modifier of the MAP1 LC3 family (By similarity). Required both for the formation and autophagic degradation of polyubiquitin-containing bodies, called ALIS (aggresome-like induced structures) and links ALIS to the autophagic machinery (By similarity). Involved in midbody ring degradation (By similarity).

	Accession number (NCBI Gene)		
STRING network genes	**Rattus norvegicus**	**Mus musculus**	**Annotation**
Stbd1	305234	52331	Starch-binding domain-containing protein 1; Acts as a cargo receptor for glycogen. Delivers its cargo to an autophagic pathway called glycophagy, resulting in the transport of glycogen to lysosomes.
Tgm2	56083	21817	Protein-glutamine gamma-glutamyltransferase 2; Catalyzes the cross-linking of proteins and the conjugation of polyamines to proteins; Belongs to the transglutaminase superfamily.
Ugt8a	50555	22239	2-hydroxyacylsphingosine 1-beta-galactosyltransferase; Catalyzes the transfer of galactose to ceramide, a key enzymatic step in the biosynthesis of galactocerebrosides, which are abundant sphingolipids of the myelin membrane of the central nervous system and peripheral nervous system; Belongs to the UDP-glycosyltransferase family.
Ulk1	360827	22241	Unc-51 like autophagy activating kinase 1.
Ulk2	303206	29869	Unc-51 like autophagy activating kinase 2.
Urm1			Ubiquitin-related modifier 1; Acts as a sulfur carrier required for 2-thiolation of mcm(5)S(2)U at tRNA wobble positions of cytosolic tRNA(Lys), tRNA(Glu) and tRNA(Gln).
Uvrag	308846	78610	Similar to UV radiation resistance associated, isoform CRA_d; UV radiation resistance associated gene.
Wdfy3	305164	72145	WD repeat and FYVE domain containing 3.
Wdfy4	498582	545030	WDFY family member 4.
Wipi1	303630	52639	WD repeat domain, phosphoinositide interacting 1.
Wipi2	288498	74781	WD repeat domain phosphoinositide-interacting protein 2; Early component of the autophagy machinery being involved in formation of preautophagosomal structures and their maturation into mature phagosomes in response to phosphatidylinositol 3-phosphate (PtdIns3P). Recruits the ATG12- ATG5-ATG16L1 complex to omegasomes, resulting in ATG8 family proteins lipidation and starvation-induced autophagy.

Table A1.7: Primary interactions of the 8 DE genes identified by STRING analysis (Fig 3.5a)

		Probability score		
Input gene	**Interacting gene**	**Experimental evidence**	**Text-mining**	**Combined score**
Prkaa1	*Prkab1*	0.879	0.804	0.975
	Prkab2	0.741	0.781	0.941
	Prkag2	0.741	0.743	0.93
	Prkag1	0.878	0.814	0.976
	Prkag3	0.703	0.721	0.913
Pik3c3	*Ambra1*	0.159	0.836	0.856
	Atg10	0	0.896	0.896
	Atg101	0	0.893	0.893
	Atg13	0	0.933	0.933
	Atg14	0.628	0.961	0.984
	Atg16l1	0	0.841	0.841
	Atg3	0	0.915	0.915
	Atg4b	0	0.824	0.824
	Atg5	0.113	0.937	0.942
	Atg7	0	0.935	0.935
	Gabarap	0.05	0.819	0.82
	Gabarapl1	0.05	0.757	0.76
	Map1lc3a	0.05	0.809	0.81
	Map1lc3b	0.05	0.884	0.885
	Nbr1	0.058	0.81	0.813
	Pik3r4	0.891	0.967	0.996
	Pikfyve	0.158	0.817	0.839
	Rab7	0.057	0.877	0.879
	Rb1cc1	0	0.899	0.899
	Rubcn	0.277	0.9	0.924
	Sqstm1	0.058	0.766	0.77
	Ulk1	0.198	0.823	0.852
	Ulk2	0.198	0.846	0.871
	Uvrag	0.539	0.936	0.969
	Wipi1	0	0.813	0.813
	Wipi2	0	0.824	0.824
	Atg9a	0.058	0.947	0.947
	Becn1	0.885	0.979	0.997
Atg12	*Atg7*	0.869	0.969	0.995
	Atg3	0.876	0.95	0.993
	Atg10	0.61	0.96	0.983
	Atg16l1	0.233	0.935	0.948
	Map1lc3b	0.198	0.909	0.924
	Rb1cc1	0	0.908	0.908
	Map1lc3a	0.198	0.889	0.907
	Atg4b	0.153	0.885	0.898
	Ulk2	0.354	0.825	0.882
	Gabarap	0.198	0.856	0.88
	Gabarapl1	0.198	0.84	0.866

		Probability score		
Input gene	**Interacting gene**	**Experimental evidence**	**Text-mining**	**Combined score**
Atg12	*Gabarapl2*	0.198	0.832	0.859
	Ulk1	0.354	0.785	0.855
	Ambra1	0	0.714	0.714
	Atg101	0	0.892	0.892
	Atg13	0	0.916	0.916
	Atg14	0	0.912	0.912
	Atg16l2	0.197	0.758	0.797
	Atg4a	0.153	0.811	0.833
	Atg4d	0.153	0.772	0.798
	Atg5	0.884	0.985	0.998
	Atg9a	0.611	0.936	0.974
	Atg9b	0.611	0.773	0.908
	Becn1	0.409	0.95	0.969
	Nbr1	0	0.802	0.802
	Pik3c3	0.173	0.935	0.944
	Pik3r4	0	0.91	0.91
	Rab7	0	0.712	0.712
	Sqstm1	0	0.817	0.817
	Urm1	0	0.825	0.825
	Uvrag	0	0.885	0.885
	Wipi1	0.458	0.819	0.898
	Wipi2	0.458	0.842	0.911
Atg16l1	*Atg10*	0	0.915	0.915
	Atg3	0.815	0.918	0.984
	Atg4b	0	0.82	0.82
	Gabarap	0.045	0.832	0.833
	Rb1cc1	0.688	0.911	0.971
	Ulk2	0.273	0.786	0.838
	Atg101	0.644	0.821	0.933
	Atg13	0.685	0.868	0.956
	Atg14	0	0.889	0.889
	Atg4a	0	0.721	0.721
	Atg5	0.9	0.964	0.996
	Atg7	0	0.918	0.918
	Atg9a	0	0.866	0.866
	Becn1	0.051	0.915	0.916
	Gabarapl1	0.045	0.728	0.73
	Gabarapl2	0.045	0.716	0.718
	Irgm1	0.156	0.863	0.88
	Map1lc3a	0.538	0.814	0.91
	Map1lc3b	0	0.847	0.847
	Nbr1	0.118	0.802	0.818
	Nod2	0.197	0.927	0.939
	Pik3r4	0	0.818	0.818
	Rab33b	0.539	0.732	0.871

		Probability score		
Input gene	**Interacting gene**	**Experimental evidence**	**Text-mining**	**Combined score**
Atg16l1	*Sqstm1*	0.613	0.744	0.896
	Ulk1	0.685	0.738	0.914
	Uvrag	0	0.777	0.777
	Wipi1	0.118	0.763	0.782
	Wipi2	0.143	0.873	0.887
Atg16l2	*Atg10*	0	0.757	0.757
	Atg3	0.69	0.767	0.924
	Atg5	0.728	0.724	0.921
	Atg7	0	0.792	0.792
	Atg9b	0	0.731	0.731
	Becn1	0.049	0.718	0.72
Gabarapl1	*Atg3*	0.523	0.836	0.918
	Atg4b	0.543	0.797	0.903
	Ulk1	0.366	0.68	0.789
	Ulk2	0.366	0.707	0.806
	Atg13	0.144	0.726	0.755
	Atg4a	0.543	0.546	0.784
	Atg4d	0.354	0.608	0.736
	Atg5	0.204	0.796	0.83
	Atg7	0.687	0.838	0.947
	Atg9a	0.199	0.704	0.753
	Becn1	0.218	0.796	0.833
	Nbr1	0.452	0.609	0.776
	Sqstm1	0.408	0.776	0.862
	Stbd1	0.197	0.779	0.815
	Wdfy3	0.79	0.363	0.86
	Wdfy4	0.774	0.218	0.815
	Wipi1	0.245	0.703	0.766
	Wipi2	0.245	0.647	0.722
Gaa	*Aaas*	0	0.82	0.82
	Acan	0	0.831	0.831
	Aga	0	0.934	0.934
	Glyat	0	0.872	0.872
	Gucy2c	0	0.867	0.867
	Tgm2	0	0.842	0.842
	Ugt8a	0	0.836	0.836
	Ggct	0	0.897	0.897
Dram2		0	0	0

Table A1.8: Secondary interactions between 'discovered' genes (Fig 3.5a)

		Probability score		
Node 1	**Node 2**	**Experimental evidence**	**Text-mining**	**Combined score**
Aaas	Aga	0	0.828	0.828
	Glyat	0	0.768	0.768
	Gucy2c	0	0.739	0.739
Acan	Gucy2c	0	0.779	0.779
Aga	Acan	0	0.831	0.831
	Gucy2c	0	0.867	0.867
Ambra1	Atg101	0	0.703	0.703
	Atg14	0	0.842	0.842
	Atg3	0.256	0.699	0.766
	Atg5	0	0.73	0.73
	Atg7	0	0.725	0.725
	Rb1cc1	0	0.732	0.732
	Ulk2	0.135	0.68	0.711
	Uvrag	0	0.851	0.851
Atg10	Gabarap	0.057	0.767	0.771
	Ulk2	0	0.72	0.72
Atg101	Atg10	0	0.88	0.88
	Atg14	0	0.891	0.891
	Atg3	0	0.882	0.882
	Atg5	0.643	0.882	0.956
	Atg7	0	0.883	0.883
	Gabarap	0.163	0.738	0.771
	Map1lc3b	0.095	0.737	0.752
	Rb1cc1	0.696	0.937	0.98
	Ulk1	0.722	0.804	0.943
	Ulk2	0.722	0.859	0.959
	Uvrag	0	0.777	0.777
	Wipi2	0	0.743	0.743
Atg13	Ambra1	0.163	0.737	0.77
	Atg10	0	0.885	0.885
	Atg101	0.849	0.961	0.993
	Atg14	0	0.916	0.916
	Atg3	0	0.911	0.911
	Atg4b	0	0.711	0.711
	Atg5	0.643	0.937	0.976
	Atg7	0	0.914	0.914
	Gabarap	0.163	0.824	0.847
	Map1lc3a	0.163	0.721	0.757
	Map1lc3b	0.095	0.807	0.818
	Pik3r4	0	0.913	0.913
	Rb1cc1	0.799	0.959	0.991
	Ulk1	0.703	0.896	0.968
	Ulk2	0.44	0.916	0.951
	Uvrag	0	0.818	0.818
	Wipi2	0	0.818	0.818
Atg14	Atg10	0	0.847	0.847
	Atg3	0	0.889	0.889
	Atg4b	0	0.752	0.752
	Atg7	0	0.888	0.888
	Gabarap	0	0.797	0.797
	Map1lc3a	0	0.736	0.736

		Probability score		
Node 1	**Node 2**	**Experimental evidence**	**Text-mining**	**Combined score**
Atg14	Map1lc3b	0	0.804	0.804
	Rb1cc1	0	0.903	0.903
	Ulk1	0	0.803	0.803
	Ulk2	0	0.816	0.816
Atg3	Atg10	0.16	0.937	0.945
	Gabarap	0.523	0.865	0.933
	Ulk2	0.358	0.823	0.881
Atg4a	Atg10	0.183	0.709	0.752
	Atg3	0.602	0.811	0.921
	Atg5	0.119	0.819	0.834
	Atg7	0.453	0.824	0.899
	Gabarap	0.543	0.723	0.868
	Gabarapl2	0.543	0.514	0.768
	Map1lc3a	0.392	0.688	0.802
	Map1lc3b	0.354	0.691	0.792
	Ulk2	0.429	0.652	0.792
	Wipi1	0.394	0.685	0.801
Atg4b	Atg10	0.203	0.763	0.803
	Atg3	0.602	0.884	0.951
	Gabarap	0.543	0.874	0.94
	Ulk2	0.429	0.687	0.813
Atg4d	Atg10	0.154	0.682	0.72
	Atg3	0.446	0.812	0.891
	Atg5	0.116	0.792	0.808
	Atg7	0.387	0.79	0.866
	Gabarap	0.354	0.622	0.745
	Map1lc3b	0.354	0.648	0.763
Atg5	Atg10	0.53	0.936	0.968
	Atg14	0	0.915	0.915
	Atg3	0.802	0.941	0.987
	Atg4b	0.119	0.885	0.895
	Atg7	0.376	0.97	0.98
	Gabarap	0.204	0.857	0.881
	Gabarapl2	0.204	0.816	0.847
	Map1lc3a	0.555	0.91	0.958
	Map1lc3b	0.18	0.924	0.935
	Rb1cc1	0.643	0.929	0.973
	Ulk1	0.643	0.839	0.94
	Ulk2	0.406	0.847	0.905
Atg7	Atg10	0.707	0.96	0.987
	Atg3	0.901	0.951	0.995
	Atg4b	0.453	0.887	0.935
	Gabarap	0.687	0.859	0.953
	Map1lc3a	0.81	0.897	0.979
	Rb1cc1	0	0.912	0.912
	Ulk1	0.339	0.837	0.888
	Ulk2	0.339	0.844	0.892
Atg9a	Atg10	0	0.863	0.863
	Atg101	0	0.853	0.853
	Atg13	0	0.915	0.915
	Atg14	0	0.871	0.871
	Atg3	0	0.917	0.917
	Atg4a	0	0.807	0.807
	Atg4b	0	0.838	0.838

		Probability score		
Node 1	**Node 2**	**Experimental evidence**	**Text-mining**	**Combined score**
Atg9a	Atg4d	0	0.704	0.704
	Atg5	0.376	0.936	0.958
	Atg7	0.68	0.934	0.978
	Becn1	0.543	0.954	0.978
	Gabarap	0.199	0.819	0.849
	Gabarapl2	0.199	0.714	0.761
	Map1lc3a	0.176	0.802	0.83
	Map1lc3b	0.176	0.827	0.851
	Nbr1	0.135	0.788	0.809
	Pik3r4	0	0.891	0.891
	Rab7	0.159	0.795	0.82
	Rb1cc1	0	0.888	0.888
	Sqstm1	0.198	0.741	0.783
	Ulk1	0.313	0.757	0.826
	Ulk2	0.313	0.824	0.874
	Uvrag	0	0.795	0.795
	Wipi1	0.364	0.847	0.898
	Wipi2	0.364	0.838	0.893
Atg9b	Atg10	0	0.709	0.709
	Atg3	0	0.736	0.736
	Atg5	0.354	0.773	0.847
	Atg7	0.611	0.736	0.893
Becn1	Ambra1	0.197	0.947	0.955
	Atg10	0	0.909	0.909
	Atg101	0	0.884	0.884
	Atg13	0	0.934	0.934
	Atg14	0.867	0.967	0.995
	Atg3	0.509	0.939	0.968
	Atg4a	0.355	0.793	0.861
	Atg4b	0.355	0.864	0.908
	Atg4d	0.316	0.771	0.837
	Atg5	0.047	0.962	0.962
	Atg7	0.456	0.96	0.977
	Atg9b	0.424	0.761	0.856
	Gabarap	0.218	0.846	0.874
	Gabarapl2	0.218	0.798	0.835
	Map1lc3a	0.218	0.929	0.942
	Map1lc3b	0.218	0.926	0.939
	Nbr1	0	0.869	0.869
	Pik3r4	0.872	0.961	0.994
	Rab7	0.077	0.811	0.818
	Rb1cc1	0	0.915	0.915
	Rubcn	0.467	0.917	0.954
	Sqstm1	0	0.891	0.891
	Ulk1	0.175	0.85	0.871
	Ulk2	0.153	0.85	0.867
	Uvrag	0.605	0.97	0.987
	Wipi1	0.372	0.81	0.876
	Wipi2	0.372	0.811	0.876
Gabarap	Ulk2	0.366	0.726	0.819
Gabarapl2	Atg10	0.057	0.698	0.703
	Atg3	0.523	0.852	0.926
	Atg4b	0.543	0.714	0.864
	Atg7	0.687	0.83	0.944

		Probability score		
Node 1	**Node 2**	**Experimental evidence**	**Text-mining**	**Combined score**
	Ulk1	0.366	0.69	0.795
	Ulk2	0.366	0.615	0.745
Ggct	Aaas	0	0.733	0.733
	Acan	0	0.81	0.81
	Aga	0	0.889	0.889
	Glyat	0	0.87	0.87
	Gucy2c	0	0.855	0.855
	Tgm2	0	0.837	0.837
	Ugt8a	0	0.837	0.837
Glyat	Acan	0	0.778	0.778
	Aga	0	0.891	0.891
	Gucy2c	0	0.889	0.889
Irgm1	Atg10	0	0.75	0.75
	Atg5	0	0.825	0.826
Map1lc3a	Atg3	0.762	0.876	0.969
	Atg4b	0.696	0.75	0.921
	Rb1cc1	0.058	0.698	0.704
	Ulk2	0.306	0.747	0.817
Map1lc3b	Atg10	0.554	0.832	0.922
	Atg3	0.523	0.889	0.945
	Atg4b	0.354	0.814	0.875
	Atg7	0.619	0.909	0.964
	Rb1cc1	0.058	0.752	0.757
	Ulk1	0.306	0.624	0.728
	Ulk2	0.306	0.696	0.78
Nbr1	Atg10	0	0.809	0.809
	Atg101	0.156	0.8	0.824
	Atg3	0	0.88	0.88
	Atg5	0.122	0.886	0.895
	Atg7	0.109	0.888	0.896
	Gabarap	0.452	0.778	0.873
	Gabarapl2	0.452	0.711	0.835
	Map1lc3a	0.452	0.632	0.789
	Map1lc3b	0.452	0.778	0.873
	Pik3r4	0	0.702	0.702
	Wdfy3	0.171	0.697	0.738
Nod2	Irgm1	0.156	0.762	0.79
Pik3r4	Ambra1	0	0.793	0.793
	Atg10	0	0.886	0.886
	Atg101	0	0.892	0.892
	Atg14	0.725	0.919	0.977
	Atg3	0	0.889	0.889
	Atg4b	0	0.733	0.733
	Atg5	0	0.897	0.897
	Atg7	0	0.89	0.89
	Gabarap	0.045	0.749	0.75
	Map1lc3b	0.045	0.788	0.789
	Rb1cc1	0	0.84	0.84
	Ulk1	0	0.747	0.747
	Ulk2	0	0.782	0.782
	Uvrag	0.539	0.917	0.96
	Wipi2	0	0.793	0.793
Pikfyve	Pik3r4	0	0.7	0.7

		Probability score		
Node 1	**Node 2**	**Experimental evidence**	**Text-mining**	**Combined score**
Prkab1	Prkag2	0.709	0.801	0.939
Prkab2	Prkab1	0.702	0.779	0.709
	Prkag2	0.723	0.798	0.941
Prkag1	Prkab1	0.889	0.842	0.981
	Prkab2	0.751	0.818	0.952
Prkag3	Prkab1	0.704	0.793	0.936
	Prkab2	0.703	0.796	0.936
Rab7	Atg13	0	0.718	0.718
	Atg3	0	0.792	0.792
	Atg5	0.045	0.848	0.849
	Atg7	0	0.835	0.835
	Gabarap	0.118	0.711	0.734
	Map1lc3b	0.091	0.739	0.753
	Pik3r4	0.056	0.806	0.809
	Pikfyve	0	0.759	0.759
	Uvrag	0	0.708	0.708
Rb1cc1	Atg10	0	0.862	0.862
	Atg3	0	0.885	0.885
	Gabarap	0.081	0.79	0.799
	Ulk2	0.44	0.889	0.935
Rubcn	Ambra1	0	0.837	0.837
	Atg14	0	0.843	0.843
	Atg5	0	0.7	0.7
	Pik3r4	0.184	0.758	0.794
	Uvrag	0.313	0.913	0.937
Sqstm1	Atg101	0.199	0.641	0.7
	Atg13	0.199	0.733	0.777
	Atg14	0	0.723	0.723
	Atg3	0	0.802	0.802
	Atg4b	0.161	0.678	0.718
	Atg5	0.197	0.897	0.914
	Atg7	0.161	0.888	0.902
	Gabarap	0.408	0.845	0.904
	Gabarapl2	0.543	0.792	0.9
	Map1lc3a	0.626	0.845	0.939
	Map1lc3b	0.838	0.907	0.984
	Nbr1	0.575	0.9	0.956
	Rb1cc1	0	0.79	0.79
	Ulk1	0.531	0.685	0.846
	Ulk2	0.175	0.688	0.732
	Wdfy3	0.197	0.787	0.822
Tgm2	Aaas	0	0.711	0.711
	Acan	0	0.737	0.737
	Aga	0	0.846	0.846
	Glyat	0	0.855	0.855
Tgm2	Gucy2c	0	0.837	0.837
	Ugt8a	0	0.778	0.778
Ugt8a	Aaas	0	0.7	0.7
	Acan	0	0.711	0.711
	Aga	0	0.84	0.84
	Glyat	0	0.832	0.832
	Gucy2c	0	0.833	0.833
Ulk1	Atg3	0.358	0.779	0.852

		Probability score		
Node 1	**Node 2**	**Experimental evidence**	**Text-mining**	**Combined score**
	Atg4b	0.429	0.562	0.739
	Gabarap	0.366	0.604	0.738
	Map1lc3a	0.306	0.707	0.788
	Rb1cc1	0.703	0.858	0.956
Uvrag	Atg10	0	0.768	0.768
	Atg14	0	0.919	0.919
	Atg3	0	0.849	0.849
	Atg4b	0	0.719	0.719
	Atg5	0	0.89	0.89
	Atg7	0	0.865	0.865
	Map1lc3b	0	0.724	0.724
	Rb1cc1	0	0.821	0.821
	Ulk2	0	0.73	0.73
Wdfy3	Atg5	0.552	0.799	0.906
	Gabarap	0.971	0.54	0.986
	Gabarapl2	0.774	0.335	0.843
	Map1lc3a	0.887	0.338	0.922
	Map1lc3b	0.774	0.515	0.885
Wdfy4	Gabarap	0.774	0.218	0.815
	Gabarapl2	0.774	0.139	0.797
	Map1lc3a	0.774	0.249	0.823
	Map1lc3b	0.774	0.139	0.797
Wipi1	Atg10	0	0.711	0.711
	Atg101	0	0.742	0.742
	Atg13	0	0.809	0.809
	Atg14	0	0.786	0.786
	Atg3	0.453	0.774	0.871
	Atg4b	0.394	0.669	0.79
	Atg5	0.321	0.82	0.873
	Atg7	0.453	0.794	0.882
	Atg9b	0.317	0.699	0.785
	Gabarap	0.245	0.737	0.793
	Gabarapl2	0.245	0.66	0.732
	Map1lc3a	0.245	0.706	0.768
	Map1lc3b	0.245	0.711	0.772
	Pik3r4	0	0.763	0.763
	Rb1cc1	0	0.779	0.779
	Ulk1	0.426	0.701	0.821
	Ulk2	0.426	0.645	0.787
Wipi2	Atg10	0	0.722	0.722
	Atg14	0	0.789	0.789
	Atg3	0.453	0.791	0.881
	Atg4b	0.394	0.699	0.809
	Atg5	0.321	0.84	0.886
	Atg7	0.453	0.79	0.88
	Gabarap	0.245	0.776	0.823
	Gabarapl2	0.245	0.689	0.755
	Map1lc3a	0.245	0.706	0.768
	Map1lc3b	0.245	0.709	0.77
	Rb1cc1	0.046	0.811	0.812
	Ulk1	0.426	0.635	0.781
	Ulk2	0.426	0.668	0.801

Table A1.9: *Stbd1*-STRING Network gene annotation (Fig 3.5b)

	Accession number (NCBI Gene)		
STRING network genes	**Rattus norvegicus**	**Mus musculus**	**Annotation**
Ank2	362036	109676	Ankyrin 2, neuronal.
Atg3	171415	67841	Ubiquitin-like-conjugating enzyme ATG3; E2 conjugating enzyme required for the cytoplasm to vacuole transport (Cvt), autophagy, and mitochondrial homeostasis. Responsible for the E2-like covalent binding of phosphatidylethanolamine to the C-terminal Gly of ATG8-like proteins (GABARAP, GABARAPL1, GABARAPL2 or MAP1LC3A).
Atg4b	316640	66615	Cysteine protease; Cysteine protease required for the cytoplasm to vacuole transport (Cvt) and autophagy.
Atg5	365601	11793	Autophagy protein 5; Involved in autophagic vesicle formation. Conjugation with ATG12, through a ubiquitin-like conjugating system involving ATG7 as an E1-like activating enzyme and ATG10 as an E2-like conjugating enzyme, is essential for its function. The ATG12-ATG5 conjugate acts as an E3-like enzyme which is required for lipidation of ATG8 family proteins and their association to the vesicle membranes.
Atg7	312647	74244	Ubiquitin-like modifier-activating enzyme ATG7; E1-like activating enzyme involved in the 2 ubiquitin- like systems required for cytoplasm to vacuole transport (Cvt) and autophagy. Activates ATG12 for its conjugation with ATG5 as well as the ATG8 family proteins for their conjugation with phosphatidylethanolamine. Both systems are needed for the ATG8 association to Cvt vesicles and autophagosomes membranes.
Atg12	67526	361321	Ubiquitin-like protein ATG12; Ubiquitin-like protein involved in autophagy vesicles formation. Conjugation with ATG5 through a ubiquitin-like conjugating system involving also ATG7 as an E1-like activating enzyme and ATG10 as an E2-like conjugating enzyme, is essential for its function. The ATG12-ATG5 conjugate acts as an E3-like enzyme which is required for lipidation of ATG8 family proteins and their association to the vesicle membranes.
Becn1	114558	56208	Beclin-1; Plays a central role in autophagy. Acts as core subunit of the PI3K complex that mediates formation of phosphatidylinositol 3-phosphate; different complex forms are believed to play a role in multiple membrane trafficking pathways: PI3KC3-C1 is involved in initiation of autophagosomes and PI3KC3- C2 in maturation of autophagosomes and endocytosis.

Ccdc62			Coiled-coil domain containing 62.
Epm2a	114005	13853	Laforin; Plays an important role in preventing glycogen hyperphosphorylation and the formation of insoluble aggregates, via its activity as glycogen phosphatase, and by promoting the ubiquitination of proteins involved in glycogen metabolism via its interaction with the E3 ubiquitin ligase NHLRC1/malin.
Gabarapl1	689161	57436	Gamma-aminobutyric acid receptor-associated protein-like 1; Ubiquitin-like modifier that increases cell-surface expression of kappa-type opioid receptor through facilitating anterograde intracellular trafficking of the receptor. Involved in formation of autophagosomal vacuoles. Whereas LC3s are involved in elongation of the phagophore membrane, the GABARAP/GATE-16 subfamily is essential for a later stage in autophagosome maturation (By similarity).
Gbe1	288333	74185	Glucan (1,4-alpha-), branching enzyme 1.
Gyg1	81675	27357	Glycogenin-1; Self-glucosylates, via an inter-subunit mechanism, to form an oligosaccharide primer that serves as substrate for glycogen synthase.
Gys1	690987	14936	Glycogen [starch] synthase, muscle; Transfers the glycosyl residue from UDP-Glc to the non- reducing end of alpha-1,4-glucan; Belongs to the glycosyltransferase 3 family.
Gys2	25623	232493	Glycogen [starch] synthase, liver.
Mccc1	294972	72039	Methylcrotonoyl-CoA carboxylase subunit alpha, mitochondrial; Biotin-attachment subunit of the 3-methylcrotonyl-CoA carboxylase, an enzyme that catalyzes the conversion of 3- methylcrotonyl-CoA to 3-methylglutaconyl-CoA, a critical step for leucine and isovaleric acid catabolism.
Nbr1	303554	17966	Next to BRCA1 gene 1 protein; Acts probably as a receptor for selective autophagosomal degradation of ubiquitinated targets.
Nhlrc1	364682	105193	E3 ubiquitin-protein ligase NHLRC1; E3 ubiquitin-protein ligase. Together with the phosphatase EPM2A/laforin, appears to be involved in the clearance of toxic polyglucosan and protein aggregates via multiple pathways.
Nudt6	207120	229228	Nucleoside diphosphate-linked moiety X motif 6; May contribute to the regulation of cell proliferation; Belongs to the Nudix hydrolase family.
Ppp1r3b	192280	244416	Protein phosphatase 1 regulatory subunit 3B; Acts as a glycogen-targeting subunit for phosphatase PP1. Facilitates interaction of the PP1 with enzymes of the glycogen metabolism and regulates its activity.

Ppp1r3d	689995	228966	Protein phosphatase 1, regulatory subunit 3D.
Ppp1r5	60340	53412	Protein phosphatase 1 regulatory subunit 3C; Acts as a glycogen-targeting subunit for PP1 and regulates its activity.
Pygb	25739	10078	Glycogen phosphorylase, brain form
Pygl	64035	110095	Glycogen phosphorylase, liver form
Pygm	24701	19309	Glycogen phosphorylase, muscle form.
Sqstm1	113894	18412	Sequestosome-1; Autophagy receptor that interacts directly with both the cargo to become degraded and an autophagy modifier of the MAP1 LC3 family (By similarity). Required both for the formation and autophagic degradation of polyubiquitin-containing bodies, called ALIS (aggresome-like induced structures) and links ALIS to the autophagic machinery (By similarity). Involved in midbody ring degradation (By similarity).
Stbd1	305234	52331	Starch-binding domain-containing protein 1; Acts as a cargo receptor for glycogen. Delivers its cargo to an autophagic pathway called glycophagy, resulting in the transport of glycogen to lysosomes.
Ugp2			UDP-glucose pyrophosphorylase 2, isoform CRA_b; UDP-glucose pyrophosphorylase 2.
Ulk1	360827	22241	Unc-51 like autophagy activating kinase 1.
Wdfy3	305164	72145	WD repeat and FYVE domain containing 3.
Wdfy4	498582	545030	WDFY family member 4.

Table A1.10: Primary interactions of *Stbd1* by STRING analysis (Fig 3.5b)

		Probability score		
Input	**Interacting gene**	**Experimental evidence**	**Text-mining**	**Combined score**
Stbd1	*Gyg1*	0.777	0.413	0.863
	Epm2a	0.72	0.493	0.851
	Gabarapl1	0.181	0.787	0.819
	Gbe1	0.72	0.326	0.803
	Gys2	0.653	0.34	0.761
	Ccdc62	0	0.759	0.759
	Ppp1r5	0.619	0.362	0.746
	Ppp1r3d	0.653	0.214	0.715
	Gys1	0.654	0.204	0.712

Table A1.11: Secondary interactions of gene associated with *Stbd1* (Fig 3.5b)

		Probability score		
Node 1	**Node 2**	**Experimental evidence**	**Text-mining**	**Combined score**
Ank2	*Gabarapl1*	0.856	0.049	0.857
Atg3	*Atg12*	0.903	0.956	0.995
Atg4b	*Atg3*	0.611	0.843	0.936
	Gabarapl1	0.589	0.819	0.922
	Atg12	0.146	0.848	0.865
Atg5	*Atg12*	0.852	0.977	0.996
	Atg3	0.858	0.956	0.993
	Becn1	0	0.963	0.963
	Ulk1	0.63	0.795	0.921
	Nbr1	0.12	0.876	0.887
	Wdfy3	0.595	0.694	0.871
	Atg4b	0.114	0.848	0.86
	Wdfy4	0.595	0.667	0.859
	Gabarapl1	0.315	0.775	0.839
Atg7	*Atg3*	0.857	0.957	0.993
	Atg12	0.844	0.958	0.993
	Becn1	0.592	0.957	0.981
	Atg5	0.464	0.963	0.979
	Gabarapl1	0.616	0.837	0.935
	Atg4b	0.588	0.847	0.934
	Nbr1	0.108	0.878	0.886
	Sqstm1	0.162	0.854	0.873
	Ulk1	0.409	0.788	0.869
Becn1	*Atg12*	0.434	0.955	0.973
	Atg3	0.604	0.929	0.97
	Atg4b	0.421	0.819	0.89
	Gabarapl1	0.199	0.774	0.811
Ccdc62	*Mccc1*	0	0.834	0.834
Epm2a	*Nhlrc1*	0.181	0.94	0.949
	Gys1	0.42	0.534	0.718
Gabarapl1	*Atg3*	0.605	0.777	0.908
	Atg12	0.194	0.822	0.85
Gbe1	*Gys1*	0.654	0.877	0.955

		Probability score		
Node 1	**Node 2**	**Experimental evidence**	**Text-mining**	**Combined score**
	Gyg1	0.771	0.639	0.913
	Gys2	0.595	0.721	0.882
	Ugp2	0	0.873	0.873
Gys1	*Gyg1*	0.767	0.453	0.867
	Pygb	0	0.813	0.813
	Pygl	0	0.799	0.799
	Gyg1	0.767	0.644	0.913
Gys2	*Ppp1r3b*	0.756	0.342	0.832
	Pygl	0	0.812	0.812
	Pygb	0	0.79	0.79
	Pygm	0	0.765	0.765
	Atg3	0	0.874	0.874
Nbr1	*Gabarapl1*	0.634	0.592	0.844
	Becn1	0	0.807	0.807
	Atg12	0	0.789	0.789
Nudt6	*Gyg1*	0	0.864	0.864
Ppp1r3b	*Gys1*	0.784	0.282	0.838
	Gyg1	0.755	0.26	0.81
	Gys1	0.602	0.575	0.823
	Epm2a	0.169	0.762	0.794
Ppp1r5	*Nhlrc1*	0.169	0.702	0.742
	Gys2	0.617	0.338	0.735
	Gyg1	0.615	0.288	0.714
	Ppp1r3d	0.617	0.817	0.704
Pygm	*Gys1*	0	0.811	0.811
	Nbr1	0.527	0.847	0.924
	Atg5	0.181	0.857	0.878
	Becn1	0	0.861	0.861
Sqstm1	*Gabarapl1*	0.432	0.735	0.843
	Atg12	0	0.766	0.766
	Wdfy3	0.181	0.721	0.762
	Ulk1	0.405	0.575	0.736
	Atg3	0	0.728	0.728
Ugp2	*Gys1*	0	0.792	0.792
	Gys2	0	0.735	0.735
	Atg3	0.43	0.792	0.876
Ulk1	*Becn1*	0.171	0.848	0.868
	Atg12	0.42	0.779	0.866
	Gabarapl1	0.42	0.71	0.824
	Atg4b	0.534	0.479	0.747
Wdfy3	*Gabarapl1*	0.856	0.315	0.897
Wdfy4	*Gabarapl1*	0.833	0.286	0.875

Appendix 2

Table A2.1: Sequence and expression elements of the AAV-*Gabarapl1*

	Location on viral genome
5' Inverted Terminal Repeat (5' ITR)	1-141
3' Inverted Terminal Repeat (3' ITR)	3537-3676
Cardiac Troponin promoter (cTnT)	235-663
Gabarapl1 cDNA	754-2476
Gabarapl1 coding sequence	944-1297
WPRE element	2568-3159
BGH poly(A) element	3225-3452

```
CCTGCAGGCAGCTGCGCGCTCGCTCGCTCACTGAGGCCGCCCGGGCAAAG   50
CCCGGGCGTCGGGCGACCTTTGGTCGCCCGGCCTCAGTGAGCGAGCGAGC  100
GCGCAGAGAGGGAGTGGCCAACTCCATCACTAGGGGTTCCTGCGGCAATT  150
CAGTCGATAACTATAACGGTCCTAAGGTAGCGATTTAAATACGCGCTCTC  200
TTAAGGTAGCCCCGGGACGCGTCAATTGAGTACTTCTCTCGGGGTGGGGG  250
ATAAAAGCAGTCTGGGCTTTCACATGACAGCATCTGGGGCTGCGGCAGAG  300
GGTCGGGTCCGAAGCGCTGCCTTATCAGCGTCCCCAGCCCTGGGAGGTGA  350
CAGCTGGCTGGCTTGTGTCAGCCCCTCGGGCACTCACGTATCTCCATCCG  400
ACGGGTTTAAAATAGCAAAACTCTGAGGCCACACAATAGCTTGGGCTTAT  450
ATGGGCTCCTGTGGGGGAAGGGGGAGCACGGAGGGGGCCGGGGCCGCTGC  500
TGCCAAAATAGCAGCTCACAAGTGTTGCATTCCTCTCTGGGCGCCGGGCA  550
CATTCCTGCTGGCTCTGCCCGCCCCGGGGTGGGCGCCGGGGGGACCTTAA  600
AGCCTCTGCCCCCCAAGGAGCCCTTCCCAGACAGCCGCCGGCACCCACCG  650
CTCCGTGGGACCTGCTAGCGTTTAAACTTAAGCTTGGTACCGAGCTCGGA  700
TCCACTAGTCCAGTGTGGTGGAATTCCCGGGATATCGTCGACCCACGCGT  750
CCGCAGGCCGCGAGATCTCCAGGTCCTTCTCTGGACGTTTAGCCACGTAT  800
GCGGCGACTGGCGCGTGGGAGCTGACGCGGGTGGAGCGATTGTGATAAGG  850
CTGACATTGACTGGGGGTGGCCAGACGCGAGACGCAGTCATCAGCGCGCG  900
CAGCAGGCCCCGTCCGGGGAGCCCCTACATCCTGAGGTCCATC<b>ATG</b>AAGT  950
TCCAGTATAAGGAGGACCACCCCTTCGAGTATCGGAAAAAGGAAGGTGAA 1000
AAGATTAGGAAGAAATACCCGGACCGGGTGCCGGTCATCGTGGAGAAGGC 1050
TCCTAAAGCCAGGGTCCCTGATCTGGATAAGAGGAAGTACCTTGTGCCCT 1100
CCGACCTCACTGTTGGCCAGTTCTACTTCTTAATCCGGAAGAGGATCCAC 1150
CTGAGACCTGAGGACGCCTTATTCTTCTTTGTCAACAACACCATCCCTCC 1200
CACCAGTGCTACCATGGGCCAGCTGTATGAGGACAACCACGAGGAAGACT 1250
ATTTTCTGTATGTGGCCTACAGTGATGAAAGTGTCTATGGAAAA<b>TGA</b>GGC 1300
AGAAGCCCAGCAGATGGGAGCACCTGGACTTGGGGGTAGGGGAGGGGTGC 1350
GCGTGGGACTTGGGGAACCAGAGGGAGGGCTCCCAACCATGGAGGAGACG 1400
CAAGGTGAAGACATCGGGAAACATCACACCGCACACGCTGTCGTCTTTTT 1450
TTCACAAGCTCAATTGTTACTTTTCTCTGCTTCCTCAGCCCAGGAAGAAC 1500
TTGTGTTGCATTGGCTGTGAGAGCGGGATGGGGACGACATGAATCACAGC 1550
TTTGCTGTGAGCTTTCTCTCGTGCAGTTTCATCAGAGGTTTGGGAGGAGG 1600
GCAGGTGGCCGCTAGAGAAGAATACAATTTAGCAGCAACTGCCGGCTCTT 1650
TGGGCAGAGGTTTGATTTTTGGCATTTGTACAAGCCGCACGGGCAAAGGG 1700
GGAAAAGAATGCCGTAGGGGACCACACCTAAGGGACCAAAAGATACCCAC 1750
TGTCACTGAAGCATTGTACCCCTAACCTCTGTCTCCATACCTTCCTCTCC 1800
TAGTCCTTTTCTTCCACCCAGGCTTCATAGCTCCGCCCCAGTTGTGGCAG 1850
GAGACATTCGAACAGACGTTTAGACGTTTAGAGTCCTCTTGGAAAATAGG 1900
GCCGTGCGGGAACGGTTATGATTGCCAGCGTTTTGGATGGCATTAAACTG 1950
GAGTTCAGGGTTGAACATGTCCTGCTCCTCATCCCATAAGTACCTTGGAC 2000
TTTCAGGAGCCTCAGGATCAGTCCTCTAGCATTTCCTTCACCTTTCTCAT 2050
GTACAGGGGCAGCGTGTCTGTGTGTGGAGGGTCCGGGTTACAAGGTAAGC 2100
TAGGTTGCCCACTTGCCCACTCGTCCTCTCCCTGCTGCAGTCTCTTGGGT 2150
CTCACACGCACTGCAAATGCTAAGCGATGGCCAGCTGTCTCCCTCCGTGG 2200
CATCTGCTATTCAAAGAAGATGGAGTGAGAGGGGCGCCAGAGTTTCATGG 2250
GGGCTTTACTCATTCATTTCATTTAGGGACTCTGTGGGGGGAGGGGCAGG 2300
CATTGCATTCTCACATGACATTTCAATTCATCTCTACCAATGAAGAGCGT 2350
CCTCCCTGTTGGGAGCAATCTGTACGTCTGTTTTGTCAGCTTCAGGTTCT 2400
GGTACTTTGAAGTCAATGCTGTCAGGCCAGGGAAATAAAATAATTGCTTA 2450
CCTTAAAAGTCAAAAAAAAAAAAAAAGGGCGGCCGCTCGAGTCTAGAGGG 2500
CCCTTCGAAGGTAAGCCTATCCCTAACCCTCTCCTCGGTCTCGATTCTAC 2550
GCGTACCGGTTAATCGATAATCAACCTCTGGATTACAAAATTTGTGAAAG 2600
ATTGACTGGTATTCTTAACTATGTTGCTCCTTTTACGCTATGTGGATACG 2650
```

```
CTGCTTTAATGCCTTTGTATCATGCTATTGCTTCCCGTATGGCTTTCATT 2700
TTCTCCTCCTTGTATAAATCCTGGTTGCTGTCTCTTTATGAGGAGTTGTG 2750
GCCCGTTGTCAGGCAACGTGGCGTGGTGTGCACTGTGTTTGCTGACGCAA 2800
CCCCCACTGGTTGGGGCATTGCCACCACCTGTCAGCTCCTTTCCGGGACT 2850
TTCGCTTTCCCCCTCCCTATTGCCACGGCGGAACTCATCGCCGCCTGCCT 2900
TGCCCGCTGCTGGACAGGGGCTCGGCTGTTGGGCACTGACAATTCCGTGG 2950
TGTTGTCGGGGAAATCATCGTCCTTTCCTTGGCTGCTCGCCTGTGTTGCC 3000
ACCTGGATTCTGCGCGGGACGTCCTTCTGCTACGTCCCTTCGGCCCTCAA 3050
TCCAGCGGACCTTCCTTCCCGCGGCCTGCTGCCGGCTCTGCGGCCTCTTC 3100
CGCGTCTTCGCCTTCGCCCTCAGACGAGTCGGATCTCCCTTTGGGCCGCC 3150
TCCCCGCATCGAAACCCGCTGATCAGCCGGTCATCATCACCATCACCATT 3200
GAGTTTAAACCCGCTGATCAGCCTCGACTGTGCCTTCTAGTTGCCAGCCA 3250
TCTGTTGTTTGCCCCTCCCCCGTGCCTTCCTTGACCCTGGAAGGTGCCAC 3300
TCCCACTGTCCTTTCCTAATAAAATGAGGAAATTGCATCGCATTGTCTGA 3350
GTAGGTGTCATTCTATTCTGGGGGGTGGGGTGGGGCAGGACAGCAAGGGG 3400
GAGGATTGGGAAGACAATAGCAGGCATGCTGGGGATGCGGTGGGCTCTAT 3450
GGCTTCTGAGGCGGAAAGAACCAGATCCTCTCTTAAGGTAGCATCGAGAT 3500
TTAAATTAGGGATAACAGGGTAATGGCGCGGGCCGCAGGAACCCCTAGTG 3550
ATGGAGTTGGCCACTCCCTCTCTGCGCGCTCGCTCGCTCACTGAGGCCGG 3600
GCGACCAAAGGTCGCCCGACGCCCGGGCTTTGCCCGGGCGGCCTCAGTGA 3650
GCGAGCGAGCGCGCAGCTGCCTGCAG                          3676
```

Figure A2.1: Linear genomic sequence of the AAV9-cTnTp-m*Gabarapl1*-WPRE. The cardiac Troponin promoter (cTnTp, light blue) and the *Gabarapl1* cDNA (green) are shown. Each line is 50 nucleotides long.

Table A2.2: Concentration and purity of cardiac DNA extracted to measure viral copy numbers

Sample ID	[DNA] ng/ul	A260/280	A260/230
2	1078.8	2.01	2.17
3	439.9	1.97	1.94
4	730.8	2.04	2.25
5	1795.6	2.03	2.23
7	774.3	2.03	2.25
9	355.9	2.10	2.11
10	568.1	1.94	1.87
13	490.9	2.02	2.22
16	818.4	2.02	2.15
17	974.3	2.04	2.19
18	1139.6	2.02	2.27
21	1225.9	2.04	2.23
22	359.8	1.95	1.83
24	1645.0	1.94	2.25
29	811.7	2.03	2.29
30	760.5	1.97	2.12
32	834.1	1.99	2.11
33	847.2	2.02	2.01
34	1106.6	2.04	2.26
36	1143.3	2.01	2.22
37	988.5	2.04	2.11
38	725.0	2.00	2.25
40	905.1	2.00	2.27
41	1344.9	2.01	2.21
42	769.0	2.02	2.17
43	1108.4	2.01	2.18
44	951.5	1.99	2.07
45	1021.0	2.03	2.15
46	743.8	2.01	2.26
47	932.0	2.02	2.20
48	865.5	2.01	2.26
50	1088.6	2.02	2.17
51	998.3	2.04	2.17
52	968.8	2.01	2.24
79	617.7	2.03	1.97
83	920.8	1.71	1.67
85	1050.0	2.03	2.22
86	397.7	2.04	2.25
87	944.1	2.03	2.26
88	874.5	2.00	2.05
89	601.3	1.96	1.95
90	719.5	2.01	2.21
92	416.9	1.79	1.63

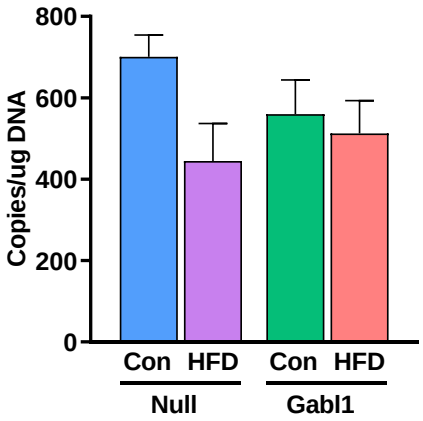

Figure A2.2: Cardiac viral copies 12 weeks post-AAV administration. Data presented as mean±SEM, *p<0.05.